UNIVERSIDAD NACIONAL AUTÓNOMA DE MÉXICO

Posgrado en Ciencias de la Tierra

Instituto de Geología

Origen de las rocas de alta presión en el centro del Complejo Acatlán, Puebla, México

T E S I S

Para obtener el grado de

Doctor en Ciencias de la Tierra

(Geología Estructural y Tectónica)

PRESENTA:

Gonzalo Humberto Galaz Escanilla

MIEMBROS DEL JURADO EXAMINADOR:

Dr. John Duncan Keppie Moorhouse, Instituto de Geología, UNAM (Tutor)

Dr. Fernando Ortega Gutiérrez, Instituto de Geología, UNAM

Dr. Gustavo Tolson Jones, Instituto de Geología, UNAM

Dr. Peter Schaaf, Instituto de Geofísica, UNAM

Dr. Luigi Solari Lovati, Centro de Geociencias, UNAM

MÉXICO, D.F., JUNIO 2013

Dedicatoria

Un mar de emociones, el país del corazón, la cuidad del cariño, un mundo de paciencia..., quisiera dedicar esta tesis a mi familia querida y humanitaria. En especial a mis padres Rosa María y Gonzalo, mi hermana Betzabé, mis tíos “Nana” y “Luchín”, y mis abuelos Ana, Susana, Humberto y Luis, por sus enseñanzas, amor y apoyo incondicional. Sin ellos nada hubiese sido posible...

Poema "Elogio de las piedras", Gabriela Mistral.

Las piedras arrodilladas, las piedras que cabalgan y las que no quieren voltearse nunca, como un corazón demasiado rendido.

Las piedras que descansan de espaldas, como guerreros muertos y tienen sus llagas tapadas de puro silencio, no de venda.

Las piedras que tienen los gestos esparcidos, perdidos como hijos: en una sierra la ceja y en el poyo[*] un tobillo. Las piedras que se acuerdan de su rostro junto y querrían reunirlo, gesto a gesto, algún día.

Las piedras amodorradas, ricas de sueños, como la pimienta de esencia, pesadas de sueño, como el árbol de coyunturas, la piedra, que aprieta salvajemente su tesoro de sueño absoluto.

Las piedras arrodilladas, las piedras incorporadas, las piedras que cabalgan y las que no quieren voltearse, igual que corazones demasiado rendidos.

La piedra cabezal para el Jacob de nuca fuerte, la piedra enjuta como el número, sin bochorno y sin rocío igual que el número.

La piedra redondeada que es solamente un gran párpado, sin pestaña, como el de Matusalem. La cumbre en garfios de los Andes místicos, que era una llama sin danza, parada como la Sara de Lot y que no quiso contestar en mi infancia y no me contesta todavía.

Las piedras con sobresalto de oro o de plata, con punzadura súbita de cobre, que están asombradas del intruso. Piedras turbadas por sus almendras de metal, como por el dardo invisible.

Las piedras arrodilladas, las piedras incorporadas, las piedras que corren en falange o en muchedumbre, sin llegar a ninguna parte.

Las piedras mayores de los ríos, de costado escurridizo, como el abogado, y que tienen las mismas vegetaciones lacias, que se pegan a la cabellera de las ahogadas. Las piedras suaves que pueden tocar al desollado y no lo hieren y pasan sobre su cuerpo con la propia lengua de su madre y no se cansan.

Las piedras menores de los ríos, los guijarros pintados como el fruto y que, ellos sí, pueden cantar. Yo también tuve cinco años y cuando los puse debajo de mi almohada, alborotaban como un montón de niños que se ahogaban o bien hacían ronda en torno del núcleo de mi sueño, dueños de él, guijarros pueriles venidos a mis sábanas por jugar conmigo.

Las piedras que no quieren ser lápidas ni fuente, por no recibir el gesto ajeno y se rehúsan a la inscripción intrusa para hacer subir algún día el gesto, el habla de ellas mismas.

Las piedras mudas, de tener el corazón más cargado de pasión que sea dable y que por no despertar su almendra vertiginosa, sólo por eso no se mueven.

---

[*] Banco de piedra u otro material que normalmente se construye en una casa pegado a una pared o junto a la puerta.

Agradecimientos

En primer lugar deseo agradecer al Dr. J. Duncan Keppie, quien me mostró una geología de alta calidad con una fascinación y un amor único, además de muchas otras cosas de la vida. En segundo lugar quisiera agradecer al Dr. J. Brendan Murphy por su gran apoyo en esta tesis, especialmente en geoquímica e isótopos de Nd, pero además por su muy "buena onda". Un especial agradecimiento al Dr. Fernando Ortega Gutiérrez, por las gratas discusiones geológicas y de fútbol, su genial apoyo en petrología, pero fundamentalmente por su calidad personal y afecto brindado. Agradecer las valiosas sugerencias y discusiones realizadas por los Dres. Gustavo Tolson, Jaroslav Dostal, Mariano Elías, James K.W. Lee, Luigi Solari, Dante Morán, Elena Centeno y Peter Schaaf. Quisiera también agradecer al Dr. Francisco Hervé, quien me brindo la pasión inicial por esta hermosa ciencia.

La presente tesis no podría haberse concretado sin el apoyo de muchos técnicos académicos de los diferentes laboratorios de la UNAM, entre ellos, Dr. Carlos Ortega-Gutiérrez, M.Sc. Consuelo Macías-Romo, Dra. M. Amabel Ortega-Rivera, Ing. Teodoro Hernández-Treviño y el Ing. Carlos Linares-López. A todos los funcionarios del Instituto de Geología, por su gran labor y colaboración, en especial agradecer a mis "secres" queridas María Luisa, Gloria, Nora y Aida, además de nuestro equipo de cómputo Rosario, Francisco y Fabricio, por su dedicación y ayuda.

A mis compañeros de la "banda geológica y amigos", Daniel, Lucy, Berlaine, Carlos, Carlitos, Mario, Elisa, Elías, Emilio, Rosalva, Fernando, Lors, Judith, Aarón, Karina, Charles, Alma, Valerie, Sandra, Rafa, Beto vetas, Edith, Rodrigo, Fabián, Roy, Vampi, Dianita, Caro, Mildred, Dafne, Julio, Marisol, Tocayo, Betillo, entre otros, por compartir muchos, pero muchos gratos momentos "extra-tesis",…si el Depa-dela-muerte y Chingadera´s Bar hablaran, uff!. Sin su apoyo esta tesis hubiese sido mucho más difícil. Perdónenme si olvidé a alguien, pero son muchos los amigos que encontré en México.

Al equipo de fútbol del Instituto de Geología, personificado en nuestro D.T. Gonzalo ("El tocayo"), además del Atlético Firenze y Borbotones FC, por las gratos momentos compartiendo el deporte rey, ah!, y los "terceros tiempos".

Esta Tesis fue realizada gracias al apoyo de una beca de doctorado otorgada por intermedio de CONACYT, y al financiamiento mediante los proyectos PAPIIT N° IN100108-3, CONACYT N° CB-2005-1:24894, e IGCP-597.

Resumen

El Complejo Acatlán constituye el basamento metamórfico Paleozoico del Terreno Mixteco, sur de México. Se compone principalmente de dos cinturones de alta presión (facies eclogita y esquistos azules), orientados ~N-S, que se encuentran emplazados en rocas de bajo grado metamórfico. La génesis y exhumación de terrenos metamórficos de alta presión se asocian fundamentalmente con regímenes convergentes, ya sea colisión o subducción, siendo esta discriminación clave en la evolución paleozoica del sur de México. Con este objetivo se realizó un estudio integrado en el margen oeste del cinturón central de alta presión (Suite Piaxtla), con énfasis en la localidad de Tehuitzingo.

La unidad metamórfica de bajo grado en Tehuitzingo está constituida por samitas y pelitas, cuya población de circones más joven produce una edad U-Pb de 481 ± 16 Ma, la cual constituye un límite superior para sus depósitos. La petrología, estructural, isótopos de Nd y poblaciones de circones, sugieren su correlación con depósitos paleozoicos de bajo grado ubicados en el margen opuesto del cinturón central de alta presión, indicando que forman parte de un mismo terreno. Por su parte, la Suite Piaxtla está compuesta por un granitoide (482 ± 3 Ma), un esquisto de mica (circón detrítico concordante más joven: 433 ± 3 Ma), peridotitas serpentinizadas y acumulados gabroicos. Un *klippe* de vergencia W es interpretado como el contacto tectónico que yuxtapone inicialmente las unidades metamórficas de bajo grado y de alta presión. Generalmente esta estructura se encuentra sobreimpuesta por numerosas fallas laterales derechas. Datos petrológico-estructurales indican que este *klippe* se inició durante el pico metamórfico en facies eclogita (~16 kbar y 750 °C), continuando durante la segunda fase de deformación penetrativa en facies epidota-anfibolita (~5 kbar y 470 °C). Una tercera fase de deformación en facies esquistos verdes (~2.7 kbar y 350 °C) común en ambas unidades, indica que la yuxtaposición se produce en la etapa final del desarrollo de este *klippe*. Edades Ar-Ar en muscovita obtenidas desde ambas unidades sugieren que esta yuxtaposición se produjo durante el Misisípico (329–316 Ma).

Diversos parámetros obtenidos desde el cinturón central de alta presión, indican que este *klippe* representa una zona de extrusión de tipo serpentinítica asociada a un régimen de subducción: (1) la naturaleza de sus protolitos; (2) patrones P-T-t; (3) altas profundidades alcanzadas (40–70 km); (4) bajas tasas de exhumación (1.6–2.3 mm/año) y gradientes termales (5.9–8.7 °C/km). Por otro lado, datos geoquímicos indican que los acumulados gabroicos de Tehuitzingo poseen una afinidad toleítica de arcos de islas inmaduros, con características típicas de magmas de antearco/arco. Sin embargo, la única evidencia acerca de la posibilidad de un arco en el Complejo Acatlán la constituye una población de circones ígneos detríticos del Devónico Medio–Misisípico (405–330 Ma) en sedimentos carboníferos. Un proceso de subducción-erosión es inferido como el principal mecanismo que permite la remoción, enterramiento y consecuente metamorfismo de rocas de antearco/arco. Poblaciones de circones e isótopos de Nd obtenidos desde variados protolitos del Complejo Acatlán, sugieren que este proceso de subducción-erosión se desarrolló sobre

el margen occidental de Gondwana en el Devónico Medio-Misisípico. El desarrollo de un canal de subducción de tipo serpentinítico posibilita la exhumación de la Suite Piaxtla, permitiendo su yuxtaposición tectónica en la corteza superior durante el Misisípico.

Los parámetros generados en esta tesis son consistentes con los obtenidos en terrenos metamórficos de alta presión generados en régimen de subducción alrededor del mundo, y muy contrastantes a los obtenidos desde terrenos generados en un régimen colisional. Por lo tanto constituyen una gran herramienta en su reconstrucción tectónica.

Tabla de Contenidos

Lista de Figuras

Capítulo 1

Introducción

1.1. Introducción general: rocas metamórficas de alta presión

En una definición "simplista", rocas metamórficas son aquellas que han sido sometidas a un conjunto de procesos físico-químicos que modifican su textura y/o su composición mineralógica, sin perder su estado sólido. La presión (P) y temperatura (T) son los principales agentes del metamorfismo, no obstante, existen factores catalizadores que favorecen las reacciones metamórficas, tales como la presencia de fluidos, la porosidad del protolito, los esfuerzos desviatorios locales, el tiempo, entre otros. Las rocas metamórficas de alta presión son aquellas que han sido sometidas a presiones superiores a ~7 kbar (facies esquistos azules y eclogitas), es decir, profundidades corticales superiores a 20 km, considerando un gradiente litostático de presión en profundidad de 0.3 kbar/km.

Por más de 50 años los geólogos tectónicos han logrado complementar la petrología metamórfica con estudios estructurales, geoquímicos, y más recientemente isotópicos, con la finalidad de asociar los diferentes "productos" metamórficos con ambientes tectónicos específicos. Históricamente se ha considerado que las rocas metamórficas de alta presión son generadas en márgenes convergentes, interpretándolas como suturas oceánicas obductadas producto de una convergencia continental-continental (e.g., Liou *et al.*, 2004; Ernst, 2005, 2010; Fig. 1a). Ejemplos mundiales lo constituyen las ofiolitas de alta presión generadas en los orógenos colisionales del Himalaya, los Pirineos, los Urales o los Alpes. Posteriormente en los 90's algunos autores reportaron rocas de alta presión (facies esquistos azules) generadas en zonas divergentes de *rift*, mejor conocidas como complejos de núcleo metamórfico, donde rocas miloníticas profundas son exhumadas a través de una falla de despegue (e.g., Jansen y Schuiling, 1976; Lister *et al.*, 1984; Fig. 1b). No obstante, en la actualidad se ha determinado que estas rocas constituían un basamento previamente metamorfoseado bajo un régimen convergente, el cual es posteriormente exhumado mediante un proceso de *rift* sobreimpuesto (e.g., Kapp *et al.*, 2000[1]; Brun y Sokoutis, 2007; Brun y Faccenna, 2008; Huet *et al.*, 2011). Así, el gran adelgazamiento cortical producto de la extensión, impide que el metamorfismo sin-*rift* supere las condiciones P-T de facies anfibolita-esquistos verdes. Sin embargo, estudios recientes han reportado fragmentos de

[1] Las citas pueden ser encontradas en el Capítulo Referencias. Sin embargo, las citas de los artículos incluidos en esta Tesis se encuentran contenidas en los mismos.

litósfera oceánica (y rocas asociadas) sometidos a alta presión durante convergencia continental-oceánica (subducción; Fig. 1c). Posteriormente estas rocas son exhumadas por medio de un canal de subducción (Ernst *et al.*, 1997; Liou *et al.*, 2004; Stöckhert y Gerya, 2005; Guillot *et al.*, 2009), por zonas internas estructuralmente debilitadas de la placa superior (Chemenda *et al.*, 2001; Keppie *et al.*, 2010b), o por una combinación de ambas zonas (Butler *et al.*, 2011).

Recientemente se han realizado algunas recopilaciones de diversos parámetros relacionados a la exhumación de rocas de alta presión en más de 80 afloramientos alrededor del mundo (e.g., Guillot *et al.* 2009; Agard *et al.*, 2009). Basándose fundamentalmente en la naturaleza de sus protolitos, profundidades alcanzadas, patrones P-T-t, tasas de exhumación y gradientes termales, propusieron tres tipos de regímenes convergentes dominantes para su génesis: ***subducción (acrecionario o serpentinítico)*** y ***continental*** (Figs. 1a,c). La principal diferencia entre los regímenes de subducción acrecionario o serpentinítico la constituye el tipo, proporciones y profundidades que alcanzan sus protolitos: (1) el régimen acrecionario se caracteriza por una gran cantidad de sedimentos marinos que incorporan fragmentos de litósfera oceánica y en ocasiones partes del prisma acrecionario-antearco, que alcanzan una profundidad máxima de ~40 km; mientras que (2) en régimen serpentinítico los protolitos se componen de peridotitas abisales y/o rocas de suprasubducción generadas en la cuña del manto, con escaso material continental adicionado, que alcanzan una profundidad máxima de ~70 km.

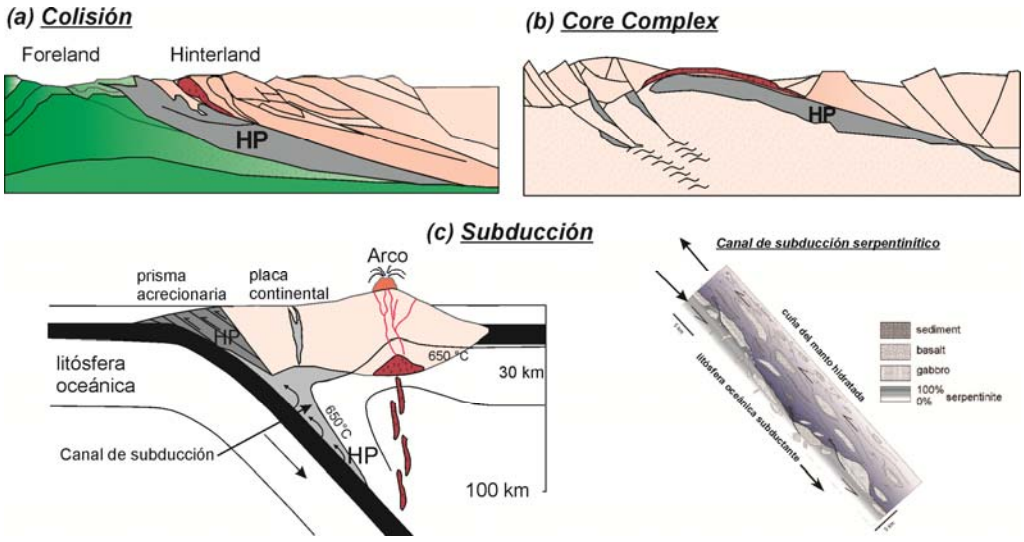

Fig 1. Algunos mecanismos de exhumación propuestos para rocas metamórficas de alta presión.

En régimen de convergencia continental (tipo alpina) los protolitos son fundamentalmente continentales, y por lo tanto de más baja densidad que las rocas mantélicas circundantes en profundidad, generando una alta flotabilidad y en consecuencia altas tasas de exhumación (sobre 20 mm/año), así como altos gradientes termales (sobre 15 °C/km). Estos parámetros son muy importantes y contrastantes con respecto a un régimen de subducción (acrecionario o serpentinítico), donde sus tasas de exhumación varían entre 1–10 mm/año y sus gradientes termales son menores a 10 °C/km.

La comprensión y determinación de estos parámetros de exhumación son fundamentales en la discriminación del ambiente tectónico de formación de rocas de alta presión. Esto ha derivado en la reinterpretación de numerosos terrenos metamórficos de alta presión alrededor del mundo (e.g., Keppie *et al.*, 2010a), permitiendo grandes avances en la comprensión de la dinámica terrestre. En este contexto, las rocas metamórficas de alta presión (Suite Piaxtla) en Tehuitzingo, Complejo Acatlán, México, constituyen un laboratorio natural, el cual es el objetivo central de la presente tesis.

1.2. Complejo Acatlán: presentación de la problemática

El Complejo Acatlán se distribuye en un área de ~22,000 km^2, limitada por las coordenadas ~16°40’–18°50’de latitud norte y ~97°30’–99°20’de longitud oeste, a lo largo del margen suroccidental de la República Mexicana (Fig. 2). Constituye el basamento Paleozoico del Terreno Mixteco, cuyo margen norte se encuentra cubierto por secuencias volcánicas y volcaniclásticas cenozoicas pertenecientes al Cinturón Volcánico Transmexicano (Fig. 2a). Hacia el sur, se encuentra en contacto con el Terreno Chatino (o Xolapa; Mesozoico–Cenozoico), mediante la cenozoica Falla Chacalapa-La Venta de régimen transtensional-siniestral (Fig. 2b; Tolson, 2005). El límite occidental del Terreno Mixteco lo constituye la cretácica tardía Falla Papalutla, que cabalga rocas del Complejo Acatlán sobre calizas cretácicas de la Plataforma Guerrero-Morelos (Cerca *et al.*, 2007). Finalmente hacia el oriente, la zona de cizalla dextral Caltepec (Pérmico) yuxtapone este terreno contra el Terreno Oaxaquia (Elías-Herrera y Ortega-Gutiérrez, 2002), cuyo basamento lo constituye el Complejo Oaxaqueño (~1 Ga; Keppie *et al.*, 2003).

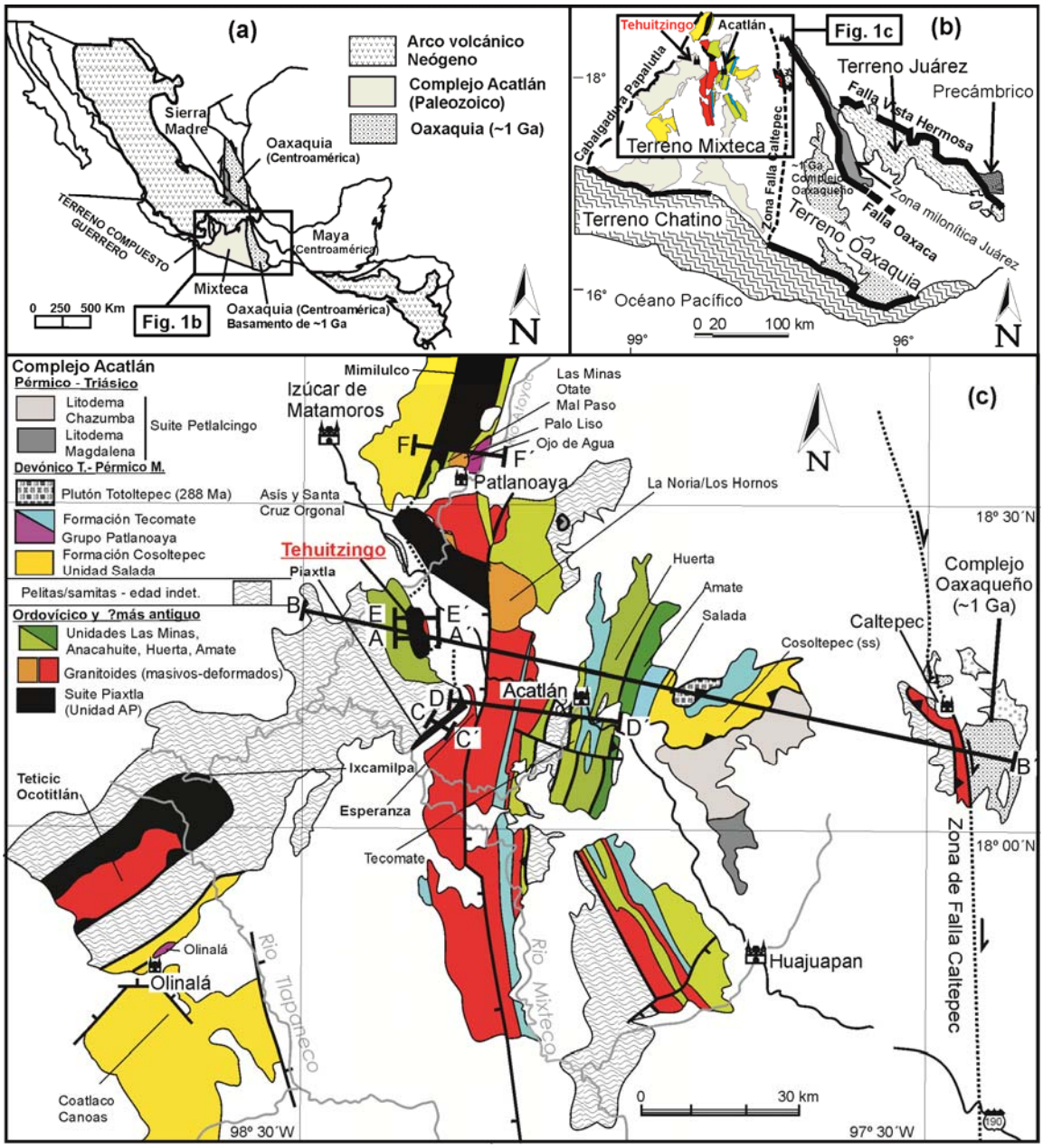

Fig. 2. (a) Localización de los principales complejos metamórficos del sur de México; (b) Mapa detallado de los complejos metamórficos del sur de México; (c) Mapa geológico del Complejo Acatlán entre las ciudades de Izúcar de Matamoros (al norte) y las ciudades Olinalá-Tamazulapan (al sur). Modificado desde Keppie *et al*. (2008b).

Las rocas paleozoicas del Complejo Acatlán pueden ser subdivididas en dos unidades metamórficas, una de bajo grado y otra de alta presión (Fig. 2c). La unidad de bajo grado está compuesta principalmente por dos secuencias: (1) una secuencia clástica

depositada durante el Neoproterozoico–Ordovícico, que se encuentra intruida por una suite ígnea bimodal emplazada en un ambiente de *rift* durante el Ordovícico–Silúrico (480–440 Ma; Murphy *et al.*, 2006; Keppie *et al.*, 2008b; Ortega-Obregón *et al.*, 2009); y (2) una secuencia marina somera del Devónico Tardío–Pérmico consistente de samitas, pelitas y algunas rocas volcánicas máficas. Esta unidad se encuentra afectada por un metamorfismo en facies esquistos verdes (~3 kbar y ~350 °C) y al menos una retrogresión a facies sub-esquistos verdes (Meza-Figueroa *et al.*, 2003; Galaz *et al.*, 2013a).

Por otro lado, la suite metamórfica de alta presión (Suite Piaxtla) consiste de: (1) una secuencia sedimentaria (pelitas y samitas) depositadas durante el Neoproterozoico–Ordovícico, la cual se encuentran intruida por una suite ígnea bimodal (granitoides y eclogitas retrogradadas) relacionada a *rift*, similar a aquella que intruye a la unidad de bajo grado metamórfico; y (2) cuerpos máficos-ultramáficos que han sido atribuidos a variados ambientes tectónicos, tales como, *rift* continental, peri-arco, arco de islas (IAB), islas oceánicas (OIB) y ofiolítico (MORB) (Meza-Figueroa, 1998; Proenza *et al.*, 2004; Murphy *et al.*, 2006; Morales-Gámez *et al.*, 2009; Keppie *et al.*, 2012b). Esta unidad fue afectada por un metamorfismo en facies eclogita (11–16 kbar y 500–750°C), sobreimpuesto por al menos dos retrogresiones a facies anfibolita y esquistos verdes (Talavera-Mendoza *et al.*, 2002; Meza-Figueroa *et al.*, 2003; Reyes-Salas, 2003; Vega-Granillo *et al.*, 2007; Middleton *et al.*, 2007; Ramos-Arias *et al.*, 2012; Galaz *et al.*, 2013a).

Las rocas de la Suite Piaxtla se encuentran emplazadas tectónicamente en la unidad de bajo grado, formando dos cinturones metamórficos de alta presión ubicados al centro (Mimilulco-Piaxtla) y occidente (Ixcamilpa-Olinalá) del Complejo Acatlán (Fig. 2c). El cinturón occidental de alta presión ha sido interpretado como un *klippe* (cabalgadura plegada), que yuxtapone la unidad metamórfica de alta presión sobre la unidad de bajo grado mediante una falla inversa de vergencia oeste (Ramos-Arias *et al.*, 2012). Por su parte, el límite oriental del cinturón central ha sido interpretado como una zona de cizalla lístrica N-S, con vergencia oeste y componente normal (Ramos-Arias *et al.*, 2008), sin embargo, la edad e interpretación tectónica del contacto occidental de este cinturón aún no han sido determinadas. En consecuencia, su mecanismo de exhumación se encuentra actualmente bajo debate, generándose diversas hipótesis publicadas (Fig. 3):

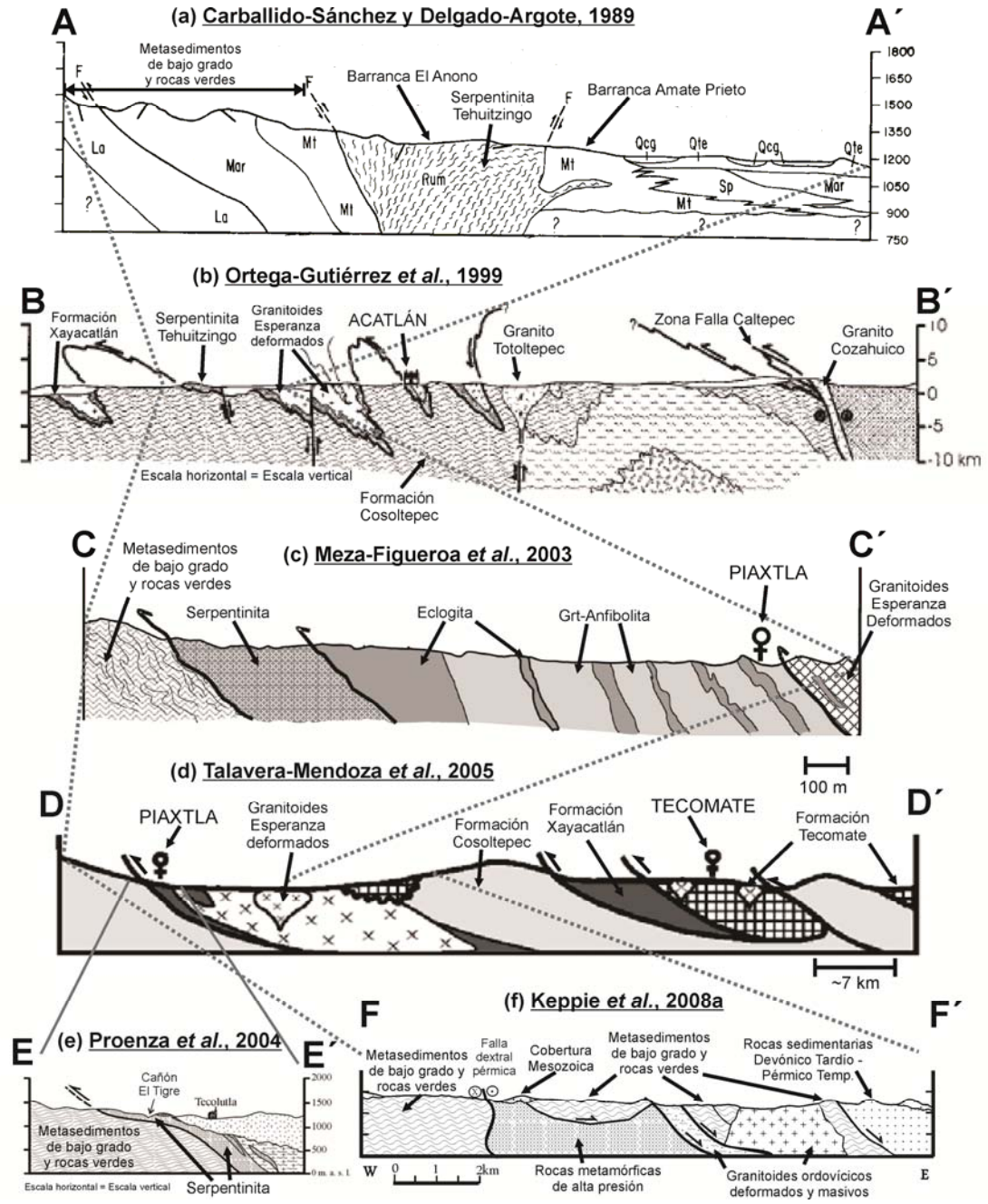

Fig. 3. Secciones previas realizadas en el Complejo Acatlán. (a) Carballido-Sánchez y Delgado-Argote (1989); (b) Ortega-Gutiérrez *et al.* (1999); (c) Meza-Figueroa *et al.* (2003); (d) Talavera-Mendoza *et al.* (2005); (e) Proenza *et al.* (2004); (f) Keppie *et al.* (2008a). Localización de las secciones se indican en la Fig. 2c.

(1) Un diapiro que se emplaza, a través de *fallas inversas reactivadas*, en la unidad metamórfica de bajo grado durante el Cretácico Tardío–Paleógeno (Fig. 3a; Carballido-Sánchez y Delgado-Argote, 1989);

(2) Una extensa napa plegada y trasportada hacia el occidente desde la Zona de Falla Caltepec, que ha sido interpretada como la sutura del Océano Iapetus, producida durante la *convergencia continental* ordovícica (colisión tipo alpina) entre masas gondwánicas (Complejo Oaxaqueño) y laurencianas (Fig. 3b; Ortega-Gutiérrez, 1981; Ortega-Gutiérrez *et al.*, 1999);

(3) Una cabalgadura plegada del Devónico Temprano–Carbonífero compuesta de múltiples napas, extruidas durante un complejo proceso de *convergencia continental* (múltiples colisiones tipo alpina) entre terrenos peri-gondwánicos y laurencianos (Fig. 3c; Meza-Figueroa *et al.*, 2003);

(4) La napa inferior de un terreno compuesto de al menos siete bloques peri-gondwánicos y laurencianos acrecionados durante el Paleozoico Inferior mediante sucesivos procesos de *convergencia continental* donde fueron cerrados los océanos Iapetus, Reico, además de pequeñas cuencas oceánicas asociadas (Fig. 3d; Talavera-Mendoza *et al.*, 2005; Vega-Granillo *et al.*, 2009);

(5) Una napa ofiolítica perteneciente al Océano Iapetus, obductada durante el Ordovícico Tardío–Silúrico Temprano mediante un proceso de *convergencia continental*. La composición de cromitas incluidas, sugiere que esta napa ofiolítica fue generada en un ambiente de periarco (Fig. 3e; Proenza *et al.*, 2004);

(6) Un corrimiento que representa el límite inferior de una zona de extrusión, generada mediante un proceso de *convergencia continental-oceánica* que afectó al Complejo Acatlán durante el Devónico–Carbonífero (Fig. 3f; Keppie *et al.*, 2008b, 2010b, 2012b). El límite superior del cinturón central de alta presión lo constituye una zona de cizalle normal-lístrica generada durante el Devónico–Carbonífero (Ramos-Arias *et al.*, 2008; Keppie *et al.*, 2010b).

En la actualidad, esta discusión ha derivado en la interpretación de las rocas metamórficas de alta presión (Suite Piaxtla) del Complejo Acatlán, como el resultado del cierre de una o múltiples cuencas oceánicas existentes entre los océanos Iapetus y Reico (Ortega-Gutiérrez *et al.*, 1999; Talavera-Mendoza *et al.*, 2005; Vega-Granillo *et al.*, 2007, 2009). En contraparte, ha sido interpretada como un cuerpo metamórfico generado y extruido en la placa superior mediante un proceso de subducción-erosión (convergencia continental-oceánica), desarrollado en el margen sur del Océano Reico durante el

Carbonífero (Keppie *et al.*, 2008a, 2012b). Con el objetivo de resolver el debate relacionado a la naturaleza de los protolitos, temporalidad de eventos, ambiente tectónico de formación, así como el mecanismo de exhumación de la Suite Piaxtla, esta tesis presenta diversos estudios a sus afloramientos en la localidad de Tehuitzingo[2], Estado de Puebla, México. Entre las metodologías aplicadas destacan petrología primaria y metamórfica, estructural, geoquímica, geocronología U-Pb, Ar-Ar, e isotopía de Nd.

1.3. Tehuitzingo: acceso al área de estudio y descripción geológica general

El área estudiada se encuentra en el Municipio de Tehuitzingo, porción suroeste del Estado de Puebla, México (Fig. 2a), a una distancia de ~220 km al sur-sureste de Ciudad de México y ~90 km al sur de la Ciudad de Puebla. Esta área se compone de cerros con alturas no superiores a los ~1,300 m.s.n.m., pertenecientes a una cadena orientada ~norte-sur que forma parte de la Sierra Mixteca. Se accede por la Carretera Internacional MEX-190, también conocida como Av. Cristóbal Colón, que nace desde la carretera México-Cuernavaca y transita por las ciudades de Izúcar y Acatlán, entre las cuales se encuentra localidad de Tehuitzingo (Fig. 4). Desde esta localidad nace hacia el oeste una terracería que permite acceder a las localidades de Tlachinola y Tecoluta, límites norte y oriental respectivamente de la zona de estudio. Desde la salida sur de Tehuitzingo, nace hacia el oeste la Carretera Federal Tehuitzingo-Axutla (MEX-602), que pasa por la localidad de Atopoltitlán, límite sur del área de trabajo.

En Tehuitzingo la Suite Piaxtla se encuentra yuxtapuesta tectónicamente contra la unidad metamórfica de bajo grado mediante fallas sub-verticales, orientadas ~N-S y que presentan indicadores cinemáticos dextrales-oblicuos. Cercano a la localidad de Atopoltitlán, esta suite se encuentra cabalgando a la unidad metamórfica de bajo grado a lo largo de una falla inversa plegada, cuyos indicadores cinemáticos indican que el "bloque de techo" (Suite Piaxtla) cabalga hacia el oeste.

[2] Tehuitzingo, palabra compuesta de origen azteca que significa: *"tehuiztli": piedras agudas / "tzin": diminutivo / "co": en*. Por lo tanto se traduce: "en las piedritas agudas", posiblemente en referencia a los grandes cristales aciculares de serpentina presentes en la Serpentinita Tehuitzingo.

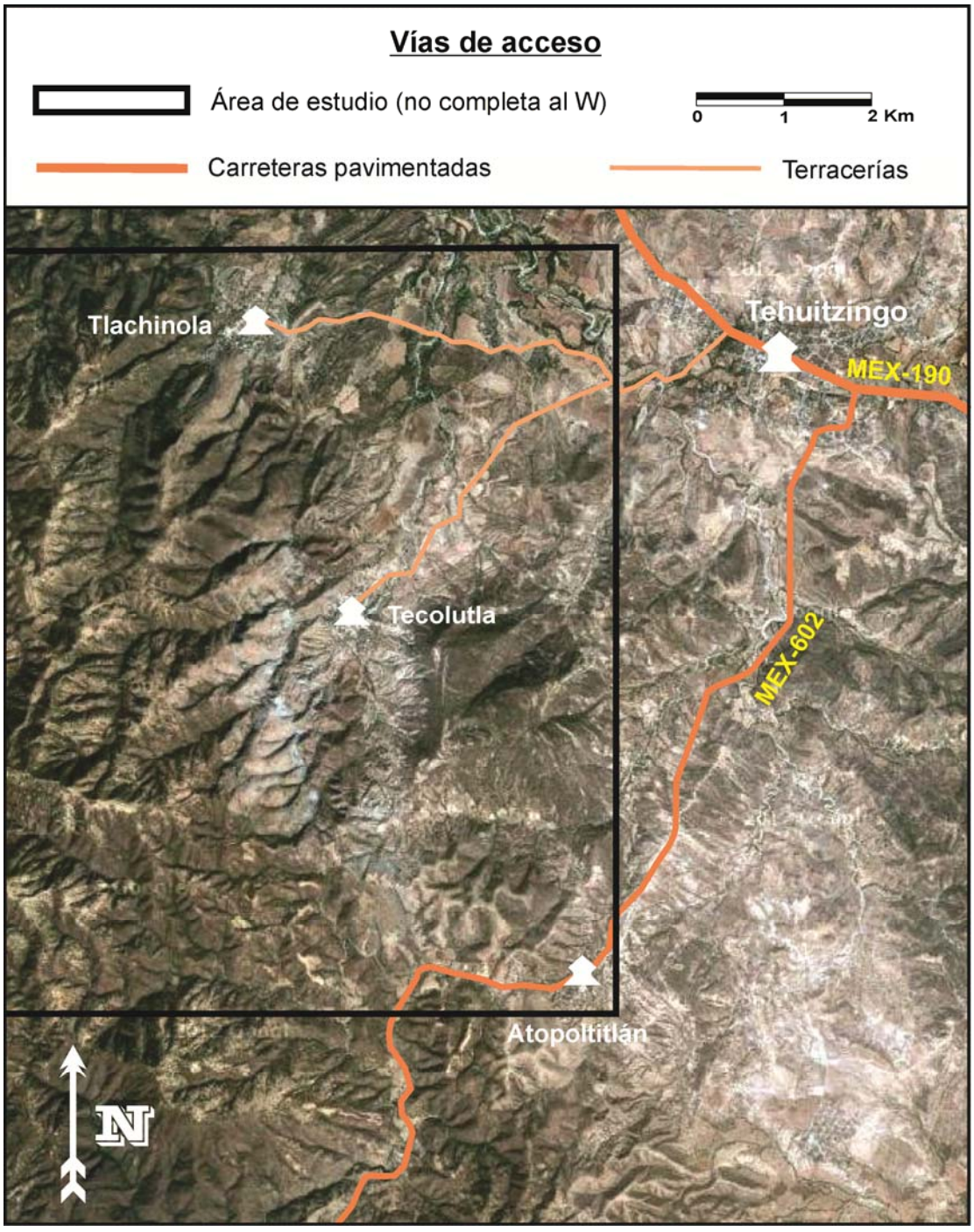

Fig. 4. Plano topográfico mostrando las vías de acceso al área de estudio. MEX-190, también conocida como Carretera Cristóbal Colón; MEX-602, también conocida como Carretera Federal Tehuitzingo-Axutla.

La Suite Piaxtla está compuesta fundamentalmente de una harzburgita serpentinizada (Serpentinita Tehuitzingo) formada por cristales aciculares y fibrosos de

serpentina, coexistiendo crisotilo, lizardita y antigorita, con asociados minerales de magnetita, calcita, mica blanca y talco, además de accesorios como cromita, clinocloro, cuarzo, anfíbol, y epidota (González-Mancera, 2001). Este cuerpo serpentinítico contiene pequeños bloques de otras litologías limitados por fallas, tales como, gabro, granitoide y esquisto de mica que presentan una deformación con fábrica planar. La mineralogía secundaria y la penetrativa polideformación dúctil registrada en esta suite, sugieren que ha sido sometida a condiciones metamórficas de alta presión.

La unidad metamórfica de bajo grado está conformada por pelitas y samitas cuarzo-feldespáticas que también presentan una deformación con fábrica planar. Además, existen unidades de rocas más jóvenes que no constituyen mayor interés para el presente estudio, tales como, un lente de conglomerado polimíctico (Jurásico?) yuxtapuesto mediante fallas contra la Suite Piaxtla, además de una discordante cobertura sedimentaria conformada por dos secuencias, una formada por areniscas lacustres pertenecientes a la Formación Tehuitzingo (Pleistoceno?; Calderón-García, 1956), y otra conteniendo areniscas, lutitas y un conglomerado polimíctico pobremente consolidado.

1.4. Objetivos específicos en las rocas Paleozoicas de Tehuitzingo

(1) Establecer la estructura, con énfasis en las relaciones de contacto entre unidades geológicas del Paleozoico (Capítulo 2).
(2) Determinar la trayectoria P-T-t de las unidades geológicas, a partir de la determinación de las condiciones del pico metamórfico y sus retrogresiones (Capítulo 2).
(3) Calcular las tasas de exhumación y gradientes termales a las cuales fueron sometidas las rocas de la Suite Piaxtla (Capítulo 2).
(4) Determinar la firma geoquímica e isotopía de Nd de la Suite Piaxtla, estableciendo el ambiente tectónico de formación de los protolitos de alta presión (capítulo 3).
(5) Establecer la implicancia en la evolución geográfica Paleozoica del margen occidental de Gondwana (Capítulos 2, 3, 4, 5 y 6).

Capítulo 2

Un *klippe* plegado de alta presión en Tehuitzingo sobre el margen occidental de una zona de extrusión, Complejo Acatlán, sur de México

A high-pressure folded klippe at Tehuitzingo on the western margin of an extrusion zone, Acatlán Complex, southern México. ***Gondwana Research, 2013, p. 641–660***

Gonzalo Galaz E., J. Duncan Keppie, James K.W. Lee, Amabel Ortega-Rivera

Gondwana Research 23 (2013) 641–660

Contents lists available at SciVerse ScienceDirect

Gondwana Research

journal homepage: www.elsevier.com/locate/gr

A high-pressure folded klippe at Tehuitzingo on the western margin of an extrusion zone, Acatlán Complex, southern México

Gonzalo Galaz E. [a,*], J. Duncan Keppie [a], James K.W. Lee [b], Amabel Ortega-Rivera [c]

[a] Departamento de Geología Regional, Instituto de Geología, Universidad Nacional Autónoma de México, México D.F., 04510, México
[b] Department of Geological Sciences and Geological Engineering, Queen's University, Kingston, Ontario, Canada K7L 3N6
[c] Instituto de Geología, Universidad Nacional Autónoma de México, Estación Regional del Noroeste, Apartado Postal 1039, Hermosillo, Sonora, 83000, México

ARTICLE INFO

Article history:
Received 13 December 2011
Received in revised form 22 April 2012
Accepted 22 April 2012
Available online 15 May 2012

Handling Editor: S. Kwon

Keywords:
Acatlán Complex
Extrusion
P-T-t high-pressure metamorphism
Tectonics
Geochronology

ABSTRACT

High-pressure (HP) rocks at Tehuitzingo, on the western margin of the HP belt within the Paleozoic Acatlán Complex (southern México), occur in a klippe that was thrust over low-grade clastic rocks. The youngest detrital zircon cluster in the low-grade rocks yielded U-Pb ages of 481 ± 16 Ma, which provide an older limit for deposition. The HP rocks are composed of metabasites, serpentinite, granite (482 ± 3 Ma) and mica schist (youngest concordant detrital zircon: 433 ± 3 Ma). The schist and granite are inferred to be high-grade equivalents of lower Paleozoic, low-grade rocks exposed elsewhere in the Acatlán Complex, from which they are inferred to have been removed by subduction erosion. Mineral analyses indicate that the subducted rocks underwent HP metamorphism and polyphase deformation at depths of ~50 km (~16 kbar and 750 °C: eclogite facies). Subsequent retrogression passed through epidote-amphibolite to greenschist facies, which was synchronous with W-vergent thrusting over the low-grade clastic rocks. Deposition of the low-grade rocks and thrusting are bracketed between either 481–329 Ma (Ordovician-Mississippian), and was followed by F_3 synformal folding. Cooling through ca. 385 °C is indicated by 329 ± 1 and 316–317 ± 2 Ma, $^{40}Ar/^{39}Ar$ muscovite plateau ages in HP rocks, which are 5–17 my younger than those of the adjacent Piaxtla eclogites suggesting younger exhumation. The petrology, P-T conditions and ages of the Piaxtla Suite is consistent with an extrusion channel within the Acatlán Complex along the active western margin of Pangea during the Carboniferous. Detrital zircon populations in the low-grade psammite (ca. 481, 520–650, 720, 750, 815, 890, 1050 and 2750 Ma) and the HP schist (ca. 457–480, 534, 908, 954–1150, 1265, 1845 and 2035 Ma) indicate derivation from the Ordovician Acatlán granitoids, Neoproterozoic Brasiliano orogens, 900–750 Ma Goiás arc (Amazonia), 1–1.3 Ma Oaxaquia, and more ancient sources in Oaxaquia/Amazonia.

1. Introduction

The deep burial and exhumation of high-pressure (HP) rocks are generally attributed to subduction and buoyancy of the lower density, subducted material (Dobrzhinetskaya, 2012). Based on the lithology, the peak P-T conditions and P-T-t paths of HP rocks, three types of subduction regime have been proposed by Guillot et al. (2009): *accretionary*, *serpentinite* and *continental-type*. Accretionary-type subduction mainly underplates HP sedimentary rocks that are exhumed slowly (<5 mm/year) over a long period. The serpentinite-type subduction zones consist of protoliths originating in both subducted abyssal peridotites and in the hydrated mantle wedge that are extruded up a thick serpentinized subduction channel (1–10 km; Ernst et al., 1997; Liou et al., 2004; Guillot et al., 2009) or into the upper plate (Chemenda et al., 2001; Keppie et al., 2010). In serpentinite-type subduction, exhumation at 1–10 mm/year is driven by decoupling and buoyancy of the low-viscosity serpentinite that may be related to slab retreat. The continental-type subduction (or Alpine-type), the UHP/HP continental protoliths are exhumed very quickly (up to 40 mm/year), and occurs predominantly during the transition from oceanic to continental subduction by diapirism, rebound, extrusion or core complex development. Exhumation of the latter rocks is mainly driven by buoyancy, delamination, crustal extension and asthenospheric return flow.

In this context, the Tehuitzingo serpentinite and associated lenses of HP rocks (metabasites, metaschist and granitoid) occur along the western margin of the median HP belt that bisects the Paleozoic Acatlán Complex of southern México (Fig. 1). However, the structural geometry of the Tehuitzingo serpentinite is in doubt and several hypotheses have been published for the nature, age and tectonic interpretation of the western boundary (Fig. 2):

(i) a *Late Cretaceous-Paleogene* diapir intruded into low-grade host rocks with reverse-fault reactivated boundaries (Fig. 2a) (Carballido-Sánchez and Delgado-Argote, 1989);

* Corresponding author. Tel.: +52 55 56224300; fax: +52 55 56224289.
E-mail address: ggalaz@ing.uchile.cl (G. Galaz E.).

1342-937X/$ – see front matter
doi:10.1016/j.gr.2012.04.011

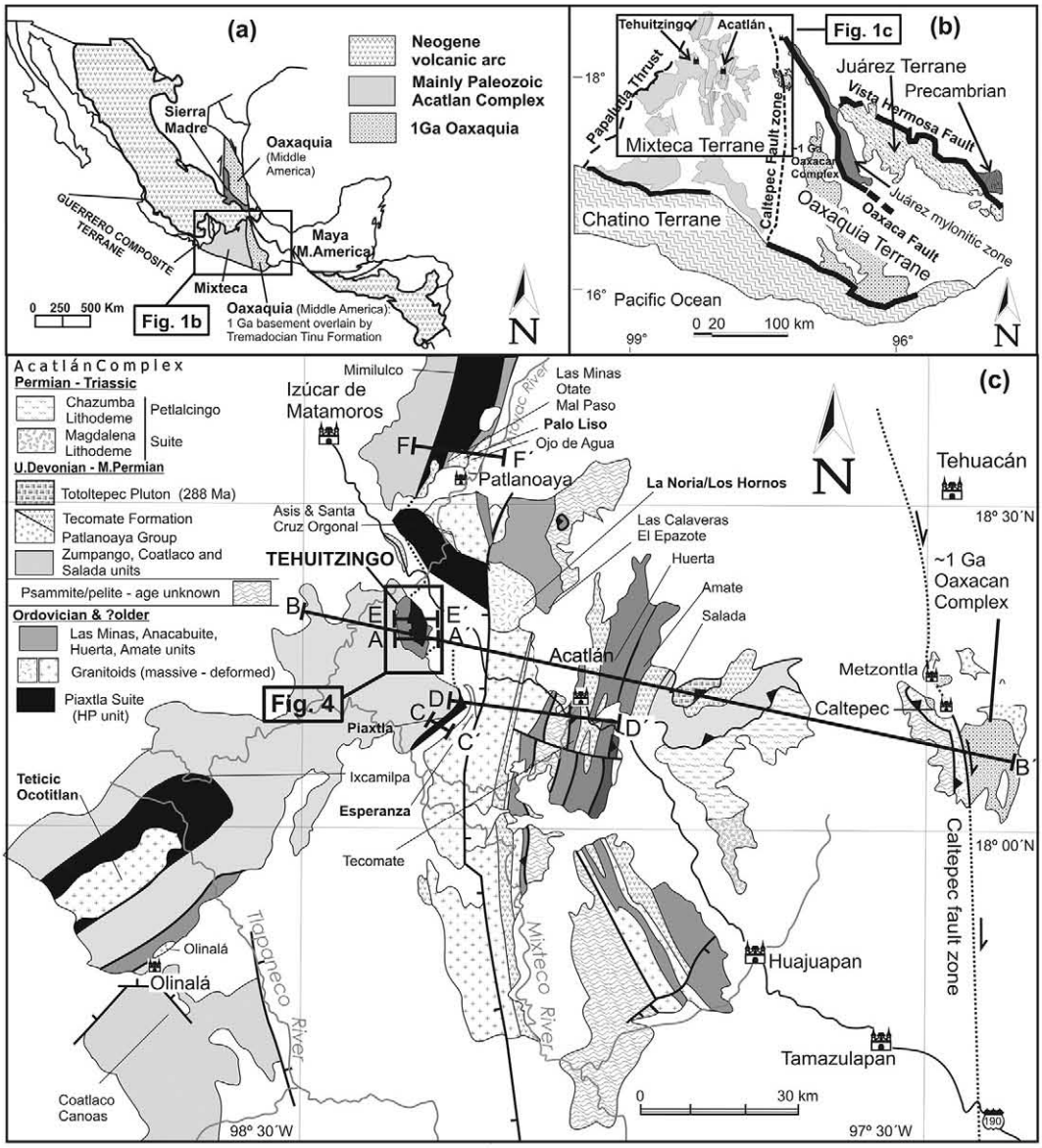

Fig. 1. (a) Location of the main metamorphic complexes in southern México; (b) detailed map of the metamorphic complexes; (c) geological map of the Acatlán Complex between Izúcar de Matamoros city (to the north) and the Olinalá-Tamazulapan cities (to the south)(modified after Keppie et al., 2008a). The study area is shown as a black rectangle.

(ii) an *Ordovician* folded thrust that forms part of an extensive nappe transported westwards from the Caltepec fault zone marking the continental-type subduction boundary between the Acatlán and Oaxacan complexes and interpreted as the Iapetus ocean suture (Fig. 2b) (Ortega-Gutiérrez, 1981; Ortega-Gutiérrez et al., 1999).

(iii) an *Early Devonian-Carboniferous* folded thrust composed of multiple nappes, including an intra-oceanic arc, produced by complex process of extrusion followed by continental-type subduction between peri-Gondwanan terranes and Laurentia (Fig. 2c)(Meza-Figueroa et al., 2003).

(iv) the lowest thrust slice of a *Lower Paleozoic* nappe stack composed of at least six accreted blocks, produced by successive continental-type subduction within the Iapetus and Rheic oceans and associated small ocean basins (Fig. 2d)(Talavera-Mendoza et al., 2005; Vega-Granillo et al., 2009);

(v) a *Late Ordovician-Early Silurian* obducted slice of oceanic lithosphere along the Iapetus suture (continental-type subduction), in which the chromites composition suggest derivation of the serpentinites from supra-subduction zone harzburgites in a periarc environment (Fig. 2e)(Proenza et al., 2004). However, the use of chromite composition in discriminating between tectonic environments is still under discussion (Power et al., 2000; Proenza et al., 2004); and

(vi) a *Permian* dextral transcurrent fault superimposed on a *Devono-Carboniferous* thrust lying along the lower boundary of an extrusion zone into the Acatlán Complex (accretionary or serpentinite-type; Fig. 2f)(Keppie et al., 2008a, 2010, 2011): the upper boundary of the median HP belt is bounded by a Devono-Carboniferous listric normal shear zone (Ramos-Arias et al., 2008; Keppie et al., 2010).

This controversy has led to the assignment of the HP rocks to between one and five oceanic tracts within the Iapetus and Rheic oceans (Fig. 3a) (Ortega-Gutiérrez et al., 1999; Talavera-Mendoza et al., 2005; Vega-Granillo et al., 2007, 2009). Conversely, Keppie et al. (2008a, 2011) suggested that the HP rocks were extruded into the Acatlán Complex (upper plate) during the Carboniferous oceanic-continental convergence zone along the western margin of Pangea with protoliths that formed along the southwestern margin of the Rheic Ocean (Fig. 3b and c). In order to resolve the debate about the structural geometry and origin of the Tehuitzingo serpentinites and

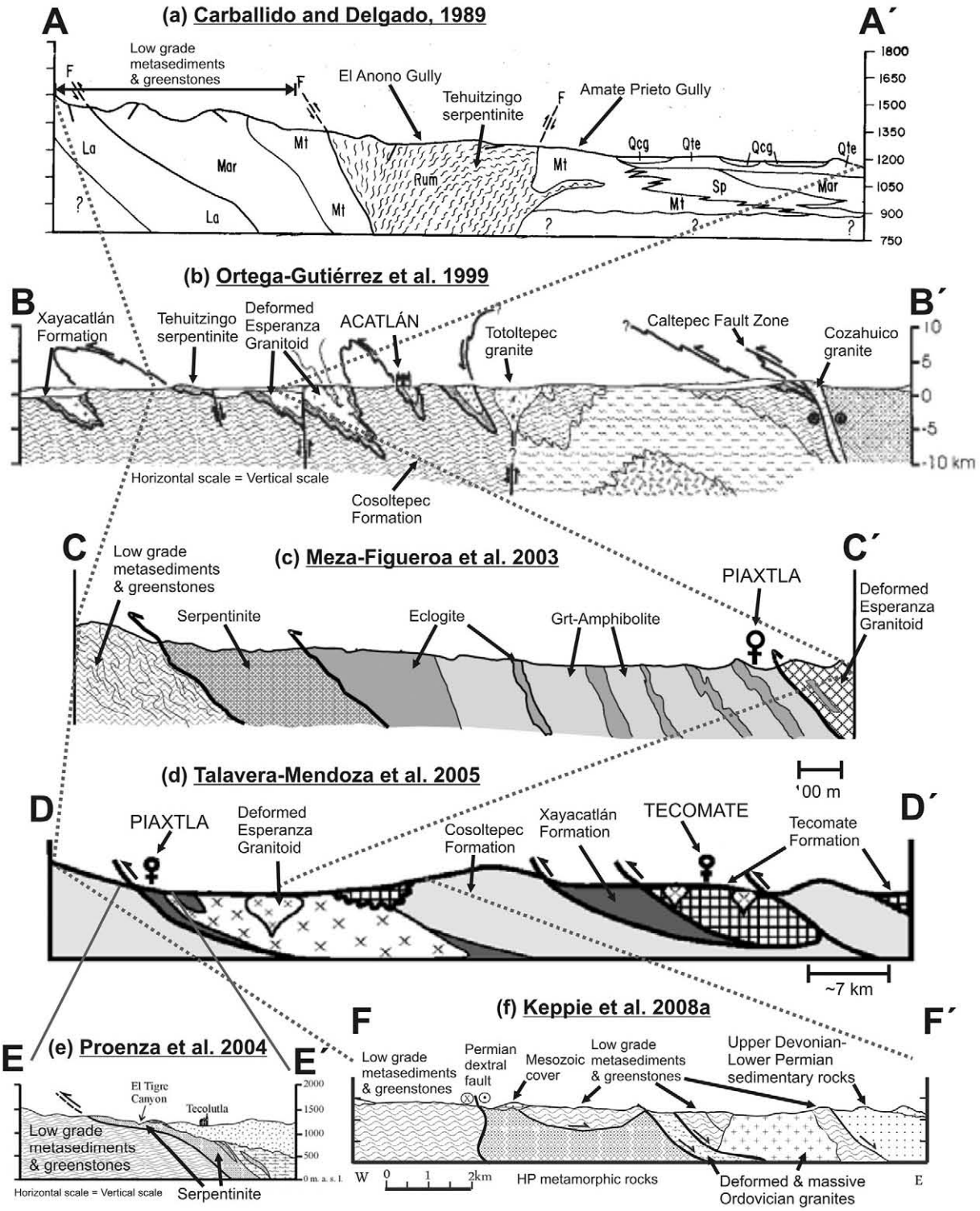

Fig. 2. Previous cross-sections of the Acatlán Complex: (a) Carballido-Sánchez and Delgado-Argote (1989); (b) Ortega-Gutiérrez et al. (1999); (c) Meza-Figueroa et al. (2003); (d) Talavera-Mendoza et al. (2005); (e) Proenza et al. (2004); (f) Keppie et al. (2008a). Locations are indicated on the Fig. 1c.

associated rocks was reexamined. We present evidence to show that the structure is a folded klippe with protoliths of Ordovician granitic, clastic and amphibolitic rocks that were subjected to Devono-Carboniferous HP metamorphism. These HP rocks were then exhumed by west-vergent thrusting below a serpentinized subduction channel within the Acatlán Complex. This occurred by subduction erosion of the upper plate at an oceanic-continental convergence zone on the western edge of Pangea.

2. Geological Setting

The predominantly Paleozoic Acatlán Complex is bounded by three tectonic contacts (Fig. 1): (i) to the east, the Permian, Caltepec dextral ductile shear zone juxtaposes the Acatlán Complex against the ca. 1 Ga Oaxacan Complex (Elías-Herrera and Ortega-Gutiérrez, 2002); (ii) to the south, the Cenozoic, sinistral transtensional Chacalapa–La Venta fault places the complex against the Mesozoic-

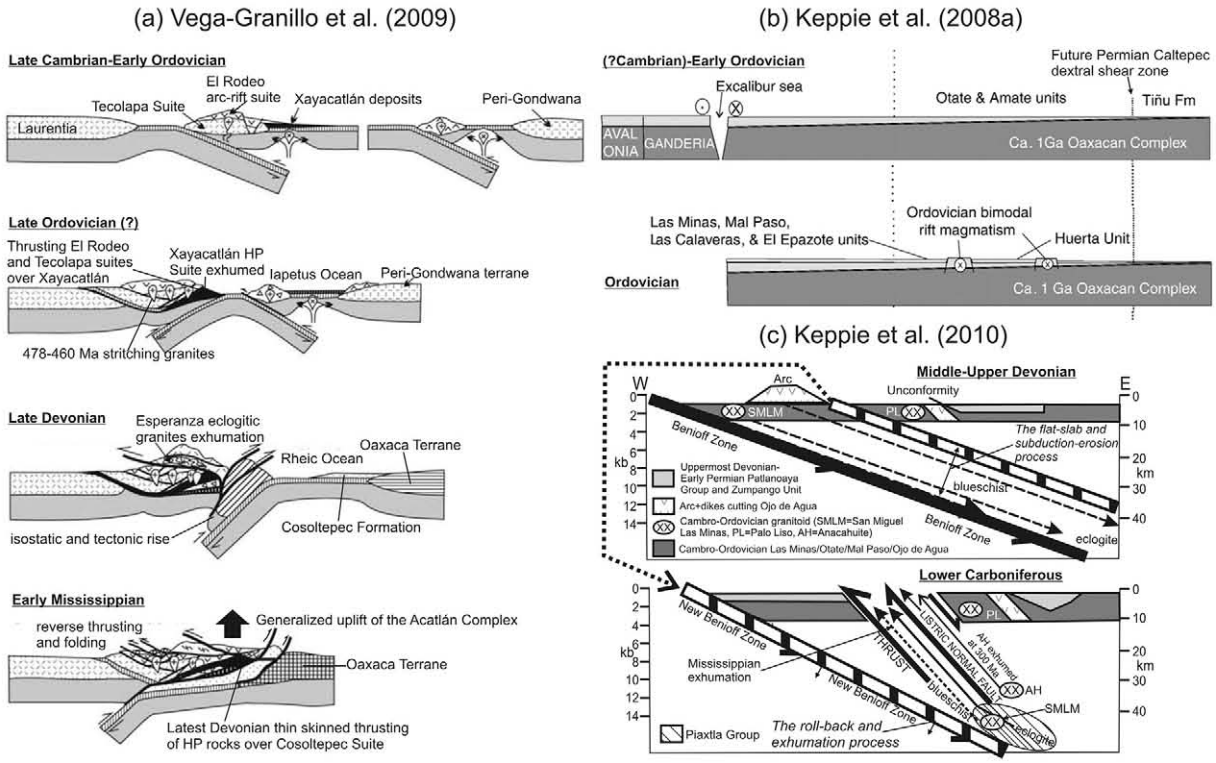

Fig. 3. Different tectonic models for Acatlán Complex: (a) Vega-Granillo et al. (2009); and (b) Keppie et al. (2010).

Cenozoic Xolapa Complex (Tolson, 2005); and (iii) to the west, the Late Cretaceous Papalutla thrust places the Acatlán Complex over the Cretaceous Morelos-Guerrero Platform (Cerca et al., 2006). The northern margin of the Acatlán Complex is covered by volcanic and volcaniclastic sequences of the Cenozoic Transmexican Volcanic Belt (Fig. 1a).

Although the Acatlán Complex has been the subject of debate over the past dozen years (c.f. Ortega-Gutiérrez et al., 1999; Talavera-Mendoza et al., 2005; Vega-Granillo et al., 2007; Keppie et al., 2008a; Vega-Granillo et al., 2009; Keppie et al., 2010, 2011), a gradually accumulating database has resolved some of the main issues. The Paleozoic rocks of the Acatlán Complex can be subdivided into low- and high-grade assemblages (Fig. 1b) (Keppie et al., 2008a,b, and references therein; Ramos-Arias and Keppie, 2011). The low-grade assemblage is composed of: (i) a Neoproterozoic-Ordovician clastic sequence intruded by ca. 480–440 Ma bimodal, rift-related igneous rocks; and (ii) a latest Devonian-Permian shallow marine sequence (>906 m) consisting of metapsammites, metapelites and tholeiitic mafic volcanic rocks. The HP metamorphic rocks occur in the N-S, Piaxtla-Mimilulco median belt and in the Ixcamilpa klippe rooted in the median belt. Rocks of the HP suite consist of: (i) a Neoproterozoic-Ordovician rift-shelf (metapsammite) package intruded by bimodal (retrogressed eclogite/amphibolite, granitoid) rift-related intrusions that are similar to those of the low-grade sequence; (ii) periarc ultramafic bodies, and possibly (iii) arc and MORB rocks. The age of HP metamorphism has been variously assigned to the Ordovician, Silurian and Carboniferous (Ortega-Gutiérrez et al., 1999; Talavera-Mendoza et al., 2005; Vega-Granillo et al., 2007, 2009) or just to the Carboniferous (Elías-Herrera et al., 2007; Middleton et al., 2007; Keppie et al., 2011; Ramos-Arias et al., 2011). Neoproterozoic-Ordovician rocks of both the HP suite and the low-grade sequence are associated with megacrystic granitoids of Ordovician age that contain concordant inherited zircons ranging in age from ca. 900 to 1300 Ma, suggesting a source in the Oaxacan Complex. Concordant ages of detrital zircons in both the low- and high-grade Cambro-Ordovician metasedimentary rocks indicate a provenance in local Ordovician plutons and/or ca. 1–1.3 Ga Oaxacan basement, together with distal northwestern Gondwana sources including an unique source in the 900–750 Ma Goiás magmatic arc within the Brasiliano orogen (Keppie et al., 2008a; Nance et al., 2009). The 900–750 Ma ages are particularly significant because they discriminate Amazonian sources from those of Laurentia.

3. Tehuizingo area

In the Tehuitzingo area, a HP unit (Piaxtla Suite) is tectonically juxtaposed against a low-grade unit along N-S structures (Fig. 4). The low-grade unit is predominantly made up of greenschist facies, metapelitic and metapsammitic rocks that have a planar fabric composed mainly of white mica and chlorite indicating low-temperature ductile deformation. The HP unit mainly consists of serpentinized harzburgite with small marginal fault blocks composed of different lithologies, such as metabasite, metagranitoid and metasedimentary rocks. The serpentinized harzburgites contain ellipsoidal metabasite lenses up to several meters in size, which have fine grained margins that may reflect an original intrusive relationship. The long axes of the ellipsoidal lenses are parallel to the foliation indicating ductile deformation. On the other hand, the high-grade metasedimentary rocks have a composite foliation where S_1 is parallel to the S-planes of a S-C fabric and the S_2 planes are subparallel to the borders of the lenses and oriented ~128/27° (dip direction/dip angle), and C_2 planes oriented ~147/58°.

Along the southern margin of the area, the Piaxtla serpentinites are thrust over the psammite-pelite unit along a gently NW-dipping thrust (320/15°), on which there are slickensides that plunge westwards (290/12°). These, together with associated recumbent folds, S-C fabrics and thrust horses indicate thrusting towards the west (Fig. 4e and f). Cutting across this thrust zone are several N-S vertical faults with subhorizontal slickensides. Along the western margin of the serpentinites in the north and central parts of the area, the HP/low-grade contact is a sub-vertical, N-S fault (107/87°), on which are slickensides with oblique dextral kinematics that plunge at 17/

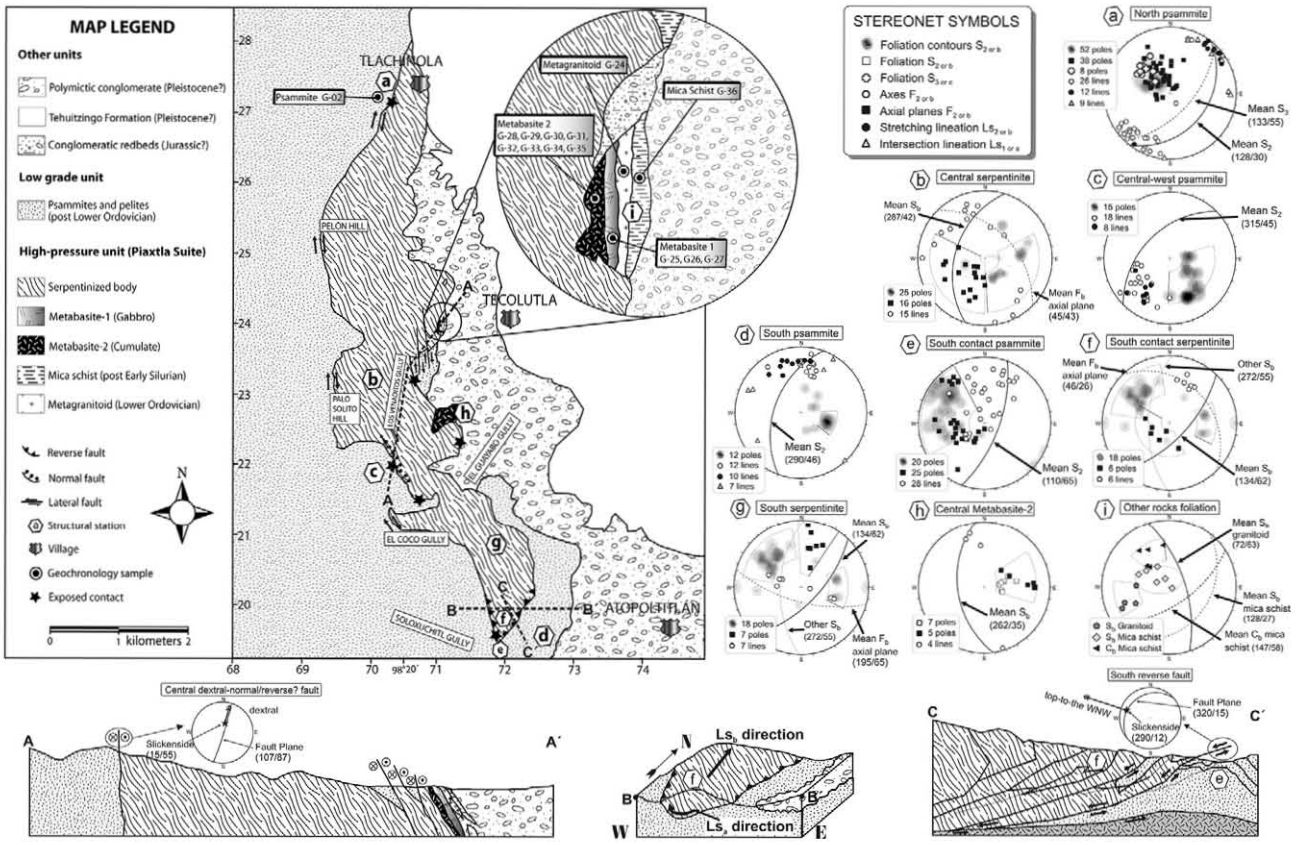

Fig. 4. Geological map of the Tehuitzingo area and cross-sections in Tecolutla (A-A´) and Atopoltitlán (B-B´ and C-C´) localities. Enlargement of the middle map shows an outcrop of the high-grade metamorphic unit. Also shown are the structural stations and data plotted in lower-hemisphere equal-angle stereonets (dip direction/dip notation for this paper).

55° (Fig. 4c). Similar low-grade psammite-pelite rocks occur along the eastern margin of the serpentinite (west of Tecolutla), where a N-S fault separates them (Fig. 4b). At Tecolutla, a fault-bounded lens of red polymictic conglomerate is juxtaposed against the serpentinite body and lenses of metabasite, metasedimentary and granitoid rocks. The redbeds are petrologically similar to Middle Jurassic rocks elsewhere (Fig. 4). The eastern margin of the serpentinites is generally unconformably overlain by lacustrine sandstones of the (?)Pleistocene Tehuizingo Formation (Calderón-García, 1956) that in turn is unconformably overlain by (?)Pleistocene polymictic conglomerates, sandstones and shales.

4. Petrography and mineral chemistry

4.1. Piaxtla Suite: high-grade rocks

The ultramafic rocks are composed almost entirely of decussate, acicular and fibrous serpentine crystals (coexisting chrysotile, lizardite and antigorite) and aggregates that make up 95% of the rock. Associated minerals include magnetite, calcite, white mica and talc (4%), and accessory chromite, clinochlore, undulose quartz, amphibole and epidote (1%).

The *metabasite-1* is melanocratic with a planar fabric and nemato-grano-poikiloblastic textures. It is composed mainly of calcic-amphiboles (~60%; actinolite and edenite types), albite (Ab_{98-99}), zoisite, Mg-Fe-chlorite (ripidolite-sheridanite types), titanite and rutile (Figs. 5, 6 and 7). The equilibrium metamorphic mineralogy manifests as: (a) an incipient high-pressure association with rare rutile and garnet ($Alm_{60-61}Sps_{1-3}Prp_{8-11}Grs_{27-28}$; mostly replaced by chlorite pseudomorphs); (b) a medium-grade metamorphic association of actinolite-edenite, zoisite and Mg-Fe-chlorite; and (c) a low-grade association composed of quartz, Mg-Fe-chlorite, actinolite, epidote, muscovite and titanite.

The *metabasite-2* is melanocratic with a planar fabric, nemato-grano-poikiloblastic textures and massive structure. It is composed mainly of albite (Ab_{98}), calcic-amphibole (edenite), muscovite, garnet ($Alm_{60-61}Sps_{1-3}Prp_{8-11}Grs_{27-28}$), rutile, zoisite, Mg-Fe-chlorite, titanite and calcite (Figs. 5, 6 and 7). The equilibrium metamorphic mineralogy occurs in: (a) a high-pressure metamorphism association of almandine garnet and rutile; (b) a medium-grade association with magnesium-hornblende, zoisite and Mg-Fe-chlorite; and (c) a low-grade association consisting Mg-Fe-chlorite (ripidolite-sheridanite types), actinolite, epidote, titanite, muscovite and calcite.

The leucocratic *granitoid* is foliated, phaneritic and equigranular with grano-poikiloblastic textures. It is composed mainly of undulose quartz and feldspar with rare almandine garnet ($Alm_{71-74}Sps_{2-3}Prp_{7-8}Grs_{15-19}$) and rutile indicating high pressure metamorphism. The granitoid is altered to a low-grade association consisting of Mg-Fe-chlorite (ripidolite type), quartz, albite (Ab_{99-100}), phengite, and zoisite (Figs. 5, 6 and 7), with accessory minerals, such as titanite altering rutile, and leucoxene. Accessory zircon and apatite also occur.

The *mica schist* has planar fabric, is medium-grained (0.25-0.5 mm) and has a lepido-grano-porphyroblastic texture. A quartz-arenite protolith is indicated by the undulose quartz (23%), feldspar (7%) and muscovite (5%). The high-pressure metamorphic association is composed by porphyroblasts of almandine garnet ($Alm_{70-72}Sps_{1-6}Prp_{6-9}Grs_{18-21}$; 9%) and rutile (4%) (Fig. 5). The medium-grade association is characterized by phengite (27%), amphibole and zoisite in the presence of quartz. The low-grade association consists of quartz (6%), albite (5%), Mg-Fe-chlorite (ripidolite type) (8%), epidote (4%) and rare titanite (Fig. 7). In the mica schist, some garnets are totally altered to Fe-Mg-chlorite (ripidolite type), clinochlore and epidote, the rutile margins are altered to titanite and leucoxene, amphibole

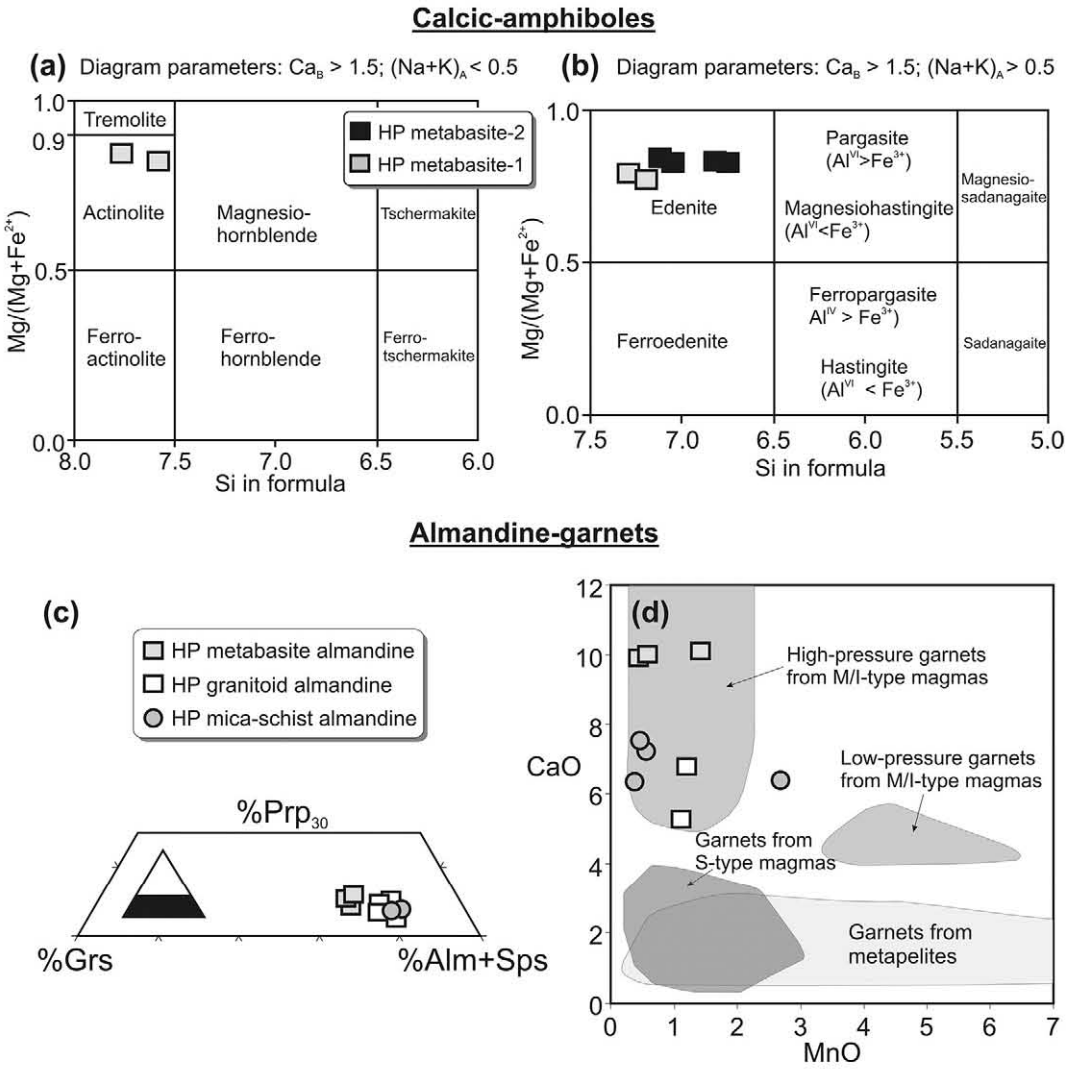

Fig. 5. Amphibole and garnet mineral chemistry: (a) Calcic-amphiboles classification diagram according to Leake et al. (1997) for low (Na + K) content; (b) Calcic-amphiboles classification diagram for higher (Na + K) content; (c) Classification diagram for garnet; (d) CaO vs MnO almandine diagram by Harangi et al. (2001) to discriminate their possible sources (Note the clear separation of almandine from M/I-type and S-type magmas based on its CaO content).

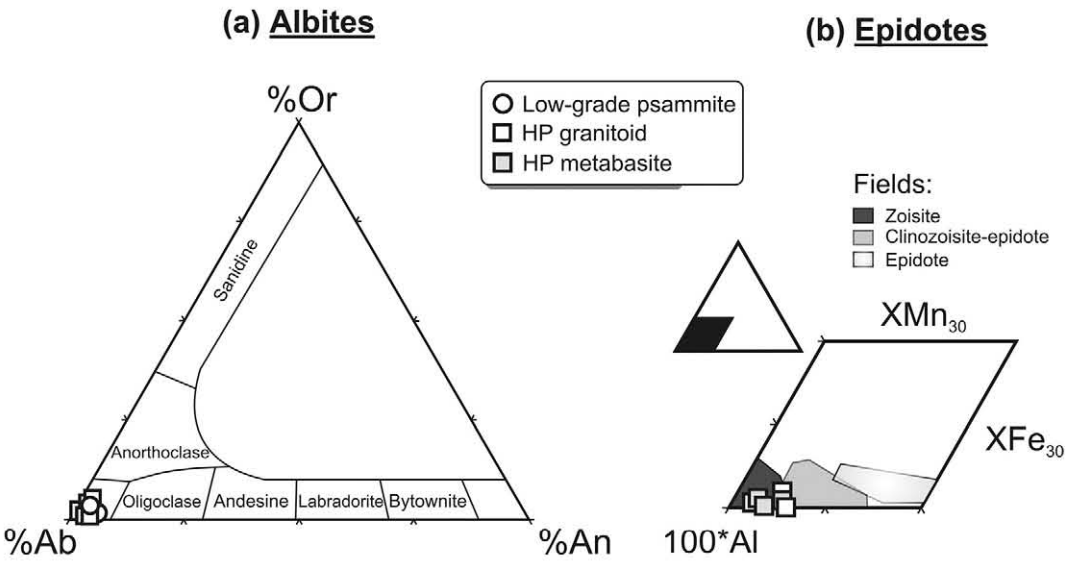

Fig. 6. Feldspar and epidote mineral chemistry: (a) Ab-An-Or ternary classification diagram for feldspars; (b) Epidote classification proposed by Grapes and Hoskin (2004) based on the octahedral Al, Fe and Mn cation totals at one of the three Y sites. X*Fe* = 100*Fe^{3+}/[Fe^{3+} + Al] and X*Mn* = 100*Mn/[Mn + Al].

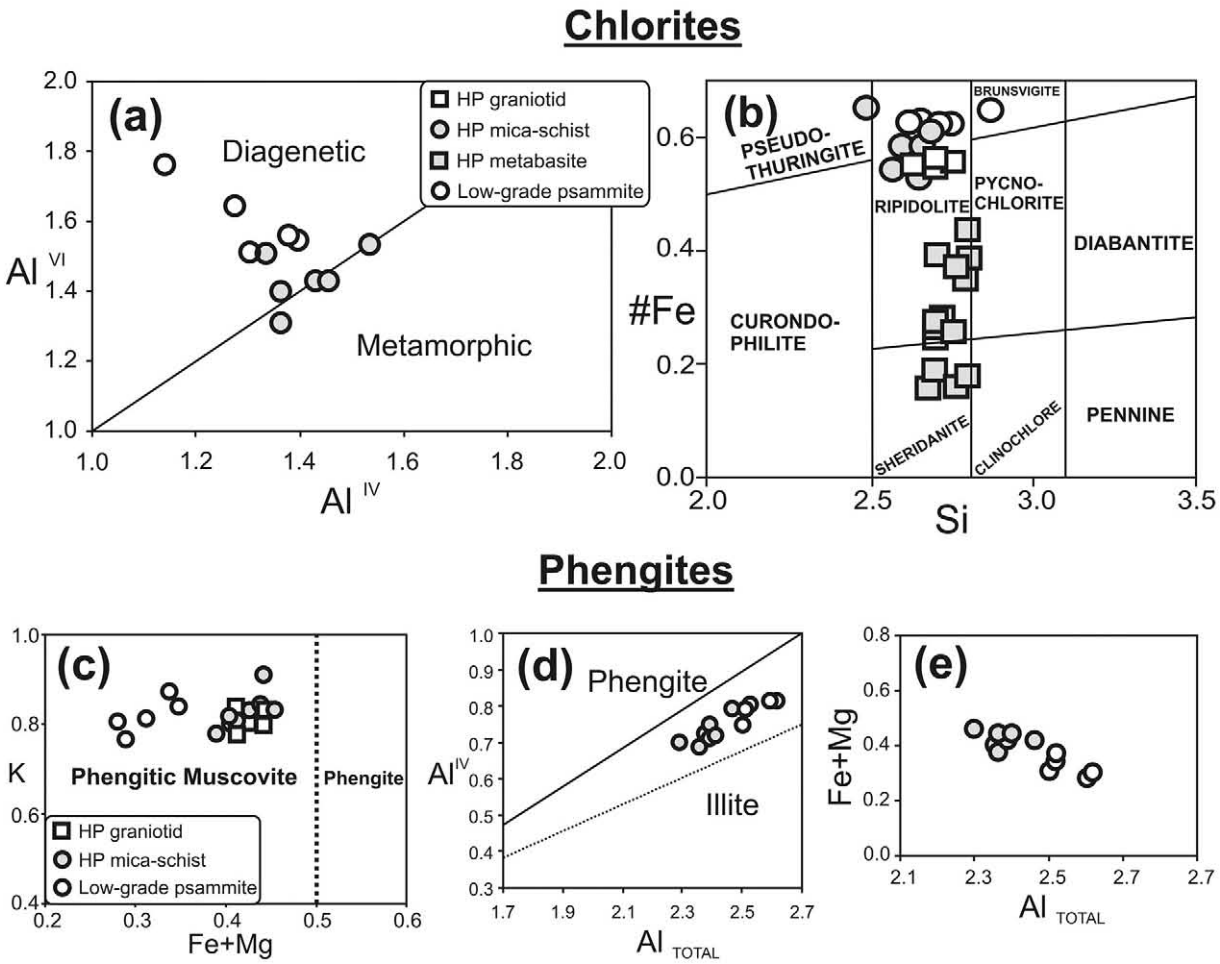

Fig. 7. Chlorite and phengite mineral chemistry: (a) Al^{IV} vs Al^{VI} genetic discrimination diagram for metasedimentary chlorites according Wiewiora and Weiss (1990); (b) Si vs #Fe ($=Fe^{2+}/[Fe^{2+}+Mg]$) classification diagram for chlorites according to Hey (1954); (c) Fe + Mg vs K classification diagram for phengitic muscovite and phengite; (d) Al_{total} vs Al^{IV} phengite-illite discrimination diagram (Weaver and Broekstra, 1984) adapted for sedimentary phengites; (e) Al_{total} vs Fe + Mg diagram (Weaver and Broekstra, 1984), showing some degree of tschermakitic replacement.

pseudomorphs are completely altered to titanite and Ca-Ti minerals, and finally clinochlore pseudomorphs are partially to completely altered to indeterminated phyllosilicates and magnetite.

4.2. Psammite-pelite unit: low-grade rocks

The *metapsammite* has a planar fabric and a granolepidoblastic texture. It is composed mainly of primary minerals, such as quartz, feldspar and accessory zircon, which suggests a medium-grained quartz-arenitic protolith (0.25-0.5 mm). The equilibrium secondary mineralogy is composed of quartz, albite (Ab_{99-100}), Mg-Fe-chlorite (ripidolite type), phengite, epidote, calcite and leucoxene (Figs. 6 and 7), indicating low-grade metamorphism.

The *metapelite* has a planar fabric and a granolepidoblastic texture. It is mainly composed of quartz, feldspar and accessory zircon, all of which suggests a shaly protolith (<0.06 mm grain size). The secondary mineralogy is identical to the psammitic rocks, namely quartz, albite, Mg-Fe-chlorite (ripidolite type), phengite, epidote, calcite and leucoxene, which also indicate a low-grade metamorphism.

5. Structure

Structures in both the Piaxtla Suite and the psammite-pelite unit display a sequence of three sets of structures. However, as some of them probably developed at different metamorphic grades and times, they are given different subscripts: numerical in the psammite-pelite unit (e.g., S_1, S_2, and S_3), and alphabetic in the Piaxtla Suite (e.g., S_a, S_b, S_c).

5.1. Psammite-pelite unit: low-grade rocks

The psammitic and pelitic rocks show three phases of penetrative deformation. Bedding is generally transposed into parallelism with the S_2 foliation. The more competent psammitic rocks preferentially display the first two sets of structures (D_1 and D_2), whereas the pelitic rocks better preserve the last two sets of structures (D_2 and D_3).

The earliest structures (D_1) are preserved as rare isoclinal folds (F_1) in the bedding with fold axes plunging at 225/50° (Fig. 4a). The D_1 deformation is accompanied by an axial plane foliation (S_1) defined by layers of quartz, albite and aligned muscovite ± chlorite. The L_1 lineation defined by the intersection between S_1-S_0 plunges gently northeastwards (20–60)/(0-7°) (Fig. 4a and d).

The second set of structures is defined by ubiquitous, asymmetric, isoclinal to tight, Class 1B, 1 C and 2, F_2 folds (Fig. 8), which have an axial planar foliation (S_2) composed of aligned muscovite and iron oxide that is accompanied by a L_2 stretching lineation of quartz. Although there is slight north–south variability in the orientations of the D_2 structures, the S_2 foliation and the S_2 axial planes are generally parallel, as are the F_2 fold axes and stretching lineations, $L_{1/2}$. This parallelism is consistent with the observed type 3 interference patterns of Ramsay and Huber (1987). Mean orientations of the second structures is as follows: (a) in the *north* (Fig. 4a), the S_2 foliation oriented ~128/30°, is roughly parallel to the S_2 axial planes (~149/33°), with

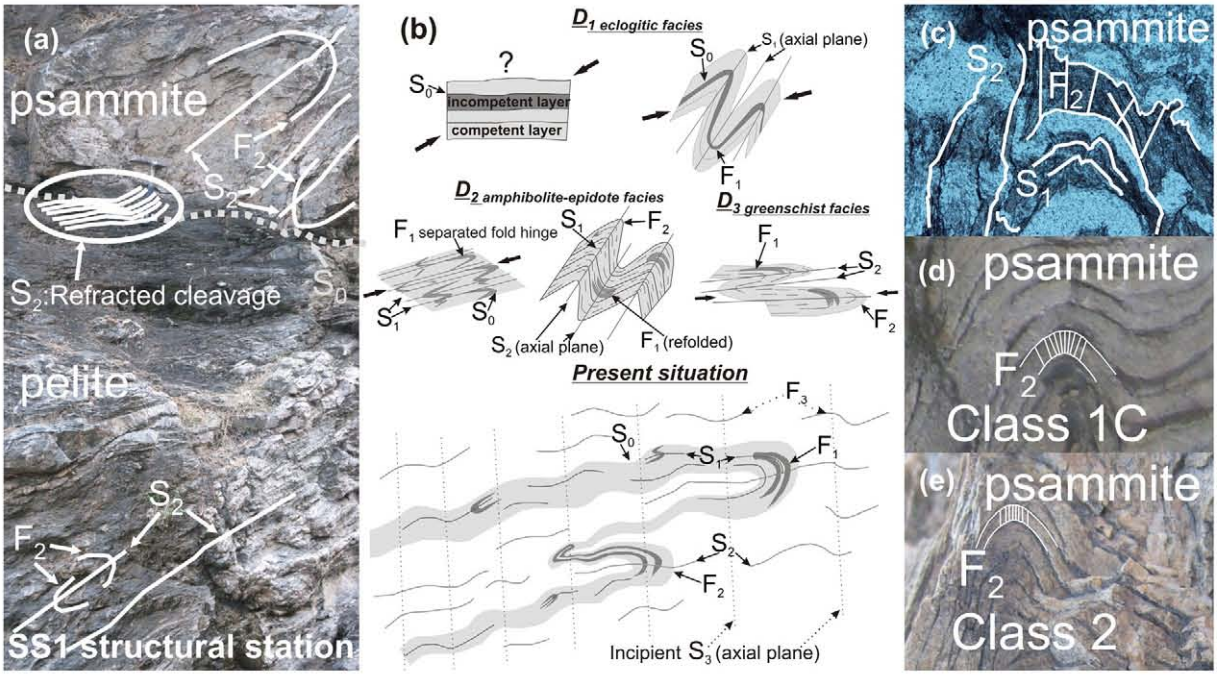

Fig. 8. Structures in the low-grade unit: (a) photograph shows the relationship between folding and foliations; (b) evolution of the structural phases; (c) microphotograph of S_1 and S_2 foliations in psammite and its relationship with the folding; (d) and (e) photographs showing the fold classification of Ramsay (1967).

the F_2 fold axes plunging gently to the southwest (220–240)/(0-15°) and the stretching lineation plunging gently to the northeast (35–60)/(0-7°); (b) in the *center* (Fig. 4c), the foliation is oriented ~315/45° with F_2 fold axes plunging to the southwest (210–260)/5-50° parallel to the stretching lineation (210–235)/5-50°; (c) in the *south* (Fig. 4d), the S_2 foliation is oriented ~290/46°, the F_2 fold axes plunging to the NNE (0–20)/5-30°, and L_2 stretching lineation plunges to the north (345–12)/5-30°; and (d) at the *southern contact* zone (Fig. 4e), the S_2 axial plane foliation is oriented ~110/65°, the F_2 axial planes are oriented at 87/45° with an average F_2 fold axis plunging to N/47°.

The third set of structures (D_3) was only observed in the northern part of the study area (Fig. 4a), where it is expressed as open-gentle, Class 1B, symmetrical F_3 folds with NNE-trending axial planes (~124/69°) and sub-horizontal F_3 fold axes plunging to south (~207/23°) parallel to the F_2 axes. The F_3 folds deform the S_2 axial planes (Fig. 8b) and are accompanied by an incipient axial plane S_3 foliation composed of muscovite and iron oxides oriented at ~133/55°. A late crenulation cleavage with a different orientation was also observed.

5.2. Piaxtla Suite: high pressure rocks

In the Piaxtla Suite, all observed lithological contacts are tectonic in character. Despite the rheological contrasts, three sets of penetrative structures were recognized in most lithologies (Fig. 9).

The oldest S_a foliation was observed only on a microscopic scale in the metabasites, granitoid and mica-schist: subsequent deformation in the serpentinites completely obliterated the earliest structures. This deformation (D_a) is defined by oriented growth of garnet and rutile (S_a) suggesting development under eclogite facies conditions.

The second set of structures (D_b) is the most penetrative and is manifested in *metabasite* by tight-close, Class 1 C-2, F_b folds with axial planes dipping at ~257/59°, and F_b fold axes plunging to the north (340–360)/10-30° (Fig. 9). These folds are accompanied by an axial planar foliation (S_b) oriented at ~262/35° and composed of aligned amphibole-zoisite-clinochlore-titanite that bends around garnet-rutile porphyroblasts. In the *granitoid*, tight folds in the S_a foliation are accompanied by an axial planar S_b composite foliation defined by muscovite-chlorite-epidote oriented at ~72/63°. D_b in the *mica-schist* comprises an S-C foliation whose S planes are parallel to the F_b axial planes: S_b is oriented at ~128/27° and C_b planes dip at ~147/58°. The *serpentinite* shows very variable structures possibly due to its ductile rheology. In the central subdomain (Fig. 4b), the serpentinite is folded by tight F_b folds with axial planes oriented ~45/43° and an axial planar S_b foliation defined by aligned serpentine oriented at ~287/42°. In the southern subdomain (Fig. 4g), the serpentinite displays S_b axial planes oriented at ~195/65° and the main S_b foliation oriented at ~134/62°, with a secondary foliation at ~272/55°. Note that the serpentinitic body is the only lithology where the S_b foliation is not sub-parallel to F_b fold axial planes. This second set of structures is accompanied by alteration of S_a garnet rims and the generation of new syntectonic garnets where the S-shaped internal foliation forms syntectonic millipede structures that are rotated but continuous with the Sb external foliation (Fig. 9a-d).

A third set of structures (D_c) is defined by open F_c folds with broad wavelengths accompanied by an axial plane foliation (S_c) composed by aligned crystals of muscovite, chlorite and iron oxides. These structures are accompanied by alteration crowns in the S_a garnets and a strong retrogression in the S_b garnets that produces garnet pseudomorphs of clinochlore-Fe-Mg-chlorite. In addition, hornblende is altered and/or replaced by actinolite-clinochlore, whereas rutile rims are altered to titanite.

6. Geothermobarometry

Several geothermometers and geobarometers have been used to obtain the P-T conditions of the deformational events that affected to both the HP and low-grade rocks. These P-T condition determinations are difficult due to the common polymetamorphism, compositional mineral zoning and the inherent problem of choosing the correct equilibrium reactions.

6.1. Analytical Methods

Six samples were selected from the Piaxtla Suite and low-grade psammite-pelite unit for polished sections. Mineral analyses were

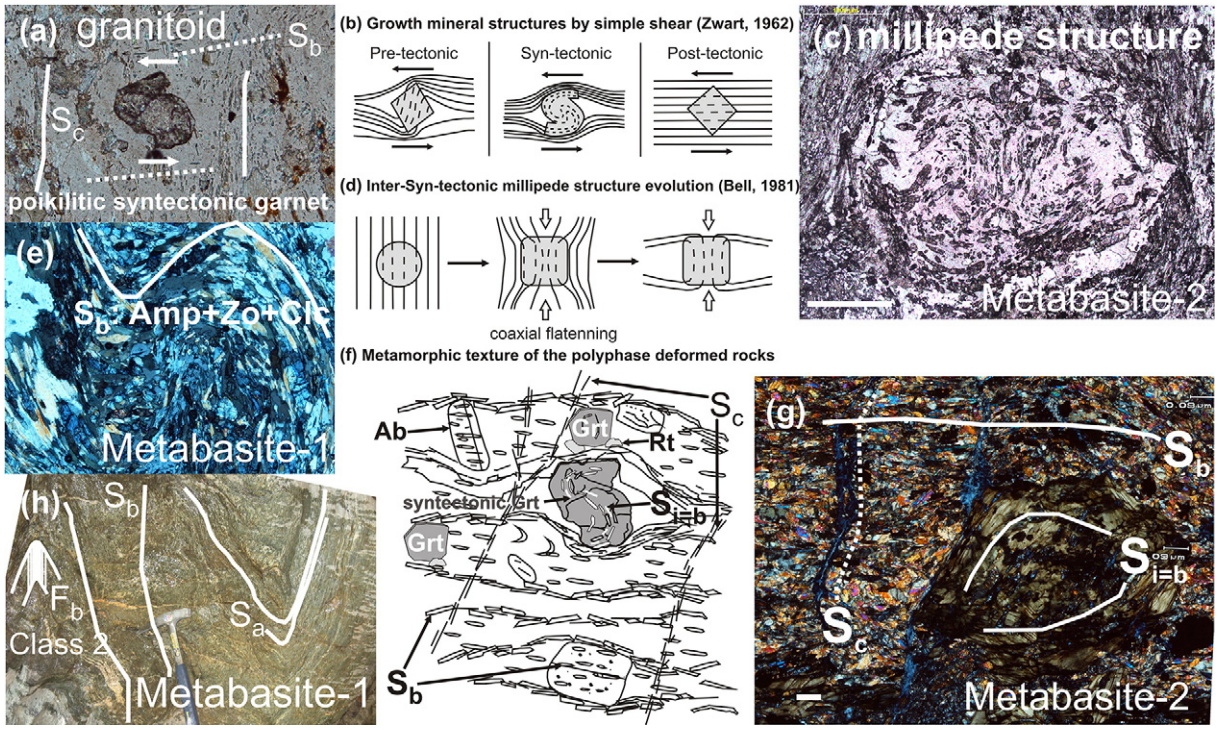

Fig. 9. Structures in the high-pressure unit: (a) microphotograph of poikilitic garnet, syntectonic with S_b foliation in granitoid; (b) relationship between deformation and mineral growth by Zwart (1962); (c) microphotograph of millipede structure in metabasite-2; (d) evolution of a syntectonic millipede structure by Bell (1981); (e) microphotograph of folded S_b foliation in metabasite-1; (f) polyphase deformation in the HP rocks; (g) microphotograph showing structural phases in metabasite-2; (h) microphotograph showing the fold classification by Ramsay (1967) and S_a, $S_{i=b}$ internal = external foliation in metabasite-1. Mineral abbreviations, Grt: garnet; Amp: amphibole; Zo: zoisite; Ab: albite; Clc: clinochlore; Rt: rutile.

performed using a scanning electron microprobe (EPMA) JEOL JXA-8900R at the University Laboratory of Petrology (LUP), Institute of Geophysics, UNAM. The results of the WDS analyses (wavelength dispersive X-ray spectroscopy) are showed in Appendix A.

6.2. Results

Fe-Mg exchange between garnet and muscovite (GM) was examined using a re-calibration of the GM geothermometer for HP metapelites (Wu and Zhao, 2006). The nine pairs of GM analyses of the HP *mica schist* give a D_a average temperature of 758 ± 28 °C.

We also used a geothermometer based on the variation of Zr content in rutile with temperature, which is applicable to various rocks types with an absolute uncertainty of 50 °C (Zack et al., 2004). In the HP *granitoid* four rutile analyses yielded a D_a average temperature of 741 ± 50 °C (Table 1). Five analyses performed in the HP *metabasite-1* gave highly variable D_a temperatures of 452, 629 and 720 °C (±50), the latter being consistent with the D_a temperature in the HP granitoid and mica-schist.

Geobarometers that relate the aluminum content in amphibole to pressure (Hollister et al., 1987; Schmidt, 1992) were also used. These yielded variable average pressures of 1.9 ± 0.6 kbar from two edenites in HP metabasite-1, and 3.4 ± 0.6 kbar and 4.8 ± 0.6 kbar from two edenites in HP metabasite-2 (Table 2). Using these pressures, it is possible to apply the edenites-tremolite/plagioclase thermometer (Holland and Blundy, 1994), which gave consistent D_b average temperatures of 471 ± 35 °C for HP *metabasite-1* and of 473 ± 35 °C for HP *metabasite-2* (Table 3).

Cathelineau (1988) suggested an empirical thermometer based on the tetrahedral aluminum content (Al^{IV}) in pure chlorites (i.e., interleaved layers of chlorites > 80%). Later Jowett (1991) introduced a correction due to the influence of iron that is applicable only to chlorites with Fe/[Fe + Mg] < 0.6. Both conditions are satisfied by the twenty-four analyzed chlorites in the HP rocks (Table 4), which yielded D_c average temperature of 345 ± 14 °C from ten chlorites of the *metabasite-1*, 343 ± 18 °C from four chlorites of the *metabasite-2*, 370 ± 12 °C from four chlorites of the *granitoid*, and 398 ± 23 °C from six chlorites of the *mica schist*. On the other hand, five chlorites of the low-grade *psammite* do not satisfy the condition of Jowett (Fe/[Fe + Mg] < 0.6), so only the Cathelineau temperatures with an average D_1 temperature of 356 ± 33 °C were determined.

The phengite barometer of Massonne and Szpurka (1997) is based on the variation of Si content with pressure, according to the

Table 1
Results of zirconium-in-rutile thermometer (Zack et al., 2004) applied to HP metabasite and granitoid of the Acatlán Complex.

Litology	HP granitoid			HP metabasite-1		
Sample	G24-c1.2	G24-c3.1	G24-c3.2	G27-c1.1	G25-c1.1	G25-c2.1
ZrO_2 (%wt.)	0.040	0.052	0.054	0.041	0.005	0.020
Zr (ppm)	296.0	385.0	400.0	304.0	37.0	148.0
T (±50 °C)	717	751	756	720	452	629

Table 2
Results of Al-in-amphibole barometer (Hollister et al., 1987; Schmidt, 1992) applied to HP metabasites of the Acatlán Complex.

Lithology	Metabasite-1		Metabasite-2			
Sample	G25-c2.1	G25-c2.2	G31-c1.1	G31-c1.2	G31-c2.1	G31-c2.2
Mineral	Edenite	Edenite	Edenite	Edenite	Edenite	Edenite
Al^{total}	1.09	0.96	1.36	1.32	1.65	1.64
P_H (kbar)*	1.4	0.6	2.9	2.7	4.5	4.5
P_S (kbar)**	2.2	1.6	3.5	3.3	4.8	4.8
$P_{AVG.}$ (kbar)	1.9 ± 0.6		3.4 ± 0.6		4.8 ± 0.6	

*P_H (±1 kbar) = 5.64*Al_{TOT}-4.76 (Hollister et al., 1987).
**P_S (±0.6 kbar) = 4.76*Al_{TOT}-3.01 (preferred values from Schmidt, 1992) magnetite/ilmenite + quartz + anorthite = tremolite + orthoclase + tschermakite.

Table 3
Results of amphibole-plagioclase thermometer (Holland and Blundy, 1994) applied to HP metabasites of the Acatlán Complex.

Lithology	HP Metabasite-1		HP Metabasite-2			
Amp smp.	G25-c2.1	G25-c2.2	G31-c1.1	G31-c1.2	G31-c2.1	G31-c2.2
SiO2	49.79	49.90	49.09	49.28	46.81	46.61
TiO2	0.11	0.12	0.11	0.09	0.18	0.18
Al2O3	6.34	5.56	8.03	7.77	9.65	9.55
FeO*	8.55	8.23	6.71	6.05	6.95	6.97
MgO	17.83	18.20	18.33	18.52	18.12	17.95
CaO	10.78	10.70	10.71	10.95	11.14	11.64
Na2O	2.15	1.91	2.59	2.50	2.87	2.67
K2O	0.11	0.10	0.06	0.03	0.03	0.05
Total	95.65	94.72	95.61	95.20	95.75	95.62
Plg smp.	G25-c1.1	G25-c1.1	G27-c2.1	G25-c1.1	G27-c2.1	G25-c1.1
X_{Ab}	98.37	98.37	98.55	98.37	98.55	98.37
X_{An}	1.32	1.32	1.20	1.32	1.20	1.32
Input P(kbar)*	1.9	1.9	3.4	3.4	4.8	4.8
T_{HB**} (°C)	470.7	471.0	455.5	452.7	492.1	490.8
T_{HB**} (°C) $_{AVG.}$	471 ± 35		473 ± 35			

Minerals abbreviations: Amp: amphibole; Plg: plagioclase.
* Input pressure from Al-in-amphibole thermometer (Schmidt, 1992).
**HB: Ed-Tr-Plg thermometry recalibration reaction edenite + albite = richterite + anorthite.

tschermakitic substitution vector: [Mg, Fe^{2+}] + Si = Al^{IV} + Al^{VI}. For this calculation, we used the computer program package PERPLE_X (Connolly, 1990), thermodynamic data for mineral end members and H_2O given by Holland and Powell (1998, updated in 2002), and the solid-solution models from database PERPLE_X (solution_model.dat file). The calculations were undertaken in the system Na_2O-K_2O-CaO-FeO-O_2-MnO-MgO-Al_2O_3-SiO_2-TiO_2-H_2O and the O_2 contents were estimated according to Massonne et al. (2007). We derived P-T diagrams contoured with isopleths of Si content per formula unit (p.f.u.) in phengite for a low-grade *psammite*, HP *granitoid* and HP *mica-schist* of Tehuitzingo (Fig. 10). These graphical results were outlined and smoothed together in commercial graphic editors according to Connolly (2005). Then, we introduced the equilibrium temperature of the mineral association at which phengite formed to estimate the pressure. This resulted in a D_a average pressure of 16.3 ± 0.7 kbar from seven phengites in the HP *mica schist* and 7.1 ± 0.8 kbar from five phengites in the HP *granitoid*. The low-grade *psammite* gave D_1 average pressure of 2.7 ± 1.2 kbar from five phengites.

6.3. Geothermobarometric implications

The geothermobarometric results (Table 5) suggest a common prograde metamorphic history for the Tehuitzingo HP rocks: (a) a metamorphic peak in the eclogite facies (with zoisite-amphibole) under a temperature of ~750 °C and a pressure of ~16 kbar, indicating that these rocks reached depths of at least 50 km (Fig. 11); (b) retrogression to epidote-amphibolite facies, with a temperature of ~472 °C and variable pressures between ~7.1 and 3.4 kbar; (c) retrogression to greenschist facies with a temperature of ~360 °C at undetermined

Table 4
Results of AlIV in chlorite thermometer applied to low-grade psammite and HP rocks (metabasites, granitoid and mica schist) of the Acatlán Complex; TC: Cathelineau (1988) temperature; TJ: Jowett (1991) temperature; and Xc = {([Mg + Fe + AlIV + Ti]-3)/3}*100 (chlorite layers percent in interleaved chlorite-smectite).

Lithology	Low-grade psammite					HP granitoid			
Sample	G02-c1.1	G02-c1.2	G02-c3.1	G02-c3.2	G02-c3.3	G24-c1.1	G24-c1.2	G24-c2.1	G24-c2.2
Al^{IV}	1.28	1.14	1.30	1.39	1.38	1.37	1.31	1.32	1.27
Al^{VI}	1.64	1.76	1.51	1.55	1.55	1.37	1.39	1.38	1.38
Al_{TOT}	2.91	2.90	2.82	2.94	2.93	2.74	2.70	2.70	2.66
Al^{IV}_J	1.34	1.20	1.36	1.46	1.44	1.43	1.37	1.37	1.33
Fe/(Fe + Mg)	0.62	0.65	0.61	0.63	0.63	0.55	0.56	0.56	0.56
Xc (%)	99.93	96.02	96.35	94.44	94.72	99.27	100.00	97.98	100.00
T_C (°C)	348.6	304.5	357.4	386.4	382.7	379.4	361.5	361.7	348.6
T_J (°C)	357.4	314.7	366.0	395.2	391.5	385.8	368.3	368.6	355.6
T_C (°C) $_{AVG.}$	356 ± 33					363 ± 13			
T_J (°C) $_{AVG.}$	365 ± 32					370 ± 12			

Lithology	HP mica schist						HP metabasite-2			
Sample	G12-c1.1	G12-c1.2	G12-c1.3	G12-c2.1	G12-c3.1	G12-c3.2	G31-c1.1	G31-c1.2	G31-c2.1	G31-c2.2
Al^{IV}	1.35	1.36	1.42	1.52	1.34	1.44	1.22	1.31	1.24	1.33
Al^{VI}	1.41	1.29	1.43	1.53	1.50	1.43	1.26	1.20	1.20	1.14
Al_{TOT}	2.76	2.65	2.85	3.05	2.84	2.87	2.48	2.51	2.44	2.48
Al^{IV}_J	1.41	1.42	1.48	1.59	1.40	1.50	1.23	1.33	1.26	1.35
Fe/(Fe + Mg)	0.59	0.54	0.58	0.65	0.60	0.54	0.18	0.18	0.16	0.16
Xc (%)	100.48	80.62	65.87	88.03	91.44	90.77	100.00	98.76	99.46	91.00
T_C (°C)	374.3	376.5	394.8	429.0	368.1	402.3	330.0	361.4	337.6	367.7
T_J (°C)	382.0	382.6	402.0	438.2	376.3	408.2	324.9	356.0	331.8	361.7
T_C (°C) $_{AVG.}$	391 ± 23						349 ± 18			
T_J (°C) $_{AVG.}$	398 ± 23						344 ± 18			

Lithology	HP metabasite-1					HP metabasite-1				
Sample	G27-c1.1	G27-c1.2	G27-c2.1	G27-c2.2	G27-c2.1	G25-c1.1	G25-c1.2	G25-c1.3	G25-c2.1	G25-c2.2
Al^{IV}	1.21	1.22	1.21	1.21	1.31	1.31	1.30	1.27	1.31	1.31
Al^{VI}	1.31	1.22	1.13	1.25	1.29	1.24	1.24	1.21	1.25	1.28
Al_{TOT}	2.51	2.44	2.34	2.46	2.60	2.54	2.54	2.48	2.56	2.59
Al^{IV}_J	1.24	1.25	1.26	1.25	1.34	1.33	1.33	1.30	1.34	1.34
Fe/(Fe + Mg)	0.39	0.35	0.44	0.44	0.39	0.26	0.26	0.25	0.25	0.25
Xc (%)	100.00	100.00	100.00	100.00	100.00	97.90	100.00	100.00	100.00	96.87
T_C (°C)	326.4	330.0	328.3	327.5	358.3	359.4	358.1	347.7	360.3	360.1
T_J (°C)	328.1	330.5	331.6	330.8	359.7	356.6	355.3	344.9	357.2	357.1
T_C (°C) $_{AVG.}$	334 ± 14					357 ± 5				
T_J (°C) $_{AVG.}$	336 ± 13					354 ± 5				
Average T(°C)	345 ± 14									

Note: bold numbers are the most appropriate temperatures depending on whether the requirement of Jowett (1991) is satisfied or not.

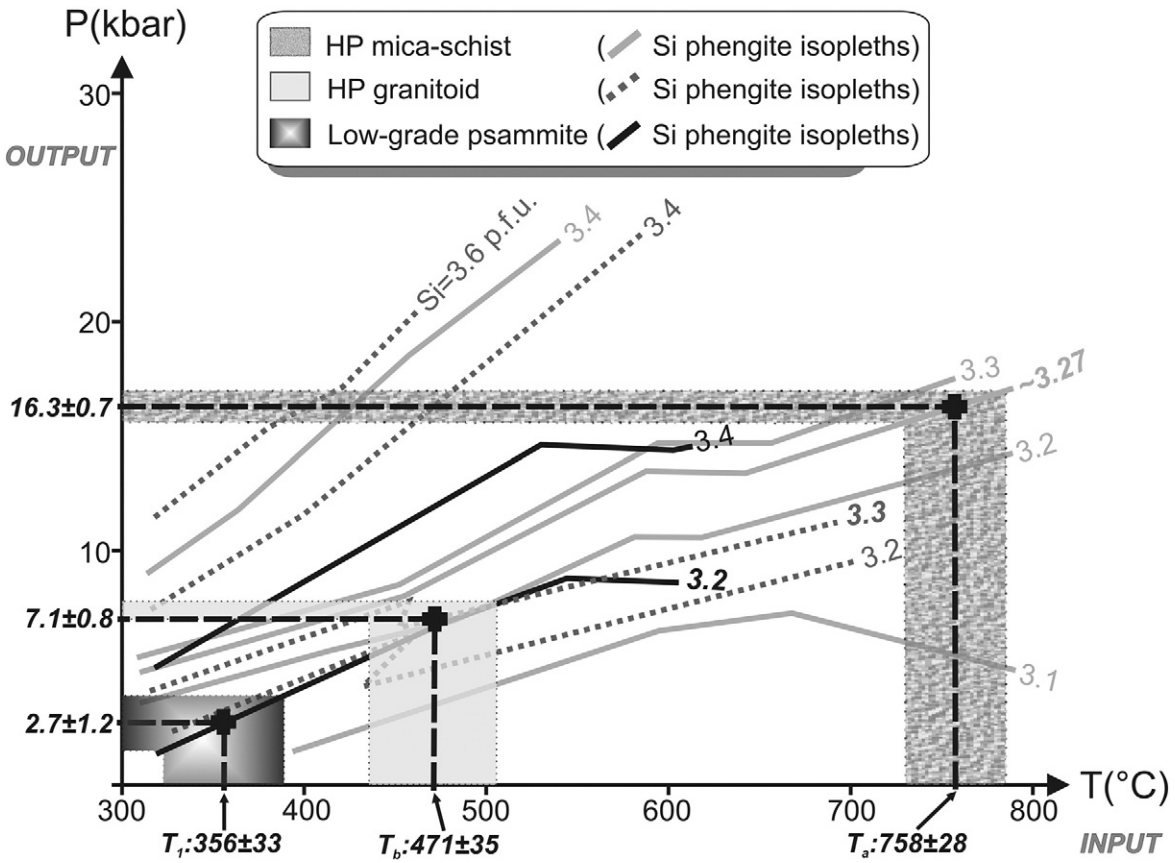

Fig. 10. HP and low-grade rocks of Acatlán Complex plotted on P-T field of phengite contoured with isopleths for Si p.f.u. in phengite. The temperatures for psammite, T_1, calculated using Al-in-chlorite thermometer; T_b in HP granitoid calculated using amphibole-plagioclase thermometer; and T_a in HP mica schist calculated using garnet-muscovite thermometer.

pressures. The variability in some results may be due to mobility in some chemicals during retrogression.

In the low-grade unit, three different metamorphic facies were recognized. The oldest gave temperatures of ~356 °C and pressures of ~2.7 kbar (Table 5). This temperature is the same as that determined for the greenschist stage of the HP rocks suggesting a common event with similar P-T conditions.

The P-T peak determined for the Tehuitzingo HP rocks differs from those documented in other parts of the Acatlán Complex (Fig. 11; e.g., Meza-Figueroa et al., 2003; Middleton et al., 2007; Ramos-Arias et al., 2011), possibly because the latter used the isopleths diagram proposed by Massonne and Szpurka (1997). However, the use of a diagram prepared for another rock can lead to errors because the isopleths vary depending on the mineralogy and bulk chemical

Table 5
Summary of the HP and low-grade rocks geothermobarometry of the Acatlán Complex.

High Pressure Unit									
Lithology	1st assn.	Results	Method	2nd assn.	Results	Method	3rd assn.	Results	Method
Metabasite-1	Grt + Rt	P: undet. T: **720 ± 50 °C**	Zr-in-Rt	Amp + Zo + Plg + Clc	P: 1.9 ± 0.6 kbar **T: 471 ± 35 °C**	Al-in-Amp Ed-Tr-Plg	Qtz + Ms + Chl + Act + Ep + Ttn	P: undet. **T: 345 ± 14 °C**	Al-in-Chl
Metabasite-2	Grt + Rt	P: undet. T: undet.		Amp + Zo + Plg + Clc	**P: 4.8 ± 0.6 kbar** **P: 3.4 ± 0.6 kbar** **T: 473 ± 35 °C**	Al-in-Amp Al-in-Amp Ed-Tr-Plg	Qtz + Ms + Chl + Act + Ep + Ttn + Cal	P: undet. **T: 343 ± 18 °C**	Al-in-Chl
Granitoid	Grt + Rt	P: undet. **T: 741 ± 50 °C**	Zr-in-Rt	Zo + Phg + Ab + Ttn	**P: 7.1 ± 0.8 kbar** T: undet.	Si-in-Phg	Ms + Chl + Qtz	P: undet. **T: 370 ± 12 °C**	Al-in-Chl
Mica schist	Grt + Rt + Phg	**P: 16.3 ± 0.7 kbar** **T: 758 ± 28 °C**	Si-in-Phg Grt-Ms	Amp + Zo + Phg + Plg	P: undet. T: undet.		Qtz + Ab + Chl + Ep + Ttn	P: undet. **T: 398 ± 23 °C**	Al-in-Chl

Low Grade Unit							
Lithology	1st assn.	Results	Method	2nd assn.	Results	3rd assn.	Results
Psammite	Qtz + Ab + Chl + Ms + Ep + Cal	**P: 2.7 ± 1.2 kbar** **T: 356 ± 33 °C**	Si-in-Phg Al-in-Chl	Ms + Op	P: undet. T: undet.	Ms + Op	P: undet. T: undet.

Minerals abbreviations: Grt: garnet; Rt: rutile; Phg: Phengite; Act: actinolite; Ed: edenite; Tr: tremolite; Amp: amphibole; Zo: zoisite; Plg: plagioclase; Ab: albite; Phg: phengite; Clc: clinochlore; Ttn: titanite; Chl: chlorite; Ms: muscovite; Qtz: quartz; Ep: epidote; Cal: calcite; Lcx: leucoxene; Op: opaque.
Note: bold numbers are consistent results interpreted as the P-T conditions of each assemblage. Inconsistent calculations may be due to the loss of certain elements in the mineral phases involved.

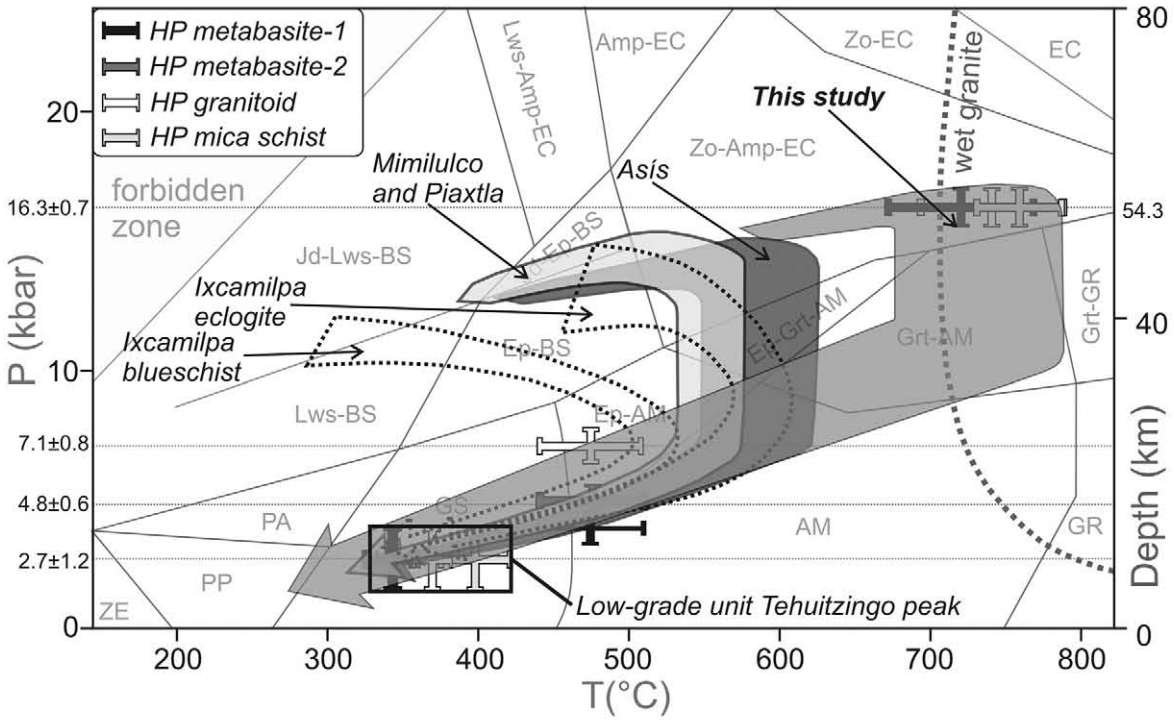

Fig. 11. Pressure-temperature trajectory of subduction-exhumation to mesozonal crustal levels of HP thrust sheet at Tehuitzingo compared with other HP rocks of Acatlán Complex: Asís (Middleton et al., 2007); Mimilulco and Piaxtla (Meza-Figueroa et al., 2003); and Ixcamilpa (Ramos-Arias et al., 2011). Depth calculated using an average geothermal gradient of 0.3 kbar/km. Facies abbreviations, ZE: zeolite; PP: prehnite-pumpellyite; PA: pumpellyite-actinolite; GS: greenschist; BS: blueschist; AM: amphibolite; GR: granulite; EC: eclogite. Minerals abbreviations, Lws: lawsonite; Jd: jadeite; Ep: epidote; Zo: zoisite; Amp: amphibole; Grt: garnet; Coe: coesite; Dia: diamond.

composition of each rock. In contrast, we derived P-T diagrams contoured with isopleths of Si content per formula unit (p.f.u.) in phengite for the Tehuitzingo rocks, with which were estimated its pressure peaks. On the other hand, the peak temperature was calculated using standard methods similar to those previously used in other studies.

Using the antigorite stability field, peak P-T conditions of ~550 °C and ~9 kbar for Piaxtla serpentinite in Tehuitzingo were estimated by González-Mancera (2001). However, Ulmer and Trommsdorff (1995) have shown that antigorite in subduction zones is stable up to ~720 °C and ~20 kbar suggesting higher grades of metamorphism. The P-T conditions determined for retrogression through epidote-amphibolite to greenschist facies are very similar to those reported previously in Acatlán Complex.

7. U-Pb Geochronology

7.1. Sample Preparation

Three samples were collected for U-Pb geochronology, a low-grade psammite (G-02), collected in the El Zapote Gully, near Tlachinola (Fig. 3), and two rocks from the high-grade metamorphic unit: a metagranite (G-24) and mica schist (G-36), collected in the quarry near the mouth of the Los Venaditos Gully, near Tecolutla (Fig. 3). These samples were crushed and pulverized to less than 200 μm, followed by concentration of heavy minerals using a Wilfley Table and separation of magnetic and nonmagnetic minerals using a Frantz isodynamic magnetic separator. This final concentrate was placed in ethanol and zircon was extracted by hand-picking using a binocular microscope. These zircons were mounted in epoxy resin, polished to expose their cores and edges, and photographed under cathodoluminescense using an ELM-3R luminoscope connected to a digital camera. These images are important for choosing points to analyze and for subsequent interpretation of the ages.

7.2. Analytical Methods

The zircons were analyzed by laser ablation–inductively coupled plasma–mass spectrometry (LA-ICP-MS) at the Geosciences Center, Campus Juriquilla, UNAM. The excimer laser-ablation system Resolution M-50 (LPX220, Lambda Physik) is coupled to a Thermo Xii quadrupole ICP-MS to perform fast and reliable U-Pb age determinations. The standard analytical parameters used were a spot laser diameter of 34 μm, a fluence of 8 J/cm^2-shot on the target, which produced a flat-bottom ablation crater of about 25 μm depth.

At least 80 zircons from the granitoid (G-24) were mounted of which 40 were randomly analyzed. At least 200 zircons were mounted from the metasedimentary rocks, G-02 and G-36, with random analysis of 135 and 130 grains, respectively. Statistically, this number is greater than the optimal number of 117 grains for obtaining a 95% confidence that no fraction of the population ≥0.05 was missed (Vermeesch, 2004). Zircons with fractures and/or inclusions and/or a diameter less than 34 μm were omitted from the analysis to minimize Pb-loss and ensure that each ablation pit was entirely located within a single zircon grain.

Inter-element fractionation was monitored by analyzing fragments of a large concordant zircon crystal "Plesovice" from Rumania with a known (ID-TIMS) age of 336 ± 0.25 Ma (2σ) and U-Th concentrations were monitored by analyzing a NIST 610 glass. For the purposes of this paper, we consider an analysis concordant when there is an overlap of $^{206}Pb/^{238}U$, $^{207}Pb/^{235}U$ and $^{207}Pb/^{206}Pb$ ages. The $^{208}Pb/^{232}Th$ age was omitted because it is very susceptible to contamination by common Pb in HP rocks (Compston et al., 1984). Based on studies of isotope mobility with time, we used the $^{206}Pb/^{238}U$ age for ages below the 1 Ga, and the $^{207}Pb/^{206}Pb$ age for ages over 1 Ga (Gehrels et al., 2006).

Data were filtered according to precision (generally 10% cutoff) and discordance (generally 20% cutoff), then plotted on the U-Pb Tera-Wasserburg diagram. Weighted mean and frequency histograms/probability density distribution were performed using Isoplot v.3.00 (Ludwig, 2003). Gehrels et al. (2006) consider ages to be

reliable if three or more analyses performed in different grains yield overlapping $^{206}Pb/^{238}U$, $^{207}Pb/^{235}U$ and $^{207}Pb/^{206}Pb$ ages, however other authors define a reliable age if there is one concordant analysis with low errors (e.g., Jeffries et al., 2003; Vermeesch, 2004). The U-Pb analyses are shown in Appendix A (Table A8).

7.3. Results

The low-grade psammite (G-02, UTM_{NAD27}: 140570108/2026916) yielded concordant ages that range from 498 ± 2 Ma to 1873 ± 17 Ma with population peaks at ca. 520, 560–650, 720, 750, 815, 890, 1050 and 2750 Ma (Fig. 12a). The cluster of seven concordant zircons produces a weighted mean age of 481 ± 16 Ma (Early Ordovician, 95% conf., MSWD: 6.0), and a single detrital zircon produces a nearly concordant age of 334 ± 2 Ma (Mississippian; Fig. 12b). These ages provide an older limit on the time of deposition of this psammite horizon as <480 Ma or <334 Ma depending on the weight placed on the single young zircon, however, we conservatively take the ~480 Ma age to provide the more robust older limit for the time of deposition. These low-grade rocks may be correlated with the

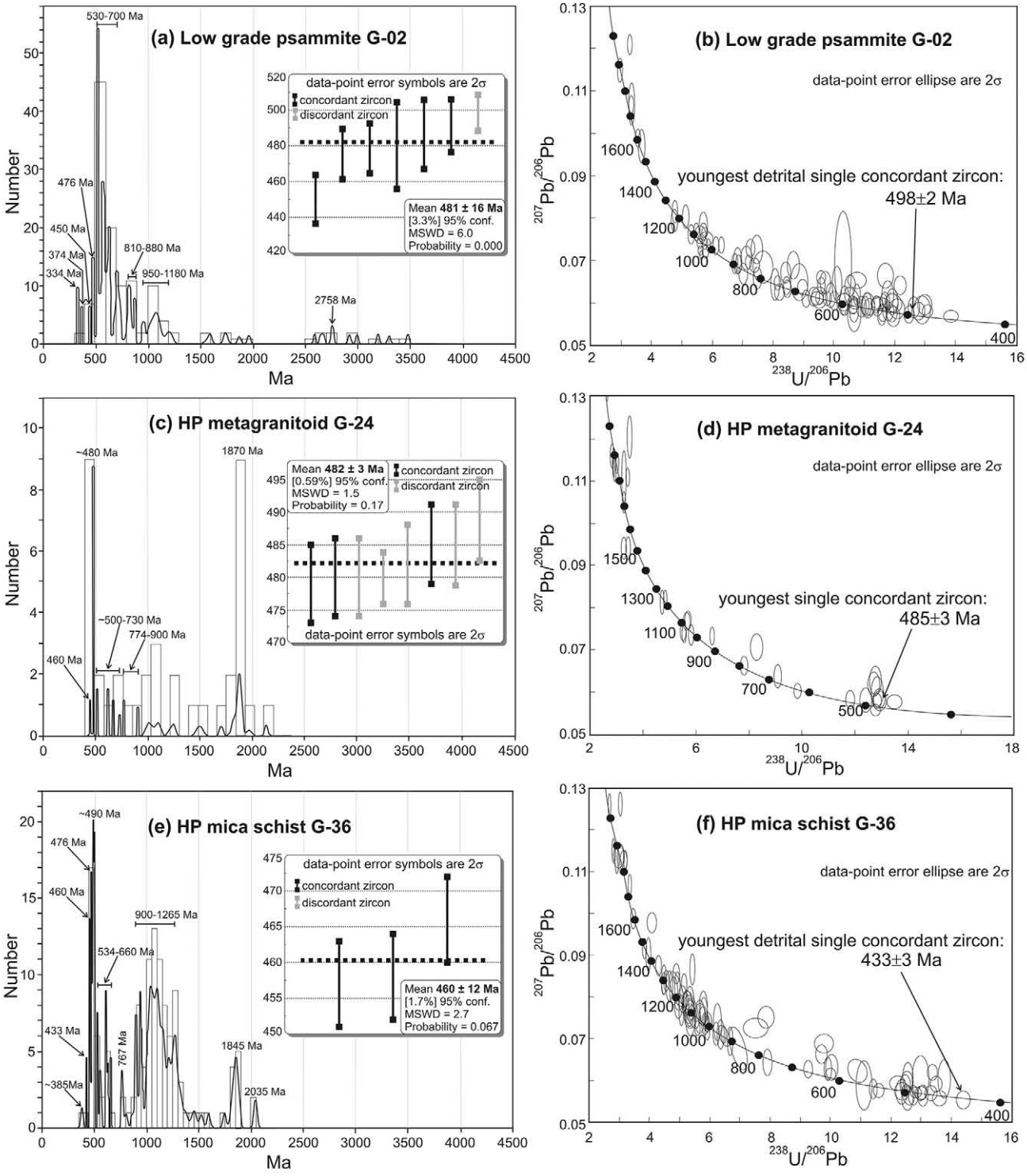

Fig. 12. U-Pb Tera-Wasserburg (TW), weighted average (WA) and combined binned frequency and probability density distribution (FPDD) diagrams for the Tehuitzingo samples: (a) and (b) low-grade psammite; (c) and (d) HP granitoid; (e) and (f) HP mica schist.

Table 6
^{40}Ar-^{39}Ar analyses of muscovite and hornblende from Tehuitzingo HP rocks, Acatlán Complex, southern México.

S	Power (watts)	^{36}Ar	^{37}Ar	^{38}Ar	^{39}Ar	^{40}Ar	$^{36}Ar/^{40}Ar$	$^{39}Ar/^{40}Ar$	r	Ca/K	$\%^{40}Ar$ Atm	$\%^{39}Ar$	$^{40}Ar^*/^{39}K$	Age
AOR 1119: **G-24 Muscovite - HP metagranitoid** - *Plateau age: 316.04 ± 1.13 Ma (steps 7-15: 73.4% Ar release), MSWD: 7.961*														
1	0.50	1.969 ± 0.054	2.984 ± 1.560	1.882 ± 0.093	53.240 ± 0.341	674.080 ± 1.309	0.002927 ± 0.000081	0.079168 ± 0.000531	0.021	0.103	86.27	1.34	1.71 ± 0.31	46.7 ± 8.3
2	0.75	0.271 ± 0.026	1.389 ± 1.335	0.948 ± 0.070	64.3551 ± 0.432	386.792 ± 0.872	0.000703 ± 0.000068	0.167218 ± 0.001192	0.007	0.039	20.65	1.62	4.74 ± 0.13	126.6 ± 3.3
3	1.00	0.346 ± 0.028	1.739 ± 1.356	1.369 ± 0.070	101.311 ± 0.520	826.791 ± 1.608	0.000419 ± 0.000034	0.122989 ± 0.000678	0.008	0.031	12.35	2.55	7.12 ± 0.09	187.1 ± 2.3
4	1.25	0.387 ± 0.038	1.208 ± 1.540	1.723 ± 0.102	129.048 ± 0.715	1322.158 ± 2.107	0.000293 ± 0.000029	0.097892 ± 0.000566	0.004	0.017	8.64	3.24	9.33 ± 0.10	241.4 ± 2.5
5	1.50	0.314 ± 0.062	3.901 ± 4.314	3.425 ± 0.239	267.003 ± 1.646	3102.496 ± 5.676	0.000101 ± 0.000020	0.086284 ± 0.000556	0.003	0.027	2.98	6.71	11.24 ± 0.10	287.1 ± 2.4
6	1.75	0.325 ± 0.107	4.235 ± 5.322	5.701 ± 0.379	443.380 ± 2.875	5501.741 ± 7.615	0.000059 ± 0.000020	0.080785 ± 0.000537	0.001	0.017	1.74	11.14	12.16 ± 0.11	308.7 ± 2.5
7	2.00	0.258 ± 0.099	6.579 ± 6.685	7.576 ± 0.483	595.104 ± 2.775	7516.529 ± 12.113	0.000034 ± 0.000013	0.079362 ± 0.000393	0.001	0.020	1.01	14.95	12.47 ± 0.08	315.9 ± 1.8
8	2.25	0.172 ± 0.081	8.010 ± 7.100	5.810 ± 0.446	476.868 ± 2.939	5992.687 ± 7.4	0.000028 ± 0.000014	0.079766 ± 0.000503	0.001	0.031	0.84	11.98	12.43 ± 0.09	315.0 ± 2.2
9	2.37	0.101 ± 0.045	15.927 ± 3.824	3.355 ± 0.275	262.158 ± 1.545	3250.633 ± 4.774	0.000030 ± 0.000014	0.080842 ± 0.000492	0.001	0.111	0.88	6.59	12.26 ± 0.09	311.0 ± 2.1
10	2.47	0.150 ± 0.066	36.728 ± 6.387	5.235 ± 0.365	410.967 ± 2.317	5176.032 ± 8.284	0.000027 ± 0.000013	0.079584 ± 0.000468	0.001	0.164	0.80	10.33	12.46 ± 0.09	315.7 ± 2.1
11	2.58	0.108 ± 0.058	30.860 ± 4.143	3.600 ± 0.223	285.600 ± 1.869	3588.27 ± 5.787	0.000028 ± 0.000016	0.079778 ± 0.000539	0.001	0.198	0.82	7.18	12.43 ± 0.10	315.0 ± 2.4
12	2.67	0.125 ± 0.060	20.291 ± 8.134	4.434 ± 0.396	364.293 ± 1.943	4646.329 ± 7.247	0.000026 ± 0.000013	0.078588 ± 0.000438	0.001	0.102	0.76	9.15	12.63 ± 0.09	319.5 ± 2.0
13	3.00	0.131 ± 0.063	10.291 ± 4.601	3.743 ± 0.249	293.735 ± 1.793	3766.118 ± 4.963	0.000034 ± 0.000017	0.078176 ± 0.000489	0.001	0.064	1.00	7.38	12.66 ± 0.10	320.3 ± 2.4
14	3.25	0.083 ± 0.039	7.355 ± 2.830	2.470 ± 0.189	197.761 ± 1.128	2479.949 ± 3.235	0.000033 ± 0.000016	0.079934 ± 0.000469	0.001	0.068	0.97	4.97	12.39 ± 0.09	314.0 ± 2.2
15	7.00	0.005 ± 0.017	1.229 ± 1.270	0.434 ± 0.050	34.950 ± 0.238	448.342 ± 1.003	0.000010 ± 0.000039	0.078136 ± 0.000561	-0.001	0.064	0.30	0.88	12.76 ± 0.17	322.6 ± 4.0
AOR 1133: **G-36 Muscovite - HP mica schist** - *Plateau age: 317.33 ± 1.46 Ma (steps 3-11: 91.0% Ar release), MSWD: 3.77*														
1	1.80	0.244 ± 0.023	0.503 ± 2.221	0.250 ± 0.044	6.761 ± 0.125	105.462 ± 0.490	0.002316 ± 0.000215	0.064226 ± 0.001231	0.013	0.136	68.29	1.73	4.92 ± 1.00	131.2 ± 25.7
2	2.10	0.082 ± 0.017	0.083 ± 2.764	0.381 ± 0.049	28.200 ± 0.257	319.455 ± 1.064	0.000257 ± 0.000052	0.088510 ± 0.000863	0.005	0.005	7.57	7.24	10.44 ± 0.20	267.9 ± 4.9
3	2.30	0.066 ± 0.017	0.223 ± 3.584	0.957 ± 0.060	75.724 ± 0.439	958.639 ± 1.956	0.000069 ± 0.000018	0.079180 ± 0.000488	0.003	0.005	2.04	19.43	12.37 ± 0.10	313.4 ± 2.4
4	2.40	0.024 ± 0.013	0.491 ± 3.013	0.573 ± 0.071	46.596 ± 0.411	595.100 ± 1.117	0.000040 ± 0.000021	0.078484 ± 0.000710	0.001	0.019	1.17	11.95	12.59 ± 0.14	318.6 ± 3.3
5	2.50	0.019 ± 0.014	0.192 ± 2.884	0.301 ± 0.044	23.643 ± 0.203	297.838 ± 0.863	0.000064 ± 0.000047	0.079573 ± 0.000723	0.001	0.015	1.89	6.07	12.33 ± 0.21	312.4 ± 4.9
6	2.70	0.029 ± 0.016	0 ± 2.374	0.816 ± 0.068	62.989 ± 0.393	796.568 ± 1.178	0.000036 ± 0.000020	0.079265 ± 0.000509	0.000	0.000	1.07	16.16	12.48 ± 0.11	316.0 ± 2.6
7	2.80	0.021 ± 0.013	0.517 ± 2.535	0.502 ± 0.051	39.977 ± 0.288	512.469 ± 1.322	0.000041 ± 0.000026	0.078192 ± 0.000601	0.000	0.024	1.22	10.26	12.63 ± 0.14	319.0 ± 3.2
8	2.90	0.018 ± 0.015	0.448 ± 2.655	0.406 ± 0.043	31.639 ± 0.268	405.224 ± 0.847	0.000044 ± 0.000038	0.078262 ± 0.000685	0.000	0.026	1.30	8.12	12.61 ± 0.18	319.0 ± 4.2
9	3.00	0.012 ± 0.013	0.311 ± 2.482	0.221 ± 0.036	17.524 ± 0.216	224.509 ± 0.866	0.000055 ± 0.000057	0.078238 ± 0.001013	0.000	0.032	1.62	4.50	12.57 ± 0.27	318.1 ± 6.3
10	3.30	0.015 ± 0.013	0.176 ± 3.124	0.346 ± 0.039	27.281 ± 0.228	350.775 ± 0.796	0.000044 ± 0.000038	0.077957 ± 0.000678	0.000	0.012	1.29	7.00	12.66 ± 0.18	320.2 ± 4.2
11	3.50	0.018 ± 0.015	0 ± 2.797	0.390 ± 0.046	29.428 ± 0.260	384.073 ± 0.981	0.000047 ± 0.000040	0.076799 ± 0.000708	0.001	0.000	1.38	7.55	12.84 ± 0.20	324.3 ± 4.5

AOR 1103: **G-25 Hornblende - HP metabasite-1** - *Plateau age: 373.07 ± 32.42 Ma (steps 3-8: 93.0% Ar release), MSWD: 1.405*

1	0.75	1.156 ± 0.027	7.353 ± 0.270	0.363 ± 0.039	0.224 ± 0.030	336.718 ± 0.572	0.003428 ± 0.000080	0.000651 ± 0.000088	0.001	61.381	101.29	2.30	−19.89 ± 36.88	−656.3 ± 1467.6
2	2.00	0.561 ± 0.024	22.768 ± 0.427	0.165 ± 0.032	0.459 ± 0.026	167.803 ± 0.433	0.003305 ± 0.000142	0.002638 ± 0.000154	0.003	94.134	97.65	4.70	8.87 ± 16.00	229.9 ± 389.7
3	2.50	0.117 ± 0.015	149.230 ± 1.258	0.074 ± 0.031	1.013 ± 0.040	35.849 ± 0.261	0.002101 ± 0.000430	0.025346 ± 0.001142	0.006	300.779	62.03	10.39	14.96 ± 5.09	372.5 ± 114.6
4	3.00	0.131 ± 0.016	175.333 ± 1.511	0.138 ± 0.026	2.703 ± 0.057	59.847 ± 0.307	0.001368 ± 0.000261	0.043144 ± 0.00979	0.005	124.426	40.37	27.71	13.81 ± 1.82	346.4 ± 41.6
5	3.50	0.077 ± 0.018	71.162 ± 0.881	0.146 ± 0.029	1.335 ± 0.035	33.188 ± 0.265	0.001730 ± 0.000531	0.038751 ± 0.001117	0.006	101.378	51.04	13.69	12.62 ± 4.08	319.1 ± 94.5
6	4.00	0.049 ± 0.019	44.843 ± 0.634	0.055 ± 0.032	0.897 ± 0.033	23.400 ± 0.223	0.001574 ± 0.000796	0.037026 ± 0.001463	0.003	94.821	46.45	9.20	14.45 ± 6.4	361 ± 144.8
7	5.00	0.048 ± 0.013	65.308 ± 0.797	0.057 ± 0.026	0.776 ± 0.032	22.919 ± 0.231	0.001292 ± 0.000568	0.031869 ± 0.001431	0.003	163.786	38.13	7.95	19.4 ± 5.38	469.8 ± 114.7
8	7.00	0.155 ± 0.020	254.169 ± 1.810	0.245 ± 0.037	2.346 ± 0.044	60.709 ± 0.288	0.001387 ± 0.000327	0.035727 ± 0.000753	0.004	214.676	40.91	24.06	16.53 ± 2.73	407.4 ± 60.3

AOR 1118: **G-28 Muscovite - HP metabasite-1** - *Plateau age: 328.74 ± 1.17 Ma (steps 6-14: 99.3% Ar release), MSWD: 1.194*

1	0.50	0.224 ± 0.024	0.515 ± 1.217	0.175 ± 0.041	5.126 ± 0.095	100.247 ± 0.516	0.002240 ± 0.000240	0.051209 ± 0.000992	0.013	0.184	66.10	0.20	6.60 ± 1.40	173.9 ± 35.0
2	0.75	0.161 ± 0.023	0.757 ± 1.329	0.206 ± 0.036	12.864 ± 0.182	202.335 ± 0.540	0.000797 ± 0.000114	0.063699 ± 0.000918	0.003	0.108	23.50	0.51	12.00 ± 0.56	304.8 ± 13.1
3	1.00	0.172 ± 0.022	0.698 ± 1.341	0.451 ± 0.045	33.368 ± 0.235	487.311 ± 0.868	0.000354 ± 0.000045	0.068614 ± 0.000500	0.003	0.038	10.44	1.31	13.05 ± 0.22	329.0 ± 5.0
4	1.25	0.269 ± 0.045	1.532 ± 2.084	1.906 ± 0.127	150.819 ± 0.789	2063.439 ± 3.429	0.000131 ± 0.000022	0.073252 ± 0.000403	0.003	0.019	3.85	5.93	13.12 ± 0.11	330.8 ± 2.6
5	1.50	0.114 ± 0.050	1.486 ± 4.005	3.117 ± 0.370	241.037 ± 1.304	3207.660 ± 5.016	0.000035 ± 0.000016	0.075315 ± 0.000425	0.001	0.011	1.04	9.47	13.14 ± 0.10	331.1 ± 2.2
6	1.75	0.260 ± 0.050	1.985 ± 2.269	2.413 ± 0.152	194.682 ± 1.163	2618.006 ± 4.611	0.000099 ± 0.000019	0.074530 ± 0.000465	0.003	0.019	2.93	7.65	13.02 ± 0.11	328.5 ± 2.6
7	2.00	0.173 ± 0.046	2.010 ± 3.064	2.798 ± 0.241	221.047 ± 1.405	2936.500 ± 3.625	0.000059 ± 0.000016	0.075447 ± 0.000490	0.001	0.017	1.74	8.69	13.02 ± 0.11	328.5 ± 2.4
8	2.25	0.148 ± 0.038	1.801 ± 2.591	2.674 ± 0.237	213.980 ± 1.101	2825.318 ± 5.761	0.000052 ± 0.000014	0.075910 ± 0.000421	0.003	0.015	1.54	8.41	12.97 ± 0.09	327.2 ± 2.1
9	2.37	0.146 ± 0.047	2.754 ± 3.907	3.567 ± 0.236	293.505 ± 1.545	3861.229 ± 6.485	0.000038 ± 0.000018	0.076188 ± 0.000422	0.002	0.017	1.11	11.53	12.98 ± 0.09	327.4 ± 2.0
10	2.47	0.127 ± 0.062	3.503 ± 3.235	3.338 ± 0.218	260.466 ± 1.446	3431.693 ± 5.956	0.000037 ± 0.000018	0.076074 ± 0.000444	0.001	0.025	1.09	10.23	13.00 ± 0.10	328.0 ± 2.4
11	2.58	0.079 ± 0.045	5.290 ± 3.172	2.696 ± 0.185	217.384 ± 1.133	2859.266 ± 4.367	0.000027 ± 0.000016	0.076202 ± 0.000415	0.001	0.045	0.80	8.54	13.02 ± 0.09	328.3 ± 2.2
12	2.67	0.085 ± 0.040	9.183 ± 3.061	2.902 ± 0.221	228.243 ± 1.306	3001.266 ± 4.292	0.000028 ± 0.000013	0.076217 ± 0.000450	0.001	0.074	0.82	8.97	13.01 ± 0.09	328.2 ± 2.2
13	3.00	0.027 ± 0.014	3.169 ± 1.612	0.767 ± 0.061	61.010 ± 0.368	802.067 ± 1.322	0.000032 ± 0.000018	0.076239 ± 0.000478	0.000	0.095	0.96	2.40	12.99 ± 0.11	327.7 ± 2.5
14	7.00	0.132 ± 0.071	18.084 ± 6.908	5.025 ± 0.338	411.532 ± 2.226	5431.958 ± 8.519	0.000023 ± 0.000013	0.075933 ± 0.000429	0.001	0.080	0.69	16.17	13.08 ± 0.09	329.7 ± 2.1

AOR 1110: **G-31 Muscovite - HP metabasite-2** - *Plateau age: 307.74 ± 27.33 Ma (steps 5-8: 79.55% Ar release), MSWD: 1.665*

1	0.50	0.445 ± 0.029	8.601 ± 1.713	0.363 ± 0.062	0.546 ± 0.047	128.057 ± 0.632	0.003457 ± 0.000224	0.004214 ± 0.000369	0.005	29.167	102.11	4.18	-5.04 ± 15.73	-145.2 ± 471.7
2	1.00	0.458 ± 0.030	3.972 ± 1.264	0.241 ± 0.041	0.536 ± 0.040	136.972 ± 0.639	0.003336 ± 0.000218	0.003896 ± 0.000293	0.005	13.624	98.56	4.11	3.67 ± 16.58	98.9 ± 434.5
3	1.50	0.704 ± 0.038	1.894 ± 0.978	0.237 ± 0.041	0.680 ± 0.047	209.925 ± 0.760	0.003353 ± 0.000182	0.003234 ± 0.000223	0.004	5.106	99.08	5.21	2.83 ± 16.71	76.6 ± 443.1
4	2.00	0.220 ± 0.022	5.534 ± 1.266	0.131 ± 0.033	0.908 ± 0.058	67.594 ± 0.375	0.003226 ± 0.000323	0.013385 ± 0.000857	0.005	11.198	95.27	6.96	3.5 ± 7.15	94.4 ± 187.9
5	2.50	0.173 ± 0.021	48.044 ± 3.125	0.140 ± 0.038	2.242 ± 0.073	68.335 ± 0.448	0.002330 ± 0.000311	0.032350 ± 0.001097	0.010	39.811	68.79	17.17	9.63 ± 2.87	248.5 ± 69.2
6	3.00	0.100 ± 0.020	87.352 ± 3.314	0.234 ± 0.040	3.456 ± 0.093	63.346 ± 0.444	0.001193 ± 0.000310	0.053675 ± 0.001528	0.007	47.091	35.16	26.47	12.07 ± 1.75	306.5 ± 40.8
7	3.37	0.055 ± 0.018	24.586 ± 2.395	0.066 ± 0.028	0.924 ± 0.052	27.003 ± 0.283	0.001788 ± 0.000683	0.033602 ± 0.001970	0.005	49.637	52.78	7.07	14.04 ± 6.09	351.8 ± 138.6
8	7.00	0.128 ± 0.020	176.232 ± 4.982	0.216 ± 0.043	3.766 ± 0.088	71.447 ± 0.553	0.001102 ± 0.000278	0.051045 ± 0.001303	0.011	88.567	32.50	28.84	13.21 ± 1.65	333.0 ± 38.0

Ordovician Las Minas, Huerta and Amate units in the eastern part of the Acatlán Complex.

The HP granitoid (G-24, UTM_{NAD27}: 140571085/2023811) yielded concordant ages ranging from 485 ± 3 to 1878 ± 14 Ma with population peaks at ca. 500, 522, 623, 774, 900 and 1875 Ma (Fig. 12c). This rock has a single concordant zircon with the younger age of 485 ± 3 Ma (Fig. 12d), and a weighted mean age of 482 ± 3 Ma (95% conf., MSWD: 1.5) calculated using the 8 youngest zircons (3 concordant and 5 discordant). As these ages are the same within error, they are interpreted to date the time of intrusion as Early Ordovician.

The HP mica schist (G-36, UTM_{NAD27}: 140571085/2023811) is tectonically juxtaposed against the metagranitoid and yielded concordant detrital ages between 433 ± 3 and 2039 ± 16 Ma with population peaks at ca. 457–480, 534, 908, 954, 1090, 1150, 1265, 1845 and 2035 Ma (Fig. 12e). The three youngest concordant zircons produce a weighted mean age of 460 ± 12 Ma (Middle to Late Ordovician, 95% conf., MSWD: 2.7), and a single detrital zircon produces the youngest concordant age of 433 ± 3 Ma (Early Silurian, Fig. 12f). Thus, deposition of this rock definitely took place after the Middle Ordovician, and possibly after the Early Silurian.

7.4. Provenance of detrital zircons

The oldest detrital zircons in both clastic rocks yielded ages between 2750 and 1845 Ma, and a main peak at 1850 Ma, which may have been derived from either Amazonia and/or Laurentia or their recycled products (Fig. 12a, c and e). There is also a considerable population of zircons between 1265 and 900 Ma, with the main peak at ~1050 Ma, possibly derived from the Oaxacan Complex, although it is not possible to discriminate between sources in Laurentia and/or Amazonia and/or the Pannotia terranes (Sureda and Omarini, 1999). However, these rocks contain a significant population of zircons between 900 and 750 Ma, which has an unique source in the Goiás Magmatic Arc of Amazonia (Keppie et al., 2008a), implying that these units were located adjacent to Amazonia during their deposition. These rocks also have 750 to 530 Ma detrital zircon populations, which are most likely derived from the pan-African/Brasiliano orogens (Unrug, 1996). The 550–500 Ma zircons could have been derived from either Laurentia, Amazonia, Acatlán Complex itself or others peri-Gondwanan terranes.

8. $^{40}Ar/^{39}Ar$ Geochronology

8.1. Analytical Methods

Six samples of the HP rocks were collected from the central outcrop in Tecolutla (UTM: 140571085/2023811). Muscovites were separated from samples of metagranitoid (G-24), mica schist (G-36), metabasite-1 (G-25 and G-28) and metabasite-2 (G-31), whereas hornblende was obtained from a sample of metabasite-1 (G-25). Minerals were pretreated and concentrated by standard techniques and later selected by handpicking under a binocular microscope from fractions that ranged in size from 40–60 mesh at the mineral separation laboratory at UNICIT-Universidad Nacional Autónoma de México, Campus-Juriquilla, Querétaro, Qro. The muscovite and hornblende separates were loaded into Al-foil packets and irradiated together with Hb3gr (1072 Ma) as a neutron-fluence monitor at the McMaster Nuclear Reactor (Hamilton, Ontario). $^{40}Ar/^{39}Ar$ analyses were performed by laser step-heating techniques described by Clark et al. (1998) at the Geochronology Research Laboratory of Queen's University, Kingston, Ontario, Canada. The data are given in Table 6 and plotted in Fig. 13. All data have been corrected for blanks, mass discrimination, and neutron-induced interferences. For the purposes of this paper, a plateau age is obtained when the apparent ages of at least three consecutive steps, comprising a minimum of 50% of the $^{39}Ar_k$ released, agree within 2σ error with the integrated age of the plateau segment. Errors shown in Table 6 and on the age spectrum represent the analytical precision at ±2σ.

8.2. Results

Muscovite from the HP metagranitoid (G-24) yielded a robust plateau age of 316 ± 1 Ma (MSWD = 7.9) with 73.4% of the total ^{39}Ar released between steps 7 and 15 (Fig. 13a). The first four steps are associated with high atmospheric contamination and some contributions of Ar from other minor contaminating phases.

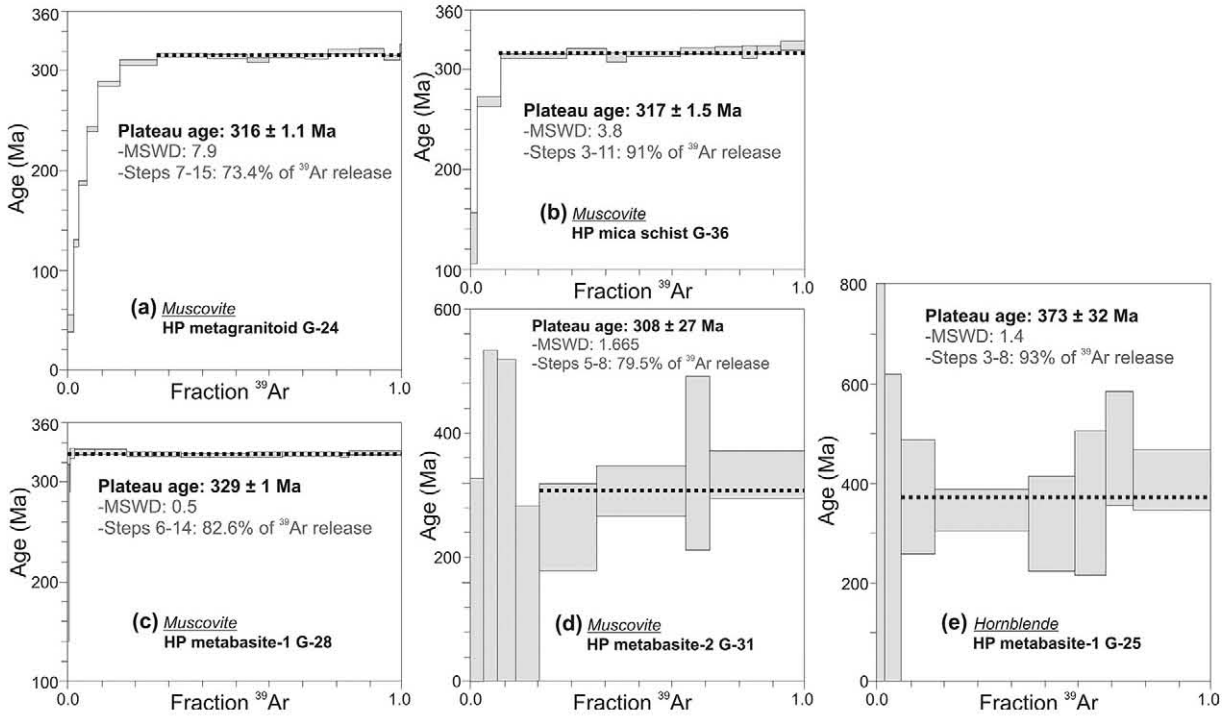

Fig. 13. $^{40}Ar/^{39}Ar$ spectra for the Tehuitzingo HP rocks: (a) muscovite from metagranitoid; (b) muscovite from mica schist; (c) muscovite from metabasite-1; (d) muscovite from metabasite-2; and (e) hornblende from metabasite-1.

Muscovite from the HP mica schist (G-36) yielded a plateau age of 317 ± 1.5 Ma (MSWD = 3.8) with a 91% of the total ^{39}Ar released between steps 3 and 11 (Fig. 13b). The first two steps are associated with high atmospheric contamination and some contributions of Ar from other minor contaminating phases.

Muscovite from HP metabasite-1 (G-28) yielded a plateau age of 329 ± 1 Ma (MSWD = 0.5) with 83% of total ^{39}Ar released between steps 6 and 14 (Fig. 13c). The first two steps are associated with high atmospheric contamination and some contributions of Ar from other minor contaminating phases.

Muscovite from HP metabasite-2 (G-31) yielded a plateau age of 308 ± 27 Ma (MSWD = 1.665) with a 79.55% of the total ^{39}Ar released between steps 5 and 8 (Fig. 13d). The large uncertainty in the first four steps is product of low K contents in the sample; this may also be due to contamination from a high Ca/K phase, such as amphibole.

Hornblende from HP metabasite-1 yielded a plateau age of 373 ± 32 Ma (MSWD = 1.4) with a 93% of total ^{39}Ar released between steps 3 and 8 (Fig. 13e). The large uncertainties are due to low amounts of ^{39}Ar, possibly due to low K content in the amphibole (Table 6).

8.3. Interpretation of ^{40}Ar/^{39}Ar Ages

Excess argon in eclogite-facies rocks is often a problem in the interpretation of ^{40}Ar/^{39}Ar ages (e.g., Boundy et al., 1997; Baxter et al., 2002), and it is possible that the rocks of the Tehuitzingo region have been exposed to varying amounts of excess argon. However, the HP metagranitoid (G-24) and mica schist (G-36) muscovites have similar crystal sizes (~0.3 mm) and produce consistent plateau ages of 316 ± 1 and 317 ± 1.5 Ma, respectively. This data consistency added to the lack of any evidence of excess Ar in the age spectra (Fig. 13a and b) and the similar degree and style of deformation (see above) of both rocks, supports a common history of burial and exhumation. These muscovite ages are therefore inferred to date the cooling-through ~385 °C using the grain size of 0.3 mm and an assumed cooling rate of 15 °C/my (Hames and Bowring, 1994).

The muscovites analyzed in the HP metabasites (G-28 and G-31) also yield consistent plateau ages of 329 ± 1 and 308 ± 27 Ma, although the latter has large errors. The best data (329 ± 1 Ma) was used to define cooling through ~385 °C.

The 373 ± 32 Ma plateau age obtained from a hornblende of HP metabasite-1 is older than both the 353–346 Ma metamorphic zircon ages (Elías-Herrera et al., 2004; Middleton et al., 2007) and the 330–345 Ma ^{40}Ar/^{39}Ar hornblende plateau ages recorded in the HP rocks extruded from the median HP zone to the east (Keppie et al., 2011). These observations suggest that metabasite-1 has been affected by excess argon. The large errors are consistent with the low K content of the hornblende compared with the muscovite.

9. Discussion

The Paleozoic Acatlán Complex at Tehuitzingo records several N-S dextral shear zones that bounded packages of HP-HT (Piaxtla Suite) and low-grade rocks. However, in the Atopoltitlán area (Fig. 4), there is a gently NW-dipping thrust (klippe) that we interpret as the original structural contact between these units. Thrusting is inferred to have started during D_a under peak metamorphic conditions of eclogite facies (with zoisite and amphibole) and continued during the second phase of penetrative and progressive deformation under epidote-amphibolite facies. ^{40}Ar/^{39}Ar hornblende plateau ages in the neighboring Piaxtla area indicate that this took place after ca. 345 Ma (Keppie et al., 2011), which is within error of the ^{40}Ar/^{39}Ar hornblende plateau age of 373 ± 32 Ma obtained at Tehuitzingo from a HP metabasite-1. As the greenschist facies deformation at ~2.7 kbar and 350 °C is common to both the HP and low-grade rocks, it is inferred that they were juxtaposed during the final stage of W-vergent thrusting by ca. 329–316 Ma. ^{40}Ar/^{39}Ar dating of muscovite in the northern low-grade rocks (Patlanoaya area) has yielded an age of 347 ± 3 Ma for its oldest foliation (Ramos-Arias et al., 2008) suggesting that extrusion affected the low-grade rocks throughout much of the Mississippian. Combining all the age data from the Tehuitzingo HP rocks indicates a cooling rate of 10-17 °C/my (Fig. 15).

Lithological data, structural data, and U-Pb detrital zircon ages indicate that the low-grade sedimentary rocks at Tehuitzingo may be correlated with the Ordovician low-grade sedimentary rocks to the east of the HP central belt at Acatlán Complex (Las Minas, Huerta and Amate units) rather than the Permian Tecomate Formation as was suggested by Carballido-Sánchez and Delgado-Argote (1989). This correlation indicates that the Early Paleozoic rocks to the east and west of the HP belt are part of the same terrane with a common evolution

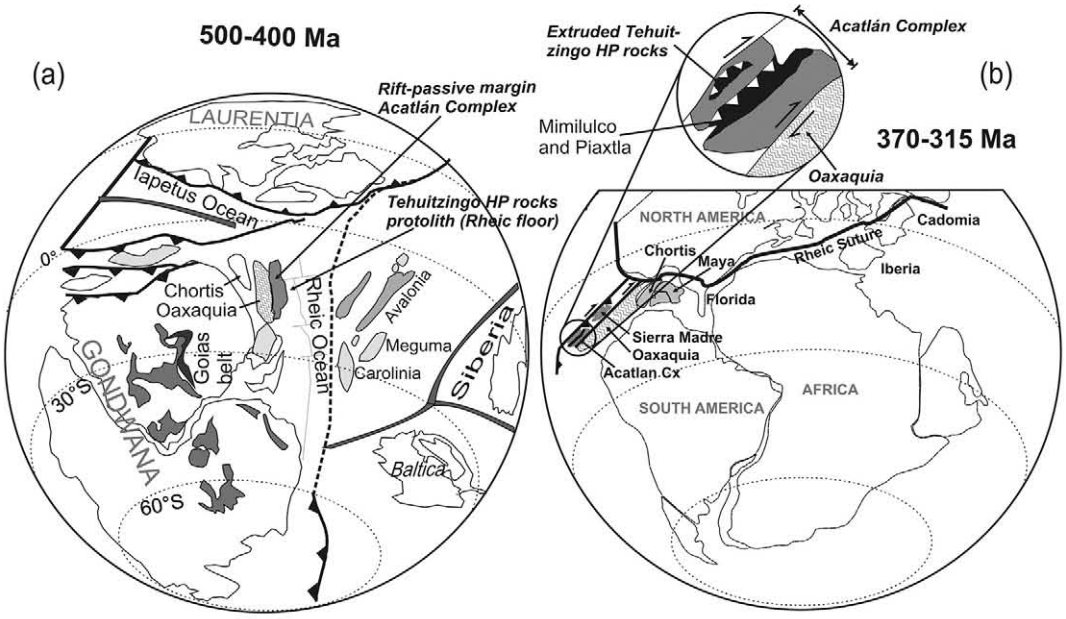

Fig. 14. Gondwana continental-reconstruction with the paleo-position of the Acatlán Complex: (a) Cambrian-Ordovician; and (b) Early-Late Mississippian. Modified after Keppie et al. (2008a).

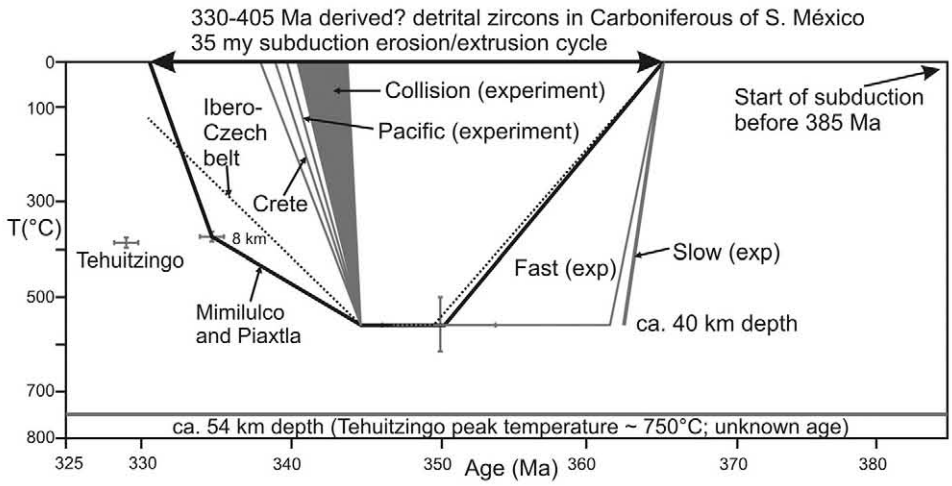

Fig. 15. Temperature-time data for the Tehuitzingo HP rocks compared with Mimilulco and Piaxta HP rocks.

(Keppie et al., 2008a; Ortega-Obregón et al., 2009; Keppie et al., 2010) rather than multiple terranes with a complex history of accretion (Ortega-Gutiérrez et al., 1999; Vega-Granillo et al., 2009). It also suggests that, rather than marking an oceanic suture, the HP rocks were extruded into the upper plate during subduction, as proposed by Keppie et al. (2008a). Geochronological constraints indicate that the subduction erosion and extrusion cycle occurred within the Carboniferous. That this took place on the western margin of Pangea is indicated by the presence of mid-Continent (USA) fauna in the Carboniferous rocks lying above neighboring Oaxaca Complex (Navarro-Santillán et al., 2002).

Furthermore, HP rocks at Acatlán Complex from Tehuitzingo, Cuatlaxtecoma Unit (Ixcamilpa) and Esperanza Suite (Piaxtla) have an estimated exhumation rate between 0.3-1.0 mm/year over a 13–20 Ma period. This very slow exhumation rate range is consistent with accretionary- and serpentinite-type subductions, which are considerably slower than the higher rates recorded in continental-type subduction (up to 40 mm/year). Furthermore, a serpentinite-subduction regime is consistent with: (i) the oceanic lithosphere affinity of the Tehuitzingo Serpentinite protolith and its associated metabasite lenses (Galaz-Escanilla et al., 2009) are typical of serpentinite-type subduction (e. g., Coleman, 1971); and (ii) the P-T-t pattern of HP Tehuitzingo rocks (Fig. 11) is similar to exhumation in a serpentinite-subduction channel (e.g., Guillot et al., 2009) from depths of ~54 km, which is deeper that the maximum, 40–45 km depth for HP rocks in the accretionary-type subduction.

The exhumation of the ultramafic rocks was probably facilitated by the high increase in volume (up to 50%) during serpentinization (O'Hanley, 1996), which decreased their density, viscosity and shear strength, which, in turn, increases their Poisson ratio (~0.29), allowing it to be highly ductile leading to their extrusion by buoyancy. The associated granitoid and metasedimentary rocks have an inheritantly lower density than the surrounding rocks also leading to their exhumation by buoyancy (Chemenda et al., 2001). Some authors report that the buoyancy force by itself is insufficient to exhume ultramafic rocks, so additional factors are needed, such as channel-flow decoupling, crustal extension, and delamination.

10. Conclusions

The tectonic evolution of the rocks in the Tehuitzingo area can be summarized as follows:

(1) *Lower Ordovician* (482–485 Ma: Tremadocian) intrusion of granitoids and metabasites of the Piaxtla Suite;
(2) *Post-lowest Ordovician* (post-481 Ma) deposition of low-grade psammite/pelite correlated with low-grade sediments to the east of the median HP belt;
(3) *Post- Early Silurian* deposition of clastic rocks (HP mica schist) adjacent to Amazonia along the southern margin of the Rheic ocean (Fig. 14a);
(4) *Late Devonian-Pennsylvanian* subduction-erosion of forearc HP rocks (based on geochemical data of Galaz-Escanilla et al., 2009) on the western margin of Pangea, HP-HT deformation and subduction-channel extrusion of the Piaxtla Suite at a cooling rate of 10-17 °C/my, which led to tectonic juxtaposition of the HP and low-grade rocks by 329–317 Ma (upper Mississippian: Fig. 14b);
(5) *Lower Permian* low-grade dextral deformation that obliterated most of the original contacts between HP and low-grade rocks;
(6) *Jurassic* deposition of the conglomeratic red beds and subsequent deformation that placed them in tectonic contact with the Acatlán Complex;
(7) Erosional period between *Cretaceous-Neogene* followed by deposition of the lacustrine Tehuitzingo Formation (*Pleistocene?*) and unconformably overlying *Pleistocene?* polymictic conglomerate.

Acknowledgements

Thanks for field assistance are due to graduate students Daniel Bolaños, Fabián Durán, Berlaine Ortega and Mario Ramos (UNAM). Assistance with U-Pb samples preparation to Valerie Pompa, Consuelo Macías, Carlos Ortega, Ofelia Pérez (All MSc., UNAM), and the Eng. Teodoro Hernández (UNAM) is also gratefully acknowledged. We thank Eng. Carlos Linares (UNAM) for help in the microprobe measurements. Valuable comments were provided by the Drs. Fernando Ortega, Mariano Elías, Luigi Solari (All UNAM) and Hans Massonne (Stuttgart University). This study was financed through projects PAPIIT N° IN100108-3, CONACYT N° CB-2005-1:24894, and IGCP 597. JKWL would like to acknowledge financial support through an NSERC Discovery grant.

Appendix A. Supplementary data

Supplementary data to this article can be found online at http://dx.doi.org/10.1016/j.gr.2012.04.011.

References

Baxter, E.F., DePaolo, D.J., Renne, P.R., 2002. Spatially correlated anomalous $^{40}Ar/^{39}Ar$ "age" variations in biotites about a lithologic contact near Simplon Pass, Switzerland: A mechanistic explanation for excess Ar. Geochimica et Cosmochimica Acta 66 (6), 1067–1083.
Bell, A.M., 1981. Foliation development: the contribution, geometry and significance of progressive bulk inhomogeneous shortening. Tectonophysics 75, 273–296.

Boundy, T.M., Hall, C.M., Li, G., Essene, E.J., Halliday, A.N., 1997. Fine-scale isotopic heterogeneities and fluids in the deep crust: a $^{40}Ar/^{39}Ar$ laser ablation and TEM study of muscovites from a granulite-eclogite transition zone. Earth and Planetary Science Letters 148, 223–242.

Calderón-García, A., 1956. Estratigrafía del Mesozoico y tectónica del sur del Estado de Puebla, México: México D. F. Congreso Geológico Internacional 20. Libro-guía de la excursión A-11, pp. 9–33.

Carballido-Sánchez, E.A., Delgado-Argote, L.A., 1989. Geología del cuerpo serpentinítico de Tehuitzingo, Estado de Puebla. Interpretación preliminar de su emplazamiento. Revista Mexicana de Ciencias Geológicas 8 (2), 134–148.

Cathelineau, M., 1988. Cation site occupancy in chlorites and as a function of temperature. Clay Minerals 23, 471–485.

Cerca, M., Ferrari, L., López-Martínez, M., Martiny, B., Iriondo, A., 2006. Late Cretaceous shortening and early Tertiary shearing in the central Sierra Madre del Sur, southern Mexico: Insights into the evolution of the Caribbean-North American plate interaction. Tecrtonics 26, TC3007. http://dx.doi.org/10.1029/2006TC001981.

Chemenda, A.I., Hurpin, D., Tang, J.-C., Stephan, J.-F., Buffet, G., 2001. Impact of arc-continent collision on the conditions of burial and exhumation of UHP/LT rocks: experimental and numerical modeling. Tectonophysics 342, 137–161.

Clark, A.H., Archibald, D.A., Lee, A.W., Farrar, E., Hodgson, C.J., 1998. Laser probe $^{40}Ar/^{39}A$rages of early- and late-stage alteration assemblages, Rosario porphyry copper-molybdenum deposit, Collahuasi District, I Region, Chile. Economic Geology 93 (3), 326–337.

Coleman, R.G., 1971. Plate tectonic emplacement of upper mantle peridotites along continental edges. Journal of Geophysical Research 76, 1212–1222.

Compston, W., Williams, I.S., Meyer, C., 1984. U-Pb geochronology of zircons form lunar Breccia 73217 using a sensitive high mass-resolution ion microprobe. Journal of Geophysical Research 89, 525–534.

Connolly, J.A.D., 1990. Multivariable phase diagrams; an algorithm based on generalized thermodynamics. American Journal of Science 290, 666–718.

Connolly, J.A.D., 2005. Computation of phase equilibria by linear programming: A tool for geodynamic modeling and its application to subduction zone decarbonation. Earth and Planetary Science Letters 236, 524–541.

Dobrzhinetskaya, L.F., 2012. Microdiamonds – Frontiers of ultrahigh-pressure metamorphism. Gondwana Research 21, 207–223.

Elías-Herrera, M., Ortega-Gutiérrez, F., 2002. Caltepec fault zone: An Early Permian dextral transpressional boundary between the Proterozoic Oaxacan and Paleozoic Acatlán complexes, southern Mexico, and regional implications. Tectonics 21 (3), 220–234.

Elías-Herrera, M., Ortega-Gutiérrez, F., Sánchez Zavala, J.L., Reyes-Salas, A.M., Macias-Romo, C., Iriondo, A., 2004. New Geochronological and Stratigraphic Data Related to the Paleozoic Evolution of the High-pressure Piaxtla Grop, Acatlán Complex, southern Mexico: IV reunion nacional de ciencias de la tierra. Libro de Resumenes, p. 150.

Elías-Herrera, M., Ortega-Gutiérrez, F., Sánchez Zavala, J.L., Iriondo, A., Ortega-Rivera, A., 2007. Conflicting stratigraphic and geochronological data from the Acatlán Complex: "Ordovician" granite intrude metamorphic and sedimentary rocks of Devonian-Permian age. Eos Transactions AGU 88 (23) (Joint Assembly Supplement, Abstract T41A-12).

Ernst, W.G., Marayama, S., Wallis, S., 1997. Buoyancy-driven, rapid exhumation of ultrahigh-pressure metamorphosed continental crust. Proceedings of the National Academy of Science USA 94, 9532–9537.

Galaz-Escanilla, G., Keppie, J.D., Solari, L., 2009. Complejo Acatlán en al área de Tehuitzingo, Estado de Puebla, sur de México: Evidencias de su evolución tectónica. Reunión Anual de la Unión Geofísica Mexicana: Geos, 29(1). GET-11.

Gehrels, G., Valencia, V., Pullen, A., 2006. Detrital zircon geochronology by laser ablation multicollector ICPMS at the Arizona LaserChron Center. In: Olszewski, T. (Ed.), Geochronology: Emerging opportunities: Paleontology Society Papers, 12, pp. 67–76.

González-Mancera, G., 2001. Mineralogía y petrología de las serpentinitas del cuerpo ultramáfico de Tehuitzingo, Estado de Puebla. Tesis de Maestría, Universidad Nacional Autónoma de México, 103 pp.

Grapes, R.H., Hoskin, P.W.O., 2004. Epidote Group Minerals in Low–Medium Pressure Metamorphic Terranes. Reviews in Mineralogy and Geochemistry 56, 301–345.

Guillot, S., Hattori, K., Agard, P., Schwartz, S., Vidal, O., 2009. Exhumation Processes in Oceanic and Continental Subduction Contexts: A Review. In: Lallemand, S., Funiciello, F. (Eds.), Subduction Zone Geodynamics. Springer-Verlag, Berlin Heidelberg, pp. 175–205.

Hames, W.H., Bowring, S.A., 1994. An empirical evolution of the argon diffusion geometry in muscovite. Earth and Planetary Science Letters 124, 161–167.

Harangi, Sz, Downes, H., Kósa, L., Szabó, Cs, Thirlwall, M.F., Mason, P.R.D., Mattey, D., 2001. Almandine garnet in calc-alkaline volcanic rocks of the Northern Pannonian Basin (Eastern- Central Europe): geochemistry, petrogenesis and geodynamic interpretations. Journal of Petrology 42, 1813–1843.

Hey, M.H., 1954. A new review of the chlorites. Mineralogical Magazine 80, 277–292.

Holland, T., Blundy, J., 1994. Non-ideal interactions in calcic amphiboles and their bearing on amphibole-plagioclase thermometry. Contributions to Mineralogy and Petrology 116, 433–447.

Holland, T.J.B., Powell, R., 1998. An internally consistent thermodynamic data set for phases of petrological interest. Journal of Metamorphic Geology 16, 309–343.

Hollister, L.S., Grissom, G.C., Peters, E.K., Stowell, H.H., Sisson, V.B., 1987. Confirmation of the empirical correlation of Al in hornblende with pressure of solidification of calc-alkaline plutons. American Mineralogist 72, 231–239.

Jeffries, T.E., Fernández-Suárez, J., Corfu, F., Gutiérrez-Alonso, G., 2003. Advances in U-Pb geochronology using a frequency quintupled Nd:YAG based laser ablation system ($\lambda = 213$ nm) and quadrupole based ICP-MS. Journal of Analytical Atomic Spectrometry 18, 847–855.

Jowett, E.C., 1991. Fitting iron and magnesium into the hydrothermal chlorite geothermometer. GAC/MAC/SEG Joint Annual Meeting, Program with Abstract 16, p. A62.

Keppie, J.D., Dostal, J., Murphy, J.B., Nance, R.D., 2008a. Synthesis and tectonic interpretation of the westernmost Paleozoic Variscan orogen in southern Mexico: From rifted Rheic margin to active Pacific margin. Tectonophysics 461, 277–290.

Keppie, J.D., Dostal, J., Miller, B.V., Ramos-Arias, M.A., Morales-Gámez, M., Nance, R.D., Murphy, J.B., Ortega-Rivera, A., Lee, J.W.K., Housh, T., Cooper, P., 2008b. Ordovician–earliest Silurian rift tholeiites in the Acatlán Complex, southern Mexico: Evidence of rifting on the southern margin of the Rheic Ocean. Tectonophysics 461, 130–156.

Keppie, J.D., Nance, R.D., Ramos-Arias, M.A., Lee, J.W.K., Dostal, J., Ortega-Rivera, A., Murphy, J.B., 2010. Late Paleozoic subduction and exhumation of Cambro-Ordovician passive margin and arc rocks in the northern Acatlán Complex, southern Mexico: Geochronological constraints. Tectonophysics 495, 213–229.

Keppie, J.D., Nance, R.D., Dostal, J., Lee, J.K.W., Ortega-Rivera, A., 2011. Constraints on the subduction erosion/extrusion cycle in the Paleozoic Acatlán Complex of southern Mexico: Geochemistry and geochronology of the type Piaxtla Suite. Gondwana Research. http://dx.doi.org/10.1016/j.gr.2011.07.020.

Leake, B.E., Woolley, A.R., Arps, C.E.S., Birch, W.D., Gilbert, M.C., Grice, J.D., Hawthorne, F.C., Kato, A., Kisch, H.J., Krivovichev, V.G., Linthout, K., Laird, J., Mandarino, J.A., Maresch, W.V., Nickel, E.H., Rock, N.M.S., Schumacher, J.C., Smith, D.C., Stephenson, N.C.N., Ungaretti, L., Whittaker, E.J.W., Youzhi, G., 1997. Nomenclature of amphiboles: report of the Subcommittee on Amphiboles of the International Mineralogical Association, Commission on New Minerals and Mineral Names. The Canadian Mineralogist 35, 219–246.

Liou, J.G., Tsujimori, T., Zhang, R.Y., Katayama, I., Maruyama, S., 2004. Global UHP metamorphism and continental subduction/collision: the Himalayan mode. International Geology Review 46, 1–27.

Ludwig, K.J., 2003. Isoplot 3.00. Berkeley Geochronology Center Special Publication, 4. 70 pp.

Massonne, H.J., Szpurka, Z., 1997. Thermodynamic properties of white micas on the basis of high pressure experiments in the system K_2O-MgO-Al_2O_3-SiO_2-H_2O and K_2O-FeO-Al_2O_3-SiO_2-H_2O. Lithos 41, 229–250.

Massonne, H.J., Willner, A.P., Gerya, T.V., 2007. Densities of psammopelitic rocks at elevated temperatures and high to ultrahigh pressure conditions: What are the geodynamic consequences? Earth and Planetary Science Letters 256, 12–27.

Meza-Figueroa, D., Ruiz, J., Talavera-Mendoza, O., Ortega-Gutiérrez, F., 2003. Tectonometamorphic evolution of the Acatlán Complex eclogites (southern México). Canadian Journal of Earth Sciences 40, 27–44.

Middleton, M.D., Keppie, J.D., Murphy, J.B., Miller, B.V., Nance, R.D., 2007. P-T-t constraints on exhumation following subduction in the Rheic Ocean: eclogitic Asís Lithodeme, Piaxtla Suite, Acatlán Complex, southern Mexico. In: Linnemann, U., Nance, R.D., Zulauf, G., Kraft, P. (Eds.), The Geology of Peri-Gondwana: the Avalonian–Cadomian Belt, Adjoining Cratons and the Rheic Ocean: Geological Society of America, Special Paper, 423, pp. 489–509.

Nance, R.D., Keppie, J.D., Miller, B.V., Murphy, J.B., Dostal, J., 2009. Palaeozoic palaeogeography of Mexico: constraints from detrital zircon age data. Geological Society of London, Special Publications 327, 239–269.

Navarro-Santillán, D., Sour-Tovar, F., Centeno-García, E., 2002. Lower Mississippian (Osagean) brachiopods from the Santiago Formation, Oaxaca, Mexico: stratigraphic and tectonic implications. Journal of South American Earth Sciences 15 (3), 327–336.

O'Hanley, D.S., 1996. Serpentinites: Records of tectonic and petrological history, 34. Oxford University Press, New York. 277 pp.

Ortega-Gutiérrez, F., 1981. La evolución tectónica premisisípica del sur de México. UNAM, Revista del Instituto de Geología 5 (2), 140–157.

Ortega-Gutiérrez, F., Elías-Herrera, M., Reyes-Salas, M., Macías-Romo, C., López, R., 1999. Late Ordovician-Early Silurian continental collisional orogeny in southern México and its bearing on Gondwana-Laurentia connections. Geology 27, 719–722.

Power, M.R., Pirrie, D., Anderson, J.C.O., Wheeler, P.D., 2000. Testing the validity of chrome spinel chemistry as a provenance and petrogenetic indicator. Geology 28, 1027–1030.

Proenza, J.A., Ortega-Gutiérrez, F., Camprubí, A., Trilla, J., Elías-Herrera, M., Reyes-Salas, M., 2004. Paleozoic serpentinite-enclosed chromitites from Tehuitzingo (Acatlán Complex, southern México): a petrological and mineralogical study. Journal of South American Earth Sciences 16, 649–666.

Ramos-Arias, M.A., Keppie, J.D., 2011. U-Pb Neoproterozoic-Ordovician protolith age constraints for high-medium pressure rocks thrust over low-grade metamorphic rocks in the Ixcamilpa area, Acatlán Complex, southern Mexico. Canadian Journal of Earth Sciences 48, 45–61.

Ramos-Arias, M.A., Keppie, J.D., Ortega-Rivera, A., Lee, J.W.K., 2008. Extensional Late Paleozoic deformation on the western margin of Pangea, Patlanoaya area, Acatlán Complex, southern Mexico. Tectonophysics 448, 60–76.

Ramos-Arias, M.A., Keppie, J.D., Lee, J.W.K., Ortega-Rivera, A., 2011. A Carboniferous high-pressure klippe in the western Acatlán Complex of southern México: implications for the tectonothermal development and paleogeography of Pangea. International Geology Review 1–20. http://dx.doi.org/10.1080/00206814.2011.580634.

Ramsay, J.G., 1967. Folding and fracturing of rocks, International series in the earth planetary sciences. McGraw Hill, New York. 508 pp.

Ramsay, J.G., Huber, M.I., 1987. The techniques of modern structural geology, Volume 2: folds and fractures. Academic Press, London. 700 pp.

Schmidt, M.W., 1992. Amphibole composition in tonalite as a function of pressure: an experimental calibration of the Al-in-hornblende barometer. Contributions to Mineralogy and Petrology 110, 304–310.

Sureda, R.J., Omarini, R.H., 1999. Evolución geológica y nomenclatura pre-Gondwánica en el Noroeste de Argentina (1800–160 Ma). Acta Geológica Hispánica 34 (2–3), 197–225.

Talavera-Mendoza, O., Ruiz, J., Gehrels, G.E., Meza-Figueroa, D.M., Vega-Granillo, R., Campa-Uranga, M.F., 2005. U-Pb geochronology of the Acatlán Complex and implications for the Paleozoic paleogeography and tectonic evolution of southern Mexico. Earth and Planetary Science Letters 235, 682–699.

Tolson, G., 2005. La falla Chacalapa en el sur de Oaxaca. In: Alaniz-Álvarez, S.A., Nieto-Samaniego, A.F. (Eds.), Grandes Fronteras Tectónicas de México: Boletín de la Sociedad Geológica Mexicana, Volumen Conmemorativo del Centenario, 52(1), pp. 111–122.

Ulmer, P., Trommsdorff, V., 1995. Serpentine Stability to Mantle Depths and Subduction-Related Magmatism. Science 268 (5212), 858–861.

Unrug, R., 1996. The assembly of Gondwanaland. Episodes 19 (1–2), 11–20.

Vega-Granillo, R., Talavera-Mendoza, O., Meza-Figueroa, D., Ruiz, J., Gehrels, G., López-Martínez, M., De la Cruz-Vargas, J., 2007. Pressure-temperature evolution of Paleozoic high-pressure rocks of the Acatlán Complex (southern Mexico): implications for the evolution of the Iapetus and Rheic Oceans. Geological Society of America Bulletin 119, 1249–1264.

Vega-Granillo, R., Calmus, T., Meza-Figueroa, D., Ruiz, J., Talavera-Mendoza, O., López-Martínez, M., 2009. Structural and tectonic evolution of the Acatlán Complex, southern Mexico: Its role in the collisional history of Laurentia and Gondwana. Tectonics 28, TC4008. http://dx.doi.org/10.1029/2007TC002159.

Vermeesch, P., 2004. How many grains are needed for a provenance study? Earth and Planetary Science Letters 224, 441–451.

Weaver, C.E., Broekstra, B., 1984. Illite mica. In: Weaver, C.E. (Ed.), Shale-Slate Metamorphism in the AppalachiansDevelopments in Petrology 10, 67–97.

Wiewiora, K., Weiss, J., 1990. Crystallochemical classifications of phylosillicates based on the unified system of projection of chemical composition II: The Chlorite group. Clay Minerals 25, 83–92.

Wu, C.M., Zhao, G., 2006. Recalibration of the garnet-muscovite (GM) geothermometer and the garnet-muscovite-plagioclase-quartz (GMPQ) geobarometer for metapelitic assemblages. Journal of Petrology 47 (2), 2357–2368.

Zack, T., Moraes, R., Kronz, A., 2004. Temperature dependence of Zr in rutile: empirical calibration of a rutile thermometer. Contributions to Mineralogy and Petrology 148, 471–488.

Zwart, H.J., 1962. On the deformation of polymetamorphic mineral associations and its application to the Bosost area (Central Pyrenees). Geologische Rundschau 52, 38–65.

Capítulo 3

Acumulados máficos de antearco y sus rocas asociadas en el cinturón central del Complejo Acatlán del sur de México: restricciones geoquímicas

Mafic forearc cumulates and associated rocks in the central high-pressure belt of the Acatlán Complex of southern México: geochemical constraints.

International Geology Review, 2013, p. 1–21

Gonzalo Galaz, J. Duncan Keppie, J. Brendan Murphy

International Geology Review, 2013
http://dx.doi.org/10.1080/00206814.2013.776806

Taylor & Francis
Taylor & Francis Group

Mafic forearc cumulates and associated rocks in the central high-pressure belt of the Acatlán Complex of southern México: geochemical constraints

Gonzalo Galaz[a]*, J. Duncan Keppie[a] and J. Brendan Murphy[b]

[a]*Departamento de Geología Regional, Instituto de Geología, Universidad Nacional Autónoma de México, México D.F., México;*
[b]*Department of Earth Sciences, St. Francis Xavier University, Antigonish, Nova Scotia, Canada B2G 2W5*

(*Accepted 12 February 2013*)

The high-pressure (HP) Piaxtla Suite at Tehuitzingo contains peridotites, gabbros, and serpentinized peridotites, as well as granitoids and metasedimentary rocks. The HP mafic rocks are characterized by low SiO_2 (38–52 wt.%) and high Mg# (~48–70), Ni (100–470 ppm), and Cr (180–1750 ppm), typical of cumulate compositions. Trace elements and rare earth element (REE) primitive mantle-normalized patterns display generally flat profiles, indicative of derivation from a primitive mantle with two distinct patterns: (1) gabbroic patterns are characterized by a positive Eu anomaly, low REE abundances, and slightly depleted high REE (HREE) relative to low REE (LREE), typical of cumulus olivine, pyroxene, and plagioclase; and (2) mafic-intermediate gabbroic patterns exhibit very flat profiles characteristic of olivine and clinopyroxene as cumulus minerals. Their Nb/Y and Zr/TiO_2 ratios suggest a subalkaline character, whereas low Ti/V ratios indicate that the Tehuitzingo cumulates are island arc tholeiitic basalts that resemble modern, immature oceanic, forearc magmas. These cumulates have high values of $\varepsilon_{Nd(t)} = 5.3–8.5$ and $^{147}Sm/^{144}Nd = 0.18–0.23$, which renders calculations of model ages meaningless. Our data are consistent with the Tehuitzingo arc rocks being part of a tectonically extruded Devonian–early Carboniferous arc developed along the west margin of Gondwana.

Keywords: Acatlán Complex; bulk-rock geochemistry; juvenile cumulates; immature arc; Gondwana

Introduction

The geochemistry of polydeformed, high-pressure (HP) protoliths is critical in determining their origin and tectonic evolution. HP rocks are generally inferred to be either the vestiges of an ocean that was subducted and then structurally extruded, either along the Benioff zone (Liou *et al.* 2004; Ernst 2010) or into the upper plate (Stöckhert and Gerya 2005; Keppie *et al.* 2010; Butler *et al.* 2011). HP rocks in the Acatlán Complex of southern México (Figure 1) occur in two N–S belts and are composed of metasedimentary rocks, granitoids, amphibolites, gabbros, and serpentinites. Although still debated (see Galaz *et al.* 2013 for a review), the most recent data indicate that the western belt is a klippe derived from a central zone of Devonian and Carboniferous tectonic extrusion (Keppie *et al.* 2008b, 2011; Ramos-Arias *et al.* 2012; Galaz *et al.* 2013). Although platinum group element (PGE) abundances suggest that the ultramafic rocks formed in a peri-arc tectonic setting (Proenza *et al.* 2004), no comprehensive geochemical data are available for the complete suite of HP rocks. Here, we present geochemical data for the mafic and associated intermediate rocks at Tehuitzingo in order to determine their origin, chemical evolution, and tectonic setting. These data indicate that the igneous rocks represent cumulates formed in a peri-arc/arc environment.

Geological setting

The Acatlán Complex is one of the terranes in southern México and constitutes the Palaeozoic basement of the Mixteca terrane (Figure 1). The northern margin of the Acatlán Complex is covered by volcanic and volcaniclastic sequences of the Cenozoic Transmexican Volcanic Belt (Figure 1(A)). The other margins are tectonic contacts (Figure 1(B)): (1) to the east, the Permian, Caltepec dextral shear zone juxtaposes the Acatlán Complex against the ca. 1 Ga Oaxacan Complex (Elías-Herrera and Ortega-Gutiérrez 2002); (2) to the south, the Cenozoic, sinistral transtensional Chacalapa–La Venta fault places the complex against the Mesozoic–Cenozoic Xolapa Complex (Tolson 2005); and (3) to the west, the Late Cretaceous Papalutla Thrust places the Acatlán Complex over the Cretaceous Morelos–Guerrero Platform (Cerca *et al.* 2007).

The Palaeozoic rocks of the Acatlán Complex can be subdivided into low- and high-grade assemblages (Figure 1(C)) (Keppie *et al.* 2008a,b; and references

*Corresponding author. Email: ggalaz@ing.uchile.cl

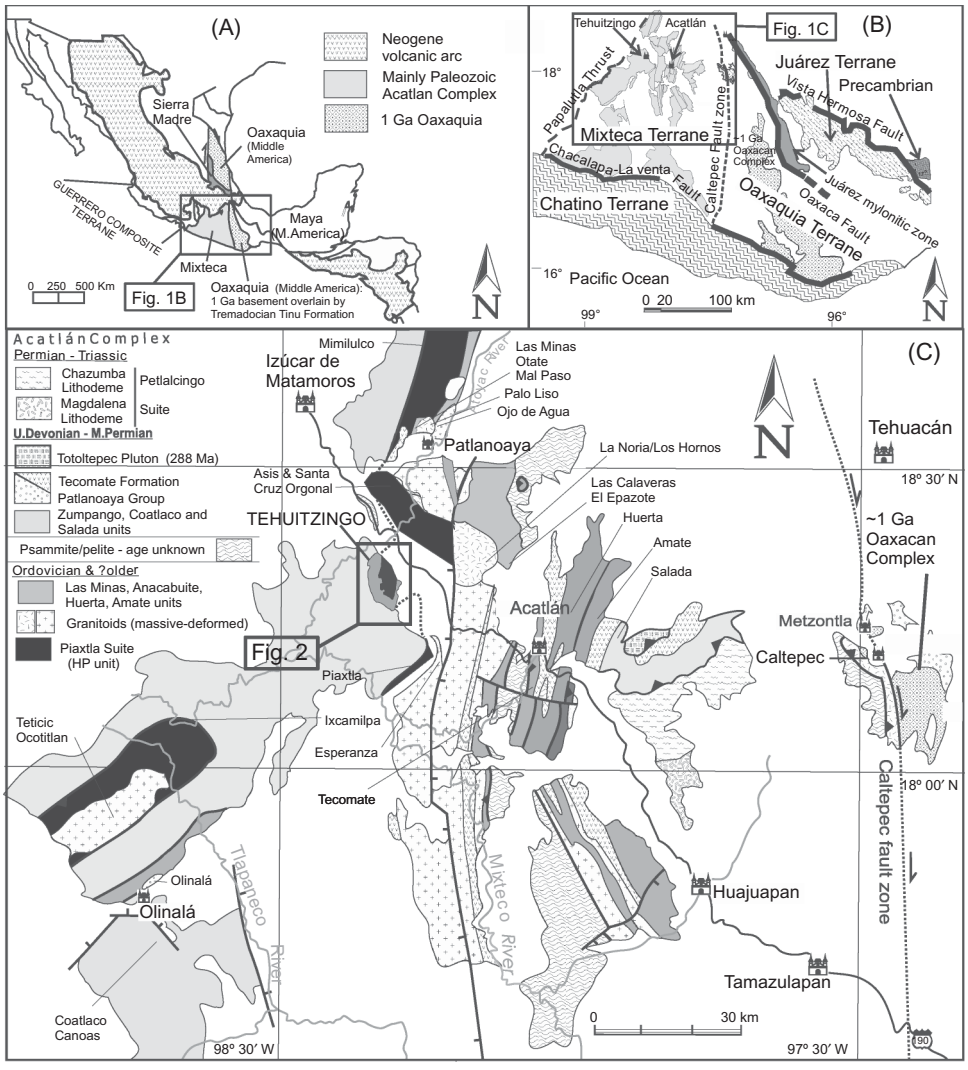

Figure 1. (A) Location of the main metamorphic complexes in southern México; (B) detailed map of the metamorphic complexes; (C) geological map of the Acatlán Complex (modified after Keppie *et al.* 2008b). The Tehuitzingo area is shown as a black rectangle.

therein). The low-grade assemblage is composed mainly of two sequences: a Neoproterozoic–Ordovician clastic sequence intruded by ca. 480–440 Ma, bimodal, rift-related, igneous rocks, and a latest Devonian–Permian shallow marine sequence consisting of metapsammites, metapelites, and some mafic volcanic rocks. The low-grade assemblage is affected by greenschist facies metamorphism (~3 kbar and ~350°C; Meza-Figueroa *et al.* 2003; Galaz *et al.* 2013). The HP metamorphic suite (Piaxtla Suite) consists of (1) a Neoproterozoic–Ordovician rift-shelf metasedimentary package (psammites and pelites) intruded by bimodal (retrogressed eclogite/amphibolite, granitoid) rift-related igneous rocks that are similar to those of the low-grade sequence; and (2) mafic–ultramafic bodies that have been attributed to a variety of tectonic settings, including continental rift, peri-arc, island arc (IAB), ocean island (OIB), and ophiolite (MORB) (Meza-Figueroa 1998; Proenza *et al.* 2004; Murphy *et al.* 2006; Morales-Gámez *et al.* 2009; Keppie *et al.* 2011). The HP suite underwent eclogite facies metamorphism (~11–16 kbar and ~500–750°C) followed by retrogressive metamorphism in the epidote–amphibolite and greenschist facies (Talavera-Mendoza *et al.* 2002; Meza-Figueroa *et al.* 2003; Galaz *et al.* 2013).

HP rocks were emplaced in the low-grade metamorphic assemblage forming two belts located in the centre (Mimilulco–Piaxtla) and west (Ixcamilpa–Olinalá) of the Acatlán Complex (Figure 1(C)). The eastern margin of the Piaxtla–Mimilulco HP belt is a N–S, normal listric shear zone with a down-dip easterly vergence (Ramos-Arias *et al.* 2008). The western margin of the central HP belt is the hanging wall of a N–S, westerly vergent folded thrust (Galaz *et al.* 2013). On the other hand, the western HP belt of Ixcamilpa–Olinalá is a klippe that was thrust over the low-grade assemblage (Ramos-Arias *et al.* 2012).

The geochemical and Sm–Nd isotopic signatures of the metasedimentary rocks in both belts are typical of rift-related passive margin sediments derived from an ancient cratonic source interpreted to be the adjacent Mesoproterozoic Oaxacan Complex (Murphy *et al.* 2006; Dostal and Keppie 2009; Ortega-Obregón *et al.* 2009). Granitoid rocks were derived by partial melting of a similar cratonic crustal source (T_{DM} ca. 1 Ga). Amphibolites exhibit a continental rift-tholeiite geochemistry and have ca. 1.25–0.75 Ga (in Asís) and ca. 1.48–0.68 Ga (in Olinalá) T_{DM} ages, indicating derivation from a subcontinental mantle source (Murphy *et al.* 2006; Ortega-Obregón *et al.* 2009). This bimodal igneous suite is inferred to have originated in an Ordovician rift-related environment by melting of both lithospheric mantle and ancient crustal components along the southern margin of the Rheic Ocean (Keppie *et al.* 2008a).

Tehuitzingo area

In the Tehuitzingo area, the western and eastern margins of the HP unit (Piaxtla Suite) are tectonically juxtaposed against the low-grade unit along subvertical N–S faults (107/87°) with oblique dextral kinematics (Figure 2). To the south, the Piaxtla Suite is thrust over the low-grade unit along a gently NW-dipping folded thrust (320/15°) with top-to-the-west kinematics (Galaz *et al.* 2013).

The low-grade unit is predominantly made up of greenschist facies, metapelitic, and metapsammitic rocks that have a planar fabric and a granolepidoblastic texture (ca. 481 Ma older limit for deposition; Galaz *et al.* 2013). They are composed mainly of primary minerals, such as quartz, feldspar, and accessory zircon, which suggest a medium-grained quartz-arenitic protolith (0.25–0.50 mm). Secondary minerals include quartz, albite, Mg–Fe–chlorite, phengite, epidote, calcite, and leucoxene, which yield a metamorphic peak of ∼3 kbar and ∼350°C (Galaz *et al.* 2013).

The HP unit mainly consists of serpentinized harzburgite (Tehuitzingo Serpentinite) formed almost entirely (95% of the rock) by decussate, acicular, and fibrous serpentine (coexisting chrysotile, lizardite, and antigorite). Associated minerals include magnetite, calcite, white mica, and talc (4%), and accessory chromite, clinochlore, undulose quartz, amphibole, and epidote (1%). The serpentinite encloses small marginal fault blocks composed of other lithologies (for more details, see Galaz *et al.* 2013). These lithologies include the following.

(1) *Metabasite-1*, which has a planar fabric and nemato-grano-poikiloblastic texture and is composed of calcic amphiboles (∼60%), albite, zoisite, Mg–Fe chlorite, titanite, and rutile. The metamorphic assemblage is an incipient HP association with rare rutile and almandine garnet, partially replaced by retrograde minerals, such as actinolite-edenite, zoisite, Mg–Fe chlorite, quartz, epidote, muscovite, and titanite.
(2) *Metabasite-2*, which has a planar fabric, nemato-grano-poikiloblastic texture and massive structure and is composed of albite, calcic amphibole, muscovite, almandine garnet, rutile, zoisite, Mg–Fe chlorite, titanite, and calcite. The metamorphic assemblage is a HP association with almandine garnet and rutile, as well as retrograde minerals, such as magnesium-hornblende, zoisite, Mg–Fe chlorite, actinolite, epidote, titanite, muscovite, and calcite.
(3) *Granitoid* (482 ± 3 Ma; Galaz *et al.* 2013), which is phaneritic, has an equigranular grano-poikiloblastic texture, and is composed of undulose quartz and feldspar with rare almandine garnet and rutile, indicating HP metamorphism. Metamorphic minerals consist of Mg–Fe chlorite, quartz, albite, phengite, zoisite, titanite, leucoxene, zircon, and apatite.
(4) *Mica schist* (maximum age of deposition ca. 433 ± 3 Ma; Galaz *et al.* 2013) has a planar fabric, medium-grained (0.25–0.5 mm), and a lepido-grano-porphyroblastic texture. A quartz-arenite protolith is indicated by the undulose quartz (23%), feldspar (7%), and muscovite (5%). The HP metamorphic association is composed of almandine garnet and rutile. Retrograde metamorphic minerals include phengite, amphibole, zoisite, quartz, albite, Mg–Fe chlorite, epidote, and rare titanite.

The HP unit records a prograde metamorphic history as follows (Galaz *et al.* 2013): (1) a metamorphic peak in the eclogite facies (∼750°C and ∼16 kbar), (2) retrogression to epidote–amphibolite facies (∼472°C and ∼7.1 to 3.4 kbar), and (3) retrogression to greenschist facies (∼360°C at undetermined pressures).

Other rock units in the study area are a more recent red polymictic conglomerate juxtaposed by fault-bounded lens against the HP unit, which in turn is unconformably overlain by a (?)Pleistocene unit composed of lacustrine sandstones of the Tehuitzingo Formation (Calderón-García 1956) and latest polymictic conglomerates, sandstones, and shales.

Geochemistry

Analytical methods

Twelve samples (ten mafic, one granitoid, and one mica-schist) were analysed by X-ray fluorescence spectrometry for major and selected trace elements (Rb, Sr, Ba, Ga, Zr, Nb, Ni, Cu, Y, Zn, Pb, Th, U, Ce, Cs, V, Cr, Co, and Ni), using a Phillips PW2400 spectrometer in the Nova Scotia Regional Geochemical Centre at Saint Mary's University, Halifax, Nova Scotia, Canada. Eight samples (six mafic, one granitoid, and one mica-schist) were analysed for rare earth elements (REE), as well as

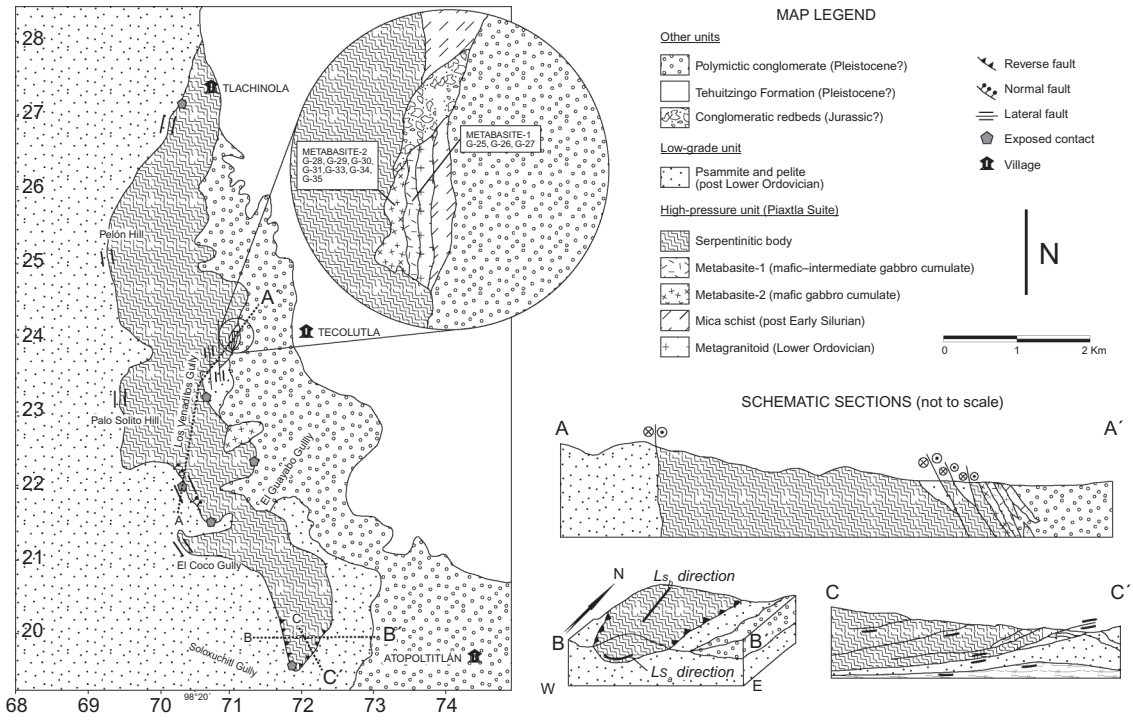

Figure 2. Geological map of the Tehuitzingo area and cross sections. The balloon in the middle map shows an outcrop of the high-grade metamorphic unit.

Y, Ba, Nb, Ta, Th, Zr, and Hf concentrations and seven samples (five mafic, one granitoid, and one mica-schist) for Nd isotopic compositions by inductively-coupled plasma mass spectrometry (ICP-MS), at Memorial University, Newfoundland, Canada. Analytical procedures, precision, and accuracy of the X-ray data are described by Dostal *et al.* (1994), the ICP-MS data are described by Ayer and Davis (1997), and analytical procedures for the Sm–Nd isotopic analyses were performed according to the methods described by Kerr *et al.* (1995). Analytical errors are generally less than 5%. T_{DM} ages are calculated using the model of DePaolo (1981, 1988) and Goldstein *et al.* (1984) for rocks with $^{147}Sm/^{144}Nd < 0.165$ (Stern 2002). The $\varepsilon_{Nd(t)}$ values are calculated for $t = 480$ Ma for granitoid, which represents the intrusive age (Galaz *et al.* 2013); for $t = 400$ Ma for peri-arc mafic cumulates (Piaxtla Suite), based on the 405–330 Ma range of igneous detrital zircons interpreted as derived from an arc (Keppie *et al.* 2012); and for $t = 430$ Ma for the mica-schist due to its maximum age of deposition of ca. 433 Ma (Galaz *et al.* 2013). The Sm–Nd isotopic data are shown in Table 1.

Table 1. Sm–Nd isotopic data for Tehuitzingo HP rocks of the Acatlán Complex.

Sample	Lithology	Nd (ppm)	Sm (ppm)	Sm/Nd	$^{143}Nd/^{144}Nd$	2σ	$\varepsilon_{Nd(0)}$	$\varepsilon_{Nd(t)}$	T_{DM1} (Ga)	T_{DM2} (Ga)
G-25	mafic-int. gab. Cum.	10.949	3.718	0.340	0.512936	6	5.81	5.37	0.947	3.904
G-26	mafic-int. gab. Cum.	5.060	1.912	0.378	0.513060	6	8.23	6.61	0.797	–
G-27	mafic-int. gab. Cum.	8.113	2.772	0.342	0.513111	6	9.22	8.73	0.936	0.852
G-30	mafic gab. Cum.	4.328	1.319	0.305	0.513058	8	8.20	8.84	0.813	0.478
G-34	mafic gab. Cum.	3.565	1.194	0.335	0.513092	6	8.86	8.57	–	0.793
G-24	granitoid	52.390	9.731	0.186	0.511983	6	−12.78	−7.61	0.759	1.751
G-36	mica-schist	37.113	7.208	0.194	0.512085	6	−10.78	−6.43	1.513	1.683

Notes: Chemical separations and isotopic analyses were determined at the Atlantic Universities Regional Isotopic Facility, Memorial University of Newfoundland, Canada. The $^{143}Nd/^{144}Nd$ ratios are measured by thermal ionization mass spectrometry, after chemical separation of Nd from Sm and other REE by ion-exchange chemistry. ε_{Nd} values are relative to $^{143}Nd/^{144}Nd = 0.512638$ and $^{147}Sm/^{144}Nd = 0.196593$ for present-day CHUR (Jacobsen and Wasserburg 1980) and $\lambda^{147}Sm = 6.54 \times 10–12$/year. T_{DM1} are calculated using the model of DePaolo (1981, 1988) and T_{DM2} calculated using a linear evolution for a mantle separated from the CHUR at 4.55 Ga and having a $\varepsilon_{Nd(0)} = 10$ (Goldstein *et al.* 1984). $\varepsilon Nd(t)$ values are calculated for $t = 480$ Ma for granitoid, which represents the intrusive age (Galaz *et al.* 2013); for $t = 400$ Ma for peri-arc mafic cumulates (Piaxtla Suite), based on the 405–330 Ma range of igneous detrital zircons interpreted as derived from an arc (Keppie *et al.* 2012); for $t = 430$ Ma for the mica-schist due to its maximum age of deposition of ca. 433 Ma (Galaz *et al.* 2013); and for the present day ($t = 0$).

Mafic rocks

Petrographic and field observations indicate that the mafic rocks (Piaxtla Suite) at Tehuitzingo have been affected by secondary processes, which modified their original chemical composition. Alteration has changed the content of alkali elements in some samples as evidenced by the wide variation in Na_2O/K_2O ratio, which ranges between 2.0 and 23.0. On the other hand, the concentrations of some major elements, high field strength elements (HFSE), REE, Th, and transition elements in the samples, probably were not modified significantly because they suffer very little remobilization during secondary alteration processes (e.g. Winchester and Floyd 1977; Pearce 1996), and their abundances exhibit a typical magmatic distribution (see below). Therefore, these latter elements are used herein to decipher primary trends in rocks that have suffered low-grade metamorphic and/or alteration events.

Generally, geochemical diagrams used for petrogenetic discrimination are applicable to liquid phases (magma) rather than to cumulates. Elements with very low partition coefficients (e.g. Zr and Nb) in early crystallization phases are incompatible with the cumulate composition and are concentrated in the pore spaces between the cumulus grains (intercumulus liquid). Their absolute abundances are lower than the liquid from which they crystallized, thus discrimination diagrams based on their abundances cannot be used reliably. However, discrimination diagrams based on ratios of incompatible elements with similar partition coefficients or on similar compatible elements are not significantly affected.

The mafic rocks are characterized by a SiO_2 between 38–52 wt.% (on a volatile-free basis) and a high Mg# (~48–70) that are typical of cumulate compositions. These rocks can be divided into two groups based on their geochemistry together with the textural distinctions made previously (Galaz *et al.* 2013):

(1) mafic-intermediate gabbroic cumulates (G-25, G-26, and G-27) that have relatively low values of Mg# (47–52), MgO (11–15 wt.%), Ni (100–180 ppm), and Cr (180–470 ppm) (Figure 3); and (2) mafic gabbroic cumulates (G-28, G-29, G-30, G-31, G-33, G-34, and G-35) that have higher values of Mg# (60–68), MgO (13–26 wt.%), Ni (260–470 ppm), and Cr (820–1750 ppm), which are characteristics of slightly differentiated cumulates.

In both groups, Ni and Cr decrease with decreasing Mg# (Figures 3(A) and 3(B)), suggesting they behaved as compatible elements, a scenario consistent with early crystallization of olivine and pyroxene as cumulate phases.

Incompatible elements, such as Zr and Nb, show a negative correlation with Mg# (Figures 3(C) and 3(D)) and

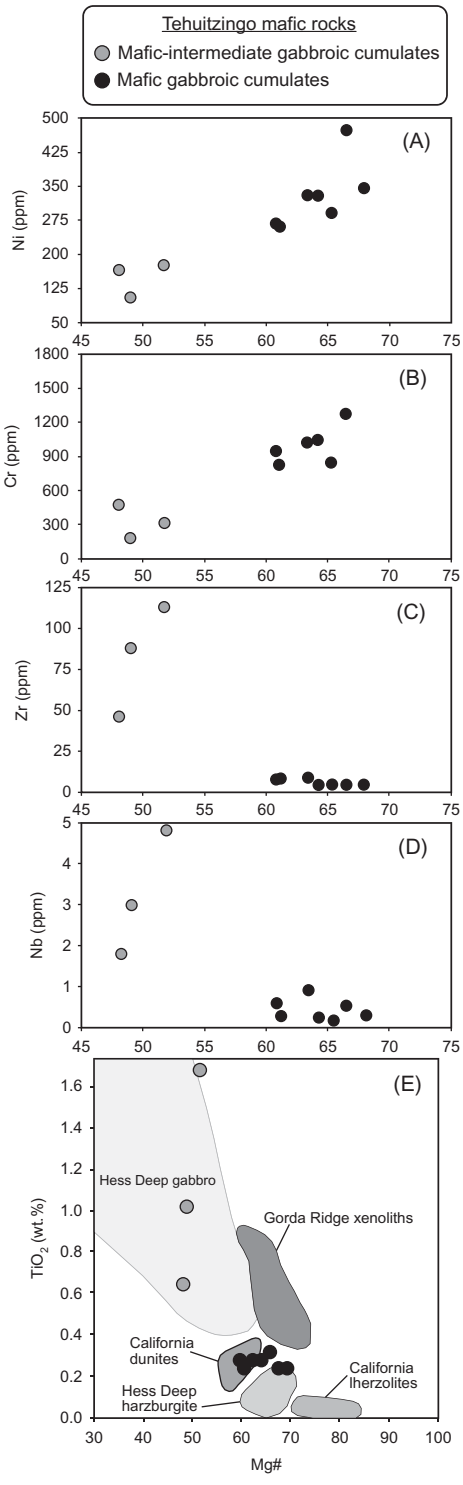

Figure 3. Mg# variation diagrams: (A) Mg# *versus* Ni; (B) Mg# *versus* Cr; (C) Mg# *versus* Zr; (D) Mg# *versus* Nb (wt.%); (E) Mg# *versus* TiO_2, where the Tehuitzingo mafic-intermediate gabbros fall in the Hess Deep gabbro cumulates field and the Tehuitzingo mafic gabbros fall between California and Hess Deep ultrabasic cumulates fields (after Davis *et al.* 2007). The mafic-intermediate gabbroic cumulates have lesser Mg#, Ni, and Cr content than mafic gabbroic cumulates and higher Zr, Nb, and Ti content. $Mg\# = 100^{*}MgO/(MgO + FeO^{t})$.

a positive correlation with TiO_2 (Figure 3(E)). The positive correlation of Zr with TiO_2, V, Y, and Nb (Figure 4) is consistent with the incompatible nature of these elements.

The Nb/Y *versus* Zr/TiO_2 diagram (Figure 5(A)) is based in ratios of incompatible elements with similar partition coefficients during fractionation of early crystallizing phases; therefore, it can be used reliably to provide an indication of magmatic affinity (Winchester and Floyd 1977). The Tehuitzingo cumulate rocks are characterized by low Nb/Y, which is typical of derivation from a subalkaline magma, and by low Zr/TiO_2, which indicates limited fractionation. The cumulate nature of the rocks precludes the use of the SiO_2 *versus* FeO^*/MgO or FeO^* *versus* FeO^*/MgO diagrams (Miyashiro 1974) to discriminate between tholeiitic and calc-alkaline magmas. However, their high Y/TiO_2 and low Zr/TiO_2 (Figure 5(B); after Lentz 1998) are characteristic of tholeiitic suites. The Ti *versus* V diagram (Figure 5(C); Shervais 1982) can be used reliably in cumulates to identify the tectonic setting because they are incompatible elements with similar partition coefficients and the discrimination between the various tectonic environments is based on the Ti/V ratios. The low Ti/V in Tehuitzingo mafic gabbroic cumulates and two of three mafic-intermediate gabbroic cumulate samples are typical of island arc tholeiites (IAT), the other sample plots in the back-arc field.

The primitive, mantle-normalized trace element and REE patterns in the Tehuitzingo cumulates display roughly flat profiles, suggesting derivation from a similar primitive spinel lherzolite (i.e. shallow) mantle source (Figure 6). The low concentrations of the incompatible trace elements and REE are attributed to the high proportion of cumulus minerals. The mafic rocks in other localities in the Acatlán Complex like Asís (Murphy *et al.* 2006), Xayacatlán, Patlanoaya, Cuaulote (Keppie *et al.* 2008a), and Olinalá (Ortega-Obregón *et al.* 2009) have distinctly different profiles in that they are richer in trace elements and display significant LREE enrichment relative to HREE, attributes interpreted to reflect a continental tholeiitic affinity.

In detail, the primitive mantle-normalized patterns of the Tehuitzingo mafic rocks show an enrichment in large ion lithophile elements (LILE), such as Rb and Ba, and a depletion in HFSE, such as Nb–Ta, Ti, Zr, and Hf (Figure 6(A)). These patterns suggest either derivation from mantle wedge (subduction) or some degree of crustal contamination. Zr and Hf negative anomalies probably reflect the volume of intercumulus liquid. The cumulates display two distinct types of REE patterns: (1) the mafic gabbroic patterns are typical of an olivine/pyroxene/plagioclase-rich cumulate, characterized by a distinct positive Eu anomaly, low REE abundances, and slightly depleted HREE relative to LREE (Figure 6(B)); and (2) the mafic-intermediate gabbroic cumulates exhibit very flat patterns, characteristic of olivine/clinopyroxene-rich early fractionation phases in

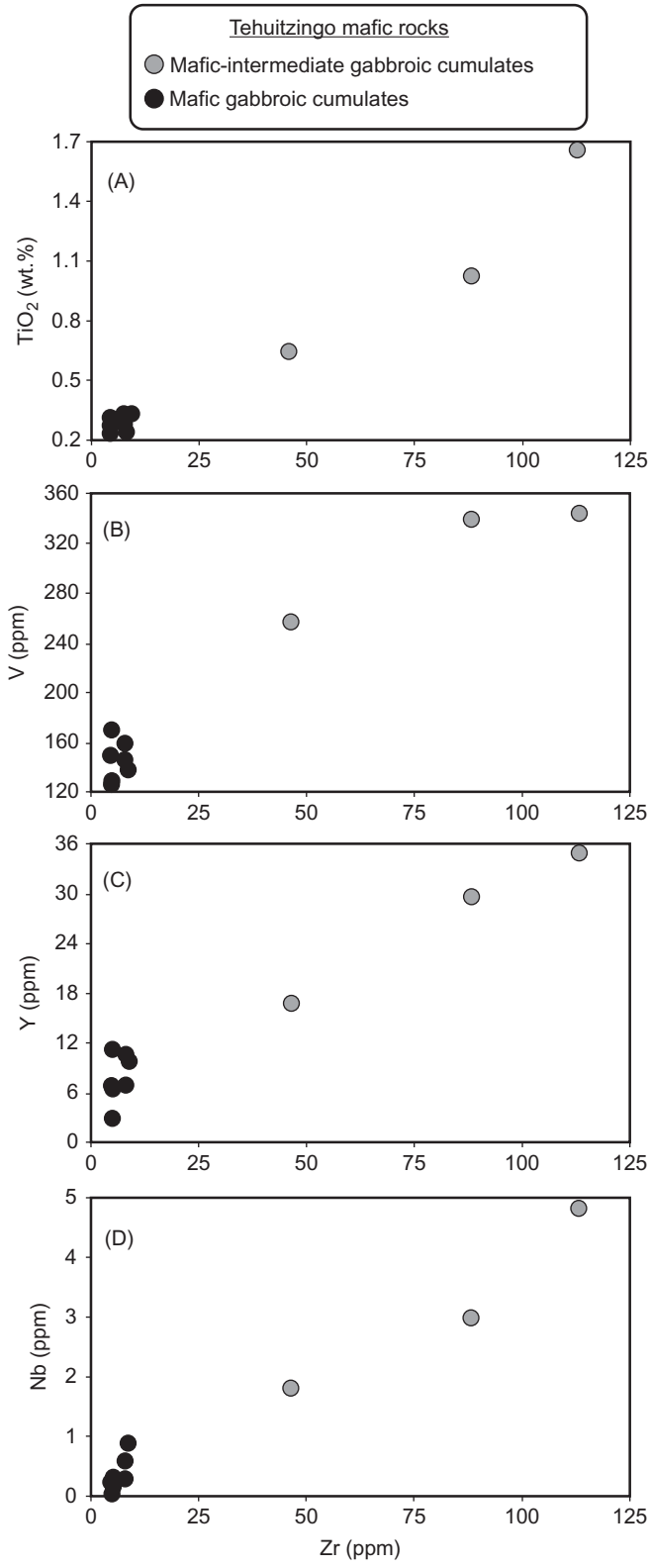

Figure 4. Zr variation diagrams: (A) Zr *versus* TiO_2; (B) Zr *versus* V; (C) Zr *versus* Y; (D) Zr *versus* Nb. The mafic-intermediate gabbroic cumulates have higher TiO_2, V, Y, and Nb content than the mafic gabbroic cumulates.

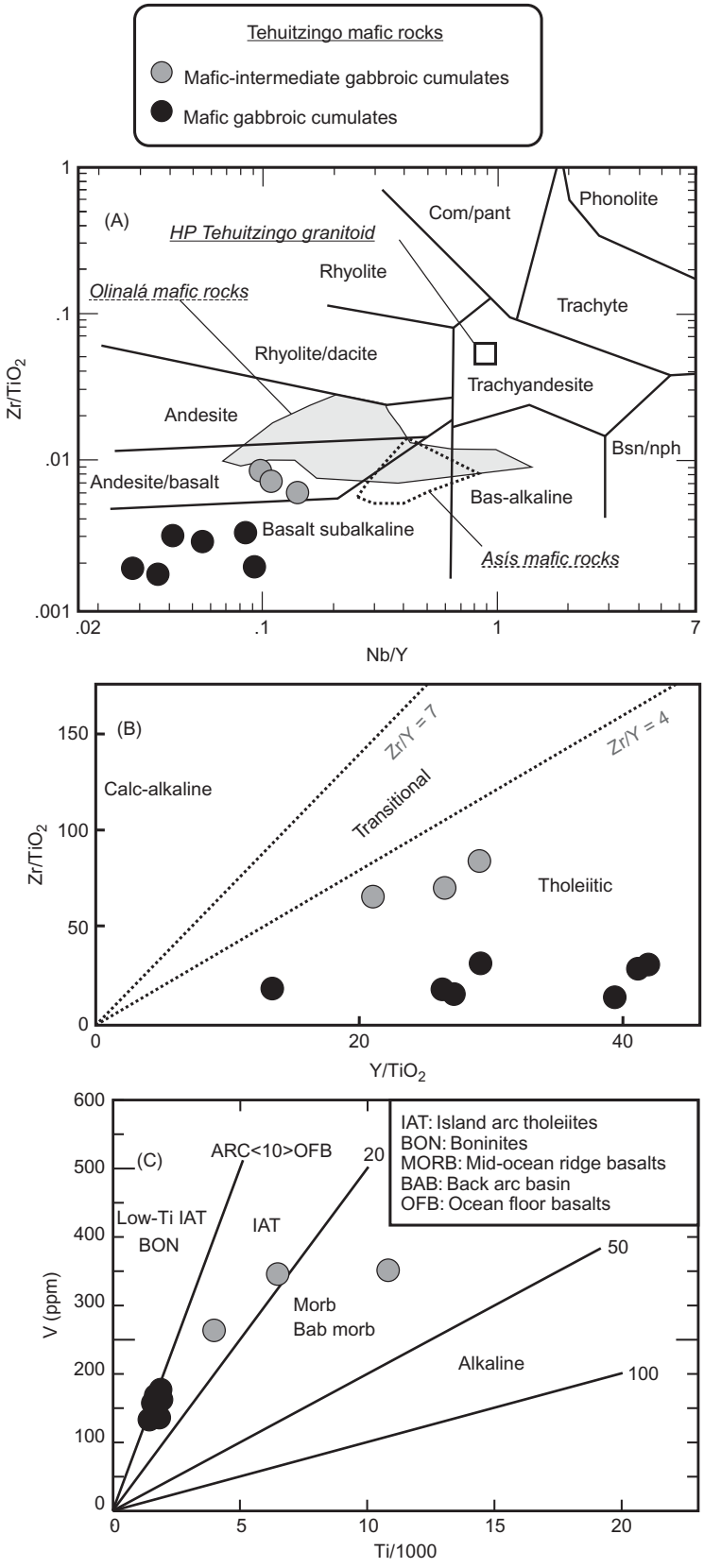

Figure 5. Classification of mafic rocks of the Acatlán Complex at Tehuitzingo plotted on (A) Nb/Y *versus* Zr/TiO_2 diagram (Winchester and Floyd 1977), where G-25, G-26, and G-27 samples fall in the intermediate subalkaline gabbros field and the others samples fall in the basic–ultrabasic subalkaline gabbros field; (B) Zr/TiO_2 *versus* Y/TiO_2 diagram (Lentz 1998); (C) Ti *versus* V diagram (Shervais 1982), where practically all cumulates fall in the island arc field, except for the G-25 sample, which falls in the back-arc field. FeO^* = total Fe as FeO.

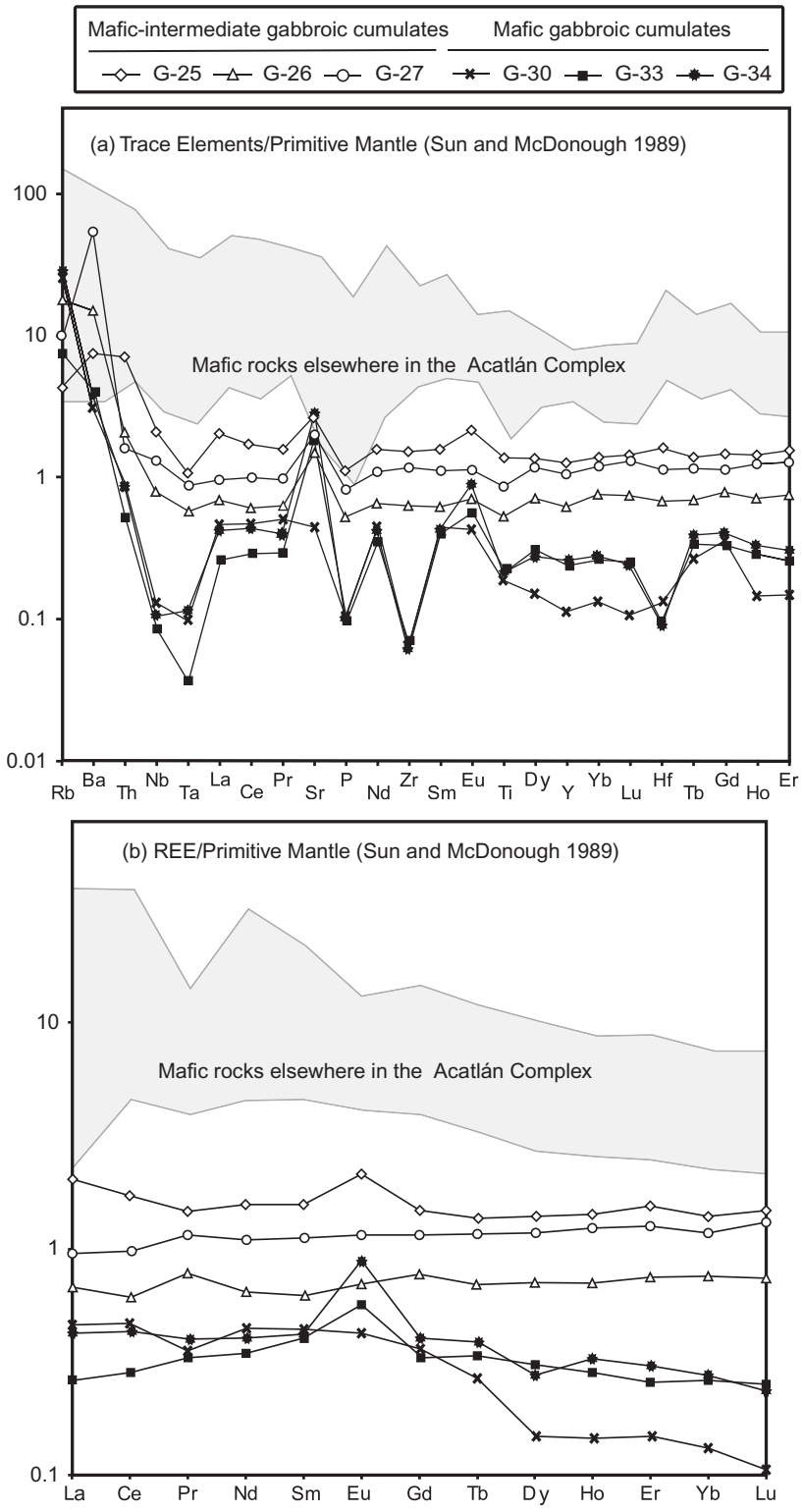

Figure 6. Tehuitzingo mafic cumulates (Piaxtla Suite) plotted on primitive mantle-normalized spider diagrams (Sun and McDonough 1989): (A) trace elements abundances, (B) rare earth elements abundances. The grey area shows other mafic rocks of the Acatlán Complex in Asís (Murphy *et al.* 2006), Xayacatlán, Patlanoaya, Cualote (Keppie *et al.* 2008a), and Olinalá (Ortega-Obregón *et al.* 2009).

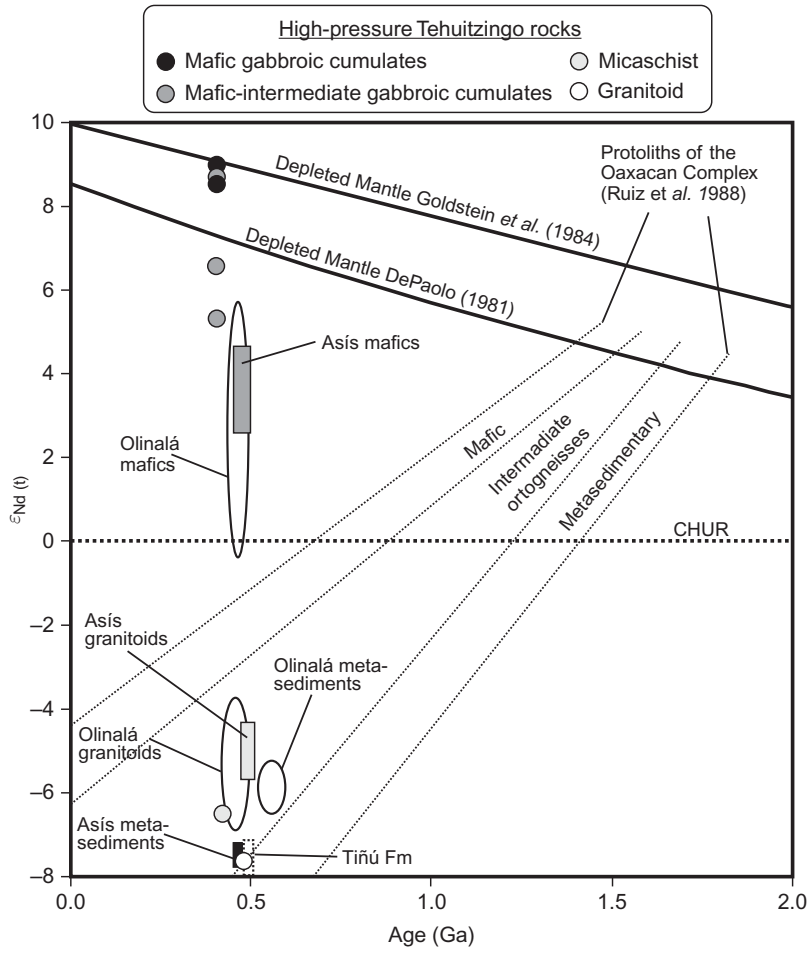

Figure 7. $\varepsilon_{Nd(t)}$ *versus* time diagram for the Tehuitzingo HP rocks compared with the Sm–Nd isotopic data from Asís (Murphy *et al.* 2006), Olinalá (Ortega-Obregón *et al.* 2009), and Oaxacan Complex (Ruiz *et al.* 1988). CHUR: Chondritic Uniform Reservoir (Jacobsen and Wasserburg 1980).

cumulates. Both REE patterns resemble the mafic plutonic rocks patterns of either ophiolitic complexes of modern oceanic environments or island arc tholeiitic basalts in immature oceanic arcs.

The Sm–Nd isotopic signature of Tehuitzingo cumulate samples has an $\varepsilon_{Nd(400\ Ma)}$ ranging from +5.37 to +8.57 (Figure 7) and high $^{147}Sm/^{144}Nd$ from 0.18 to 0.23, which renders calculations of model ages meaningless (Stern 2002). These high $\varepsilon_{Nd(t)}$ values are characteristic of juvenile magmas derived from a highly depleted mantle source and are typical of mafic complexes that are vestiges of the Rheic Ocean (Murphy *et al.* 2011). An exception is sample G-25, which has $\varepsilon_{Nd(t)}$ values similar to Asís mafic rocks. These data suggest that Tehuitzingo cumulates were derived from a highly depleted juvenile mantle source.

Granitoid rock

The HP granitoid is a syenodiorite of intermediate composition (Figure 5(A)) with SiO_2 content of ~59 wt.% (on a volatile-free basis; Table 2) and $Fe_2O_3{}^t/MgO = 2.81$. There is a clear chemical similarity between the Tehuitzingo granitoid with both the deformed and undeformed Ordovician granitoids within the Acatlan Complex (deformed: Esperanza type; Reyes-Salas 2003; Murphy *et al.* 2006; Keppie *et al.* 2008a; Ortega-Obregón *et al.* 2009) (undeformed: Palo Liso, La Noria, Zapote Negro, etc.; Miller *et al.* 2007; Hinojosa-Prieto *et al.* 2008) (Figure 8). The trace element patterns are very similar to those of upper continental crust (UCC), except for an enrichment in incompatible elements and marked Rb–Ba, Nb, Sr, and Ti depletions, which is typical of volcanic arc signatures (Figures 8(A) and 8(B)): this signature has been interpreted as inherited from a crustal source that was itself derived from a volcanic arc (Ortega-Obregón *et al.* 2009). REE patterns are characterized by relative LREE moderate enrichment, with (La/Sm)n = 2.5–5.3 (3.7 in Tehuitzingo granitoid), a flat HREE pattern with (Gd/Yb)n = 1.2–2.1 (2.1 in Tehuitzingo granitoid) and a moderate negative Eu anomaly (Figure 8(C)).

The Sm–Nd isotopic signature of Tehuitzingo granitoid has an $\varepsilon_{Nd(480\ Ma)} = -7.61$ (Figure 7), which is lower than

Table 2. Major and trace element analyses for Tehuitzingo HP rocks of the Acatlán Complex.

Sample	G-25 M-I. Cum.	G-26 M-I. Cum.	G-27 M-I. Cum.	G-28 M. Cum.	G-29 M. Cum.	G-30 M. Cum.	G-31 M. Cum.	G-33 M. Cum.	G-34 M. Cum.	G-35 M. Cum.	G-24 Granite	G-36 Mica-schist
SiO_2 (wt.%)	46.63	50.34	45.67	48.77	51.83	49.56	40.61	47.56	47.12	48.15	59.07	61.90
TiO_2	1.74	0.66	1.08	0.27	0.26	0.24	0.32	0.27	0.27	0.26	0.85	0.83
Al_2O_3	17.28	14.77	14.54	14.02	15.18	11.22	15.88	12.92	13.75	13.84	21.45	21.32
Fe_2O_3	9.66	10.19	13.45	8.26	7.22	7.35	10.51	7.88	8.13	7.92	7.05	7.80
MnO	0.12	0.15	0.20	0.13	0.11	0.13	0.17	0.13	0.13	0.13	0.08	0.06
MgO	12.19	10.99	15.44	15.04	13.26	17.95	25.52	17.15	16.98	16.01	2.51	2.46
CaO	9.29	9.48	6.73	11.53	8.45	11.00	5.52	11.33	10.83	10.88	0.35	0.19
Na_2O	2.69	3.08	2.18	1.26	3.12	2.33	0.77	2.55	2.46	2.51	7.74	0.92
K_2O	0.11	0.23	0.17	0.60	0.51	0.24	0.12	0.23	0.29	0.23	0.87	4.14
P_2O_5	0.13	0.06	0.10	0.01	0.01	0.01	0.03	0.01	0.01	0.01	0.03	0.15
L.O.I.	3.88	2.94	5.29	3.56	3.18	1.95	7.39	1.94	2.71	3.07	2.42	5.25
Total	100.01	99.99	100.01	100.01	100.00	100.00	99.99	99.98	100.01	100.00	100.00	100.00
V (ppm)	345.50	258.40	340.70	161.00	147.70	128.10	171.80	131.00	151.40	140.10	323.10	191.90
Cr	312.80	468.50	183.20	943.70	821.20	1753.70	1271.90	841.60	1041.00	1017.80	86.40	103.10
Co	45.90	37.80	42.30	47.40	44.50	49.40	78.60	54.40	54.10	56.10	11.10	10.60
Zr	113.00	46.22	88.01	7.80	7.80	4.68	4.70	4.77	4.47	8.50	333.78	178.23
Ba	47.67	93.12	335.95	185.90	157.60	19.25	14.10	25.25	23.51	37.30	785.22	938.23
La	5.05	1.70	2.38	3.70	0.70	1.15	2.00	0.65	1.06	3.10	52.15	41.83
Nd	11.50	4.71	7.96	1.60		3.28	1.40	2.52	2.94	1.20	49.87	36.88
Ni	175.20	165.90	103.90	267.50	260.70	345.90	472.00	290.80	328.70	329.60	46.20	42.10
Cu	103.40	36.90	165.70	6.80	4.30	5.90	5.30	10.10	5.30	6.60	52.00	57.40
Zn	64.20	76.40	81.60	61.70	58.30	39.10	54.80	37.40	40.80	38.30	74.20	107.20
Ga	17.30	12.10	16.10	12.50	10.10	3.70	8.30	6.60	6.30	8.50	18.50	29.20
Rb	2.40	10.30	5.20	27.50	22.00	14.50	6.10	4.20	16.00	8.50	52.80	210.80
Sr	238.50	132.30	181.70	215.60	101.40	39.90	10.50	166.90	253.40	303.70	51.00	80.40
Y	35.10	17.04	29.83	10.90	7.20	3.15	11.50	6.77	7.14	10.50	23.01	32.77
Nb	4.84	1.82	3.00	0.60	0.30	0.30		0.19	0.25	0.90	24.35	24.66
Pb	16.80	14.10	16.90	13.80	10.90	15.20	8.60	4.80	5.00	7.70	22.00	29.90
Th	0.85	0.25	0.19		3.80	0.11	6.50	0.06	0.10		17.14	13.93
U		0.10	1.10		2.60	1.40		5.20		3.50	2.60	6.50
Ce	12.94	4.59	7.34			3.50		2.14	3.28		105.26	83.98
Pr	2.06	0.82	1.28			0.66		0.38	0.52		12.53	9.65
Sm	4.11	1.63	2.93			1.17		1.07	1.11		9.22	7.77
Eu	2.19	0.71	1.17			0.43		0.57	0.90		1.76	1.43
Gd	5.36	2.86	4.24			1.31		1.23	1.48		6.80	6.42
Tb	0.92	0.46	0.78			0.18		0.23	0.26		0.93	1.01
Dy	6.24	3.21	5.31			0.68		1.39	1.26		5.24	6.21
Ho	1.42	0.71	1.24			0.15		0.29	0.33		1.08	1.26
Er	4.57	2.23	3.76			0.45		0.77	0.91		2.77	3.81
Tm	0.67	0.32	0.58			0.07		0.13	0.10		0.42	0.53
Yb	4.23	2.30	3.59			0.40		0.80	0.84		2.65	3.81
Lu	0.67	0.34	0.60			0.05		0.11	0.11		0.34	0.56
Hf	3.28	1.39	2.35			0.27		0.20	0.19		6.86	3.76
Ta	0.14	0.07	0.11			0.01		0.00	0.02		1.51	0.89
Cs			2.40	2.00	3.80	8.60	4.30		14.00	5.50	13.30	14.80

Notes: M-I. Cum.: mafic-intermediate gabbroic cumulate; M. Cum.: mafic gabbroic cumulate; wt.%: weight percent; ppm: parts per million; and L.O.I.: Lost on ignition.

those obtained in Asís and Olinalá, but close to the values of the sedimentary Tiñú Formation (Oaxacan Complex). The model age (T_{DM} = 1.76 Ga) is similar to the Tiñu Formation (1.83–1.50 Ga), as well as the granitoids in Asís (1.80–1.50 Ga) and Olinalá (1.29–1.10 Ga). The contemporaneity between the Tehuitzingo granitoid (488–479 Ma; Galaz *et al.* 2013) and the Ordovician deformed and undeformed granitoids of the complex (ca. 480–440 Ma; Ortega-Gutiérrez *et al.* 1999; Sánchez-Zavala *et al.* 2004; Talavera-Mendoza *et al.* 2005; Murphy *et al.* 2006; Miller *et al.* 2007) suggests a common derivation from an ancient Mesoproterozoic basement, possibly the Oaxacan Complex (c.f. Murphy *et al.* 2006; Ortega-Obregón *et al.* 2009).

Metasedimentary rock

The HP mica-schist has a SiO_2 content of ~62 wt.%, Al_2O_3 of ~21 wt.%, and Fe_2O_3 of ~7.8 wt.% (on a

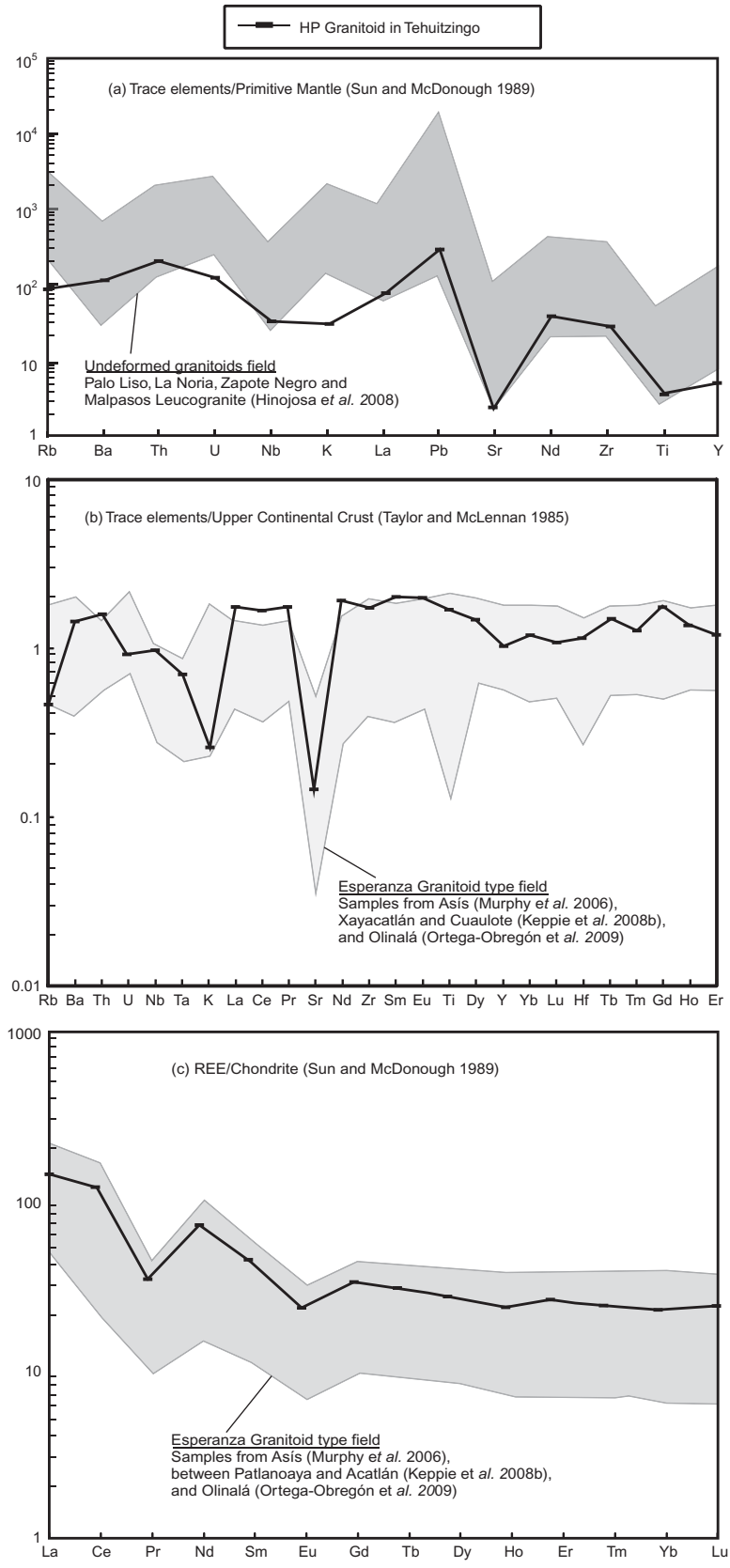

Figure 8. Tehuitzingo granitoid spider diagrams compared with other granitoids of the Acatlán Complex: (A) trace elements abundances primitive mantle-normalized (Sun and McDonough 1989); (B) trace elements abundances upper continental crust-normalized (Taylor and McLennan 1985); (C) rare earth elements abundances chondrite-normalized (Sun and McDonough 1989).

volatile-free basis; Table 2). Elements such as Al and Ti are stable during weathering and can be used to differentiate sedimentary sources. The Al_2O_3/TiO_2 ratio of ~27 is typical of a combined granitic and sedimentary source (Girty *et al.* 1996), whereas Zr–Al–Ti relative abundances are consistent with derivation from strongly peraluminous granites (Garcia *et al.* 1994) (Figure 9(A)).

Some trace elements, such as La, Th, Hf, and Cr, are stable during weathering and are therefore helpful in the discrimination of the sediment source. The ratio Cr/Th = 7.4 is within the range 2.5–17.5, which is typical of sediments derived from felsic source (Cullers 1994). On the other hand, in the binary diagram La/Th *versus* Hf (Floyd and Leveridge 1987), the mica-schist falls in the field of sediment derived from a mixture of sources of felsic and mafic compositions (Figure 9(B)). The mafic component is also supported by the high La/Th (~3), low Zr/Co (~17), and low Th/Yb (~4) in the Tehuitzingo

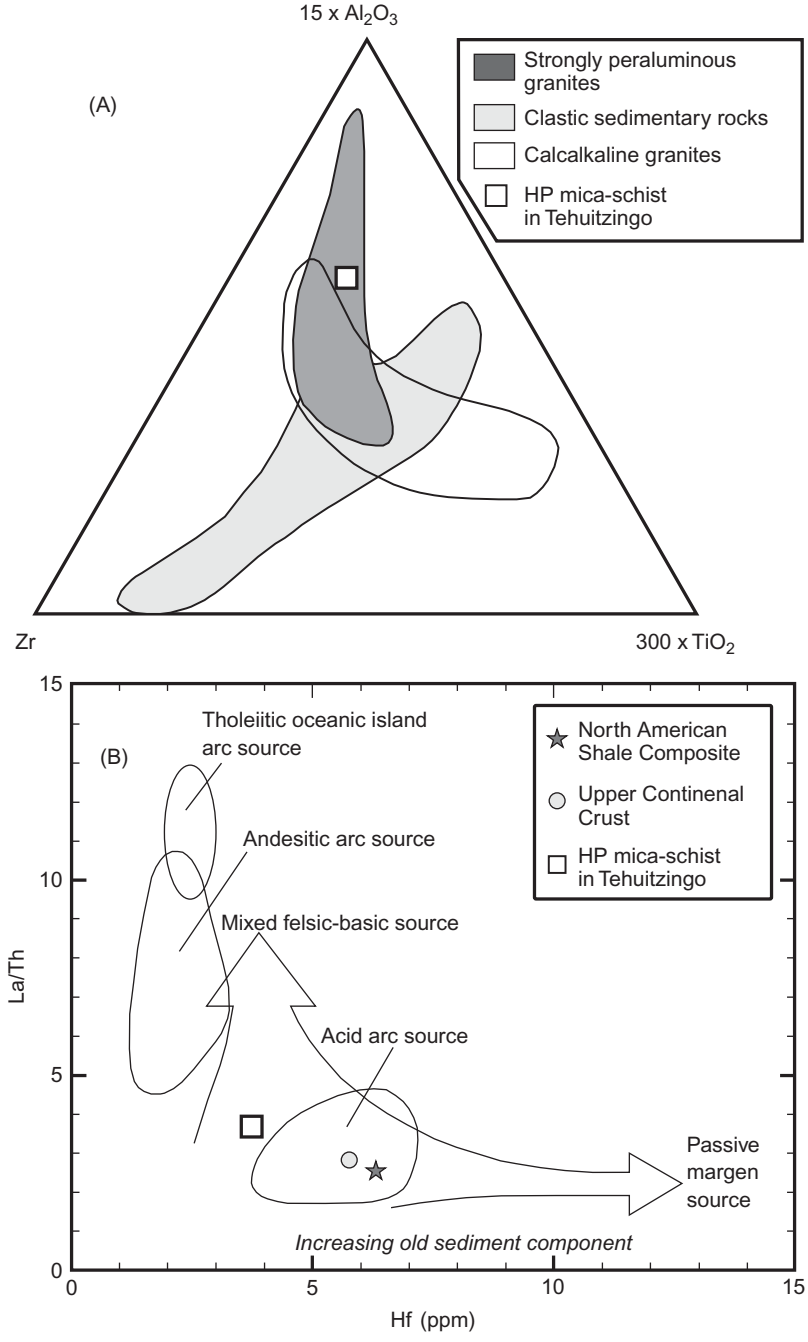

Figure 9. Tehuitzingo mica-schist source discrimination diagrams: (A) Zr–Al_2O_3(× 15)–TiO_2(× 300) diagram (Garcia *et al.* 1994); (B) Hf *versus* La/Th diagram (Floyd and Leveridge 1987).

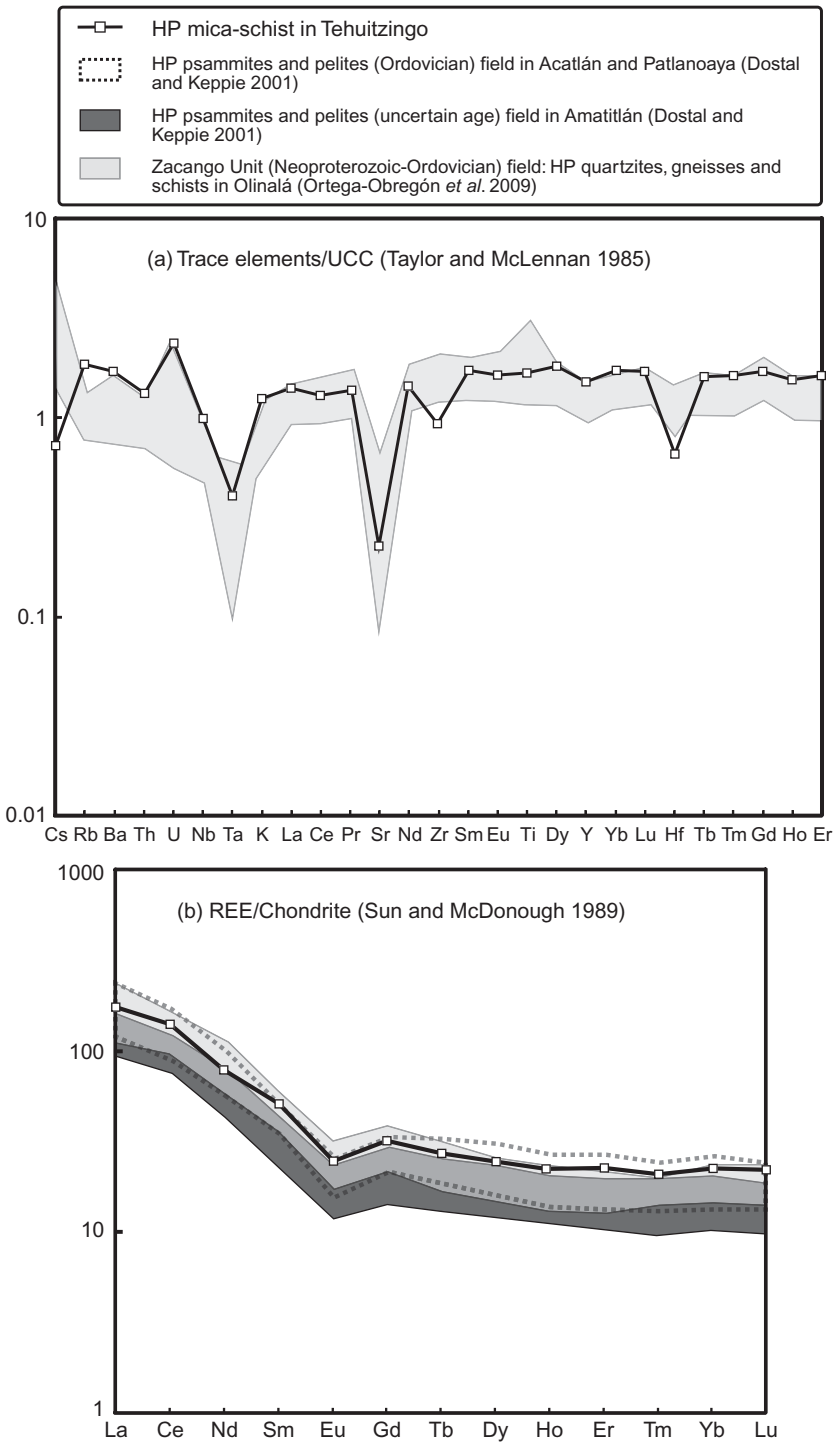

Figure 10. Tehuitzingo mica-schist spider diagrams compared with others sedimentary rocks of the Acatlán Complex: (A) trace elements abundances upper continental crust-normalized (Taylor and McLennan 1985); (B) rare earth elements abundances chondrite-normalized (Sun and McDonough 1989).

mica-schist (e.g. McLennan *et al.* 1980). The trace element UCC-normalized pattern (Figure 10(A)) is similar to sedimentary rocks at Olinalá and are characterized by enrichment in incompatible trace elements such as Rb, Ba, U, and LREE (e.g. La and Sm) relative to HFSE and HREE and pronounced negative Ni–Ta anomalies, characteristics of crustal rocks (Taylor and McLennan 1985). The REE chondrite-normalized pattern (Figure 10(B)) is

similar to sedimentary rocks of the Acatlán Complex in Olinalá, Patlanoaya, Xayacatlán, Matamoros, Amatitlán, Pitayo, and Acatlán (Dostal and Keppie 2009; Ortega-Obregón *et al.* 2009), showing LREE enrichment and a flat HREE pattern, with values of (La/Sm)n = 3.5 and (La/Yb)n = 7.9, suggesting derivation from a fractionated source rock. The moderate negative Eu anomaly (Eu/Eu* = 0.62) reflects either weathering of plagioclase in the source rock or derivation from a source rock that was fractionated with respect to plagioclase.

The Sm–Nd isotopic signature of Tehuitzingo mica-schist has an $\varepsilon_{Nd(430\ Ma)} = -6.43$, which is higher than those obtained from similar sedimentary rocks in Asís, lower than Olinalá, but consistent with migmatized metasedimentary rocks of Asís (Figure 7). The $^{147}Sm/^{144}Nd$ of 0.12 is similar to pelites–psammites (0.12–0.13) and migmatized sediments (0.11–0.12) at Asís (Murphy *et al.* 2006). The model age (T_{DM} = 1.69 Ga) is consistent with both pelites–psammites and migmatized sediment at Asís (1.86–1.68 and 1.73–1.45 Ga, respectively; Murphy *et al.* 2006), but higher than those obtained in Olinalá (1.62–1.52 Ga; Ortega-Obregón *et al.* 2009). These values are typical of a Mesoproterozoic continental crust source, such as the adjacent Oaxacan Complex, an interpretation supported by the similarity between the REE patterns of pelite–psammite elsewhere in the Acatlan Complex and the Tehuitzingo mica-schist (Dostal and Keppie 2009). Therefore, the possible sources are the recycled sediments of the Oaxacan Complex (ca. 1 Ga), the mafic–ultramafic rocks of the Piaxtla Suite, as well as the widely distributed Ordovician megacrystic granitoids in the Acatlán Complex. Consistent with these potential sources is the presence of 480–460 Ma and ca. 1.0 Ga detrital zircons populations in the mica-schist (Galaz *et al.* 2013).

Discussion

The investigated mafic rocks can be divided into two groups: (1) mafic-intermediate gabbroic cumulates with some degree of crustal contamination and (2) poorly differentiated mafic gabbroic cumulates. Trace elements and REE primitive mantle-normalized patterns suggest that they were derived from a primitive mantle source. These rocks display two distinct types of REE patterns that can be attributed to different bulk compositions: (1) gabbroic rocks with geochemical patterns typical of olivine/pyroxene/plagioclase-rich cumulates and (2) mafic-intermediate rocks with patterns characteristic of olivine/clinopyroxene-rich cumulates.

Our new petrological and geochemical data indicate that the Tehuitzingo cumulates are island arc tholeiitic basalts with features typical of the forearc of immature

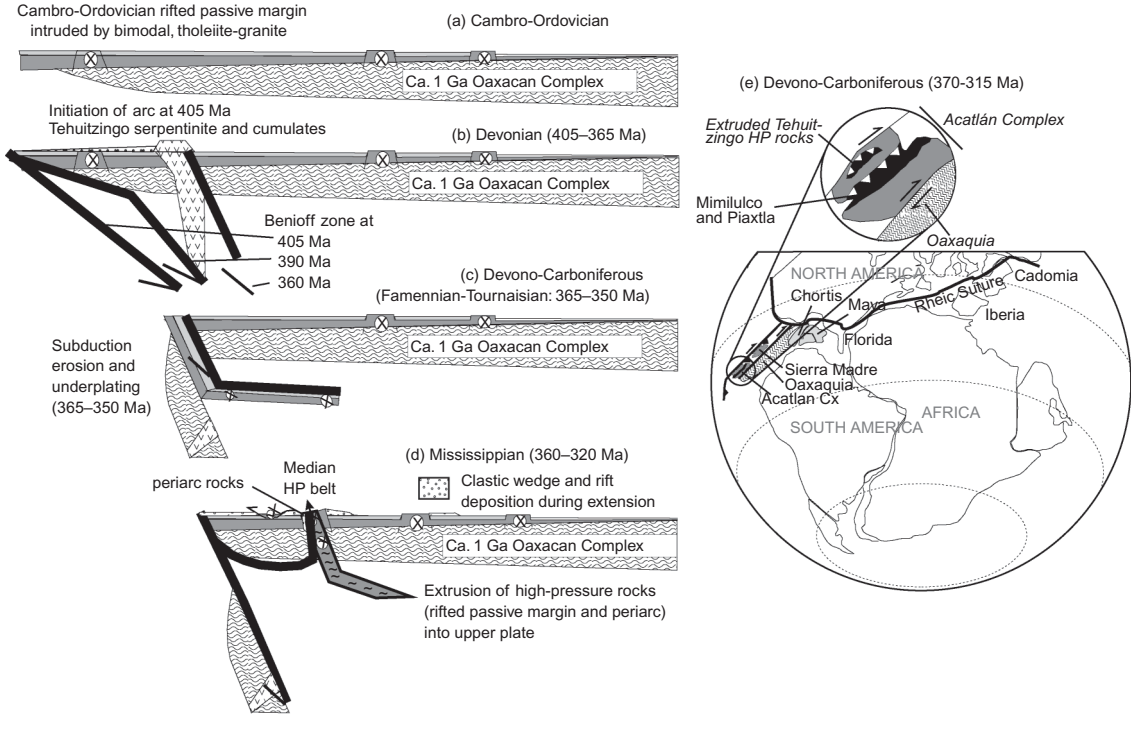

Figure 11. Acatlán Complex, Cambrian to Carboniferous, evolutionary model (modified after Keppie *et al.* 2012): (A) Cambro–Ordovician rifted passive margin intruded by bimodal rift-tholeiites, mafic rocks, and granitoids; (B) Devonian magmatic island arc represented by the Tehuitzingo serpentinite and cumulates; (C) Devono–Carboniferous subduction–erosion, underplating and HP metamorphism of the subducted rocks; (D) Mississippian extrusion of the HP rocks by a west-vergent klippe; (E) palaeogeographic reconstruction showing location of Tehuitzingo mafic rocks on the western margin of Pangea.

arc complexes in modern oceanic environments. Trace element patterns suggest modest subduction zone enrichment and/or crustal contamination. This conclusion is consistent with PGE and Au concentrations in serpentinites and associated chromitite bodies of the Tehuitzingo Serpentinite, which are interpreted to reflect an oceanic lithospheric fragment formed in a peri-arc environment (Proenza *et al.* 2004). To date, the only evidence of an arc in the Acatlán Complex is the presence of igneous detrital zircons that range in age from 405 to 330 Ma (Keppie *et al.* 2012). Keppie *et al.* (2011, 2012) proposed that the arc was removed by subduction erosion during the Late Devonian–early Carboniferous and was tectonically extruded into the Acatlán Complex in Mississippian time. In this scenario, the Tehuitzingo arc rocks could represent an extruded part of the missing arc (Figure 11), an interpretation consistent with the model of Keppie *et al.* for the Acatlán Complex, rather than the collisional or multi-collisional models previously proposed (Ortega-Gutiérrez *et al.* 1999; Talavera-Mendoza *et al.* 2005; Vega-Granillo *et al.* 2007, 2009).

The petrological, geochemical, U–Pb, and Nd isotopic data suggest that the Tehuitzingo granite may be correlated with both the Ordovician deformed (Esperanza type) and undeformed granitoids, which are widespread in the Acatlán Complex. These plutons share a common derivation from an ancient Mesoproterozoic basement, possibly the Oaxacan Complex, and their association with within-plate mafic rocks suggests they are part of a rift-related bimodal suite (Keppie *et al.* 2008a,b). Similarly, the associated mica-schist may be correlated with pre-Ordovician low-grade and HP sedimentary rocks (ca. 700–470 Ma) elsewhere in the Acatlán Complex and were derived from a mixture of mafic and felsic sources. These sources probably include mafic–ultramafic rocks of the Piaxtla Suite and either megacrystic granitoids (Acatlán Complex) and/or recycled sediments of the Oaxacan Complex.

Acknowledgements

This study was financed through projects PAPIIT N° IN100108-3, CONACYT N° CB-2005-1:24894, an NSERC Discovery Grant to J.B. Murphy, and is a contribution to IGCP 597. A CONACyT scholarship supported the studies of G. Galaz. Valuable comments were provided by Dr F. Ortega (UNAM) and Dr J. Dostal (St. Mary's University). Field assistance was provided by B. Ortega, D. Bolaños, M. Ramos, F. Durán, and C. Ortega (UNAM).

References

Ayer, J.A., and Davis, D.W., 1997, Neoarchean evolution of differing convergent margin assemblages in the Wabigoon Subprovince: Geochemical and geochronological evidence from the Lake of the Woods greenstone belt, Superior Province, Northwestern Ontario: Precambrian Research, v. 81, p. 155–178.

Butler, J.P., Beaumont, C., and Jamieson, R.A., 2011, Crustal emplacement of exhuming (ultra) high–pressure rocks: Will that be pro- or retro-side?: Geology, v. 39, p. 635–638.

Calderón-García, A., 1956, Estratigrafía del Mesozoico y tectónica del sur del Estado de Puebla, México, *in* Congreso Geológico Internacional, 20th, México D. F., Libro-guía de la excursión A-11, p. 9–33.

Cerca, M., Ferrari, L., López-Martínez, M., Martiny, B., and Iriondo, A., 2007, Late Cretaceous shortening and early Tertiary shearing in the central Sierra Madre del Sur, southern México: Insights into the evolution of the Caribbean–North American plate interaction: Tectonics, v. 26, p. 1–34. doi:10.1029/2006TC001981.

Cullers, R.L., 1994, The controls on the major and trace element variation of shale, siltstone and sandstone of Pennsylvanian–Permian age from uplifted continental blocks in Colorado to platform sediment in Kansas, USA: Geochimica et Cosmochimica Acta, v. 58, p. 4955–4972.

Davis, A.S., Clague, D.A., and Paduan, J.B., 2007, Diverse Origins of Xenoliths from Seamounts at the Continental Margin, Offshore Central California: Journal of Petrology, v. 48, no. 5, p. 829–852.

DePaolo, D., 1981, Trace element and isotopic effects of combined wallrock assimilation and fractional crystallization: Earth and Planetary Science Letters, v. 53, p. 189–202.

DePaolo, D.J., 1988, Age dependence of the composition of continental crust as determined from Nd isotopic variations in igneous rocks: Earth and Planetary Science Letters, v. 59, p. 263–271.

Dostal, J., Dupuy, C., and Caby, R., 1994, Geochemistry of the Neoproterozoic Tilemsi belt of Iforas (Mali, Sahara): A crustal section of an oceanic island arc: Precambrian Research, v. 65, p. 55–69.

Dostal, J., and Keppie, J.D., 2009, Geochemistry of low-grade clastic rocks in the Acatlán Complex of southern Mexico: Evidence for local provenance in felsic-intermediate igneous rocks: Sedimentary Geology, v. 222, p. 241–253.

Elías-Herrera, M., and Ortega-Gutiérrez, F., 2002, Caltepec fault zone: An Early Permian dextral transpressional boundary between the Proterozoic Oaxacan and Paleozoic Acatlán complexes, southern México, and regional implications: Tectonics, v. 21, no. 3, p. 220–234.

Ernst, W.G., 2010, Subduction-zone metamorphism, calc–alkaline magmatism, and convergent-margin crustal evolution: Gondwana Research, v. 18, p. 8–16. doi:10.1016/j.gr.2009.05.010.

Floyd, P.A., and Leveridge, B.E., 1987, Tectonic environment of the Devonian Gramscatho basin, south Cornwall: Framework mode and geochemical evidence from turbiditic sandstone: Journal of Geological Society (London), v. 144, p. 531–542.

Galaz, G., Keppie, J.D., Lee, J.K.W., and Ortega-Rivera, A., 2013, A high-pressure folded klippe at Tehuitzingo on the western margin of an extrusion zone, Acatlán Complex, southern México: Gondwana Research, v. 23, p. 641–660.

Garcia, D., Fonteilles, M., and Moutte, J., 1994, Sedimentary fractionation between Al, Ti, and Zr and the genesis of strongly peraluminous granites: Journal of Geology, v. 102, p. 411–422.

Girty, G.H., Ridge, D.L., Knaack, C., Johnson, D., and Al-Riyami, R.K., 1996, Provenance and depositional setting of Paleozoic chert and argillite, Sierra Nevada, California: Journal of Sedimentary Research, v. 66, p. 107–118.

Goldstein, S.L., O'Nions, R.K., and Hamilton, P.J., 1984, A Sm–Nd isotopic study of atmospheric dusts and particulates from major river system: Earth and Planetary Science Letters, v. 70, p. 221–236.

Hinojosa-Prieto, H.R., Nance, R.D., Keppie, J.D., Dostal, J.V., Ortega-Rivera, A., and Lee, J.K.W., 2008, Ordovician and Late Paleozoic–Early Mesozoic tectonothermal history of the La Noria area, northern Acatlán Complex, southern México: Record of convergence in the Rheic and paleo-Pacific Oceans: Tectonophysics, v. 461, p. 324–342.

Jacobsen, S.B., and Wasserburg, G.J., 1980, Sm–Nd evolution of chondrites: Earth and Planetary Science Letters, v. 50, p. 139–155.

Keppie, J.D., Dostal, J., Miller, B.V., Ramos-Arias, M.A., Morales-Gámez, M., Nance, R.D., Murphy, J.B., Ortega-Rivera, A., Lee, J.W.K., Housh, T., and Cooper, P., 2008a, Ordovician-earliest Silurian rift tholeiites in the Acatlán Complex, southern México: Evidence of rifting on the southern margin of the Rheic Ocean: Tectonophysics, v. 461, p. 130–156.

Keppie, J.D., Dostal, J., Murphy, J.B., Galaz-Escanilla, G., Ramos-Arias, M.A., and Nance, R.D., 2012, High pressure rocks of the Acatlán Complex, southern Mexico: Large-scale subducted Ordovician rifted passive margin extruded into the upper plate during the Devonian–Carboniferous: Tectonophysics, v. 560–561, p. 1–21.

Keppie, J.D., Dostal, J., Murphy, J.B., and Nance, R.D., 2008b, Synthesis and tectonic interpretation of the westernmost Paleozoic Variscan orogen in southern México: From rifted Rheic margin to active Pacific margin: Tectonophysics, v. 461, p. 277–290.

Keppie, J.D., Nance, R.D., Dostal, J., Lee, J.K.W., and Ortega-Rivera, A., 2011, Constraints on the subduction erosion/extrusion cycle in the Paleozoic Acatlán Complex of southern México: Geochemistry and geochronology of the type Piaxtla Suite: Gondwana Research, v. 21, p. 1050–1065. doi:10.1016/j.gr.2011.07.020.

Keppie, J.D., Nance, R.D., Murphy, J.B., and Dostal, J., 2010, The high-pressure Iberian–Czech belt in the Variscan orogen: Extrusion into the upper (Gondwanan) plate?: Gondwana Research, v. 17, p. 306–316. doi:10.1016/j.gr.2009.08.007.

Kerr, A., Jenner, G.A., and Fryer, B.J., 1995, Sm–Nd isotopic geochemistry of Precambrian to Paleozoic granitoid suites and the deep-crustal structure of the southeast margin of the Newfoundland Appalachians: Canadian Journal of Earth Sciences, v. 32, p. 224–245.

Lentz, D.R., 1998, Petrogenetic evolution of felsic volcanic sequences associated with Phanerozoic volcanic-hosted massive sulphide systems: The role of extensional geodynamics: Ore Geology Reviews, v. 12, p. 289–327.

Liou, J.G., Tsujimori, T., Zhang, R.Y., Katayama, I., and Maruyama, S., 2004, Global UHP metamorphism and continental subduction/collision: The Himalayan mode: International Geology Review, v. 46, p. 1–27.

McLennan, S.M., Nance, W.B., and Taylor, S.R., 1980, Rare earth element–thorium correlations in sedimentary rocks and the composition of the continental crust: Geochimica et Cosmochimica Acta, v. 44, p. 1833–1839.

Meza-Figueroa, D., Ruiz, J., Talavera-Mendoza, O., and Ortega-Gutiérrez, F., 2003, Tectonometamorphic evolution of the Acatlán Complex eclogites (southern México): Canadian Journal of Earth Sciences, v. 40, p. 27–44.

Meza-Figueroa, D.M., 1998, Geochemistry and characterization of intermediate temperature eclogites from the Acatlán complex, southern México [Ph.D. thesis]: Tucson, University of Arizona, 201 p.

Miller, B.V., Dostal, J., Keppie, J.D., Nance, R.D., Ortega-Rivera, A., and Lee, J.K.W., 2007, Ordovician calc-alkaline granitoids in the Acatlán Complex, southern México: Geochemical and geochronologic data and implications for the tectonics of the Gondwanan margin of the Rheic Ocean, *in* Linnemann, U., Nance, R.D., Kraft, P., and Zulauf, G., eds. The evolution of the Rheic Ocean: From Avalonian–Cadomian active margin to Alleghenian–Variscan collision: Geological Society of America, Special Paper 423, p. 465–475.

Miyashiro, A., 1974, Volcanic rock series in island arcs and active continental margins: American Journal of Science, v. 274, p. 321–355.

Morales-Gámez, M., Keppie, J.D., and Dostal, J., 2009, Carboniferous tholeiitic dikes in the Salada unit, Acatlán Complex, southern México: A record of extension on the western margin of Pangea: Revista Mexicana de Ciencias Geológicas, v. 26, no. 1, p. 133–142.

Murphy, J., Coussens, B., Braid, J., Strachan, R., Dostal, J., Keppie, J., and Nance, R., 2011, Highly depleted oceanic lithosphere in the Rheic Ocean: Implications for Paleozoic plate reconstructions: Lithos, v. 123, p. 165–175.

Murphy, J.B., Keppie, J.D., Nance, R.D., Miller, B.V., Dostal, J., Middleton, M., Fernández-Suárez, J., Jeffries, T.E., and Storey, C.D., 2006, Geochemistry and U–Pb protolith ages of eclogitic rocks of the Asís Lithodeme, Piaxtla Suite, Acatlán Complex, southern México: Tectonothermal activity along the southern margin of the Rheic Ocean: Journal of the Geological Society, v. 163, p. 683–695.

Ortega-Gutiérrez, F., Elías-Herrera, M., Reyes-Salas, M., Macías-Romo, C., and López, R., 1999, Late Ordovician–Early Silurian continental collisional orogeny in southern México and its bearing on Gondwana–Laurentia connections: Geology, v. 27, no. 8, p. 719–722.

Ortega-Obregón, C., Murphy, J.B., and Keppie, J.D., 2009, Geochemistry and Sm–Nd isotopic systematics of Ediacaran–Ordovician, sedimentary and bimodal igneous rocks in the western Acatlán Complex, southern México: Evidence for rifting on the southern margin of the Rheic Ocean: Lithos, v. 114, p. 155–167.

Pearce, J.A., 1996, A user's guide to basalt discrimination diagrams, *in* Wyman, D.A., ed. Trace element geochemistry of volcanic rocks: Applications for massive sulphide exploration: Geological Association of Canada, Short Course Notes, no. 12, p. 79–113.

Proenza, J.A., Ortega-Gutiérrez, F., Camprubí, A., Trilla, J., Elías-Herrera, M., and Reyes-Salas, M., 2004, Paleozoic serpentinite-enclosed chromitites from Tehuitzingo (Acatlán Complex, southern México): A petrological and mineralogical study: Journal of South American Earth Sciences, v. 16, p. 649–666.

Ramos-Arias, M.A., Keppie, J.D., Lee, J.W.K., and Ortega-Rivera, A., 2012, A Carboniferous high-pressure klippe in the western Acatlán Complex of southern México: Implications for the tectonothermal development and paleogeography of Pangea: International Geology Review, v. 54, p. 1–20. doi: 10.1080/00206814.2011.580634.

Ramos-Arias, M.A., Keppie, J.D., Ortega-Rivera, A., and Lee, J.W.K., 2008, Extensional Late Paleozoic deformation on the western margin of Pangea, Patlanoaya area, Acatlán Complex, southern México: Tectonophysics, v. 448, p. 60–76.

Reyes-Salas, M.A., 2003, Mineralogía y petrología de los Granitoides Esperanza del Complejo Acatlán, sur de México, [Ph.D. thesis]: Cuernavaca, Morelos, Universidad Autónoma del Estado de Morelos, 165 p.

Ruiz, J., Patchett, P.J., and Ortega-Gutiérrez, F., 1988, Proterozoic and Phanerozoic basement terranes of México from Nd isotopic studies: Geological Society of America Bulletin, v. 100, p. 274–281.

Sánchez-Zavala, J.L., Jenner, G.A., Belousova, E., and Macías-Romo, C., 2004, Ordovician and Mesoproterozoic zircons from the Tecomate Formation and Esperanza Granitoids, Acatlán Complex, Southern México: Local provenance in the Acatlán and Oaxacan complexes: International Geology Review, v. 46, p. 1005–1021.

Shervais, J.W., 1982, Ti–V plots and the petrogenesis of modern and ophiolitic lavas: Earth and Planetary Science Letters, v. 59, no. 1, p. 101–118.

Stern, R.J., 2002, Crustal evolution in the East African Orogen: A neodymium isotopic perspective: Journal of African Earth Sciences, v. 34, no. 3–4, p. 109–117.

Stöckhert, B., and Gerya, T.V., 2005, Pre-collisional high pressure metamorphism and nappe tectonics at active continental margins: A numerical simulation: Terra Nova, v. 17, p. 102–110.

Sun, S.S., and McDonough, W.F., 1989, Chemical and isotopic systematics of oceanic basalts: Implications for mantle composition and processes, *in* Saunders, A.D., and Norry, M.J., eds. Magmatism in the Ocean Basins: Geological Society London Special Publications 42, p. 313–345.

Talavera-Mendoza, O., Meza-Figueroa, D., De la Cruz, V.J.C., and Vega-Granillo, R., 2002, Esquistos azules en el complejo Acatlán, (sur de México): Implicaciones tectonometamórficas, *in* Reunión Anual de la Unión Geofísica Mexicana, Abstract, v. 22, p. 248.

Talavera-Mendoza, O., Ruiz, J., Gehrels, G.E., Meza-Figueroa, D.M., Vega-Granillo, R., and Campa-Uranga, M.F., 2005, U–Pb geochronology of the Acatlán Complex and implications for the Paleozoic paleogeography and tectonic evolution of southern México: Earth and Planetary Science Letters, v. 235, p. 682–699.

Taylor, S.R., and McLennan, S.M., 1985, The continental crust: Its composition and evolution: Oxford, Blackwell, 312 p.

Tolson, G., 2005, La falla Chacalapa en el sur de Oaxaca, *in* Alaniz-Álvarez, S.A., and Nieto-Samaniego, A.F., eds. Grandes Fronteras Tectónicas de México: Boletín de la Sociedad Geológica Mexicana, Volumen Conmemorativo del Centenario, v. 52, no. 1, p. 111–122.

Vega-Granillo, R., Calmus, T., Meza-Figueroa, D., Ruiz, J., Talavera-Mendoza, O., and López-Martínez, M., 2009, Structural and tectonic evolution of the Acatlán Complex, southern México: Its role in the collisional history of Laurentia and Gondwana: Tectonics, v. 28, p. 1–25. doi: 10.1029/2007TC002159.

Vega-Granillo, R., Talavera-Mendoza, O., Meza-Figueroa, D., Ruiz, J., Gehrels, G., López-Martínez, M., and De la Cruz-Vargas, J., 2007, Pressure–temperature evolution of Paleozoic high-pressure rocks of the Acatlán Complex (southern México): Implications for the evolution of the Iapetus and Rheic Oceans: Geological Society of America Bulletin, v. 119, p. 1249–1264.

Winchester, J.A., and Floyd, P.A., 1977, Geochemical discrimination of different magma series and their differentiation products using immobile elements: Chemical Geology, v. 20, p. 325–343.

Capítulo 4

Rocas de alta presión del Complejo Acatlán, sur de México: subducción a gran escala de un *rift* de margen pasivo Ordovícico extruido en la placa superior durante el Devónico–Carbonífero

High pressure rocks of the Acatlán Complex, southern México: Large-scale subducted Ordovician rifted passive margin extruded into the upper plate during the Devonian–Carboniferous

J. Duncan Keppie, Jaroslav Dostal, J. Brendan Murphy, Gonzalo Galaz-Escanilla, Mario A. Ramos-Arias, R. Damian Nance

Tectonophysics 560–561 (2012) 1–21

Contents lists available at SciVerse ScienceDirect

Tectonophysics

journal homepage: www.elsevier.com/locate/tecto

High pressure rocks of the Acatlán Complex, southern Mexico: Large-scale subducted Ordovician rifted passive margin extruded into the upper plate during the Devonian–Carboniferous

J. Duncan Keppie [a,*], Jaroslav Dostal [b], J. Brendan Murphy [c], Gonzalo Galaz-Escanilla [a], Mario A. Ramos-Arias [a], R. Damian Nance [d]

[a] Depto de Geología Regional, Instituto de Geología, Universidad Nacional Autónoma de México, 04510 México, D.F., México
[b] Dept. of Geology, St. Mary's University, Halifax, Nova Scotia, Canada B3H 3C3
[c] Dept. of Earth Sciences, St. Francis Xavier University, Antigonish, Nova Scotia, Canada B2G 2W5
[d] Dept. of Geological Sciences, 316 Clippinger Laboratories, Ohio University, Athens, Ohio 45701, USA

ARTICLE INFO

Article history:
Received 6 March 2012
Received in revised form 5 June 2012
Accepted 11 June 2012
Available online 4 July 2012

Keywords:
Blueschist
Acatlán Complex
Mexico
Mississippian
Paleogeography
Pangea

ABSTRACT

High pressure (HP) rocks in the Paleozoic Acatlán Complex of southern Mexico occur in a median belt extruded into the complex, which is the root zone of a klippe to the west. These HP rocks are predominantly clastic metasedimentary rocks and include a bimodal suite of amphibolites and granitoids. U–Pb LA-ICPMS zircon dating indicates that one of the amphibolites was intruded at or before 461 ± 2 Ma, and a megacrystic granitoid yielded an intrusive age of 488 +8/−7 Ma, which is within the 490–450 Ma range of other dated HP megacrystic granitoids. The amphibolites have a tholeiitic (transitional to alkalic), within-plate chemistry derived from a heterogeneous mantle by various degrees of partial melting. The host metasedimentary rocks contain detrital zircons derived both from the Acatlán granitoids and the ca. 1.0–1.3 Ga Oaxacan Complex, and are inferred to represent rifted passive margin sediments. An age of 348 +4/−1 Ma from zircons in a migmatized amphibolite is interpreted as the time of migmatization and dates decompression melting following peak pressure at depths of 45–55 km. Retrogression from 530 °C to 370 °C occurred between 343 and 335 Ma. The predominance of reasonably coherent, rifted passive margin rocks over a surface area of 10 × 90 km suggests removal of a large slice of the upper plate during flat slab subduction. This slice was subducted to depths of ca. 45–55 km where it was underplated and transferred to the overriding plate. The absence of Oaxacan Complex rocks in the HP belt suggests the Oaxacan basement was subducted to greater depths. Underplating was followed by extrusion facilitated by extension in the upper plate that produced Mississippian rift basins east of the median HP belt. Westward overthrusting of the HP rocks produced a klippe that overrode Mississippian clastic wedge sediments.

1. Introduction

High pressure (HP) rocks are commonly inferred to represent remnants of subducted ocean basins with protoliths derived from both the subducting and overriding plates including ophiolites, oceanic arcs, bimodal volcanic and continental margin deposits (Liou et al., 2004). HP rocks derived from the upper plate are inferred to have been removed by subduction erosion, which can take place either continuously in piecemeal fashion producing in a tectonic mélange (von Huene et al., 2004) or episodically as large fault-bounded slices (Keppie et al., 2009a, 2012). Most such slices are below the resolution of seismic imaging, but a few large fragments have been recorded: (i) 2 × 20 km in cross-section along the Middle America Trench (Ranero and von Huene, 2000); (ii) 20 × 100 km in Cascadia (Calvert, 2003); (iii) two ≤4 × 30 and 0–10 × 60 km wedge-shaped slices beneath southern British Columbia (Monger and Price, 2002); and (iv) a slice of the order of 50 × 250 km is inferred to have been removed off southern Mexico in 6 my (Keppie et al., 2009a,b). If such removed pieces include continental crust, they may return to the surface by extrusion. Numerical modelling (Butler et al., 2011; Stöckhert and Gerya, 2005; Warren et al., 2008a, 2008b) indicates that extrusion of HP rocks is accompanied by considerable telescoping and internal deformation, which is consistent with the general field occurrence of thin tectonic slices. In this paper, we document that most of the HP rocks in the Acatlán Complex of southern Mexico are reasonably coherent, extruded, metamorphosed rifted passive margin rocks, 10 × 90 km in dimension, and were subducted from the fore-arc of the continental margin and extruded in <20 my, factors consistent with rapid subduction erosion of a large slice.

* Corresponding author. Tel.: +52 555 622 4290; fax: +52 555 622 4289.
E-mail address: duncan@unam.mx (J.D. Keppie).

0040-1951/$ – see front matter © 2012 Elsevier B.V. All rights reserved.
doi:10.1016/j.tecto.2012.06.015

Two HP belts occur within the Paleozoic rocks of the Acatlán Complex: the median Piaxtla-Organal–Asis–Mimilulco belt and the western Ixcamilpa–Olinalá belt (Fig. 1). Recent data on the median HP belt show this to include bimodal, rift-related tholeiites at Piaxtla and Asis (Keppie et al., 2011; Murphy et al., 2006), island-arc mafic rocks at Mimilulco (Meza-Figueroa et al., 2003), and periarc ultramafic–mafic rocks at Tehuitzingo (Galaz Escanilla et al., 2009; Proenza et al., 2004). However, no geochemical data are available at Organal and data are limited at Mimilulco. The protolith age may be recorded at Asis where zircon cores in eclogite yielded an Ordovician age (interpreted as a metamorphic age by Elías-Herrera et al., 2004, but a protolith age by Middleton et al., 2007). The age of HP metamorphism is Carboniferous at Piaxtla, Asis and Mimilulco (Keppie et al., 2010, 2011; Middleton et al., 2007). In the Ixcamilpa–Olinalá belt, the HP rocks have Ordovician protolith ages (Ortega-Obregón et al., 2009; Ramos-Arias and Keppie, 2011), but only in the Olinalá area are geochemical analyses available and these indicate the presence of rift tholeiites (Ortega-Obregón et al., 2009). In this paper, we present geochemical and U–Pb LA-ICPMS zircon data for rocks from the Ixcamilpa, Mimilulco and Organal areas that indicate an Ordovician tholeiitic affinity, derivation from a rifted passive margin along the leading edge of the upper plate, and overprinting by Carboniferous HP metamorphism.

2. Geological setting

The Acatlán Complex is bounded on three sides by tectonic boundaries (Fig. 1a): (i) on its eastern side, the Permian, Caltepec dextral ductile shear zone (Elías-Herrera and Ortega-Gutiérrez, 2002) juxtaposes the Acatlán Complex against the ca. 1.0–1.3 Ga Oaxacan Complex; (ii) to the south, the sinistral transtensional, Cenozoic, Chacalapa–La Venta Fault places it against the Mesozoic–Cenozoic Xolapa Complex (Tolson, 2005); and (iii) on its western margin, the Late Cretaceous Papalutla thrust places the Acatlán Complex over the Cretaceous Morelos-Guerrero platformal strata (Cerca et al.,

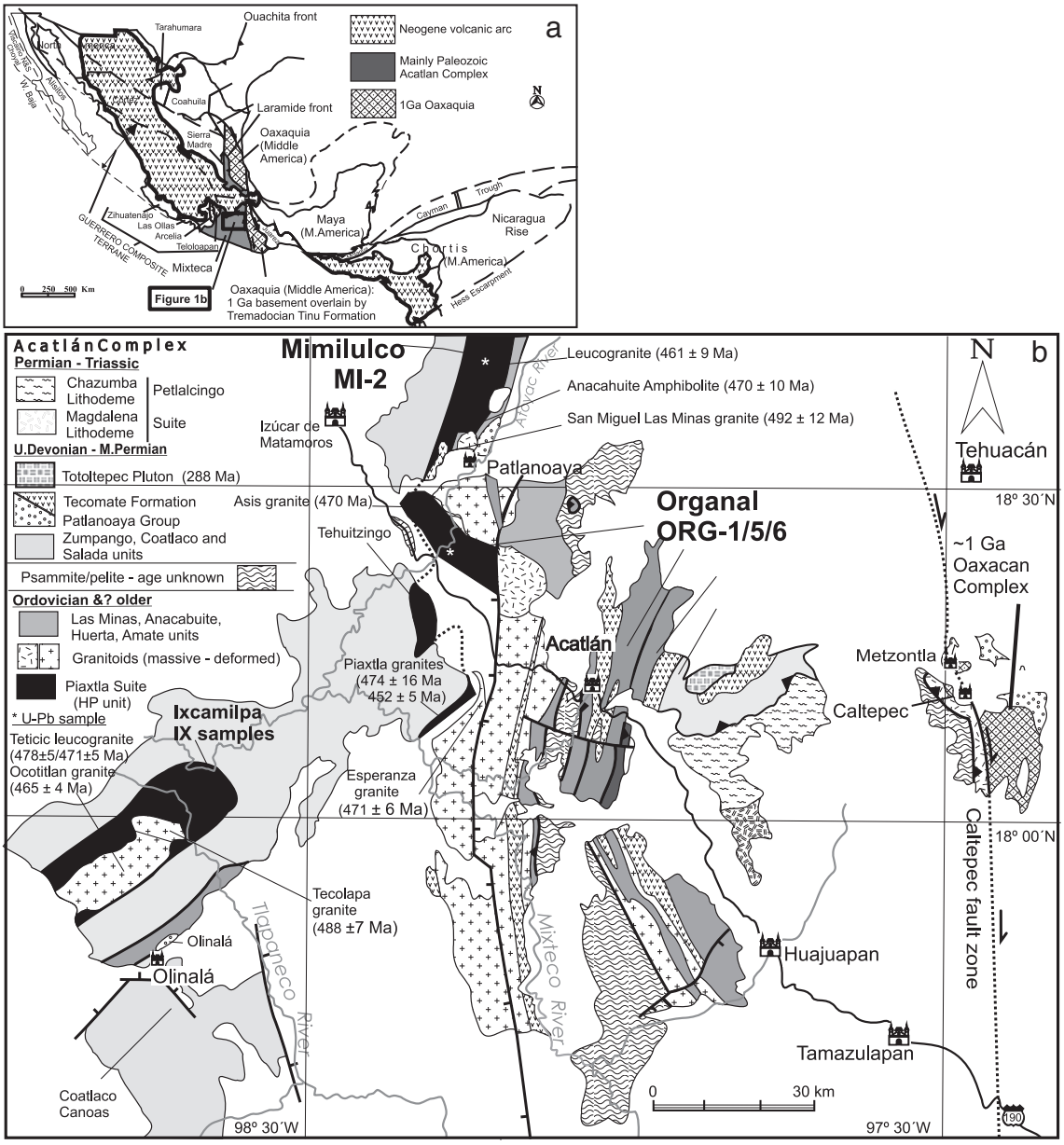

Fig. 1. Maps of Mexico showing: (a) terranes (modified after Keppie, 2004), and (b) a geological map of the Acatlán Complex (modified after Ortega-Gutiérrez et al., 1999, and Keppie et al., 2008).

2006). To the north, the Acatlán Complex is covered by volcanic and volcaniclastic sequences of Cenozoic Transmexican Volcanic Belt. The Paleozoic rocks of the Acatlán Complex may be subdivided into two assemblages of contrasting, low and high metamorphic grade, the geological records of which have been constrained by recent geochronology (Keppie et al., 2008, 2010, 2011 and references therein). The low-grade assemblage is composed of: (a) a Neoproterozoic–Ordovician clastic sequence intruded by ca. 480–440 Ma bimodal, rift-related igneous rocks; and (b) a latest Devonian–Permian shallow marine sequence (>906 m) consisting of metapsammites, metapelites and tholeiitic mafic volcanic rocks. The high-grade (HP) metamorphic assemblage consists of: (i) a Neoproterozoic–Ordovician rift-shelf sequence intruded by bimodal rift-related intrusions that are similar in age and geochemical composition to the low-grade rocks; (ii) periarc ultramafic rocks, and (iii) arc and MORB basalts. The Ordovician granitoids contain concordant inherited zircons and range in age from ca. 900 to 1300 Ma that may have been derived from the neighboring Oaxacan Complex (Keppie et al., 2008). Concordant detrital zircon ages in both the low- and high-grade Cambrian-Ordovician metasedimentary rocks indicate a provenance in local Ordovician plutons and/or ca. 1.0–1.3 Ga Oaxacan basement, and distal sources from northwestern Gondwana including the Amazonian craton

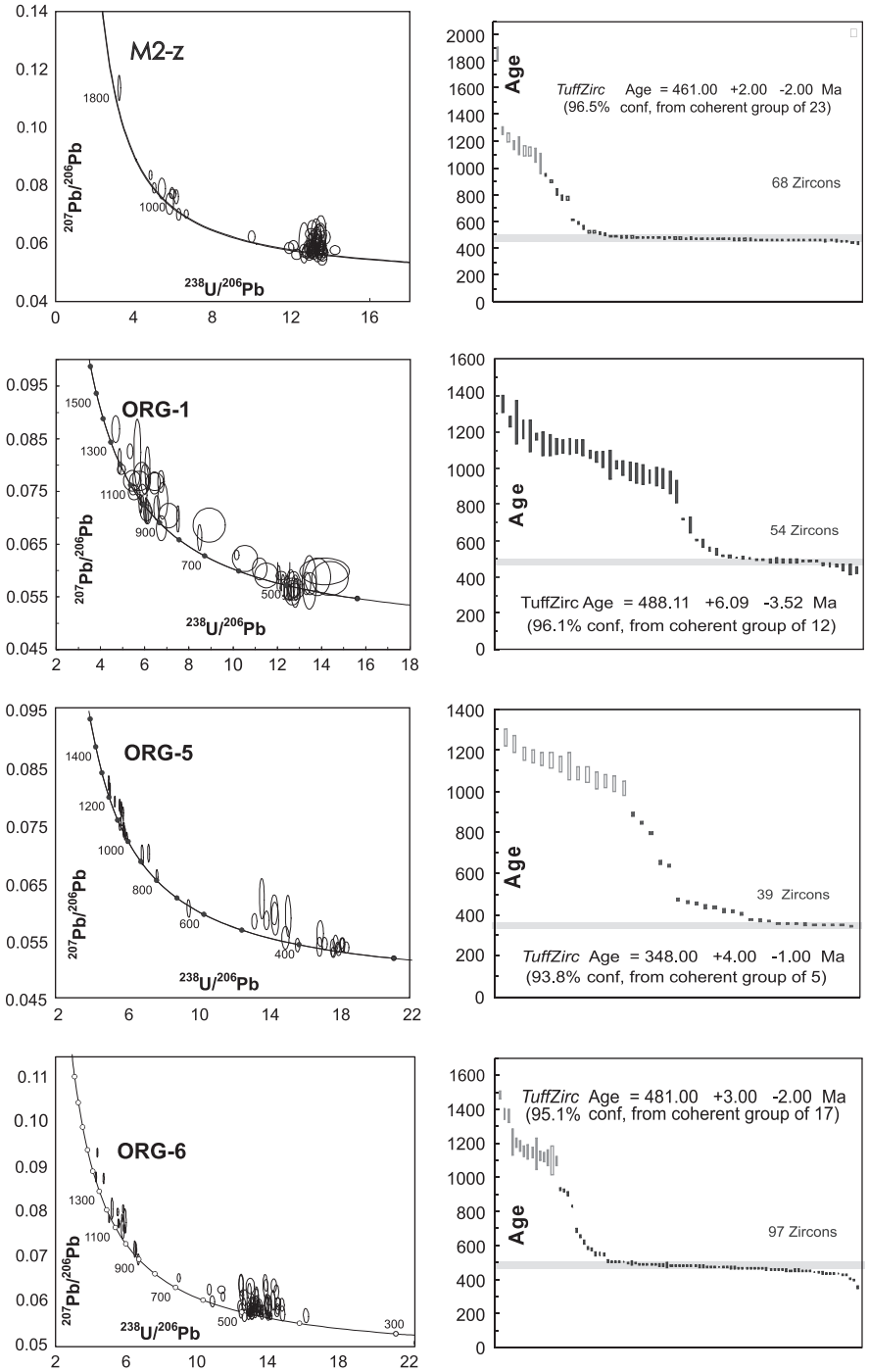

Fig. 2. U–Pb LA-ICP-MS zircon analyses of rocks in the median high pressure belt of the Acatlán Complex plotted on Tera-Wasserburg (left-hand column) diagrams, and frequency plots (right-hand column) to derive the mean $^{206}Pb/^{238}U$ age using the TuffZirc age algorithm of Ludwig and Mundil (2002): (a, b) granitic dike sample MI-2; (c, d) megacrystic granitic sheet, sample ORG-1; (e, f) migmatitic amphibolite, sample ORG-5; and (g, h) metapsammite sample ORG-6.

Table 1
LA-ICPMS U–Pb analyses of zircon from the Piaxtla Suite, Acatlán Complex, southern Mexico of: (a) a granitoid back vein cutting an amphibolite at Mimilulco (sample MI-2); (b) a megacrystic granitoid (sample ORG-1) at Organal; (c) a migmatitic amphibolite (sample ORG-5) at Organal; and (d) a metapsammite (sample ORG-6) at Organal. Errors are 1-sigma.

Corrected ratios										Corrected ages (Ma)								
M2-Z	U (ppm)	Th (ppm)	Th/U	$^{207}Pb/^{206}Pb$	$\pm1\sigma$	$^{207}Pb/^{235}U$	$\pm1\sigma$	$^{206}Pb/^{238}U$	$\pm1\sigma$	$^{206}Pb/^{238}U$	$\pm1\sigma$	$^{207}Pb/^{235}U$	$\pm1\sigma$	$^{207}Pb/^{206}Pb$	$\pm1\sigma$	Best age (Ma)	$\pm1\sigma$	% disc
Zircon_1_Mi2-z_008	87	67	0.71	0.1136	0.0018	4.78454	0.10162	0.30548	0.00255	1718	13	1782	18	1858	28	1858	28	7.53
Zircon_10_018	188	139	0.68	0.05622	0.00073	0.63049	0.00979	0.08138	0.00069	504	4	496	6	461	28	504	4	−1.61
Zircon_11_020	201	178	0.82	0.05777	0.00075	0.58524	0.00853	0.07355	0.00049	458	3	468	5	521	28	458	3	2.14
Zircon_12_021	301	64	0.20	0.07742	0.00077	1.7921	0.02147	0.16792	0.00111	1001	6	1043	8	1132	20	1132	20	11.57
Zircon_13_022	189	141	0.69	0.05913	0.00077	0.59935	0.00866	0.07361	0.00046	458	3	477	5	572	28	458	3	3.98
Zircon_14_023	251	87	0.32	0.07404	0.00089	1.3241	0.02247	0.12887	0.00155	781	9	856	10	1043	24	781	9	8.76
Zircon_15_024	61	37	0.56	0.05832	0.00193	0.60228	0.02252	0.0749	0.00064	466	4	479	14	542	71	466	4	2.71
Zircon_16_026	177	72	0.38	0.05625	0.00073	0.58914	0.00851	0.07605	0.00048	473	3	470	5	462	28	473	3	−0.64
Zircon_17_027	129	96	0.69	0.05689	0.0008	0.59963	0.00916	0.07654	0.00047	475	3	477	6	487	31	475	3	0.42
Zircon_18_028	340	443	1.21	0.06162	0.00129	0.63828	0.01405	0.07494	0.00049	466	3	501	9	661	41	466	3	6.99
Zircon_19_029	101	71	0.65	0.05833	0.00117	0.61885	0.01322	0.07708	0.00058	479	3	489	8	542	40	479	3	2.04
Zircon_2_009	697	143	0.19	0.07706	0.00068	1.7756	0.02642	0.16694	0.002	995	11	1037	10	1123	16	1123	16	4.05
Zircon_20_030	204	209	0.95	0.0633	0.00214	0.65726	0.02551	0.0753	0.00057	468	3	513	16	718	66	468	3	8.77
Zircon_21_032	95	68	0.66	0.0613	0.00197	0.62626	0.02263	0.0741	0.00055	461	3	494	14	650	63	461	3	6.68
Zircon_22_033	251	99	0.36	0.08142	0.00077	1.665	0.02808	0.14799	0.00207	890	12	995	11	1232	17	1232	17	10.55
Zircon_23_034	604	293	0.45	0.07369	0.0015	1.74211	0.05419	0.17146	0.00238	1020	13	1024	20	1033	38	1033	38	1.26
Zircon_24_035	138	109	0.73	0.05748	0.00098	0.58928	0.01086	0.07434	0.00053	462	3	470	7	510	34	462	3	1.70
Zircon_25_036	132	54	0.38	0.07915	0.00074	2.1611	0.02596	0.19802	0.0015	1165	8	1169	8	1176	17	1176	17	0.94
Zircon_26_038	283	229	0.75	0.0615	0.00123	0.64472	0.01394	0.07595	0.00062	472	4	505	9	657	39	472	4	6.53
Zircon_27_039	133	89	0.62	0.05745	0.00092	0.62501	0.01099	0.07898	0.00058	490	3	493	7	509	32	490	3	0.61
Zircon_28_040	190	134	0.65	0.0569	0.0008	0.60267	0.00941	0.07686	0.00053	477	3	479	6	488	28	477	3	0.42
Zircon_29_041	209	177	0.79	0.0585	0.00088	0.59972	0.00985	0.07435	0.0005	462	3	477	6	549	30	462	3	3.14
Zircon_3_010	177	153	0.80	0.06019	0.00283	0.65508	0.03422	0.07894	0.00068	490	4	512	21	610	94	490	4	4.30
Zircon_30_042	162	169	0.96	0.06576	0.00092	0.65113	0.01022	0.07146	0.00051	445	3	509	6	799	27	445	3	12.57
Zircon_31_044	187	126	0.62	0.05899	0.00077	0.61709	0.00936	0.07591	0.00059	472	4	488	6	567	26	472	4	3.28
Zircon_32_045	132	94	0.66	0.05729	0.0008	0.60263	0.00935	0.07635	0.00051	474	3	479	6	503	28	474	3	1.04
Zircon_33_046	221	125	0.52	0.0591	0.00077	0.67456	0.01033	0.08251	0.00067	511	4	523	6	571	26	511	4	2.29
Zircon_34_047	351	74	0.20	0.06231	0.00082	0.85916	0.01441	0.10001	0.0007	614	4	630	8	685	26	614	4	2.54
Zircon_35_048	126	59	0.43	0.07001	0.00084	1.532	0.02176	0.15888	0.00121	951	7	943	9	929	23	951	7	−0.85
Zircon_36_050	109	88	0.75	0.05779	0.00087	0.60216	0.01027	0.07561	0.00061	470	4	479	7	522	32	470	4	1.88
Zircon_37_051	144	107	0.69	0.05588	0.00084	0.56547	0.00938	0.0735	0.00052	457	3	455	6	448	32	457	3	−0.44
Zircon_38_052	111	96	0.80	0.06373	0.00115	0.65031	0.01268	0.07443	0.00056	463	3	509	8	733	37	463	3	9.04
Zircon_39_053	220	62	0.26	0.07695	0.001	1.4641	0.02906	0.13582	0.00204	821	12	916	12	1120	25	821	12	10.37
Zircon_4_011	89	58	0.61	0.06535	0.00105	0.68758	0.01215	0.07645	0.00057	475	3	531	7	786	32	475	3	10.55
Zircon_40_054	402	80	0.18	0.0577	0.00063	0.55851	0.00737	0.07024	0.00051	438	3	451	5	518	23	438	3	2.88
Zircon_41_056	128	93	0.67	0.05689	0.00085	0.61172	0.01031	0.07809	0.0006	485	4	485	6	487	32	485	4	0.00
Zircon_42_057	150	120	0.74	0.06213	0.00099	0.6218	0.01104	0.07283	0.00056	453	3	491	7	679	33	453	3	7.74
Zircon_43_058	325	254	0.72	0.05678	0.00068	0.57266	0.00782	0.07319	0.00048	455	3	460	5	483	25	455	3	1.09
Zircon_44_059	155	97	0.58	0.05839	0.00076	0.67595	0.01039	0.08399	0.00069	520	4	524	6	544	27	520	4	0.76
Zircon_45_060	163	136	0.77	0.06153	0.00171	0.63807	0.02056	0.07521	0.00055	467	3	501	13	658	57	467	3	6.79
Zircon_46_062	225	144	0.59	0.05834	0.00156	0.59906	0.01863	0.07448	0.00058	463	3	477	12	542	56	463	3	2.94
Zircon_47_063	1236	173	0.13	0.08356	0.00067	2.3709	0.02429	0.20581	0.00132	1206	7	1234	7	1282	15	1282	15	5.93
Zircon_48_064	257	258	0.93	0.06327	0.00076	0.67033	0.0103	0.07673	0.00074	477	4	521	6	717	24	477	4	8.45
Zircon_49_065	110	75	0.63	0.06087	0.00103	0.64463	0.01195	0.07672	0.00057	477	3	505	7	635	35	477	3	5.54
Zircon_5_012	225	164	0.67	0.056	0.00073	0.56974	0.00813	0.07392	0.00044	460	3	458	5	452	28	460	3	−0.44
Zircon_50_066	78	26	0.31	0.07609	0.00099	1.6969	0.02547	0.16203	0.00122	968	7	1007	10	1097	25	1097	25	3.87
Zircon_51_068	268	12	0.04	0.07015	0.00061	1.4492	0.01566	0.14984	0.00093	900	5	910	6	933	17	900	5	1.10
Zircon_52_069	182	40	0.20	0.07154	0.00136	1.2736	0.02735	0.1276	0.00128	774	7	834	12	973	37	774	7	7.19
Zircon_53_070	116	78	0.62	0.05767	0.00098	0.60403	0.0113	0.07622	0.00059	474	4	480	7	517	36	474	4	1.25
Zircon_54_071	69	32	0.42	0.07891	0.00146	2.00146	0.05452	0.18396	0.00254	1089	14	1116	18	1170	35	1170	35	6.92
Zircon_55_072	99	85	0.79	0.05884	0.00094	0.6221	0.01102	0.07673	0.00058	477	3	491	7	561	33	477	3	2.85
Zircon_56_074	661	796	1.11	0.05759	0.00058	0.5852	0.00772	0.0737	0.00063	458	4	468	5	514	21	458	4	2.14
Zircon_57_075	231	140	0.56	0.05892	0.00071	0.59897	0.00835	0.07387	0.00052	459	3	477	5	564	25	459	3	3.77

Zircon_58_076	257	176	0.63	0.05741	0.00069	0.58806	0.00803	0.0743	0.00048	462	3	470	5	507	25	462	3	1.70
Zircon_59_077	159	111	0.64	0.0574	0.00086	0.61712	0.01049	0.07797	0.00062	484	4	488	7	507	32	484	4	0.82
Zircon_6_014	152	122	0.74	0.06203	0.00087	0.64264	0.01006	0.0749	0.00052	466	3	504	6	675	29	466	3	7.54
Zircon_60_078	106	83	0.72	0.0628	0.00172	0.64177	0.02082	0.07411	0.00067	461	4	503	13	702	56	461	4	8.35
Zircon_61_080	140	111	0.74	0.05455	0.00082	0.55337	0.00916	0.07362	0.00052	458	3	447	6	394	32	458	3	−2.46
Zircon_62_081	220	193	0.81	0.06096	0.00091	0.6249	0.01029	0.07416	0.0005	461	3	493	6	638	31	461	3	6.49
Zircon_63_082	143	130	0.84	0.06035	0.00084	0.62679	0.00965	0.0756	0.00048	470	3	494	6	616	29	470	3	4.86
Zircon_64_083	81	52	0.59	0.05875	0.001	0.62655	0.01172	0.07747	0.0006	481	4	494	7	558	35	481	4	2.63
Zircon_65_084	202	147	0.67	0.05574	0.00067	0.59531	0.00807	0.07734	0.00049	480	3	474	5	442	26	480	3	−1.27
Zircon_66_085	120	88	0.68	0.06394	0.0009	0.81668	0.01506	0.09053	0.00109	559	6	606	8	740	28	559	6	7.76
Zircon_67_086	92	48	0.48	0.06621	0.00132	0.79726	0.01755	0.08456	0.00078	523	5	595	10	813	40	523	5	12.10
Zircon_68_087	328	107	0.30	0.07061	0.00071	0.9387	0.0114	0.09634	0.00066	593	4	672	6	946	20	593	4	11.76
Zircon_7_015	113	66	0.54	0.05949	0.00089	0.61878	0.01035	0.07545	0.00056	469	3	489	6	585	31	469	3	4.09
Zircon_8_016	139	103	0.69	0.06361	0.00245	0.64884	0.02792	0.07398	0.00062	460	4	508	17	729	78	460	4	9.45
Zircon_9_017	91	70	0.71	0.05826	0.00093	0.61706	0.01078	0.07677	0.00054	477	3	488	7	540	33	477	3	2.25

Isotopic ratios										Corrected ages (Ma)								
ORG 1	U ppm	Th ppm	Th/U	$^{207}Pb/^{206}Pb$	$\pm1\sigma$	$^{207}Pb/^{235}U$	$\pm1\sigma$	$^{206}Pb/^{238}U$	$\pm1\sigma$	$^{206}Pb/^{238}U$	$\pm1\sigma$	$^{207}Pb/^{235}U$	$\pm1\sigma$	$^{207}Pb/^{206}Pb$	$\pm1\sigma$	Best age (Ma)	$\pm1\sigma$	disc
ORG-1-7	252	36	0.143	17.0881	4.5	0.5611	6.5	0.0695	4.7	433	20	452	24	549	98	433	20	21.1
ORG-1-44	318	14	0.044	16.7127	3.4	0.5835	7.4	0.0707	6.5	441	28	467	28	598	74	441	28	26.3
ORG-1-24	389	50	0.129	17.0012	5	0.5871	6.1	0.0724	3.5	451	15	469	23	560	108	451	15	19.6
ORG-1-43	186	72	0.388	17.3808	3	0.5885	3.4	0.0742	1.7	461	7.5	470	13	512	65	461	8	9.9
ORG-1-44A	398	44	0.111	17.3145	7.2	0.5922	7.5	0.0744	2	462	8.7	472	28	521	159	462	9	11.2
ORG-1-6	233	19	0.082	17.3727	3	0.596	3.2	0.0751	1.2	467	5.4	475	12	513	66	467	5	9.0
ORG-1-55A	356	11	0.031	17.7357	3	0.606	3.1	0.078	0.7	484	3	481	12	468	66	484	3	−3.5
ORG-1-10	269	27	0.102	17.6185	2.4	0.6103	2.5	0.078	0.7	484	3.2	484	9.5	482	53	484	3	−0.4
ORG-1-50	189	17	0.09	17.8275	4.5	0.6038	4.7	0.08	1.2	485	5.6	480	18	456	100	485	6	−6.3
ORG-1-26	305	51	0.166	17.7713	2.0	0.6077	2.6	0.08	1.6	486	7.6	482	9.9	463	44	486	8	−5.0
ORG-1-34	307	50	0.162	15.2111	4.5	0.7107	5.1	0.08	2.5	487	12	545	22	798	94	487	12	39.0
ORG-1-36	486	80	0.165	17.4524	3.6	0.6201	4.1	0.08	2.0	487	9.4	490	16	503	79	487	9	3.2
ORG-1-13	215	49	0.226	17.7008	3.0	0.6140	4.6	0.08	3.4	489	16	486	18	472	67	489	16	−3.7
ORG-1-41	249	26	0.106	17.9222	3.4	0.6066	4.2	0.08	2.4	489	11	481	16	444	76	489	11	−10.1
ORG-1-20	134	63	0.472	17.4533	4.2	0.6264	4.3	0.08	1.2	492	5.6	494	17	503	92	492	6	2.2
ORG-1-49	293	38	0.13	17.9088	2.3	0.6134	2.4	0.08	0.5	494	2.4	486	9.1	446	51	494	2	−10.8
ORG-1-18	224	51	0.23	17.6453	3.2	0.6279	3.4	0.08	1.0	498	4.6	495	13	479	72	498	5	−4.1
ORG-1-35	169	24	0.142	16.2491	9.3	0.6902	9.5	0.08	1.8	504	8.8	533	39	658	200	504	9	23.4
ORG-1-30	645	409	0.634	17.4878	3.0	0.6431	3.0	0.08	0.5	505	2.4	504	12	499	66	505	2	−1.4
ORG-1-28	508	51	0.101	16.9417	1.1	0.6686	1.9	0.08	1.6	509	7.6	520	7.8	568	25	509	8	10.4
ORG-1-38	267	43	0.162	17.1159	3.5	0.6677	3.6	0.08	0.6	513	2.8	519	15	546	77	513	3	5.9
ORG-1-5	265	22	0.082	16.9253	3.2	0.7080	5.0	0.09	3.8	537	20	544	21	570	71	537	20	5.8
ORG-1-25	245	42	0.171	16.5812	2.8	0.7421	3.7	0.09	2.4	551	13	564	16	615	61	551	13	10.3
ORG-1-16	206	28	0.135	16.0555	3.3	0.8151	5.5	0.09	4.4	585	25	605	25	684	70	585	25	14.5
ORG-1-8	331	53	0.161	15.8828	1.2	0.8542	1.5	0.10	0.9	605	4.9	627	6.8	707	25	605	5	14.4
ORG-1-17	352	78	0.222	14.5725	3.9	1.0613	7.7	0.11	6.7	685	44	734	40	887	80	685	44	22.8
ORG-1-23	184	33	0.181	15.0950	3.0	1.0765	3.2	0.12	0.9	718	6.2	742	17	814	64	718	6	11.8
ORG-1-11	145	44	0.304	14.6983	2.9	1.3888	4.0	0.15	2.8	890	23	884	23	870	59	870	59	−2.3
ORG-1-12	95	34	0.361	14.3275	2.9	1.2822	3.0	0.13	0.7	806	4.9	838	17	922	60	922	60	12.6
ORG-1-31	413	126	0.305	14.1964	2.7	1.3710	5.9	0.14	5.2	851	42	877	35	941	55	941	55	9.6
ORG-1-55	232	36	0.154	14.0903	2.5	1.5976	3.4	0.16	2.3	975	21	969	21	957	50	957	50	−1.9
ORG-1-33	291	82	0.281	14.0887	1.8	1.6101	4.0	0.16	3.6	982	33	974	25	957	36	957	36	−2.6
ORG-1-2	109	45	0.415	14.0360	2.6	1.6063	2.8	0.16	1.0	976	8.8	973	17	964	53	964	53	−1.2
ORG-1-15	134	42	0.314	13.9819	2.7	1.6281	2.7	0.17	0.7	985	6.5	981	17	972	54	972	54	−1.3
ORG-1-45	228	40	0.174	13.9093	2.7	1.5145	3.1	0.15	1.6	917	14	936	19	983	54	983	54	6.8
ORG-1-54	302	21	0.071	13.7660	2.0	1.7235	2.2	0.17	1.0	1024	9	1017	14	1004	41	1004	41	−1.9
ORG-1-53	564	172	0.305	13.6637	1.1	1.7167	1.5	0.17	1.0	1013	9	1015	9.3	1019	22	1019	22	0.6
ORG-1-47	539	123	0.229	13.6511	3.9	1.4826	4.7	0.15	2.8	883	23	923	29	1021	78	1021	78	13.5
ORG-1-10A	198	37	0.186	13.4573	2.3	1.7370	3.7	0.17	2.9	1010	27	1022	24	1050	46	1050	46	3.8

(continued on next page)

Table 1 (*continued*)

Isotopic ratios										Corrected ages (Ma)								
ORG 1	U ppm	Th ppm	Th/U	$^{207}Pb/^{206}Pb$	±1σ	$^{207}Pb/^{235}U$	±1σ	$^{206}Pb/^{238}U$	±1σ	$^{206}Pb/^{238}U$	±1σ	$^{207}Pb/^{235}U$	±1σ	$^{207}Pb/^{206}Pb$	±1σ	Best age (Ma)	±1σ	disc
ORG-1-4	134	29	0.213	13.3722	1.5	1.8669	4.3	0.18	4.0	1073	39	1069	28	1063	30	1063	30	−1.0
ORG-1-58	156	57	0.364	13.2702	1.1	1.8953	2.7	0.18	2.5	1080	24	1079	18	1078	22	1078	22	−0.2
ORG-1-3	194	59	0.303	13.0485	2.2	1.6406	4.0	0.16	3.3	930	29	986	25	1112	45	1112	45	16.3
ORG-1-29	276	83	0.301	13.0076	1.8	1.6419	5.3	0.15	5.0	928	43	986	33	1118	36	1118	36	17.0
ORG-1-56	257	41	0.158	13.0043	2.2	1.5730	2.8	0.15	1.8	892	15	960	18	1119	44	1119	44	20.3
ORG-1-19	298	95	0.318	12.9868	2.0	1.8436	6.6	0.17	6.3	1032	60	1061	43	1121	39	1121	39	7.9
ORG-1-46	234	48	0.204	12.9784	2.1	1.9546	6.3	0.18	5.9	1089	59	1100	42	1123	41	1123	41	3.0
ORG-1-59	341	72	0.210	12.9325	3.0	1.7778	3.8	0.17	2.4	994	22	1037	25	1130	59	1130	59	12.0
ORG-1-22	257	42	0.165	12.9156	3.3	1.8194	6.5	0.17	5.6	1014	52	1052	43	1132	66	1132	66	10.4
ORG-1-57	243	70	0.290	12.6283	1.0	2.2057	3.1	0.20	3.0	1186	32	1183	22	1177	20	1177	20	−0.8
ORG-1-45A	101	20	0.198	12.6026	4.3	1.7860	4.5	0.16	1.5	975	13	1040	29	1181	84	1181	84	17.4
ORG-1-32	469	155	0.330	12.3883	2.5	2.2849	2.7	0.21	1.1	1204	13	1208	19	1215	49	1215	49	0.9
ORG-1-42	175	32	0.185	12.1322	6.3	2.0038	6.6	0.18	2.2	1047	22	1117	45	1256	122	1256	122	16.6
ORG-1-52	415	212	0.512	12.1007	1.4	2.1339	2.4	0.19	1.9	1107	20	1160	17	1261	28	1261	28	12.2
ORG-1-40	137	34	0.249	11.5155	2.4	2.5539	3.9	0.21	3.1	1246	35	1288	29	1357	47	1357	47	8.1
Corrected ratios										Corrected ages (Ma)								
ORG 5	U (ppm)	Th (ppm)	Th/U	$^{207}Pb/^{206}Pb$	±1σ	$^{207}Pb/^{235}U$	±1σ	$^{206}Pb/^{238}U$	±1σ	$^{206}Pb/^{238}U$	±1σ	$^{207}Pb/^{235}U$	±1σ	$^{207}Pb/^{206}Pb$	±1σ	Best age (Ma)	±1σ	% disc
Zircon_ORG5_001_008	77	45	0.542	0.07445	0.00082	1.79870	0.02220	0.17511	0.00098	1040	5	1045	8	1054	22	1054	22	0.5
Zircon002_009	218	1	0.005	0.05507	0.00061	0.41991	0.00501	0.05544	0.00026	348	2	356	4	415	25	348	2	2.2
Zircon003_010	292	49	0.157	0.07944	0.00062	2.10280	0.01815	0.19209	0.00071	1133	4	1150	6	1183	15	1183	15	1.5
Zircon004_011	64	22	0.320	0.08273	0.00083	2.34040	0.02576	0.20544	0.00095	1204	5	1225	8	1263	20	1263	20	1.7
Zircon005_012	67	23	0.324	0.08143	0.00081	2.27650	0.02478	0.20292	0.00087	1191	5	1205	8	1232	19	1232	19	1.2
Zircon006_014	175	100	0.535	0.07555	0.00073	1.89290	0.02238	0.18179	0.00125	1077	7	1079	8	1083	19	1083	19	0.2
Zircon007_015	33	13	0.365	0.05918	0.00175	0.57205	0.01943	0.07010	0.00066	437	4	459	13	574	64	437	4	4.8
Zircon008_016	111	1	0.010	0.05502	0.00094	0.42833	0.00760	0.05654	0.00029	355	2	362	5	413	38	355	2	1.9
Zircon009_017	55	6	0.100	0.05600	0.00129	0.51905	0.01286	0.06734	0.00062	420	4	425	9	452	51	420	4	1.2
Zircon011_020	149	64	0.401	0.07441	0.00060	1.79080	0.01618	0.17465	0.00073	1038	4	1042	6	1053	16	1053	16	0.4
Zircon013_022	178	2	0.010	0.05473	0.00077	0.41747	0.00611	0.05535	0.00024	347	1	354	4	401	31	347	1	2.0
Zircon014_023	275	1	0.005	0.05431	0.00060	0.41987	0.00499	0.05615	0.00025	352	2	356	4	384	25	352	2	1.1
Zircon015_024	129	77	0.558	0.07743	0.00070	1.88360	0.01879	0.17644	0.00076	1047	4	1075	7	1132	18	1132	18	2.6
Zircon016_026	171	2	0.009	0.05385	0.00065	0.41562	0.00554	0.05599	0.00032	351	2	353	4	365	27	351	2	0.6
Zircon017_027	77	47	0.573	0.07019	0.00102	1.43173	0.02699	0.14794	0.00099	889	6	902	11	934	30	889	6	1.4
Zircon018_028	98	13	0.122	0.06097	0.00095	0.89632	0.01648	0.10663	0.00070	653	4	650	9	638	34	653	4	−0.5
Zircon019_029	166	1	0.008	0.05484	0.00071	0.44373	0.00639	0.05862	0.00036	367	2	373	4	406	29	367	2	1.6
Zircon020_030	274	1	0.004	0.05428	0.00065	0.40872	0.00536	0.05467	0.00029	343	2	348	4	383	27	343	2	1.4
Zircon021_032	152	27	0.166	0.06656	0.00069	1.20918	0.01553	0.13175	0.00068	798	4	805	7	824	22	798	4	0.9
Zircon022_033	84	33	0.368	0.07830	0.00075	1.94210	0.02111	0.18007	0.00092	1067	5	1096	7	1154	19	1154	19	2.6
Zircon023_034	81	16	0.190	0.05969	0.00224	0.54836	0.02217	0.06663	0.00045	416	3	444	15	592	81	416	3	6.3
Zircon024_035	81	21	0.248	0.07706	0.00127	1.68406	0.03583	0.15850	0.00139	948	8	1003	14	1123	33	1123	33	5.5
Zircon025_036	190	38	0.188	0.07583	0.00061	1.87200	0.02172	0.17827	0.00150	1058	8	1071	8	1091	16	1091	16	1.2
Zircon026_038	117	22	0.173	0.07049	0.00097	1.36585	0.02168	0.14053	0.00075	848	4	874	9	943	28	848	4	3.0
Zircon027_039	143	9	0.056	0.05414	0.00099	0.42599	0.00836	0.05707	0.00027	358	2	360	6	377	41	358	2	0.6
Zircon028_040	131	5	0.039	0.05791	0.00087	0.61829	0.01037	0.07635	0.00057	474	3	489	7	526	33	474	3	3.1
Zircon029_041	71	15	0.197	0.07291	0.00160	1.04590	0.02418	0.10411	0.00074	638	4	727	12	1011	42	638	4	12.2
Zircon030_042	53	1	0.015	0.05445	0.00109	0.44676	0.00933	0.05961	0.00036	373	2	375	7	390	42	373	2	0.5
Zircon031_044	270	1	0.005	0.05347	0.00059	0.41919	0.00497	0.05694	0.00025	357	2	355	4	349	23	357	2	−0.6
Zircon032_045	141	4	0.029	0.05463	0.00076	0.48486	0.00739	0.06437	0.00033	402	2	401	5	397	29	402	2	−0.2
Zircon033_046	133	24	0.167	0.07842	0.00068	1.94350	0.01904	0.17982	0.00081	1066	4	1096	7	1158	16	1158	16	2.7
Zircon034_047	188	77	0.381	0.07886	0.00069	1.98110	0.01995	0.18245	0.00089	1080	5	1109	7	1169	16	1169	16	2.6
Zircon035_048	150	83	0.520	0.07316	0.00064	1.71250	0.01670	0.16985	0.00071	1011	4	1013	6	1018	17	1018	17	0.2
Zircon036_050	42	10	0.222	0.05884	0.00106	0.58930	0.01149	0.07257	0.00054	452	3	470	7	561	37	452	3	3.8

Zircon037_051	150	2	0.011	0.05480	0.00077	0.41754	0.00621	0.05532	0.00028	347	2	354	4	404	29	347	2	2.0
Zircon038_052	152	61	0.375	0.07390	0.00069	1.76200	0.01869	0.17313	0.00088	1029	5	1032	7	1039	18	1039	18	0.3
Zircon039_053	57	35	0.576	0.06266	0.00217	0.63908	0.02409	0.07397	0.00049	460	3	502	15	697	69	460	3	8.4
Zircon040_054	37	2	0.055	0.05684	0.00148	0.46422	0.01252	0.05946	0.00043	372	3	387	9	485	54	372	3	3.9
Zircon012_021	36	3	0.086	0.06069	0.00170	0.58861	0.01735	0.07030	0.00065	438	4	470	11	628	56	438	4	6.8

Corrected ratios										Corrected ages (Ma)								
ORG 6	U (ppm)	Th (ppm)	Th/U	$^{207}Pb/^{206}Pb$	$\pm 1\sigma$	$^{207}Pb/^{235}U$	$\pm 1\sigma$	$^{206}Pb/^{238}U$	$\pm 1\sigma$	$^{206}Pb/^{238}U$	$\pm 1\sigma$	$^{207}Pb/^{235}U$	$\pm 1\sigma$	$^{207}Pb/^{206}Pb$	$\pm 1\sigma$	Best age (Ma)	$\pm 1\sigma$	% disc
Zircon_ORG_008	142	99	0.653	0.05970	0.00066	0.59244	0.00757	0.07190	0.00047	448	3	472	5	593	23	448	3	5.1
Zircon002_009	155	61	0.372	0.05699	0.00057	0.58398	0.00658	0.07426	0.00039	462	2	467	4	491	21	462	2	1.1
Zircon003_010	181	62	0.319	0.07606	0.00056	1.79430	0.01730	0.17098	0.00108	1018	6	1043	6	1097	14	1097	14	2.4
Zircon004_011	271	88	0.305	0.05943	0.00059	0.56959	0.00701	0.06945	0.00051	433	3	458	5	583	20	433	3	5.5
Zircon005_012	308	38	0.115	0.05634	0.00042	0.56314	0.00479	0.07242	0.00030	451	2	454	3	466	16	451	2	0.7
Zircon006_014	110	50	0.422	0.05744	0.00092	0.60242	0.01087	0.07607	0.00036	473	2	479	7	508	33	473	2	1.3
Zircon007_015	102	18	0.164	0.05965	0.00076	0.76414	0.01256	0.09291	0.00073	573	4	576	7	591	26	573	4	0.5
Zircon008_016	109	47	0.409	0.09288	0.00068	2.93840	0.02567	0.22911	0.00110	1330	6	1392	7	1485	13	1485	13	4.5
Zircon009_017	49	13	0.247	0.06895	0.00083	1.43350	0.01892	0.15057	0.00083	904	5	903	8	897	23	904	5	−0.1
Zircon010_018	145	163	1.057	0.05823	0.00140	0.57753	0.01414	0.07181	0.00034	447	2	463	9	538	50	447	2	3.5
Zircon011_020	80	62	0.727	0.05969	0.00084	0.62147	0.00942	0.07550	0.00044	469	3	491	6	592	29	469	3	4.5
Zircon013_022	90	32	0.339	0.05749	0.00101	0.64134	0.01283	0.08091	0.00046	502	3	503	8	510	36	502	3	0.2
Zircon014_023	175	43	0.230	0.05633	0.00053	0.57503	0.00594	0.07394	0.00032	460	2	461	4	465	20	460	2	0.2
Zircon015_024	198	22	0.104	0.07824	0.00059	1.87960	0.01651	0.17403	0.00077	1034	4	1074	6	1153	14	1153	14	3.7
Zircon016_026	78	60	0.722	0.05899	0.00100	0.62739	0.01137	0.07696	0.00048	478	3	494	7	567	35	478	3	3.2
Zircon019_029	76	32	0.401	0.06207	0.00081	0.81117	0.01190	0.09441	0.00064	582	4	603	7	677	26	582	4	3.5
Zircon020_030	35	21	0.552	0.06039	0.00121	0.66297	0.01400	0.07954	0.00054	493	3	516	9	618	41	493	3	4.5
Zircon021_032	142	51	0.335	0.07692	0.00056	1.90580	0.01596	0.17952	0.00074	1064	4	1083	6	1119	14	1119	14	1.8
Zircon022_033	88	68	0.719	0.06060	0.00085	0.53965	0.00795	0.06455	0.00030	403	2	438	5	625	29	403	2	8.0
Zircon023_034	129	34	0.248	0.06133	0.00053	0.76200	0.01129	0.08875	0.00107	548	6	575	7	651	18	548	6	4.7
Zircon024_035	96	72	0.707	0.05990	0.00140	0.58386	0.01496	0.07070	0.00036	440	2	467	10	600	49	440	2	5.8
Zircon025_036	106	24	0.214	0.06483	0.00071	0.92529	0.01506	0.10049	0.00121	617	7	665	8	769	22	617	7	7.2
Zircon026_038	82	39	0.451	0.05761	0.00086	0.60702	0.00972	0.07631	0.00043	474	3	482	6	515	32	474	3	1.7
Zircon027_039	84	58	0.652	0.05783	0.00075	0.55484	0.00771	0.06945	0.00034	433	2	448	5	523	28	433	2	3.3
Zircon028_040	220	74	0.316	0.07145	0.00096	1.51389	0.02262	0.15368	0.00069	922	4	936	9	970	27	922	4	1.5
Zircon029_041	188	29	0.144	0.05638	0.00058	0.55564	0.00631	0.07147	0.00032	445	2	449	4	467	22	445	2	0.9
Zircon031_043	108	61	0.527	0.06591	0.00099	0.80686	0.01501	0.08853	0.00097	547	6	601	8	804	31	547	6	9.0
Zircon032_044	82	32	0.367	0.06324	0.00083	0.63431	0.00966	0.07274	0.00037	453	2	499	6	716	26	453	2	9.2
Zircon033_045	71	38	0.497	0.05801	0.00081	0.61846	0.00922	0.07726	0.00039	480	2	489	6	530	29	480	2	1.8
Zircon034_046	31	19	0.579	0.05812	0.00116	0.62421	0.01300	0.07795	0.00045	484	3	492	8	534	41	484	3	1.6
Zircon035_047	71	16	0.215	0.05908	0.00091	0.56429	0.00959	0.06928	0.00039	432	2	454	6	570	31	432	2	4.8
Zircon036_049	88	46	0.494	0.06298	0.00126	0.70894	0.01489	0.08092	0.00052	502	3	544	9	708	40	502	3	7.7
Zircon037_050	47	24	0.465	0.05902	0.00106	0.62099	0.01270	0.07639	0.00074	475	4	490	8	568	37	475	4	3.1
Zircon038_051	78	42	0.505	0.05797	0.00075	0.62122	0.00865	0.07755	0.00039	481	2	491	5	529	27	481	2	2.0
Zircon040_053	333	47	0.132	0.06677	0.00050	0.97668	0.00907	0.10609	0.00050	650	3	692	5	831	15	650	3	6.1
Zircon041_055	250	99	0.369	0.07713	0.00058	1.92130	0.01624	0.18042	0.00070	1069	4	1089	6	1125	14	1125	14	1.8
Zircon042_056	25	12	0.451	0.07122	0.00121	1.52640	0.02723	0.15513	0.00084	930	5	941	11	964	33	930	5	1.2
Zircon043_057	73	33	0.420	0.06191	0.00112	0.66532	0.01321	0.07795	0.00040	484	2	518	8	671	36	484	2	6.6
Zircon044_058	67	29	0.411	0.05771	0.00081	0.59824	0.00911	0.07516	0.00045	467	3	476	6	519	29	467	3	1.9
Zircon045_059	49	35	0.659	0.05938	0.00095	0.62141	0.01080	0.07588	0.00052	471	3	491	7	581	34	471	3	4.1
Zircon046_061	30	19	0.582	0.07682	0.00092	1.59890	0.02111	0.15054	0.00083	904	5	970	8	1117	23	1117	23	6.8
Zircon047_062	106	56	0.498	0.05731	0.00075	0.55078	0.00791	0.06963	0.00042	434	3	446	5	504	28	434	3	2.7
Zircon049_064	99	54	0.511	0.05663	0.00079	0.61253	0.00919	0.07828	0.00042	486	3	485	6	477	30	486	3	−0.2
Zircon052_068	184	114	0.580	0.05898	0.00140	0.59032	0.01540	0.07259	0.00039	452	2	471	10	566	51	452	2	4.0
Zircon053_069	27	17	0.594	0.06091	0.00128	0.63584	0.01379	0.07566	0.00041	470	2	500	9	636	44	470	2	6.0
Zircon054_070	591	158	0.251	0.05643	0.00103	0.48706	0.00998	0.06259	0.00038	391	2	403	7	470	39	391	2	3.0
Zircon055_071	97	84	0.816	0.06035	0.00121	0.63294	0.01300	0.07566	0.00036	470	2	498	8	616	42	470	2	5.6
Zircon056_073	130	39	0.285	0.07802	0.00057	2.14730	0.01841	0.19928	0.00090	1171	5	1164	6	1147	15	1147	15	−0.6
Zircon058_075	75	48	0.607	0.06178	0.00105	0.59478	0.01072	0.06979	0.00042	435	3	474	7	667	37	435	3	8.2

(continued on next page)

Table 1 (*continued*)

Corrected ratios										Corrected ages (Ma)								
ORG 6	U (ppm)	Th (ppm)	Th/U	$^{207}Pb/^{206}Pb$	$\pm 1\sigma$	$^{207}Pb/^{235}U$	$\pm 1\sigma$	$^{206}Pb/^{238}U$	$\pm 1\sigma$	$^{206}Pb/^{238}U$	$\pm 1\sigma$	$^{207}Pb/^{235}U$	$\pm 1\sigma$	$^{207}Pb/^{206}Pb$	$\pm 1\sigma$	Best age (Ma)	$\pm 1\sigma$	% disc
Zircon059_076	114	29	0.240	0.07815	0.00080	1.58249	0.02002	0.14686	0.00083	883	5	963	8	1151	21	1151	21	8.3
Zircon060_077	81	38	0.440	0.05771	0.00075	0.58897	0.00801	0.07392	0.00030	460	2	470	5	519	29	460	2	2.1
Zircon100_125	265	45	0.158	0.05766	0.00069	0.58507	0.00807	0.07351	0.00050	457	3	468	5	517	27	457	3	2.4
Zircon61_079	123	75	0.571	0.06480	0.00063	1.00580	0.01169	0.11236	0.00072	686	4	707	6	768	21	686	4	3.0
Zircon62_080	239	68	0.266	0.08024	0.00061	1.91120	0.01728	0.17240	0.00084	1025	5	1085	6	1203	15	1203	15	5.5
Zircon63_081	40	18	0.411	0.05876	0.00146	0.58404	0.01709	0.07209	0.00068	449	4	467	11	558	55	449	4	3.9
Zircon64_082	60	40	0.629	0.05694	0.00091	0.60606	0.01068	0.07717	0.00057	479	3	481	7	489	36	479	3	0.4
Zircon65_083	110	38	0.327	0.05767	0.00063	0.61943	0.00873	0.07781	0.00068	483	4	489	5	517	24	483	4	1.2
Zircon67_086	139	45	0.303	0.07186	0.00094	1.35670	0.02060	0.13693	0.00070	827	4	870	9	982	27	827	4	4.9
Zircon68_087	79	31	0.371	0.05693	0.00102	0.53516	0.01115	0.06818	0.00042	425	3	435	7	489	43	425	3	2.3
Zircon70_089	69	40	0.540	0.06299	0.00169	0.63299	0.01866	0.07288	0.00045	453	3	498	12	708	61	453	3	9.0
Zircon71_091	57	29	0.485	0.05781	0.00098	0.62508	0.01101	0.07827	0.00036	486	2	493	7	523	40	486	2	1.4
Zircon73_093	176	40	0.213	0.05649	0.00070	0.56123	0.00769	0.07206	0.00032	449	2	452	5	472	29	449	2	0.7
Zircon74_094	90	84	0.879	0.05859	0.00082	0.60551	0.00896	0.07494	0.00036	466	2	481	6	552	33	466	2	3.1
Zircon75_095	245	89	0.341	0.07937	0.00056	1.99850	0.01771	0.18189	0.00096	1077	5	1115	6	1181	15	1181	15	3.4
Zircon76_097	60	45	0.697	0.05874	0.00094	0.64857	0.01083	0.07984	0.00038	495	2	508	7	558	38	495	2	2.6
Zircon77_098	47	25	0.511	0.05714	0.00097	0.60791	0.01127	0.07718	0.00057	479	3	482	7	497	40	479	3	0.6
Zircon78_099	93	57	0.579	0.05732	0.00075	0.59306	0.00826	0.07494	0.00037	466	2	473	5	504	31	466	2	1.5
Zircon79_100	91	55	0.564	0.05861	0.00100	0.60310	0.01089	0.07461	0.00046	464	3	479	7	553	40	464	3	3.1
Zircon80_101	65	34	0.498	0.05902	0.00106	0.58911	0.01109	0.07233	0.00040	450	2	470	7	568	42	450	2	4.3
Zircon81_103	69	72	0.978	0.08712	0.00078	2.55180	0.02545	0.21218	0.00095	1240	5	1287	7	1363	19	1363	19	3.7
Zircon84_106	83	30	0.335	0.05700	0.00068	0.61132	0.00815	0.07765	0.00045	482	3	484	5	492	26	482	3	0.4
Zircon85_107	168	66	0.366	0.05713	0.00063	0.61441	0.00795	0.07791	0.00053	484	3	486	5	497	24	484	3	0.4
Zircon86_109	142	49	0.323	0.06030	0.00066	0.73725	0.00935	0.08807	0.00055	544	3	561	5	614	23	544	3	3.0
Zircon87_110	53	26	0.466	0.05850	0.00082	0.65677	0.01019	0.08132	0.00054	504	3	513	6	549	30	504	3	1.8
Zircon89_112	134	52	0.361	0.05762	0.00063	0.58966	0.00690	0.07414	0.00030	461	2	471	4	515	24	461	2	2.1
Zircon90_113	133	53	0.375	0.05889	0.00088	0.55447	0.00976	0.06829	0.00039	426	2	448	6	563	32	426	2	4.9
Zircon91_115	100	43	0.400	0.06083	0.00073	0.67840	0.00901	0.08066	0.00046	500	3	526	5	633	25	500	3	4.9
Zircon92_116	110	77	0.659	0.06002	0.00521	0.45854	0.04176	0.05541	0.00058	348	4	383	29	604	187	348	4	9.1
Zircon95_119	2402	244	0.095	0.05693	0.00057	0.60841	0.00670	0.07736	0.00036	480	2	483	4	489	22	480	2	0.6
Zircon96_121	243	45	0.174	0.06000	0.00066	0.63991	0.00761	0.07698	0.00035	478	2	502	5	604	23	478	2	4.8
Zircon98_123	151	38	0.238	0.05643	0.00043	0.55969	0.00503	0.07182	0.00034	447	2	451	3	469	17	447	2	0.9
Zircon99_124	220	96	0.411	0.05820	0.00070	0.60608	0.00803	0.07562	0.00042	470	3	481	5	537	26	470	3	2.3
Zircon018_028	164	75	0.428	0.06332	0.00150	0.70567	0.01861	0.08083	0.00053	501	3	542	11	719	53	501	3	7.6
Zircon048_063	96	28	0.277	0.05848	0.00099	0.60715	0.01112	0.07529	0.00051	468	3	482	7	548	39	468	3	2.9
Zircon057_074	52	23	0.414	0.06312	0.00114	0.67562	0.01462	0.07767	0.00093	482	6	524	9	712	41	482	6	8.0
Zircon66_085	85	35	0.383	0.08047	0.00146	2.14181	0.04511	0.19305	0.00133	1138	7	1162	15	1208	38	1208	38	2.1
Zircon69_088	63	15	0.216	0.08763	0.00074	2.81470	0.02681	0.23313	0.00100	1351	5	1359	7	1374	17	1374	17	0.6
Zircon72_092	16	8	0.440	0.06306	0.00101	0.61416	0.01070	0.07052	0.00049	439	3	486	7	710	36	439	3	9.7
Zircon88_111	86	62	0.679	0.07767	0.00166	1.81260	0.04517	0.16926	0.00114	1008	6	1050	16	1138	45	1138	45	4.0
Zircon97_122	106	58	0.515	0.05643	0.00090	0.62044	0.01094	0.07964	0.00059	494	4	490	7	469	35	494	4	−0.8
Zircon092_117	140	26	0.178	0.07607	0.00160	1.81520	0.04133	0.17304	0.00152	1029	8	1051	15	1097	42	1097	42	2.1

and the 900–750 Ma Goiás magmatic arc within the Brasiliano orogen (Keppie et al., 2008; Nance et al., 2009). The latter ages are particularly important because they allow distinction between Laurentian and Amazonian sources.

The HP belts in the Acatlán Complex have generally been inferred to occur in synformal keels of a single nappe rooted in the Caltepec shear zone (Ortega-Gutiérrez et al., 1999; Talavera-Mendoza et al., 2005; Vega-Granillo et al., 2007, 2009). Whereas this appears to be the shape of the Ixcamilpa–Olinalá klippe (Ramos-Arias and Keppie, 2011; Ramos-Arias et al., 2011), the Mimilulco–Piaxtla belt has been interpreted as an extrusion zone (bounded below by a thrust and above by a listric normal fault) within the Acatlán Complex and the root zone for the Ixcamilpa–Olinalá belt, The Ixcamilpa–Olinalá belt has been subdivided into a number of lithodemic units (from bottom to top): Coacalco, Cuatlaxtecoma, Buenavista, and Chicomala intruded by the Tecolapa granitoid (Keppie et al., 2008; Ramos-Arias et al., 2008). Low-grade, Carboniferous clastic metasedimentary rocks occur both to the east and west of the Mimilulco–Piaxtla belt. Both HP belts were collectively interpreted as oceanic remnants of either the Iapetus Ocean (Ortega-Gutiérrez, 1981; Ortega-Gutiérrez et al., 1999), or of multiple oceans within the Iapetus and Rheic oceans (Talavera-Mendoza et al., 2005; Vega-Granillo et al., 2007, 2009). Alternatively, Keppie et al. (2008, 2011) have proposed that the HP rocks were extruded into the active western margin of Pangea and that their protoliths formed along the southern passive margin of the Rheic Ocean. Resolution of the contrasting hypotheses for the origin of the HP rocks in the Acatlán Complex has important implications for paleogeographic reconstructions. Thus, further U–Pb zircon dating and geochemistry of the mafic rocks was undertaken to determine their age and tectonic setting. In order to distinguish between the various hypotheses, we undertook U–Pb zircon geochronology to determine the protolith and metamorphic ages of the HP igneous and metasedimentary rocks, accompanied by geochemistry to indicate the tectonic setting of the mafic protoliths.

3. U–Pb geochronology

3.1. Analytical methods

Four samples were collected for U–Pb zircon dating (Fig. 1) by laser ablation inductively coupled plasma mass spectrometry (LA-ICP-MS) at the Laboratorio de Estudios Isotópicos (LEI), Centro de Geociencias, UNAM, Mexico (see Solari et al., 2010 for methodology):

(i) at Mimilulco, a granitic dike (M2-z1) that cuts a wide eclogite intrusion;
(ii) at Organal, a metapsammite (ORG-6) cut by a megacrystic granite intrusive sheet (ORG-1);
(iii) at Organal, a migmatitic amphibolite (ORG-5) containing quartzo-feldspathic patches, lenses and discontinuous veins inferred to indicate partial melting.

Zircons were extracted using standard techniques for mineral separation, as described by Solari et al. (2010) for U–Pb geochronology. In the figures and tables, the ages of grains >1 Ga are $^{207}Pb/^{206}Pb$ ages (e.g., Gehrels et al., 2006) which are regarded as minimum ages due to the effect of possible Pb loss, whereas $^{206}Pb/^{238}U$ ages are used for zircons<1 Ga because the small amounts of ^{207}Pb in young grains yield imprecise $^{207}Pb/^{206}Pb$ ages. Zircon analyses with <10% normal and <5% reverse discordancy are used to date the time of intrusion in igneous rocks. The age is considered robust if it belongs to a cluster of three of more zircons with similar ages (Gehrels et al., 2006). Mean $^{206}Pb/^{238}U$ age were calculated using the TuffZirc age algorithm of Ludwig and Mundil (2002).

3.2. Results

The granitic dike (M2-z) in amphibolite at Mimilulco is characterized by purely igneous zircons with ages ranging from a single, slightly discordant analysis at ca. 1800 Ma, through a few ca. 800–1300 Ma, to a population of 23 roughly concordant zircons that define a mean age of 461 ± 2 Ma (Fig. 2a and b, Table 1). The latter age is interpreted to date the time of crystallization of the granitic vein and provides a younger age limit for intrusion of the amphibolite: Ordovician granitoids are present elsewhere in the Piaxtla Suite (Keppie et al., 2008, 2010, 2011). On the other hand, the granitic dike may be a back vein produced by melting of the country rock adjacent to the amphibolite, in which case it provides the age of intrusion of the amphibolite. The dike is unlikely to be a migmatitic leucosome because migmatization is absent in the metasedimentary host rocks and the pressure–temperature path reached a peak temperature of 560 °C at 11–15 kb (Meza-Figueroa et al., 2003), which is below the ca. 630 °C minimum melting curve for wet granite (Ernst, 2009).

The metapsammite (ORG-6) at Organal yielded detrital zircons with ages ranging from ca. 1485 Ma to 391 Ma (Fig. 2g and h, Table 1). A coherent group of 17 zircons gave a TuffZirc age of 481 + 3/− 2 Ma, which is interpreted to reflect the maximum age for deposition of the layer. There is also a significant number of zircons with ages between ca. 1100 and 1200 Ma.

The intrusive megacrystic granitic sheet (ORG-1) yielded zircon ages ranging from ca. 433 to 1357 Ma (Fig. 2c and d, Table 1). A coherent group of 12 zircons gave a TuffZirc age of 488 + 8/− 7 Ma, which is interpreted as the time of intrusion. There is also a population of zircons with ages between 940 and 1140 Ma that are inferred to represent inheritance.

The migmatitic amphibolite (ORG-5) yielded zircon ages ranging from ca. 347 to 1263 Ma (Fig. 2e and f, Table 1). A coherent group of 5 zircons gave a TuffZirc age of 348 + 4/− 1 Ma, which is inferred to date the migmatization because: (a) the zircons were probably recovered from the granitic partial melt rather than the amphibolite, which has low Zr (Table 2); and (b) the age is similar to the 346 ± 3 Ma and 353 ± 1 Ma age for peak metamorphism along strike to the north (at Asis and Mimilulco, respectively: Elías-Herrera et al., 2004; Middleton et al., 2007). These data are consistent with the P–T curve, which reached peak temperatures of 730–830 °C at 15.3–16.8 kb (Vega-Granillo et al., 2007) that lie above the ca. 650 °C minimum melt curve for wet basalt (Harry and Green, 1999). Furthermore, migmatization generally occurs as a result of decompression melting following peak metamorphism, and suggests rapid exhumation because the ages overlap.

4. Geochemistry

Whole rock major and trace elements were determined using lithium tetraborate fusion at the Activation Laboratories, Ancaster, Ontario, Canada. Major elements and some trace elements (Ba, Sr, Y and Zr) were determined by inductively coupled plasma-optical emission spectrometry, whereas other trace elements were analyzed using a Perkin Elmer Optima 3000 inductively coupled plasma mass spectrometer. Based on replicate analyses, the precision is generally between 2 and 10% for trace elements and 3–5% for major elements. Sm–Nd isotopic analyses were performed at the Atlantic Universities Regional Isotopic Facility, Memorial University of Newfoundland. Errors on $^{143}Nd/^{144}Nd$ are generally less than 0.002%. The εNd_t values are calculated using a $^{147}Sm/^{144}Nd = 0.1967$ and $^{143}Nd/^{144}Nd = 0.512638$ values for the present day chondrite uniform reservoir (CHUR) and for t = 460 Ma. ^{147}Sm decay constant is 6.54 10^{-12} y^{-1} (Steiger and Jäger, 1977), T_{DM} were calculated with respect to the De Paolo mantle model (DePaolo, 1988).

The rocks have experienced a complex metamorphic history including eclogite-blueschist facies metamorphism, which could have

Table 2
Major, selected trace element and rare earth element analyses of amphibolites and a granitoid from the Piaxtla Suite, Acatlán Complex, southern Mexico.

Sample	IX-47	IX-243	IX-245	IX-247	IX-251	IX-253	IX-285	IX-266	IX-267	IX-268	IX-276	IX-278	IX-229	IX-230	IX-231
SiO_2 (wt.%)	46.17	48.10	53.77	48.86	67.12	61.96	72.49	46.65	46.54	46.47	45.87	49.00	47.65	45.26	45.42
TiO_2	1.52	1.98	1.31	2.76	0.57	1.00	0.56	3.02	3.08	2.68	1.24	1.42	2.06	1.57	1.39
Al_2O_3	12.25	13.43	13.68	13.11	13.99	16.38	12.80	12.48	13.79	13.82	15.72	13.34	13.75	15.33	15.11
Fe_2O_3	11.94	14.18	9.80	13.77	7.17	7.49	4.84	16.79	14.14	13.91	11.02	12.81	14.02	13.98	13.35
MnO	0.19	0.20	0.21	0.20	0.08	0.11	0.04	0.23	0.17	0.17	0.17	0.15	0.20	0.21	0.20
MgO	10.17	5.83	6.01	5.80	1.95	2.01	1.17	5.80	5.94	6.97	8.75	6.76	7.25	7.78	7.16
CaO	12.48	10.93	7.63	11.07	0.91	1.81	0.76	10.84	11.68	9.98	10.55	9.65	10.50	10.61	11.49
Na_2O	1.94	2.30	5.56	2.85	4.60	3.22	2.67	2.38	2.33	3.44	2.71	4.26	3.00	2.20	2.58
K_2O	0.18	0.24	0.14	0.41	1.02	2.47	2.42	0.49	0.52	0.37	0.05	0.10	0.07	0.18	0.08
P_2O_5	0.14	0.21	0.16	0.28	0.10	0.23	0.13	0.31	0.32	0.29	0.10	0.09	0.17	0.12	0.12
LOI	2.74	1.71	1.25	0.88	1.98	2.57	2.11	1.47	1.29	1.45	2.88	2.47	2.00	2.92	3.00
Total	99.72	99.11	99.52	99.99	99.50	99.26	99.99	100.45	99.80	99.55	99.06	100.04	100.67	100.16	99.91
Mg #	62.78	44.88	54.84	45.48	35.01	34.70	32.37	40.62	45.41	49.81	61.13	51.10	50.60	52.43	51.51
Cr (ppm)	735	103	232	92	32	95	34	131	153	265	388	344	257	158	198
Ni	171	43	76	67	24	31	19	70	75	95	162	103	51	84	87
Co	49	42	23	45	12	14	8	48	40	40	41	56	42	48	47
V	281	348	259	348	69	107	71	413	401	361	242	280	415	327	335
Rb	1	0	0	0	0	0	0	0	0	0	0	0	0	2	0
Ba	69	53	31	89	287	919	663	69	161	99	19	17	34	82	79
Sr	223	231	93	353	44	176	26	329	344	234	219	94	105	135	142
Ga	15	19	15	20	17	23	16	23	24	19	16	13	18	17	17
Ta	0.37	0.42	0.24	0.74	0.49	0.73	0.49	0.62	0.90	0.70	0.08	0.06	0.11	0.07	0.07
Nb	8.0	9.0	5.0	16.6	9.9	16.5	10.1	14.0	19.7	16.5	1.2	1.1	2.1	1.3	1.3
Hf	2.26	3.88	3.08	4.58	8.48	9.40	6.49	5.51	4.89	4.38	2.44	2.43	3.17	2.39	2.38
Zr	94	167	145	194	404	438	318	232	226	191	106	91	135	96	87
Y	14	29	31	26	26	39	24	34	28	24	26	24	36	32	29
Th	0.67	0.97	2.79	1.23	5.61	8.06	5.67	1.71	1.57	1.24	0.15	0.12	0.20	0.23	4.40
La	7.12	10.74	12.04	14.28	40.98	50.97	38.09	16.26	17.31	14.11	2.34	2.22	3.51	2.77	2.38
Ce	16.52	25.42	27.09	34.33	72.83	94.74	65.03	38.89	41.56	34.17	7.19	7.47	11.13	8.45	7.51
Pr	2.44	3.64	3.74	4.80	9.44	12.44	8.57	5.47	5.83	4.84	1.32	1.41	1.96	1.57	1.36
Nd	11.58	17.29	17.99	22.92	39.45	49.84	35.62	25.99	27.66	22.94	7.16	8.21	11.91	8.97	8.11
Sm	3.18	5.17	4.49	6.05	8.40	9.98	7.86	7.08	7.15	5.64	2.85	3.26	4.44	3.46	2.88
Eu	1.11	1.59	1.33	2.07	1.71	2.41	1.64	2.20	2.38	1.88	1.07	1.11	1.50	1.25	1.09
Gd	3.20	5.41	5.09	5.54	5.93	7.91	5.97	7.07	6.64	5.51	3.79	3.94	5.77	4.61	4.23
Tb	0.54	0.94	0.89	0.95	0.95	1.24	0.95	1.20	1.10	0.93	0.72	0.75	1.07	0.92	0.81
Dy	3.23	6.16	5.98	5.61	5.64	7.56	5.38	7.38	6.73	5.51	4.72	5.00	7.41	6.29	5.55
Ho	0.62	1.22	1.25	0.99	1.00	1.39	1.04	1.36	1.22	1.02	1.02	1.00	1.58	1.37	1.16
Er	1.71	3.40	3.69	2.74	2.81	3.85	2.82	3.63	3.06	2.73	2.91	2.94	4.52	4.12	3.63
Tm	0.22	0.51	0.55	0.36	0.41	0.58	0.40	0.52	0.41	0.35	0.45	0.41	0.65	0.61	0.51
Yb	1.44	3.23	3.34	2.14	2.62	3.89	2.73	3.30	2.35	2.21	3.00	2.65	4.51	0.39	3.38
Lu	0.22	0.46	0.54	0.31	0.43	0.57	0.39	0.47	0.37	0.29	0.45	0.37	0.71	0.57	0.55

Mg# = 100 × MgO/(MgO + FeO+) mol%.

Table 2 (*continued*)

Sample	IX-235	IX-240	IX-54	IX-62	MI-1	MI-5	MI-6	MI-8	MI-10	MI-13	PIX-10	PIX-12	PIX-24	ORG-2	ORG-3
SiO_2 (wt.%)	38.77	47.18	47.22	46.62	51.07	48.10	48.03	48.23	48.81	50.66	47.07	47.93	48.25	49.46	46.50
TiO_2	1.28	1.32	2.53	1.24	1.65	1.76	1.61	1.33	0.85	0.83	1.92	1.32	2.78	1.71	3.37
Al_2O_3	15.60	14.48	14.74	16.14	14.09	15.25	14.77	15.34	14.66	16.36	14.09	13.79	13.82	13.28	14.03
Fe_2O_3	12.94	10.69	13.64	10.71	11.31	13.44	12.87	10.68	11.01	9.69	14.05	12.83	14.54	13.90	18.05
MnO	0.20	0.18	0.21	0.17	0.19	0.23	0.20	0.19	0.18	0.15	0.28	0.22	0.22	0.30	0.69
MgO	4.88	5.89	7.67	9.03	7.92	6.65	7.13	7.96	9.37	6.92	6.68	9.06	6.25	8.72	6.92
CaO	14.94	12.80	6.72	10.02	7.72	9.68	11.72	11.43	11.51	8.68	10.98	11.25	9.98	10.19	7.30
Na_2O	1.50	3.18	3.65	2.85	4.35	3.21	2.33	2.47	1.85	3.59	2.49	1.62	2.50	2.12	2.03
K_2O	1.37	0.10	0.14	0.08	0.16	0.36	0.40	0.38	0.17	0.94	0.48	0.59	0.45	0.43	0.60
P_2O_5	0.06	0.11	0.54	0.10	0.17	0.19	0.17	0.17	0.07	0.09	0.18	0.11	0.28	0.17	0.40
LOI	9.08	4.26	3.44	3.11	1.87	1.59	1.09	2.00	1.88	2.00	1.96	2.37	1.06	0.83	0.66
Total	100.63	100.19	100.51	100.07	100.50	100.47	100.31	100.18	100.36	99.90	100.18	101.09	100.13	101.11	100.54
Mg #	42.75	52.18	52.69	62.54	58.10	49.49	52.32	59.61	62.76	58.58	48.50	58.31	45.98	55.40	43.16
Cr (ppm)	489	363	237	378	410	174	255	374	488	239	158	329	160	269	113
Ni	221	136	36	151	182	77	104	97	177	87	35	62	40	110	68
Co	61	41	38	34	39	44	48	39	45	38	55	60	51	63	70
V	258	295	327	257	286	313	304	258	275	219	302	238	354	302	469
Rb	40	0	1	1	0	5	7	7	3	24	20	25	20	95	226
Ba	167	794	76	25	26	148	175	142	56	266	110	45	168	11	13
Sr	199	281	168	193	97	197	233	166	95	167	134	160	268	74	93
Ga	17	17	20	16	14	19	19	15	14	15	17	16	20	191	185
Ta	0.07	0.07	1.20	0.07	0.20	0.50	0.30	0.70	0.10	0.10	0.51	0.28	1.14	19	25
Nb	1.4	1.4	28.6	1.4	5.6	7.3	6.9	10.4	2.2	2.1	8.7	4.7	19.4	0.55	1.37
Hf	2.33	2.05	8.04	2.09	4.30	3.80	3.00	2.20	1.30	1.70	2.45	1.70	4.16	15.4	29.4
Zr	87	87	404	82	133	146	127	85	39	54	108	75	183	3.35	7.42
Y	26	28	41	24	34	32	29	27	23	20	30	23	31	133	307
Th	0.15	0.14	2.99	0.14	2.10	1.00	0.80	0.70	0.40	0.90	0.83	0.37	1.74	25	39
La	2.23	2.46	33.43	2.07	10.60	12.00	10.20	8.60	2.40	9.70	8.51	4.93	17.80	9.33	26.76
Ce	7.32	7.46	72.36	6.64	26.20	29.10	24.30	17.50	4.90	9.20	21.10	12.80	43.20	21.10	57.71
Pr	1.36	1.43	9.45	1.23	3.70	3.98	3.50	2.62	0.99	1.41	3.09	1.95	5.91	3.02	7.92
Nd	8.28	8.38	41.41	7.01	18.80	19.10	17.10	13.00	5.50	6.80	15.20	9.66	27.30	14.38	35.00
Sm	2.85	2.86	9.01	2.56	4.63	4.89	4.26	3.35	1.67	2.06	4.31	3.02	6.65	3.74	7.98
Eu	1.16	1.12	2.56	1.01	1.34	1.61	1.37	1.14	0.69	0.75	1.52	1.08	2.16	1.32	2.31
Gd	3.91	4.04	8.07	3.58	5.43	5.62	5.13	4.27	3.02	3.11	5.19	3.76	6.74	4.66	8.79
Tb	0.75	0.78	1.43	0.68	0.95	0.94	0.85	0.75	0.56	0.58	0.88	0.65	1.06	0.80	1.41
Dy	4.94	5.14	8.59	4.68	5.74	5.49	4.96	4.48	3.69	3.50	5.58	4.12	6.14	4.90	8.07
Ho	1.11	1.14	1.66	0.93	1.26	1.18	1.05	0.98	0.84	0.80	1.16	0.89	1.19	0.97	1.51
Er	3.16	3.19	4.75	2.82	3.38	3.23	3.08	2.83	2.66	2.40	3.34	2.59	3.26	2.75	4.05
Tm	0.47	0.50	0.68	0.40	0.54	0.47	0.45	0.41	0.40	0.33	0.47	0.36	0.43	0.40	0.57
Yb	3.07	3.24	4.30	2.71	3.38	2.95	2.83	2.68	2.59	2.19	2.96	2.29	2.64	2.58	3.50
Lu	0.45	0.45	0.65	0.44	0.53	0.47	0.42	0.41	0.41	0.33	0.44	0.34	0.38	0.37	0.51

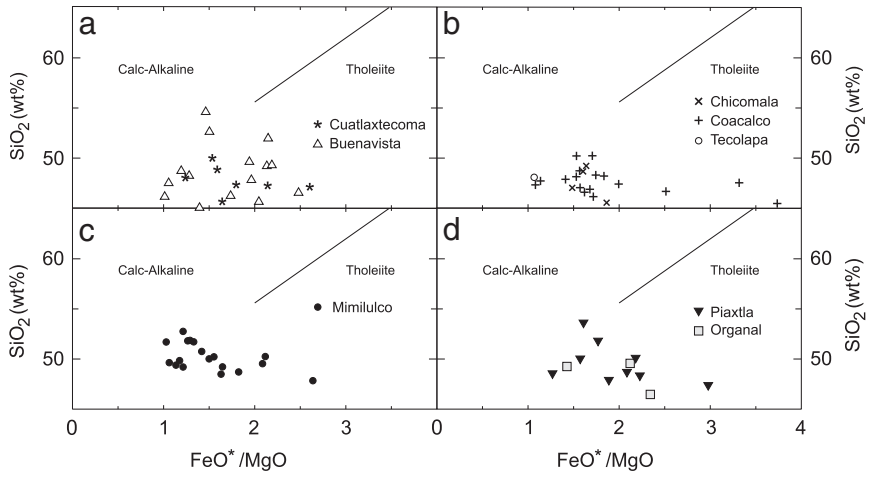

Fig. 3. FeO*/MgO vs SiO_2 (wt.%) diagrams for the HP mafic rocks (a) the Buenavista and Cuatlaxtecoma units of the Piaxtla Suite, Ixcamilpa; (b) the Coacalco, Chicomala and Tecolapa units of the Piaxtla Suite, Ixcamilpa; (c) Mimilulco group; (d) Organal and Piaxtla rocks. Tholeiite and calc-alkaline fields are after Miyashiro (1974).

potentially modified their chemical composition. Thus, to minimize the effects of possible element mobilization during metamorphism, we selected massive homogeneous samples and the discussion focuses on elements in these samples that are relatively immobile during secondary processes (Winchester and Floyd, 1977). These elements include some of the major elements, rare earth elements (REE), high field strength elements (HFSE), Th and transition elements such as Cr and Ni.

The investigation concentrated on mafic rocks of bimodal sequences in the western and central Acatlán Complex: Ixcamilpa, Mimilulco, Organal and Piaxtla: the Piaxtla data were reported by Keppie et al. (2011). The major and trace elements of the mafic rocks from the first three areas are given in Table 2 and in the Appendix. These rocks have a SiO_2 content (calculated on a volatile-free basis) mainly around 45–50 wt.% and Mg# ($100 \times MgO/MgO + FeO^*$ mol%) ranging from 64 to 35, although most of the rocks are in the range of Mg# 55–45. As Mg# decreases there is a general decrease in compatible trace elements such as Ni (from 200 to 50 ppm) and Cr (from 600 to 100 ppm) and an increase of incompatible trace elements such as HFSE. The trends are consistent with low pressure fractional crystallization. An increase of TiO_2 with increasing of FeO*/MgO accompanied by nearly constant SiO_2 in these suites (Figs. 3 and 4; Miyashiro, 1974), as well as the increasing V with decreasing Mg#, are characteristic of tholeiitic or transitional series in which fractionation of Fe-Ti oxides was not significant probably due to the low partial pressure of oxygen (Miyashiro, 1974).

4.1. Ixcamilpa

For rocks modified by secondary processes, the Zr/TiO_2 vs Nb/Y plot (Fig. 5) is typically used as a proxy for the total alkalis vs silica classification diagram. In this plot, the Nb/Y ratio measures the degree of

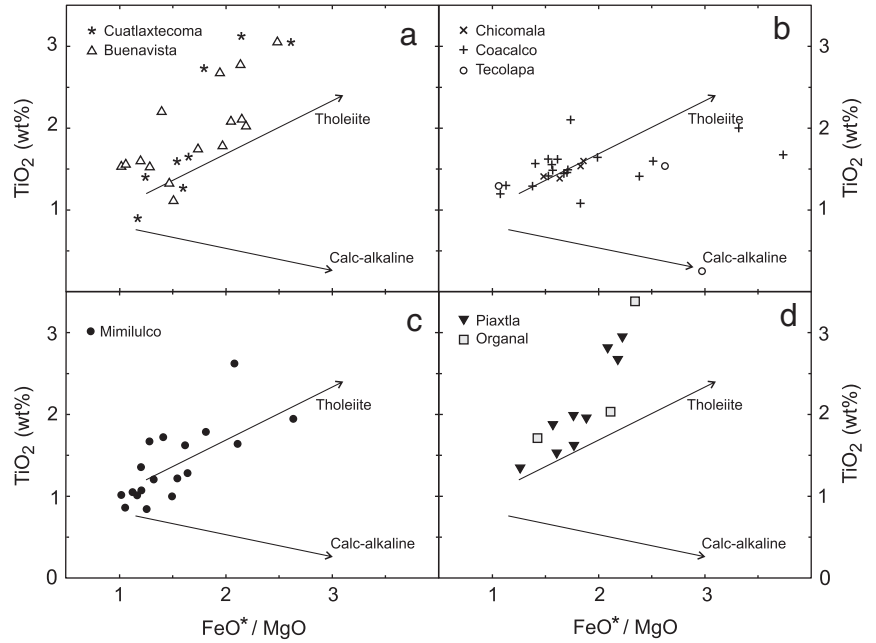

Fig. 4. FeO*/MgO vs TiO_2 (wt.%) diagrams for the HP mafic rocks (a) the Buenavista and Cuatlaxtecoma units of the Piaxtla Suite, Ixcamilpa; (b) the Coacalco, Chicomala and Tecolapa units of the Piaxtla Suite, Ixcamilpa; (c) Mimilulco group; (d) Organal and Piaxtla rocks. Vectors for tholeiitic and calc-alkaline trends are after Miyashiro (1974).

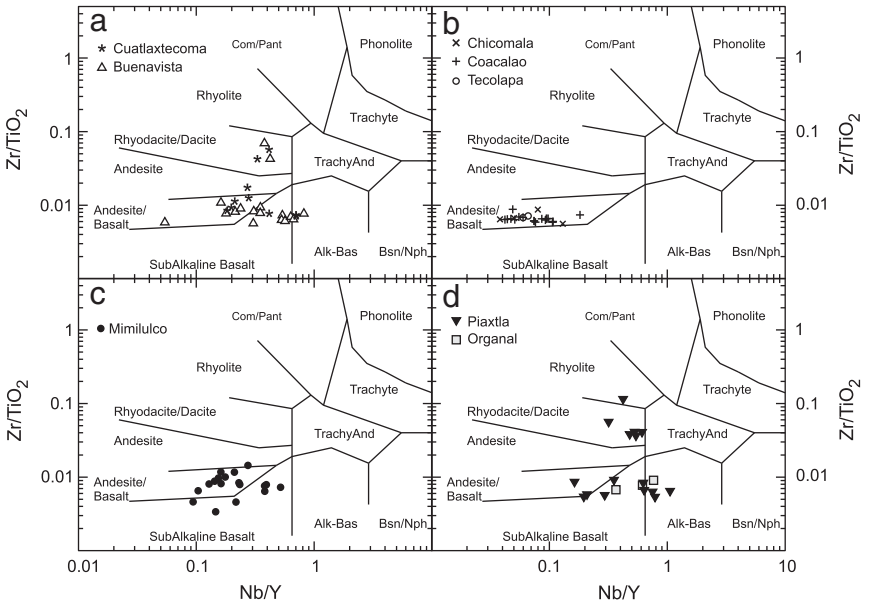

Fig. 5. Zr/TiO_2 vs Nb/Y diagram of Winchester and Floyd (1977) for the HP rocks (a) the Buenavista and Cuatlaxtecoma units of the Piaxtla Suite, Ixcamilpa; (b) the Coacalco, Chicomala and Tecolapa units of the Piaxtla Suite, Ixcamilpa; (c) Mimilulco group; (d) Organal and Piaxtla rocks. Abbreviations: Sub-AB = subalkaline basalt; Alk-Bas = alkaline basalt; TrachyAnd = trachyandesite; Bsn = basanite; Trach = trachyte; Nph = nephelinite.

alkalinity whereas the Zr/TiO_2 is an index of fractionation (Winchester and Floyd, 1977). This plot together with the Zr/TiO_2 vs SiO_2 diagram (Fig. 6) suggests that the mafic rocks correspond compositionally to subalkaline basalts, although some samples are transitional to alkali basalts. The Nb/Y ratio (Fig. 5) shows that there are two partly overlapping groups of basaltic rocks. The first group, which includes rocks of the Buenavista and Cuatlaxtecoma units, has a higher Nb/Y ratio and higher contents of strongly incompatible trace elements than the rocks of the second group from the Coacalco, Chicomala and Tecolapa units. The chondrite-normalized REE patterns of the first mafic group (Fig. 7) are enriched in light REE (LREE) with a minor fractionation of heavy REE (HREE) as indicated also by $(Gd/Yb)_n$ ~1–2 and $(La/Yb)_n$ ~2–5. On the other hand, the mantle-normalized plots of these rocks show negatively sloping patterns and some, but not all, samples display negative Nb and Ta anomalies relative to La and Th (Fig. 8). The second group with lower Nb/Y has flat or LREE-depleted patterns with $(La/Yb)_n < 1$ (typically ~0.5) and is accompanied by mantle-normalized plots with distinct depletion of strongly incompatible elements (left side of the mantle-normalized plot) but without depletion of Nb and Ta relative to Th and La. The differences between the two groups do not appear to be

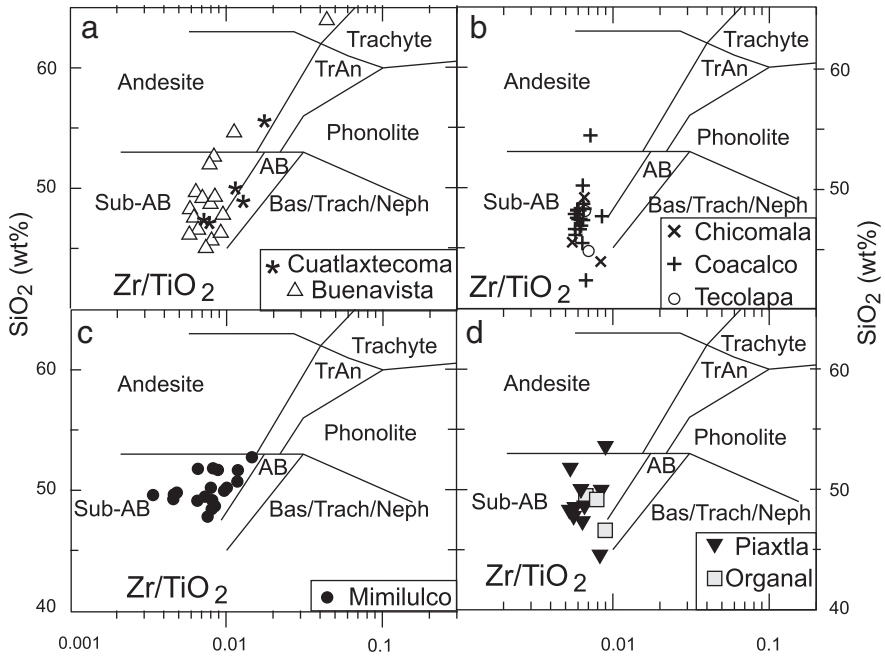

Fig. 6. Zr/TiO_2 vs SiO_2 (wt.%) diagram of Winchester and Floyd (1977) for the HP rocks (a) the Buenavista and Cuatlaxtecoma units of the Piaxtla Suite, Ixcamilpa; (b) the Coacalco, Chicomala and Tecolapa units of the Piaxtla Suite, Ixcamilpa; (c) Mimilulco group; (d) Organal and Piaxtla rocks. Abbreviations: Sub-AB = subalkaline basalt; AB = alkaline basalt; TrAn = trachyandesite; Bas = basanite; Trach = trachyte; Neph = nephelinite.

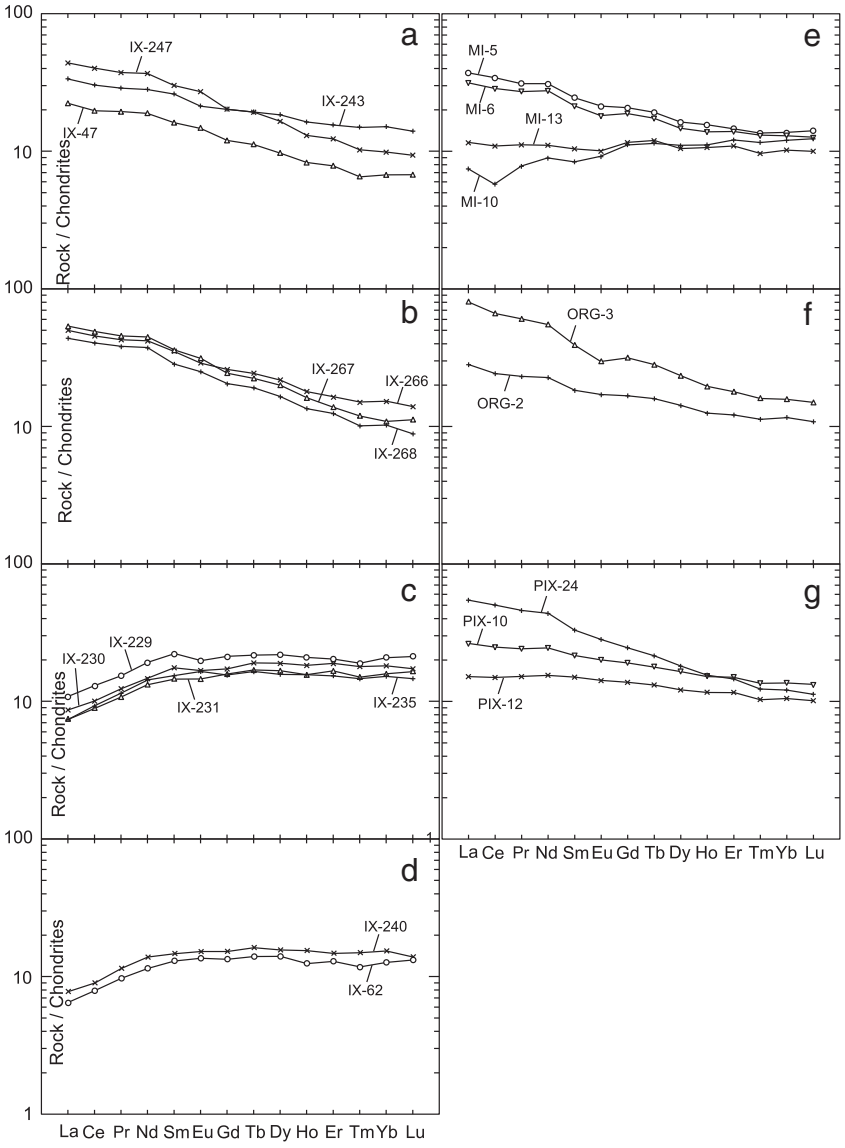

Fig. 7. Chondrite-normalized REE abundances for (a) Buenavista unit (IX-47; IX-243; IX-247); (b) Cuatlaxtecoma unit (IX-266, IX-267; IX-268); (c) Coacalco unit (IX-229; IX-230; IX-231; IX-235); (d) Chicomala and Tecolapa units (IX-62, IX-240); (e) Mimilulco samples (MI-5, MI-6; MI-10; MI-13); (f) Organal samples (ORG-2; ORG-3), (g) Piaxtla samples (PIX-10, PIX-12, PIX-24). Normalizing values are after Sun and McDonough (1989).

due to crustal contamination as both groups have a low Th/La ratio (typically <0.1), a sensitive index of crustal contamination (Sun and McDonough, 1989). The low Th/La values (~0.1) are characteristic of mantle-derived rocks uncontaminated by continental crust. Although some of the geochemical characteristics of the rocks of the second group resemble those of mid-ocean ridge basalts (MORB), the rocks are associated with felsic rocks and were likely emplaced upon the thin continental crust.

The Sm–Nd isotopic characteristics of the Ixcamilpa (IX) amphibolites are highly variable with εNd ranging from +0.8 to +8.6 and $^{147}Sm/^{144}Nd$ from 0.10 to 0.23 Table 3; Fig. 9). The first group includes most mafic samples with LREE-enriched chondrite-normalized patterns, and has relatively low ε_{Nd} (+0.8 to +5.5) and $^{147}Sm/^{144}Nd$ (0.13–0.16). These samples have low (La/Nb)n ratios (<1.5) and do not appear to be significantly contaminated by continental crust. The second group of samples have low Nb/Y ratios and depleted LREE patterns and have high positive ε_{Nd} (~+8) and high $^{147}Sm/^{144}Nd$ (~0.22) values, which resemble those expected for juvenile magmas derived from a depleted mantle source (Fig. 9). Taken together these data suggest that the isotopic range and isotopic and trace element differences between the two groups probably reflect derivation from a heterogeneous subcontinental lithospheric mantle. On the other hand, two additional IX samples (268 and 245) have LREE-enriched patterns and display distinct Nd isotopic signatures (Table 3). Sample IX-268 has an unusually low $^{147}Sm/^{144}Nd$ ratio (0.1) and young model age T_{DM} (360 Ma), which may indicate a metasomatic event that modified its mantle source. Sample IX-245 has high (La/Nb)n (> 2), Th/La ~0.23 and a distinct negative Nb anomaly on the mantle-normalized plot, which probably indicate crustal contamination. These data suggest a complex evolution of the lithospheric mantle source for the precursor of the IX mafic rocks: an heterogeneous late Proterozoic mantle source (see T_{DM} ages in Table 3) affected at ca. 360 Ma by a metasomatic event (Table 3), which was variably contaminated by the crust during ascent to the surface.

4.2. Mimilulco

The Mimilulco mafic rocks are typical of subalkaline basalts with SiO_2 ranging from 48 wt.% to 53 wt.% (Fig. 3). The basaltic rocks display

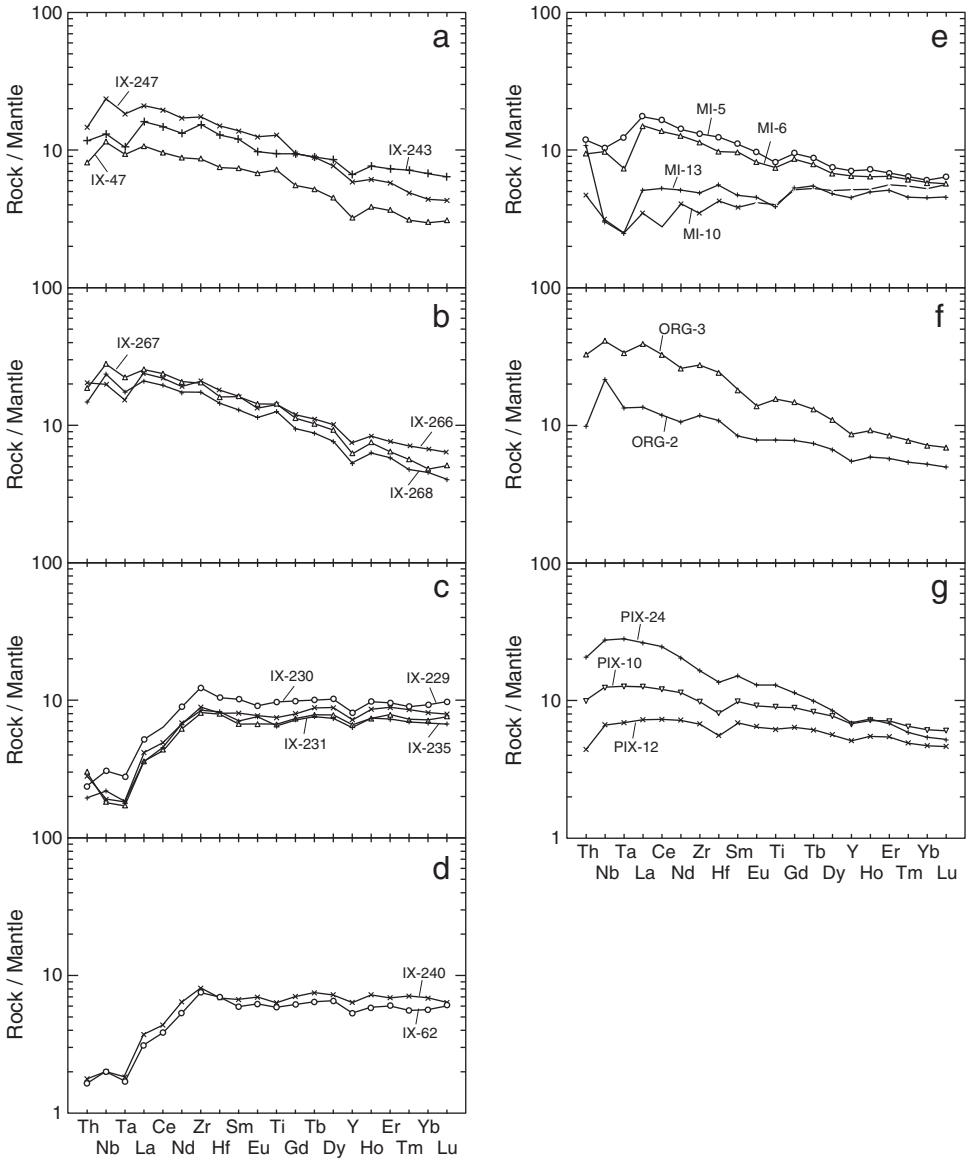

Fig. 8. Primitive mantle-normalized trace element patterns of (a) Buenavista unit (IX-47; IX-243; IX-247); (b) Cuatlaxtecoma unit (IX-266, IX-267; IX-268); (c) Coacalco unit (IX-229; IX-230; IX-231; IX-235); (d) Chicomala and Tecolapa units (IX-62, IX-240); (e) Mimilulco samples (MI-5, MI-6; MI-10; MI-13); (f) Organal samples (ORG-2; ORG-3), (g) Piaxtla samples (PIX-10, PIX-12, PIX-24). Normalizing values are after Sun and McDonough (1989).

significant compositional variations, some of which are not related to differentiation. For example, their Nb/Y (Fig. 5) ratio, which is not modified during the fractional crystallization, ranges from 0.1 to 0.6. The variations are also reflected in a wide range of chondrite-normalized REE patterns that extends from LREE-depleted to LREE-enriched with $(La/Yb)_n$ and $(La/Sm)_n$ ratios varying from ~0.5 to 2.5 and from ~0.8 to 1.5, respectively (Fig. 7). The heavy REE segment of the patterns is typically flat with $(Gd/Yb)_n$ ranging from 1 to 1.5 (Fig. 7). Likewise the mantle-normalized trace element plots of the mafic rocks show a flat to slightly negative slope, with the patterns ranging from those that peak at Nb-Ta to those that have negative Nb-Ta anomalies relative to Th and La (Fig. 8). Although the Th/La ratio is variable and probably records the limited role of crustal contamination in the evolution of some of the rocks, the positive ε_{Nd} values and the absence of a correlation of major elements with Th/La ratios suggest that the contamination cannot explain the differences in the mantle-normalized plots among the various samples. We conclude that these differences are probably related to heterogeneous mantle sources.

The Sm–Nd isotopic characteristics of the Mimilulco samples are similar to the IX samples in showing variable ε_{Nd} from +1.8 to +6.6 and $^{147}Sm/^{144}Nd$ ratios of 0.16–0.22 (Table 3, Fig. 9). Although the Th/La ratio is variable and probably records limited crustal contamination in the evolution of some rocks, the positive ε_{Nd} values and the absence of a correlation of major elements with Th/La ratios suggest that the differences exhibited in the mantle-normalized plots among the various samples are unlikely to be related to crustal contamination. We conclude that these differences are probably related to heterogeneous subcontinental lithospheric mantle sources.

4.3. Organal

The Organal mafic rocks have SiO_2 from 47 to 50 wt.%. They are subalkaline (Fig. 6) and show typical tholeiitic fractionation trends (Figs. 3 and 4). The range in Nb/Y ratio (0.3–0.8) suggests that some basalts are transitional, as observed in the other suites. The mafic rocks have moderately LREE-enriched, chondrite-normalized REE

patterns with $(La/Yb)_n$ ranging between 2 and 5 accompanied by $(La/Sm)_n$ ~1.5 and $(Gd/Yb)_n$ ~1.5 to 2. The mantle-normalized trace element patterns of mafics show a negative slope without negative Nb, Ta and Ti anomalies.

The Organal mafic samples have Sm–Nd isotopic features similar to those from Ixcamilpa and Mimilulco. The ε_{Nd} values are between +1.8 and 2.2 and the $^{147}Sm/^{144}Nd$ ratios are between 0.15 and 0.17 (Table 3, Fig. 9). On the other hand, the associated felsic rocks have a very different isotopic signature with negative ε_{Nd} values (−4.9), low $^{147}Sm/^{144}Nd$ (0.13), and T_{DM} = ca. 1.6 Ga. geochemical and Sm–Nd isotopic characteristics of the felsic rocks are inconsistent with derivation by fractional crystallization from a mafic parent, and instead are characteristic of intra-crustal melting. Such an origin is supported by the negative Nb-Ta and Ti anomalies on the mantle-normalized plot, the low $^{147}Sm/^{144}Nd$ and high T_{DM}.

4.4. Petrogenesis

The three bimodal felsic–mafic suites are potentially correlative, in terms of lithological association and age. The mafic rocks from all areas typically fall into the fields of subalkaline basalts, although the range in Nb/Y suggests some of these rocks are transitional to alkaline basalts. Relatively elevated SiO_2 contents, high Th/La, Th/Nb and La/Nb ratios and low ε_{Nd} are commonly used as indicators of crustal contamination (Neal et al., 2002), and our data suggest that some of the evolved HP rocks were affected by crustal contamination. However, this process cannot account for all of the differences among the various groups of mafic rocks.

Differences in the behavior of some incompatible trace elements and their ratios can be used to distinguish between compositional changes due to fractional crystallization, differences in degree of partial melting, depth of melting and heterogeneous source rocks. A La/Yb vs Yb diagram (Fig. 10) indicates that the variations among the mafic rocks of the Coacalco can be explained by the process of fractional crystallization, whereas those of the Mimilulco, Cuatlaxtecoma, Buenavista, Piaxtla and Organal require a heterogeneous source as well as variable degrees of partial melting.

The degree of melting and nature of the mantle source can be estimated by using the REE composition of the mafic rocks. Garnet preferentially retains heavy REE whereas all REE are strongly incompatible in spinel. Basaltic magmas derived from a garnet-bearing mantle source have a Dy/Yb ratio higher than those generated from a spinel-bearing mantle. Thus the Dy/Yb ratio reflects the depth of the melting and the La/Sm ratio is related to the degree of partial melting. The Dy/Yb vs La/Sm diagram (Fig. 11) shows that Coacalco, Chicomala and Tecolapa mafic rocks were derived from a shallow spinel-bearing mantle and their low La/Sm suggests a high degree of melting. The rocks of the Buenavista and Cutlaxtecoma units, and Organal were likely derived from a transition zone between garnet- and spinel-bearing sources by a smaller degree of melting.

The Th/Yb vs Nb/Yb diagram of Pearce (2008) can be used to evaluate lithospheric inputs. The averages of N-MORB (N-type MORB), E-MORB (E-type MORB) and OIB (ocean island basalt) form a diagonal mantle array in this graph (Fig. 12). Lavas that interacted with continental crust during the ascent or have a subduction component are displaced to higher Th/Yb values. Most of the basalts lie within

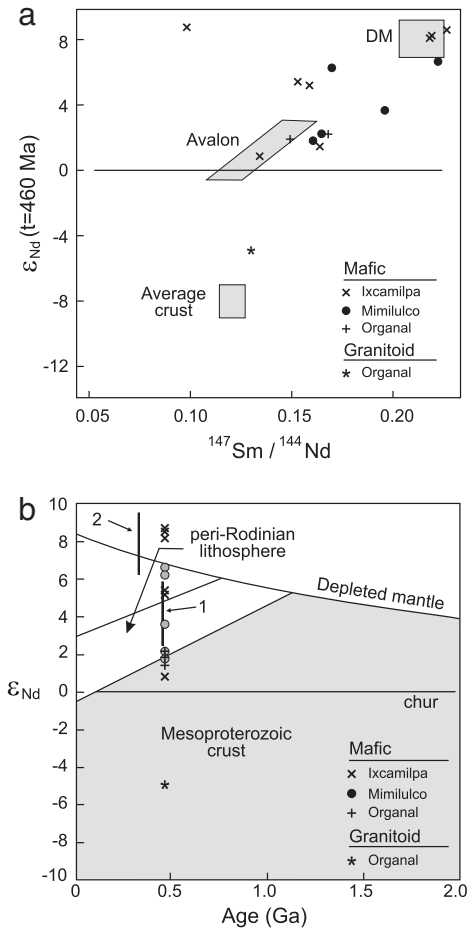

Fig. 9. Sm–Nd isotopic systematics for the HP amphibolites and one granitoid from the Piaxtla Suite, Acatlán Complex: (a) ε_{Nd} vs $^{147}Sm/^{144}Nd$ (t = 460 Ma comparing the Sn-Nd isotopic data with typical Avalonian crust, depleted mantle and the average upper continental crust (after Murphy et al., 2006); and (b) ε_{Nd} vs Time (Ma) comparing the data for amphibolites and a granitoid with the range of Asis eclogitic amphibolites depicted as line 1 (Murphy et al., 2006), and the range of Carboniferous tholeiitic basalts (Progreso and Zumpango units) of the western Acatlán Complex shown as line 2 (Ortega-Obregon et al., 2010). Compositions of pero-Rodinian oceanic lithosphere and Mesoprotereozoic continental crust (after Murphy et al., 2006) are shown for comparison. CHUR = chondritic uniform reservoir.

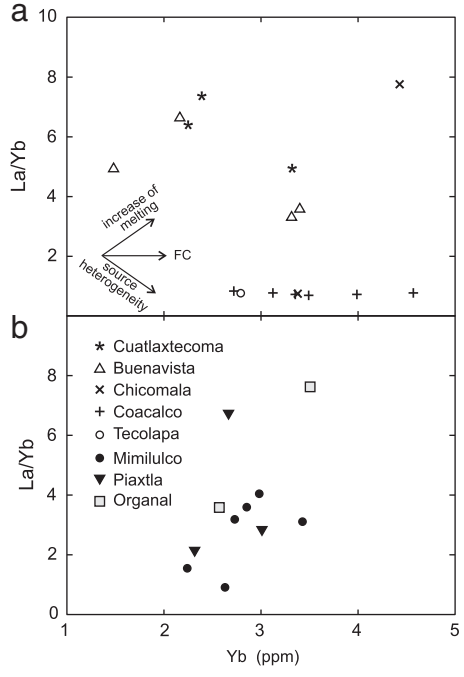

Fig. 10. Plots of La/Yb vs Yb for the mafic rocks of the Ixcamilpa area (a) and Mimilulco, Organal and Piaxla (b) areas. Vectors of degree of partial melting, fractional crystallization (FC) and source heterogeneity are after He et al. (2010).

Table 3
Sm–Nd isotopic data for Ordovician metasedimentary and metaigneous rocks of the Acatlán complex in the median HP belt at the Mimilulco, Organal and Ixcamilpa.

Sample	Nd (ppm)	Sm (ppm)	$^{143}Sm/^{144}Nd$	$^{143}Nd/^{144}Nd$		2σ	$Nd_{460\ Ma}$	T_{DM} DePaolo	T_{DM2} (Ma)
Mimilulco									
MI-1	16.65	4.55	0.1651	0.512654	±	7	2.17	1216	1556
MI-5	17.54	4.67	0.1610	0.512621	±	7	1.77	1215	1530
MI-8	11.65	3.28	0.1702	0.512876	±	7	6.21	618	962
MI-10	5.45	2.00	0.2224	0.513054	±	7	6.61		
MI-13	7.21	2.34	0.1963	0.512821	±	6	3.6	1914	2881
Organal									
ORG-1	36.34	7.84	0.1304	0.512186	±	4	−4.93	1564	1672
ORG-2	14.79	4.12	0.1683	0.512664	±	4	2.18	1267	1465
ORG-3	52.17	12.91	0.1495	0.512590	±	5	1.84	1077	1212
Ixcamilpa									
IX-54 (CM)	41.18	9.171	0.1346	0.512493	±	7	0.8	1062	1266
IX-229 (CC)	11.7	4.227	0.2185	0.51312	±	7	8.1		
IX-240 (CM)	7.942	2.88	0.2193	0.513126	±	7	8.2		
IX-245 (BV)	15.75	4.277	0.1642	0.512616	±	7	1.5	1308	1644
IX-247 (BV)	22.57	5.724	0.1533	0.512784	±	7	5.4	674	925
IX-266 (CL)	26.33	6.928	0.1591	0.512789	±	7	5.2	729	1009
IX-268 (CL)	22.57	3.691	0.0989	0.512789	±	7	8.7	360	480
IX-278 (CC)	8.136	3.049	0.2266	0.513164	±	7	8.5		

T_{DM2} calculated using a linear evolution for a mantle separated from the CHUR at 4.55 Ga and having a present day Epsilon value of +10.
T_{DM} is not given for rocks with 147/144 >0.175 according to the method of Stern.
143/144 corrected from the deviation from JNdi-1. Mean value of MUN TIMS Lab: 0.512101.
Std Dev 0.000007 N = 52.
UNITS: BV = Buenavista, CC = Coacalco blueschist, CL = Cuatlaxtecoma, CM = Chicomala.

or adjacent to a diagonal mantle array implying very limited contamination. However, some basalts plot significantly above the MORB-OIB mantle array, suggesting the involvement of a crustal or subduction component. High Th/Nb ratio relative to primitive mantle in some of these samples is also consistent with the negative Nb-Ta anomalies in the trace element patterns.

Positive ε_{Nd} values and low Th/La ratios indicate that some of these samples were derived either from a metasomatically enriched subcontinental lithospheric mantle (SCLM) of juvenile mantle, whereas other samples were affected by crustal contamination. Assuming that the mafic rocks were derived from a similar source, then their parent magma originated in SCLM.

Saunders et al. (1992) argued that continental rifting, decompression, the presence of hydrous phases in SCLM, melt injection from a plume into the lithosphere, and thermal and mechanical erosion of the lithosphere, are all processes that can generate melting of SCLM and generation of within-plate basalts. All the mafic suites have geochemical characteristics (including Ti and immobile trace elements

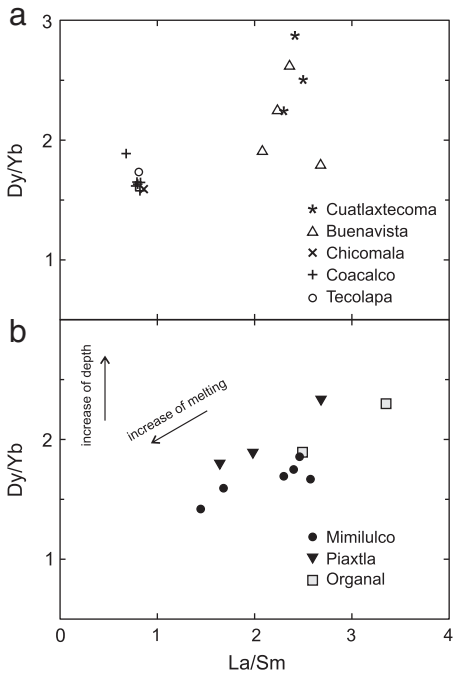

Fig. 11. Plots of Dy/Yb vs La/Sm for the mafic rocks of the Ixcamilpa area (a) and Mimilulco, Organal and Piaxtla areas (b). Vectors of degrees of partial melting and melting depth are after He et al. (2010).

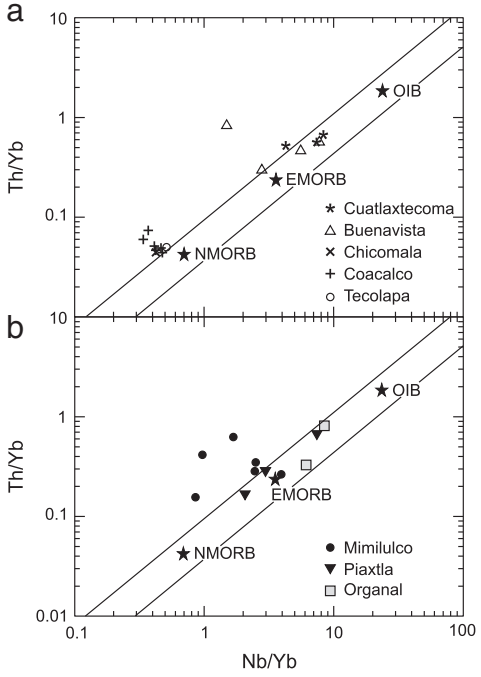

Fig. 12. Th/Yb vs Nb/Yb diagram for the mafic rocks of the Ixcamilpa area (a) and Mimilulco, Organal and Piaxtla areas (b). Mantle array (MORB-OIB) and modeling is after Pearce (2008).

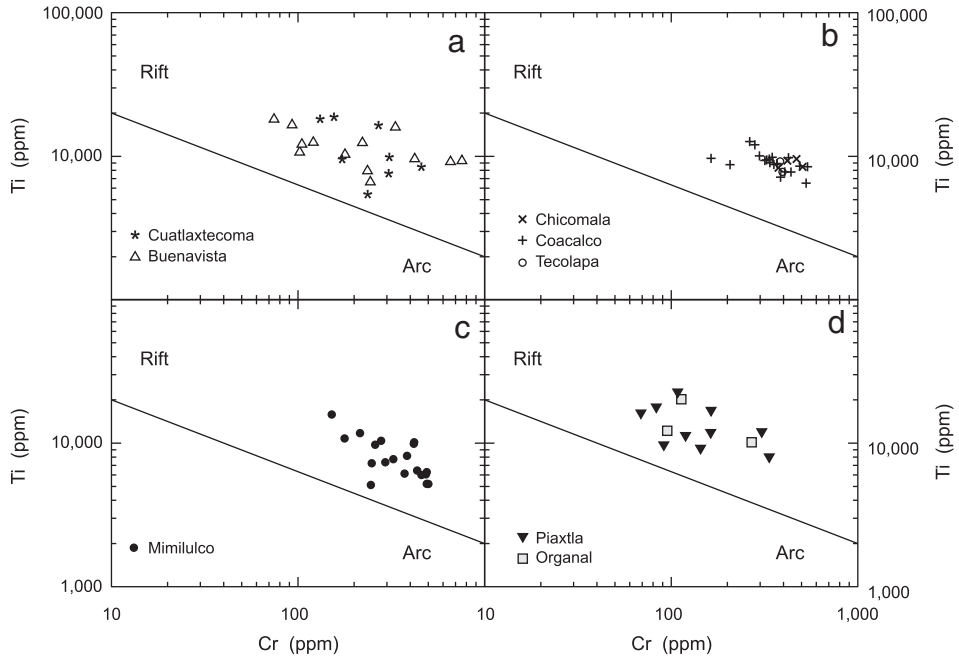

Fig. 13. Cr (ppm) vs Ti (ppm) of Pearce (1975) for the HP mafic rocks (a) the Buenavista and Cuatlaxtecoma units of the Piaxtla Suite, Ixcamilpa; (b) the Coacalco, Chicomala and Tecolapa units of the Piaxtla Suite, Ixcamilpa; (c) Mimilulco samples; (d) Organal and Piaxtla samples.

abundances, such as Zr, Cr, Y and Nb: Fig. 13) typical of within-plate, tholeiitic to transitional basalts.

Field observations show that there is a spatial and temporal relationship between the silicic and mafic rocks. However, the felsic rocks have distinct negative Nb, Ta and Ti anomalies and significantly different ε_{Nd} values suggesting that they are not directly related to the basalts. These traits together with the close spatial association of felsic and mafic rocks suggest that the felsic rocks are crustal melts related to an emplacement of the mafic magmas. Their associations with felsic rocks suggest that the rocks were emplaced upon a thin continental crust.

5. Correlations

The detrital zircon populations in the metapsammite from Organal (ORG-6) have population peaks at 1100–1200 Ma and 481 +3/−2 Ma, which are similar to those of other Acatlán HP metasedimentary rocks (Keppie et al., 2008; Nance et al., 2009; Ortega-Obregón et al., 2009; Ramos-Arias and Keppie, 2011). The nearest sources for these zircons are the adjacent Oaxacan Complex and contemporaneous Ordovician Acatlán plutons. Such plutons include the 488 +8/−7 Ma megacrystic granitoid sheet at Organal. This latter age is within the 490–450 Ma age range of other megacrystic granitoids reported in the HP belts: (i) at Mimilulco: 492 ± 12 Ma for the San Miguel Las Minas granitoid pluton intruded by a leucogranite dated at 473 +32/−24 Ma (Keppie et al., 2010), and 461 ± 9 Ma for a leucogranite (Talavera-Mendoza et al., 2005); (ii) at Asis: ca. 470 Ma for a granitic sheet (Murphy et al., 2006); (iii) the type Esperanza granitoid yielded 471 ± 6 Ma (Sánchez-Zavala et al., 2004); (iv) at Piaxtla: 474 ± 16 Ma for a granite (Talavera-Mendoza et al., 2005) and 452 ± 6 Ma (Keppie et al., 2011) for a granitoid; (v) near Ixcamilpa: 488 ± 7 Ma for the Tecolapa granitoid pluton (Ramos-Arias and Keppie, 2011); and (vi) near Olinalá: 465 ± 4 Ma for the Ocotitlan megacrystic granite, 473 ± 7 Ma for a granitic sheet near Olinalá (Ortega-Obregón et al., 2009), 478 ± 5 Ma and 471 ± 5 Ma for Tetecic leucogranites (Talavera-Mendoza et al., 2005).

At Mimilulco, the 461 ± 2 Ma age of the back veining is similar (within error) to the 470 ± 10 Ma, U–Pb zircon age reported for the Anacahuite Amphibolite (Keppie et al., 2010), and both ages lie within the range of megacrystic granitoids around Mimilulco (492 ± 12 Ma to 473 +32/−24 Ma) suggesting that the rocks form part of a bimodal suite. The rocks at Ixcamilpa, Mimilulco and Organal have similar geochemical characteristics to those at Olinalá, Asis and Piaxtla (Keppie et al., 2011; Murphy et al., 2006; Ortega-Obregón et al., 2009). The mafic rocks are amphibolites with chemical compositions corresponding to within-plate tholeiites, and some are transitional to alkaline basalts. Associated felsic rocks do not appear to be related to the amphibolites and compositionally resemble peraluminous calc-alkaline rhyolites derived by melting of the crust. Thus, in contrast to earlier studies (Meza-Figueroa et al., 2003), all of the HP mafic rocks appear to have been derived from the Ordovician rift-passive margin: the only exception are those at Tehuitzingo that have periarc affinites (Galaz Escanilla et al., 2009; Proenza et al., 2004).

The 348 +4/−1 Ma migmatization age at Organal is similar to the ~347–330 Ma (SHRIMP zircon ages determined by Middleton et al. (2007) and dates decompression melting following peak metamorphism dated at 346 ± 3 Ma and 353 ± 1 Ma at Asis and Mimilulco, respectively (metamorphic zircon ages: Elías-Herrera et al., 2004; Middleton et al., 2007). Decompression melting was followed by cooling through ca. 530 °C at 343 Ma (amphibole at Piaxtla), ca 470 °C at of 344 ± 5 Ma (glaucophane at Mimilulco), and 370 °C at 338–334 Ma (phengite)(Keppie et al., 2010, 2011).

6. Tectonic implications

The rift setting of most of the Ordovician HP mafic tholeiites, their bimodality with respect to Ordovician megacrystic granitoids, and their association with metamorphosed continental rise rocks, are all consistent with derivation from a rift-passive margin off northwestern Amazonia (Fig. 14). These HP rocks are inferred to have been extruded into the Acatlán Complex because similar low-grade, Ordovician, rift-related tholeiitic rocks and clastic metasediments occur on either side of the median HP belt (Keppie et al., 2008, 2010, 2011). Since no ophiolitic rocks occur along the Mixteca–Oaxaquia terrane boundary, the HP protoliths were probably derived from the margin of Oaxaquia lying to the west of the Acatlán Complex (Fig. 15a and b). This interpretation is consistent with similarity of the chemistry and geochronology

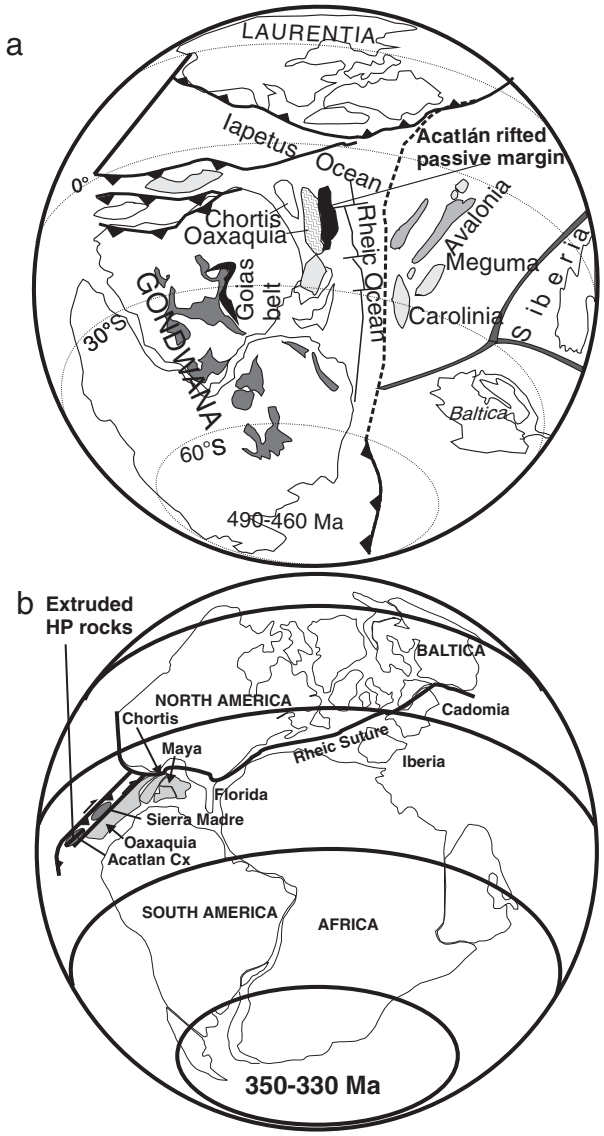

Fig. 14. Global reconstructions showing: (a) the Acatlán rifted passive margin of Oaxaquia; and (b) the Mississippian extrusion zone within the Acatlán Complex on the western margin of Pangea.

of the HP rocks and low-grade Acatlán rocks on either side of the HP belt (Keppie et al., 2008). Extrusion of the median HP belt is indicated by the bounding tectonic contacts: a thrust below and a listric shear zone above (Galaz Escanilla et al., 2009; Ramos-Arias et al., 2008). The Devonian–Carboniferous age of the HP metamorphism suggests that the HP rocks were removed from the margin by subduction erosion (Fig. 15c). This interpretation is consistent with the presence of a remnant of the arc on the eastern side of the median HP belt at Patlanoaya near Mimilulco (Fig. 1) (Keppie et al., 2010). That much of the arc was also removed by subduction erosion is indicated by the periarc affinity of the HP rocks at Tehuitzingo (Fig. 15d)(Galaz Escanilla et al., 2009; Proenza et al., 2004). Traces of this arc can also be seen in the 405–330 Ma igneous detrital zircons found in Carboniferous rocks in the Acatlán Complex and in rocks unconformably overlying the Oaxacan Complex (Keppie et al., 2008).

Subduction erosion of the upper plate is generally thought to occur by piecemeal removal of the frontal and lower margin of the upper plate (von Huene et al., 2004) resulting in the formation of a tectonic mélange. However, numerical modeling has indicated that large strips of the margin, up to 300 km wide, may be removed in one piece (D. F. Keppie et al., 2010, 2012). The presence of the 6 km wide Ordovician Tecolapa granitoid that cross-cuts two mappable units (15×25 km in surface dimension) at Ixcamilpa suggests that this slice was also removed, extruded and transported in a klippe as one large piece. This slice structurally overlies three other slices each with similar dimensions. The HP rifted passive margin rocks in the median HP belt are 10×90 km in surface dimension, and, although internally deformed, appear to form a reasonably coherent slice suggesting that they, too, were subducted in one large piece. This conclusion is consistent with the rapid (<17 my) removal of this piece, which must have occurred after 365±15 Ma, the age of the youngest detrital zircon in the HP rocks at Piaxtla (Keppie et al., 2011). The small Tehuitzingo slice is the only representative of subducted forearc (Fig. 14d: Galaz Escanilla et al., 2009; Proenza et al., 2004). Numerical experiments indicate that subducted upper plate rocks can be underplated beneath the upper plate (Keppie et al., 2009a), and such a process is envisaged for the HP rocks of the Acatlán Complex (Fig. 15c). The absence of rocks of the basement (Oaxacan Complex) in the median HP belt suggests that the basement was delaminated from the rifted passive margin and its higher density may have caused it to be subducted to greater depths (Fig. 15d).

The timing of peak temperatures is indicated by the 348 +4/−1 Ma age of metamorphic zircons in the migmatized amphibolite that followed peak pressure at depths of 45–55 km at ca 350 Ma (Keppie et al., 2011; Vega-Granillo et al., 2007). Exhumation is constrained by $^{40}Ar/^{39}Ar$ cooling ages of 342 and 334 Ma for hornblende and phengite (Keppie et al., 2010, 2011). That the HP rocks of the median belt form a reasonably coherent slice(s) is remarkable given the internal polyphase deformation, and suggests that extrusion was facilitated by extension. Such extension is consistent with the synchronous deposition of the uppermost Devonian–Lower Permian, Patlanoaya Group (363–270 Ma: Ramos-Arias et al., 2008) in a basin lying just to the east of the median HP belt. To the west of the HP belt, clastic wedge sedimentation is inferred for the Mississippian Zumpango Unit (Ortega-Obregón et al., 2009; Ramos-Arias and Keppie, 2011) (Fig. 1).

Acknowledgments

We would like to acknowledge a Papiit grant (IN103003) and a CONACyT grant (CB-2005-1/24894) to JDK, a NSF grant EAR 0308105 to RDN, and NSERC Discovery grants to JD and JBM. The paper benefitted by a constructive review by Dr. L.A. Solari and represents a contribution to the IGCP Pangea Project 597.

References

Butler, J.P., Beaumont, C., Jamieson, R.A., 2011. Crustal emplacement of exhuming (ultra) high-pressure rocks: will that be pro- or retro-side? Geology 39, 635–638.
Calvert, A.J., 2003. Seismic reflection imaging of two megathrusts in the northern Cascadia subduction zone. Nature 428, 163–167.
Cerca, M., Ferrari, L., López-Martínez, M., Martiny, B., Iriondo, A., 2006. Late Cretaceous shortening and early Tertiary shearing in the central Sierra Madre del Sur, southern Mexico: insights into the evolution of the Caribbean–North American plate interaction. Tectonics 26, TC3007. http://dx.doi.org/10.1029/2006TC001981.
DePaolo, D.J., 1988. Neodymium Isotope Geochemistry: An Introduction. Springer Verlag, New York. 187 pp.
Elías-Herrera, M., Ortega-Gutiérrez, F., 2002. Caltepec fault zone: an Early Permian dextral transpressional boundary between the Proterozoic Oaxacan and Paleozoic Acatlán Complexes, southern Mexico, and regional implications. Tectonics 21 (3), 1013. http://dx.doi.org/10.1029/2000TC001278.
Elías-Herrera, M., Ortega-Gutiérrez, F., Sánchez-Zavala, J.L., Reyes-Salas, A.M., Macias-Romo, C., Iriondo, A., 2004. New geochronological ad stratigraphic data related to the Paleozoic evolution of the high-pressure Piaxtla Group, Acatlán Complex, southern Mexico. IV reunion nacional de ciencias de la tierra, Libro de Resumenes, p. 150.
Ernst, W.G., 2009. Subduction-zone metamorphism, calc-alkaline magmatism, and convergent-margin crustal evolution. Gondwana Research 18 (1), 8–16. http://dx.doi.org/10.1016/j.gr.2009.05.010.
Galaz Escanilla, G., Keppie, J.D., Solari-Lovati, L., 2009. Complejo Acatlan en el area de Tehuitzingo, Estado de Puebla, Sur de Mexico: evidencias de su evolucion tectonica. Geos 29 (1), 48.

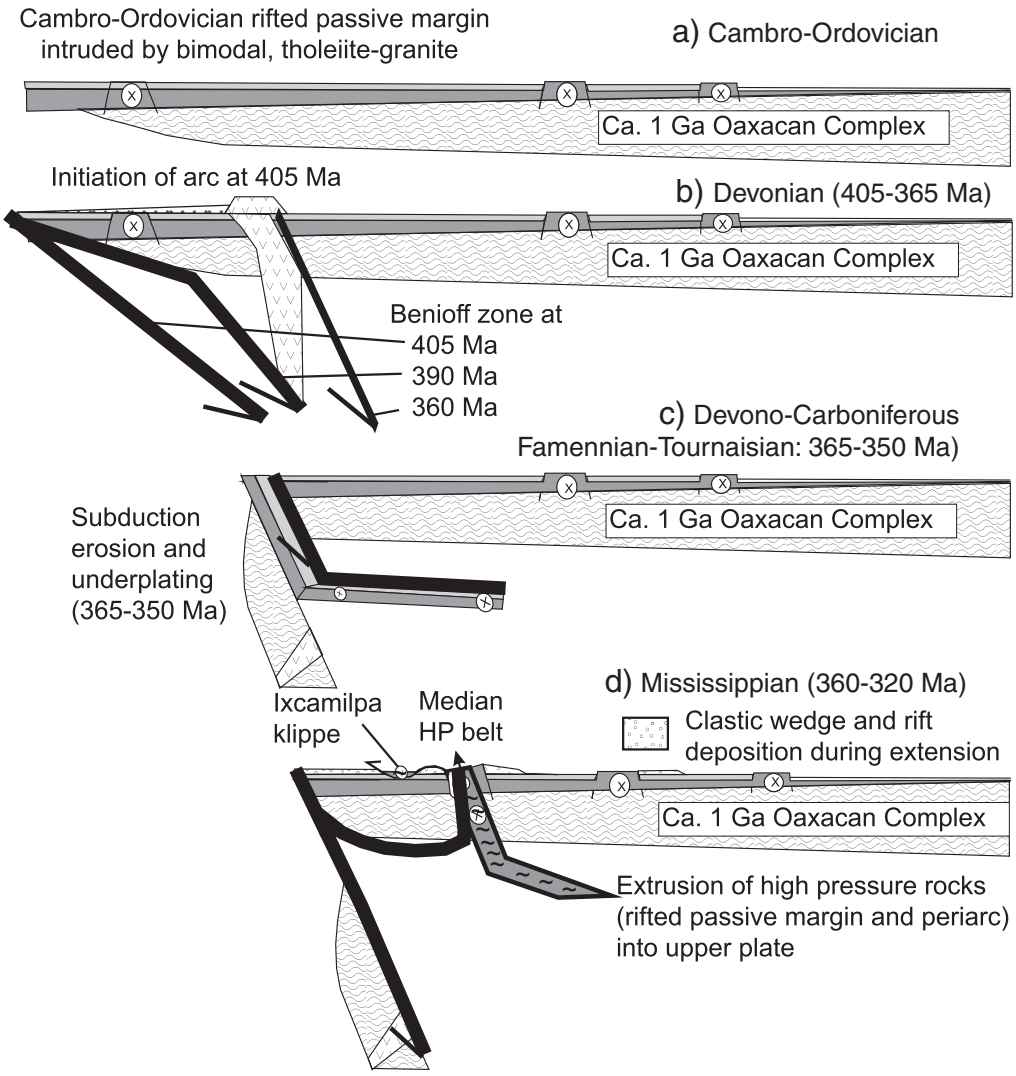

Fig. 15. Tectonic cross-sections showing the development of the Acatlán Complex in: (a) the Ordovician, (b) the Devonian, (c) the Devono-Carboniferous boundary, and (d) the Mississippian.

Gehrels, G., Valencia, V., Pullen, A., 2006. Detrital Zircon Geochronology by Laser Ablation Multicollector ICPMS at the Arizona LaserChron Center. In: Olszewski, T. (Ed.), Geochronology: Emerging Opportunities: Paleontology Society Papers, v.12, pp. 67–76.

Harry, D.L., Green, N.L., 1999. Slab dehydration and basalt petrogenesis in subduction systems involving very young oceanic lithosphere. Chemical Geology 160, 309–333.

He, Q., Xiao, L., Balta, B., Gao, R., Chen, J., 2010. Variety and complexity of the Late-Permian Emeishan basalts: reappraisal of plume–lithosphere interaction processes. Lithos 119, 91–107.

Keppie, J.D., 2004. Terranes of Mexico revisited: a 1.3 billion year odyssey. International Geology Review 46, 83–100.

Keppie, J.D., Dostal, J., Murphy, J.B., Nance, R.D., 2008. Synthesis and tectonic interpretation of the westernmost Paleozoic Variscan orogen in southern Mexico: from rifted Rheic margin to active Pacific margin. Tectonophysics 461, 277–290.

Keppie, D.F., Currie, C.A., Warren, C., 2009a. Subduction erosion modes: comparing finite element numerical models with the geological record. Earth and Planetary Science Letters 287, 241–254.

Keppie, J.D., Morán-Zenteno, D.J., Martiny, B., González-Torres, E., 2009b. Synchronous 29–19 Ma arc hiatus, exhumation, and subduction of forearc in southwestern Mexico. In: James, K.H., Lorente, M.A., Pindell, J. (Eds.), Origin and Evolution of the Caribbean Plate: Geological Society of London, Special Publications, 328, pp. 169–179. http://dx.doi.org/10.1144/SP328.7.

Keppie, J.D., Nance, R.D., Ramos-Arias, M.A., Lee, J.K.W., Dostal, J., Ortega-Rivera, A., Murphy, J.B., 2010. Late Paleozoic subduction and exhumation of Cambro-Ordovician passive margin and arc rocks in the northern Acatlán Complex, southern Mexico: geochronological constraints. Tectonophysics 495, 213–229. http://dx.doi.org/10.1016/j.tecto.2010.09.019.

Keppie, J.D., Nance, R.D., Dostal, J., Lee, J.K.W., Ortega-Rivera, A., 2011. Constraints on the subduction erosion/extrusion cycle in the Paleozoic Acatlán Complex of southern Mexico: geochemistry and geochronology of the type Piaxtla Suite. Gondwana Research 21, 1050–1065. http://dx.doi.org/10.1016/j.gr.2011.07.020.

Keppie, D.F., Hynes, A.J., Lee, J.K.W., Norman, M., 2012. Oligocene-Miocene back-thrusting in southern Mexico linked to the rapid subduction erosion of a large forearc block. Tectonics 31, TC2008. http://dx.doi.org/10.1029/2011TC002976.

Liou, J.G., Tsujimori, T., Zhang, R.Y., Katayama, I., Maruyama, S., 2004. Global UHP metamorphism and continental subduction/collision: the Himalayan model. International Geology Review 46, 1–27.

Ludwig, K.R., Mundil, R., 2002. Extracting reliable U–Pb ages and errors from complex populations of zircons from Phanerozoic tuffs. Geochimica et Cosmochimica Acta 66, 463A Goldchmidt Conference Abstracts.

Meza-Figueroa, D., Ruiz, J., Talavera-Mendoza, O., Ortega-Gutiérrez, F., 2003. Tectonometamorphic evolution of the Acatlán Complex eclogites (southern México). Canadian Journal of Earth Sciences 40, 27–44.

Middleton, M.J.D., Murphy, J.B., Miller, B.V., Nance, R.D., Ortega- Rivera, A., Lee, J.K.W., 2007. P–T–t constraints on exhumation following subduction in the Rheic Ocean from eclogitic rocks in the Acatlán Complex of southern México. In: Linnemann, U., Nance, R.D., Zulaf, G., Kraft, P. (Eds.), The evolution of the Rheic Ocean: from Avalonian–Cadomian active margin to Alleghenian–Variscan collision: Geological Society of America, Special Paper, 423, pp. 437–452. http://dx.doi.org/10.1139/e02-093.

Miyashiro, A., 1974. Volcanic rock series in island arcs and active continental margins. American Journal of Science 274, 321–355.

Monger, J., Price, R., 2002. The Canadian Cordillera: geology and tectonic evolution. Canadian Society of Economic Geologists Recorder 2002, 1–36 February 2002.

Murphy, J.B., Keppie, J.D., Nance, R.D., Miller, B.V., Middleton, M., Fernández-Suarez, J., Jeffries, T.E., 2006. Geochemistry and U–Pb protolith ages of eclogitic rocks of the Asis Lithodeme, Piaxtla Suite, Acatlán Complex, southern Mexico: Cambro-Ordovician rift-passive margin sequence cut by an Ordovician arc on the southern

margin of the Rheic Ocean. Journal of the Geological Society of London 163, 683–695.
Nance, R.D., Keppie, J.D., Miller, B.V., Murphy, J.B., Dostal, J., 2009. Palaeozoic palaeogeography of Mexico: Constraints from detrital zircon age data. Geological Society of London Special Publication 327, 239–269.
Neal, C.R., Mahoney, J.J., Chazey III, W.J., 2002. Mantle sources and the highly variable role of continental lithosphere in basalt petrogenesis of the Kergulen Plateau and Broken Ridge LIP: results from ODP Leg 183. Journal of Petrology 43, 1177–1205.
Ortega-Obregon, C., Keppie, J.D., Murphy, J.B., 2010. Geochemistry of Carboniferous low metamorphic grade sedimentary and tholeiitic igneous rocks in the western Acatlán Complex, southern Mexico: deposition along the active western margin of Pangea. Revista Mexicana de Ciencias Geológicas 27 (2), 238–253.
Ortega-Gutiérrez, F., 1981. Metamorphic belts of southern México and their tectonic significance. Geofísica Internacional 20 (3), 177–202.
Ortega-Gutiérrez, F., Elías-Herrera, M., Reyes-Salas, M., Macias-Romo, C., López, R., 1999. Late Ordovician–Early Silurian continental collision orogeny in southern Mexico and its bearing on Gondwana–Laurentia connections. Geology 27, 719–722.
Ortega-Obregón, C., Keppie, J.D., Murphy, J.B., Lee, J.K., Ortega-Rivera, A., 2009. Geology and geochronology of Paleozoic rocks in western Acatlán Complex, southern Mexico: evidence for contiguity across an extruded high-pressure belt and constraints on Paleozoic reconstructions. Geological Society of America Bulletin 121, 1678–1694. http://dx.doi.org/10.1130/B26597.1.
Pearce, J.A., 1975. Basalt geochemistry used to investigate past tectonic settings on Cyprus. Tectonophysics 25, 41–67.
Pearce, J.A., 2008. Geochemical fingerprinting of oceanic basalts with applications to ophiolite classification and the search for Archean oceanic crust. Lithos 100, 14–48.
Proenza, J.A., Ortega-Gutiérrez, F., Camprubi, A., Trilla, J., Elías-Herrera, M., Reyes-Salas, M., 2004. Paleozoic serpentinite-enclosed chromitites from Tehuatzingo (Acatlán Complex, southern Mexico): a petrological and study. Journal of South American Earth Sciences 16, 649–666.
Ramos-Arias, M.A., Keppie, J.D., 2011. U–Pb Neoproterozoic–Ordovician protolith age constraints for high- to medium-pressure rocks thrust over low-grade metamorphic rocks in the Ixcamilpa area, Acatlán Complex, southern Mexico. Canadian Journal of Earth Sciences 48, 45–61.
Ramos-Arias, M.A., Keppie, J.D., Ortega-Rivera, A., Lee, J.W.K., 2008. Extensional late Paleozoic deformation on the western margin of Pangea, Patlanoaya area, Acatlán Complex, southern México. Tectonophysics 448, 60–76.
Ramos-Arias, M., Keppie, J.D., Lee, J.K.W., Ortega-Rivera, A., 2011. A Carboniferous high-pressure klippe in the western Acatlán Complex of southern Mexico: implications for the tectonothermal development and paleogeography of Pangea. International Geology Review. http://dx.doi.org/10.1080/00206814.2011.580634.
Ranero, C.R., von Huene, R., 2000. Subduction erosion along the Middle America convergent margin. Nature 404, 748–755.
Sánchez-Zavala, J.L., Jenner, G.A., Belousova, E.A., Macías-Romo, C., 2004. Ordovician and Mesoproterozoic zircons from the Tecomate Formation and Esperanza Granitoids, Acatlán Complex, southern Mexico: local provenance in the Acatlán and Oaxacan Complexes. International Geology Review 46, 1005–1021.
Saunders, A.D., Storey, M.R., Kent, W., Norry, M.J., 1992. Consequences of plume–lithosphere interactions. In: Story, B.C., Alabaster, T., Pankhurst, R.J. (Eds.), Magmatism and the Causes of Continental Breakup: Geological Society London, Special Publications, 68, pp. 41–59.
Solari, L.A., Gómex-Tuena, A., Bernal, J.P., Pérez-Arvizu, O., Tanner, M., 2010. U–Pb Zircon Geochronology with an Integrated LA-ICP-MS Microanalytical Workstation: Achievements in Precision and Accuracy. Geostandards and Geoanalytical Research 34 (1), 5–18.
Steiger, R.H., Jäger, E., 1977. Subcommission on geochronology: convention on the use of decay constants in geo- and cosmochronology. Earth and Planetary Science Letters 36, 359–362.
Stöckhert, B., Gerya, T.V., 2005. Pre-collisional high pressure metamorphism and nappe tectonics at active continental margins: a numerical simulation. Terra Nova 17, 102–110.
Sun, S.S., McDonough, W.F., 1989. Chemical and isotopic systematics of oceanic basalts: implications for mantle composition and processes. In: Saunders, A.D., Norry, M.J. (Eds.), Magmatism in the ocean basins: Geological Society London Special Publication, 42, pp. 313–345.
Talavera-Mendoza, O., Ruiz, J., Gehrels, G.E., Meza-Figueroa, D.M., Vega-Granillo, R., Campa-Uranga, M.F., 2005. U–Pb geochronology of the Acatlán Complex and implications for the Paleozoic paleogeography and tectonic evolution of southern Mexico. Earth and Planetary Science Letters 235, 682–699.
Tolson, G., 2005. La Falla Chacalapa en el sur de Oaxaca. Boletin Sociedad Geolóica Mexicana LVII (1), 111–122.
Vega-Granillo, R., Talavera-Mendoza, O., Meza-Figueroa, D., Ruiz, J., Gehrels, G.E., López-Martínez, M., de La Cruz-Vargas, J.C., 2007. Pressure–temperature-time evolution of Paleozoic high-pressure rocks of the Acatlán Complex (southern Mexico): implications for the evolution of the Iapetus and Rheic Oceans. Geological Society of America Bulletin 119, 1249–1264.
Vega-Granillo, R., Calmus, T., Meza-Figueroa, D., Ruiz, J., Talavera-Mendoza, O., López-Martínez, M., 2009. Structural and tectonic evolution of the Aacatlán Complex, southern México: its role in collisional history of Laurentia and Gondwana. Tectonics 28, 1–25. http://dx.doi.org/10.1029/2007TC002159.
Von Huene, R., Ranero, C.R., Vannucchi, P., 2004. Generic model of subduction erosion. Geology 32, 913–916.
Warren, C., Beaumont, C., Jamieson, R., 2008a. Modelling tectonic styles and ultrahigh pressure (UHP) rock exhumation during the transition from oceanic subduction to continental collision. Earth and Planetary Science Letters 1–2, 129–145.
Warren, C., Beaumont, C., Jamieson, R., 2008b. Formation and exhumation of ultra-high pressure rocks during continental collision: role of detachment in the subduction channel. G3 Geochemistry Geophysics Geosystems 9, Q04019. http://dx.doi.org/10.1029/2007GC001839.
Winchester, J.A., Floyd, P.A., 1977. Geochemical discrimination of different magma series and their differentiation products using immobile elements. Chemical Geology 20, 325–343.

Capítulo 5

Amalgamación y desmembramiento de Pangæa: el ejemplo tipo del ciclo supercontinental

Amalgamation and Breakup of Pangæa: the type example of the supercontinent cycle

J. Duncan Keppie, Gonzalo Galaz-Escanilla, Maria Helbig, Mortiz Kirsch

GSA Cordilleran Section, 108th Annual Meeting
Field Trip 1
31 March–4 April 2012

Amalgamation and Breakup of Pangæa: the type example of the supercontinent Cycle

International Geological Correlation Program Project #597: Late Paleozoic–Early Mesozoic of the Acatlán and Ayu complexes, southern Mexico: events on the periphery of Pangæa synchronous with amalgamation and breakup

J. Duncan Keppie
Gonzalo Galaz-Escanilla
Departamento de Geología Regional, Insituto de Geología, Universidad Nacional Autónoma de México, 04510 Mexico, D.F.
Maria Helbig
Mortiz Kirsch
Centro de Geociencias, Universidad Nacional Autónoma de México, Campus Juriquilla, 76230 Querétaro, QRO, Mexico

INTRODUCTION

There is widespread acceptance that between 300 and 200 million years ago, all of the Earth's continental land masses were assembled into a giant supercontinent, Pangæa, surrounded by a superocean, Panthalassa. However, different configurations have been proposed, e.g., Pangæa A1, A2, B, and C (Fig. 1A). Reconstructions based on Mexican paleomagnetic data have been used to support both A and B models:

(a) PANGEA-A. A Permo-Triassic Pangea-A reconstruction where southern Mexico lies approximately in its present location relative to North America (Fang et al., 1989, Alva-Valdivia et al., 2002);

(b) PANGEA-B. A Pangea-B reconstruction placing southern Mexico off eastern Canada during the Jurassic (Fig. 1B: Böhnel, 1999).

There are also Middle American variants of the Pangea-A reconstruction:

(i) southwestern Mexico is placed either along the western margin of Pangea (Fig. 1C and 1D: Keppie, 2004, Keppie et al., 2008, 2010), or within Pangea between the Maya terrane and southern USA (Fig. 1E: Talavera-Mendoza et al.,2005, Vega-Granillo et al., 2007, 2009);

(ii) the Yucatan block is placed either within Pangea along the southern margin of USA (Fig. 1F: Pindell and Dewey, 1982), or on the western margin of Pangea during the mid-late Permian migrating into the Gulf of Mexico by the Middle Jurassic (Steiner, 2005);

(iii) the Chortis block has generally been placed off southwestern Mexico on the western marin of Pangea (Fig. 1E)(e.g., Pindell and Dewey, 1982), or within the within Pangea along the eastern margin of Mexico (Fig. 1G: Keppie and Keppie, in review).

On this field trip we will examine the evidence for subduction-related tectonics during the Pennsylvanian-Jurassic in the Ayu and Acatlán complexes, which suggests proximity to an ocean that is more consistent with the Pangea-A model (Fig. 2).

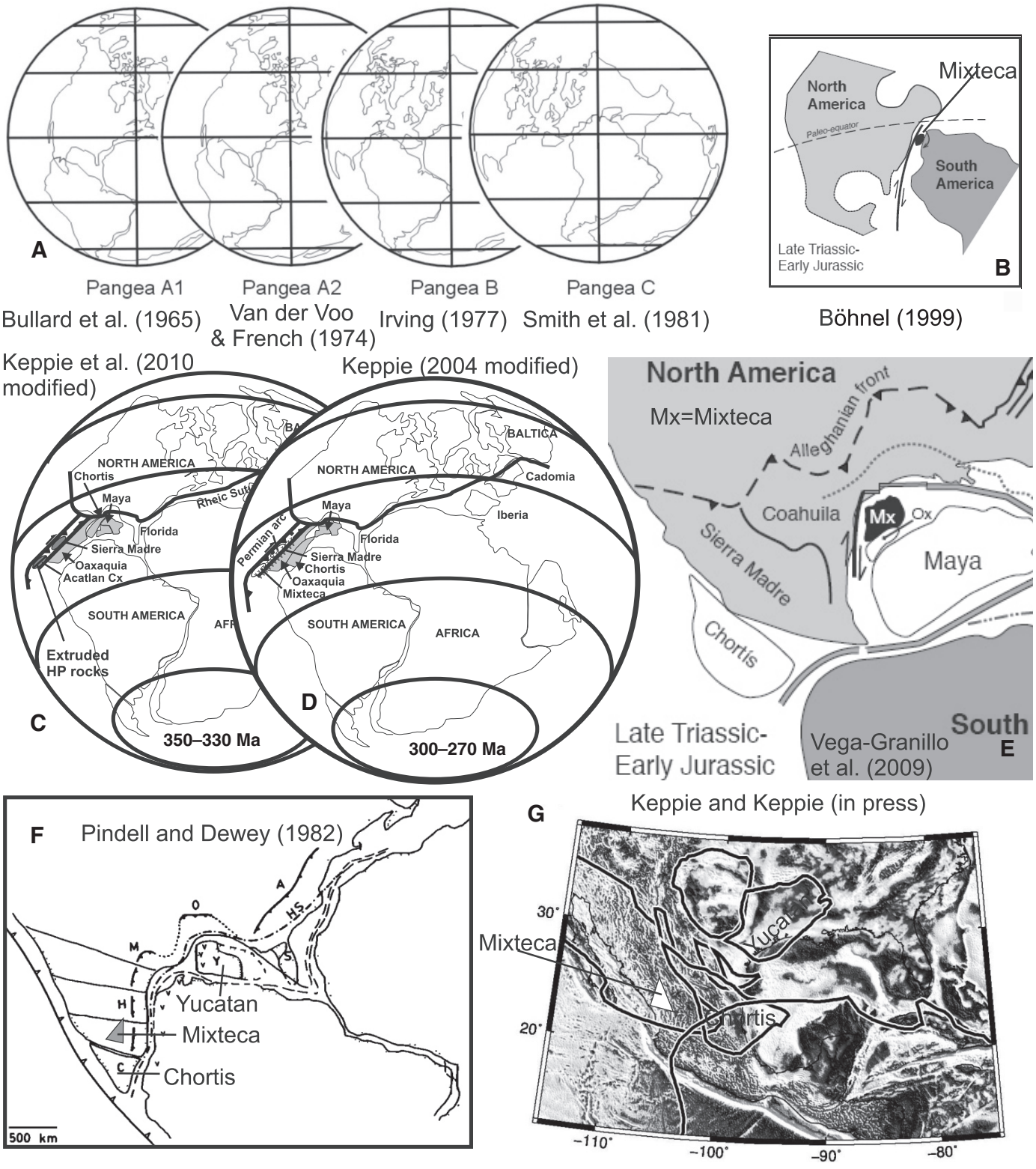

Figure 1. Reconstructions of Pangea by various authors.

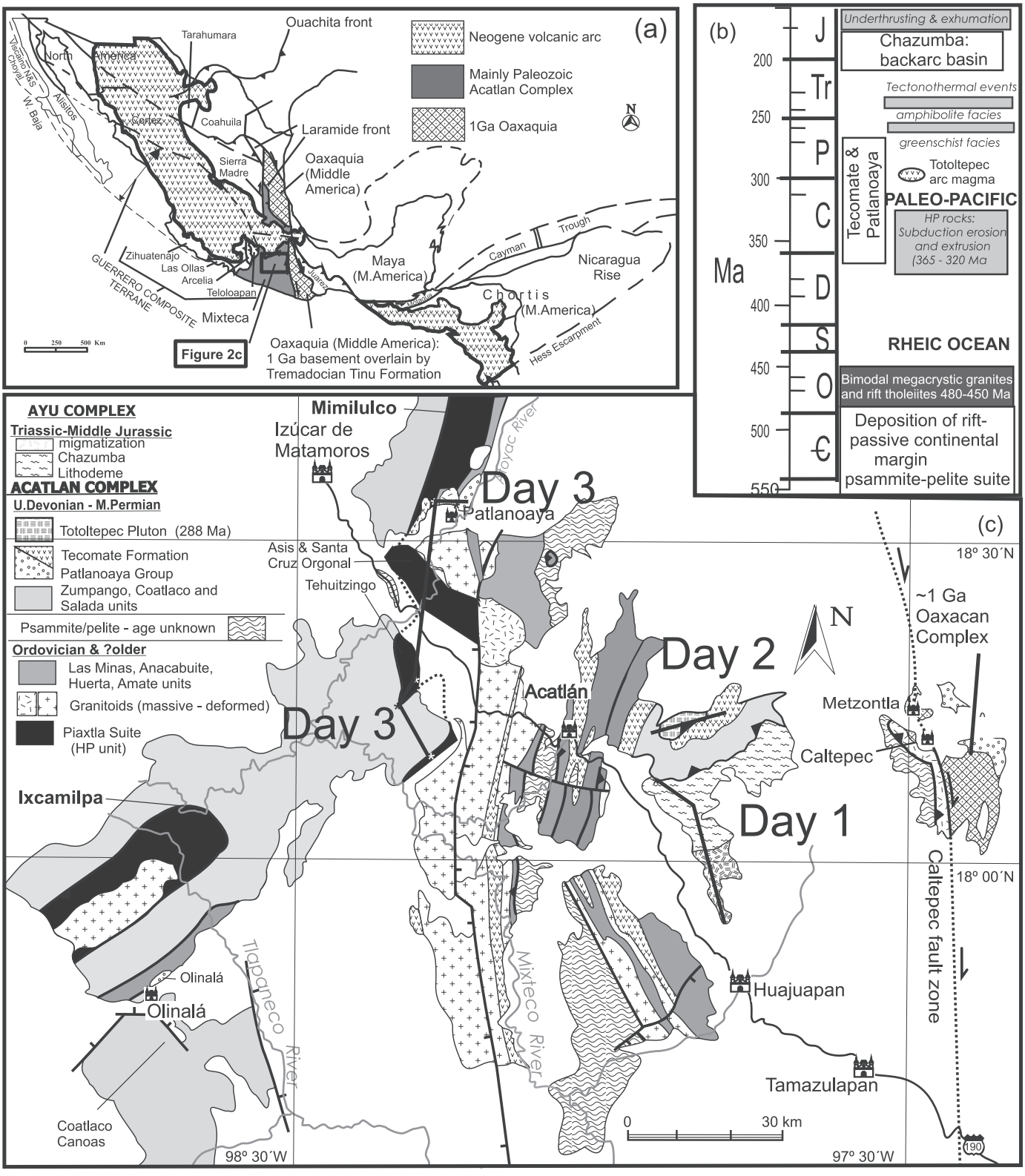

Figure 2. (A) Terranes of Middle America (after Keppie, 2004); (B) Ages od units in the Acatlán Complex; (C) Map of the Acatlán Complex (modified after Keppie et al., 2010) showing the field trip route.

DAY 1

Maria Helbig and J. Duncan Keppie

The Triassic-Jurassic Ayú Complex Southern Mexico: Evidence for Deposition on the Proximal Margin of a Backarc Basin, Underthrusting and Extrusion into the Acatlán Complex during the Breakup of Pangea-A

Helbig, M, Keppie, J.D., Murphy, J.B., and Solari, L.A., in press. U-Pb geochonological constraints on the Triassic–Jurassic Ayú Complex southern Mexico: derivation from the western margin of Pangea: Gondwana Research.

ABSTRACT

Rocks of the newly designated Ayú Complex are located in the eastern Mixteca terrane (southern Mexico), and comprise polyphase-deformed turbiditic rocks (Chazumba Lithodeme) that are intercalated with boudinaged ortho-amphibolites. In the south, the metasedimentary sequence is affected by partial melting and grades into the ~171 Ma Magdalena Migmatite. Migmatitzation was accompanied by 171–168 Ma granitoid minor intrusions and pegmatites with inherited zircon populations of ca. 260–290, 320–360, 420–480, 880–990, and 1080–1250 Ma that are also found in the Chazumba Lithodeme. Detrital U/Pb zircon ages from the migmatized and unmigmatized Chazumba Lithodeme yielded clusters of ca. 297, 266, 250, 214, 198, and 192 Ma, suggesting Upper Triassic—Lower Jurassic deposition. The MORB tholeiitic geochemistry of the amphibolites within the Chazumba Lithodeme indicates a back-arc environment with sedimentation occurring along the inboard rifted passive margin, the Upper Triassic–Lower Jurassic detrital zircons being derived from a contemporaneous, outboard magmatic arc. These characteristics suggest correlation with the lens-shaped Central terrane typified by the Potosi turbiditic fan in the rift-passive margin of Pangea that is absent west of the Mixteca terrane. The presence of this arc requires deposition adjacent to a subducting ocean and thus supports a Pangea-A reconstruction. Early Jurassic flattening of the subduction zone is inferred to have led telescoping of the Triassic–Early Jurassic back arc basin, during which the Chazumba Lithodeme was thrust beneath the Pangean margin where it was metamorphosed under amphibolite facies metamorphic conditions. It is further inferred that Middle-Upper Jurassic steepening of the subducting zone led to tectonic exhumation of the Chazumba Lithodeme by normal faulting along the reactivated Providencia Shear Zone. Deposition, underthrusting and exhumation of the Chazumba Lithodeme are synchronous with the breakup of Pangea and the opening of the Gulf of Mexico.

STOP 1-1 (W97.78834, N17.9387426: Fig. 3)
Location: Road between Sta. María Ayú and Ahuehuetitlán, riverbed of Río La Peña.

Micaceous schists and garnet-biotite gneisses are intercalated with boudinaged amphibolites, that underwent migmatization at ~171 Ma (leucosome dated by Keppie et al., 2004) and formed a mappable unit, called the Magdalena Migmatite. This tectonothermal event was accompanied by syntectonic intrusion of granitic, granodioritic and dioritic dikes and sheets (Yañez et al., 1991). A granite dike that cuts the paleosome yielded only one igneous zircon of 171 ± 4 (Middle Jurassic), whereas the rest of the dated grains are inherited zircons. Two paleosome samples of the Magdalena Migmatite yielded youngest detrital zircons of ~198 Ma (Early Jurassic) and 214 Ma (Late Triassic), respectively. Amphibolites were previously dated by Keppie et al. (2004) and showed $^{40}Ar/^{39}Ar$ cooling ages of 150 ± 2 Ma for biotite and 136 ± 2 for hornblende, suggesting rapid exhumation. Geochemically, amphibolites sampled across the Ayú Complex are MORB-like, rift-related tholeiites (Helbig et al., 2010). The majority of the ortho-amphibolites have jagged NMORB-normalized REE patterns that imply contamination either by a crustal and/or subduction component and suggest a formation in a back-arc basin.

STOP 1-2 (W97.807052°, N17.9987634°: Fig. 3)
Location: short road stop east of Tetaltepec.

Structural relationships in the Magdalena Migmatite: Large scale, close to open, upright to gently inclined parasitic fold (F_4) that folds the leucosome and boudinaged S_3-parallel granite sheets.

STOP 1-3 (W97.830789°, N18.036058°: Fig. 3)
Location: Riverbed, south of San Miguel Ixtápan.

Partially molten, and strongly deformed metasedimentary rocks that are intruded by granodiorites and pegmatites. Xenoliths are probably the metasedimentary host rock and show internal foliation as well as partial melting of the fertile domains. $^{40}Ar/^{39}Ar$ dating of a pegmatite and a granitic sheet yielded 167 ± 2 Ma for muscovite, and 155 ± 5 Ma for biotite (Keppie et al., 2004).

STOP 1-4 (W97.832239°,N18.0421378°: Fig. 3)
Location: Road section, south of San Miguel Ixtapan.

Outcrop exhibits a dike that cuts across the micaceous schists and feeds a granite sheet. The emplacement of the granite sheet is parallel to the main foliation, inflating the surrounding metapelitic host rock. The dike continues its way into the hanging metasedimentary host rock. Where in the contact with the host rock, the dike is overprinted by the same fabric as in the metasedimentary rocks. The rock is affected by later brittle normal block faulting. The fabric-parallel granite sheets show sharp contacts with the metapelites and exhibit minor pinch-and-swell structures and a distinct tectono-magmatic foliation at their margins suggesting stress-related emplacement.

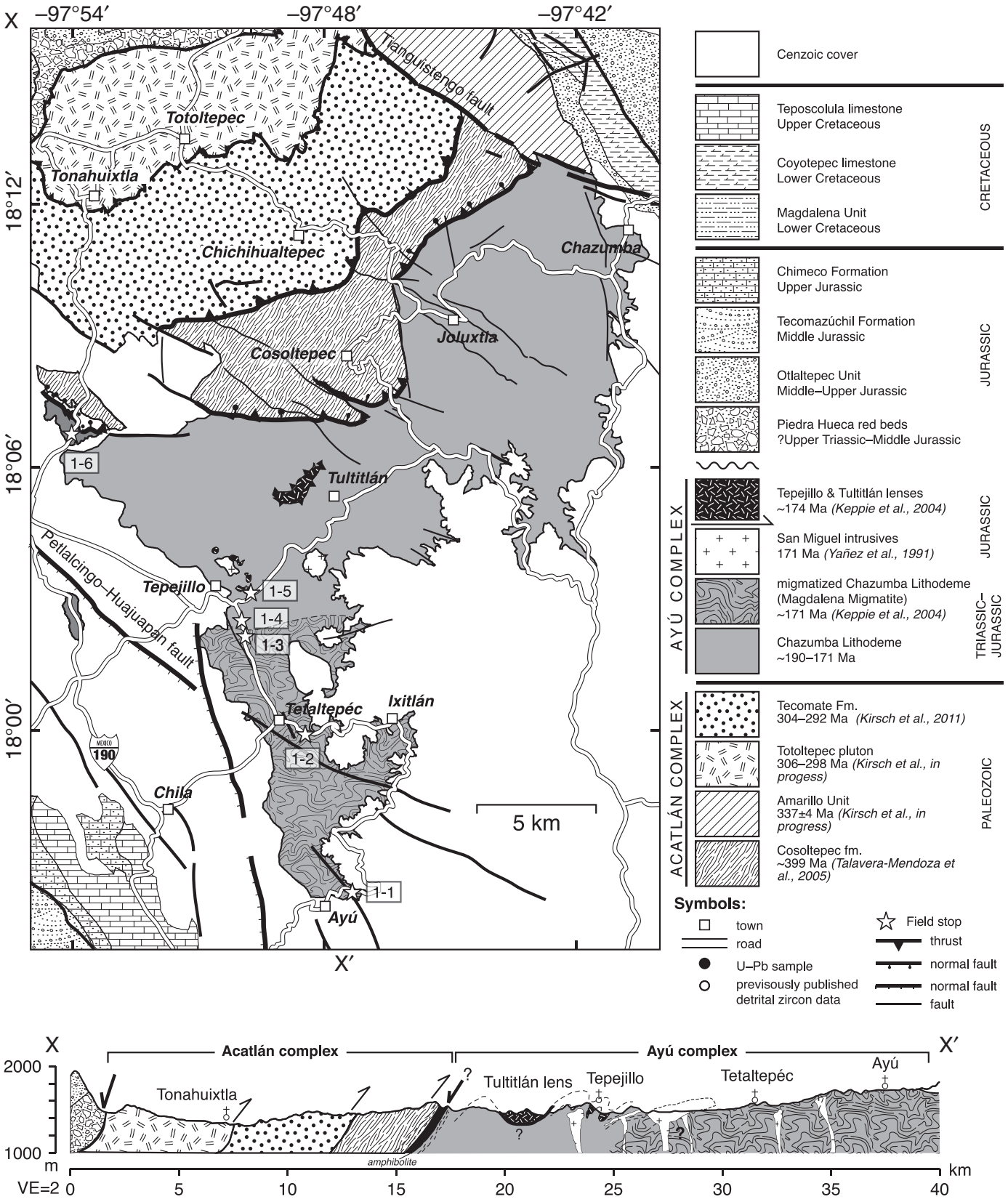

Figure 3. Geological map and section of the Totoltepec-Ayu area, southern Mexico showing field trip stops (modified after Helbig et al., in press).

STOP 1-5 (W97.828639°, N18.0526397°: Fig. 4)
Location: Foothills of the Cerro de La Peña (Cenozoic volcanic plug), north of Tejepillo; San Miguel Ixtapan road exit to Tultitlán.

Micaceous schists intercalated with minor quartzites are intruded by granites, leucogranitic and aplitic dikes. A granite dike cuts a tight, recumbent E-trending F_3 fold in the metasedimentary host rock. Small leucogranite veins that probably originate from the dike are parallel to the folded S_2 fabric. These relationships suggest that the intrusion was syn- to late-tectonic with respect to F_3. The granite is characterized by zircon inheritance and the crystallization age is inferred from the youngest grain with an age of 168 Ma. U-Pb detrital zircon analyses of a psammitic and a pelitic mica schist yielded maximum depositional ages of ~269 Ma and ~263 Ma (Middle Permian), respectively.

In the hanging wall, the mafic-ultramafic Tepejillo lens lies structurally as a nappe above the Chazumba Lithodeme (Keppie et al., 2004) and consists of four bodies that crop out along the foothills of Cenozoic volcanic plug (C. La Peña). The Tepejillo lens comprises coarse crystalline ultramafic (mainly dunite) to gabbroic rocks that are cut by diabase dikes. Geochemically, they are interpreted as part of a cumulatic body intruded into the lower continental crust (Keppie et al., 2004). The contact between the metasedimentary rocks of the Chazumba Lithodeme and the Tepejillo lens has been mapped as a folded thrust (Keppie et al., 2004). The Tultitán lens, 4 km to the northeast of the Tepejillo lens, consists of massive amphibolite and a core of metamorphosed norite. One concordant U-Pb LA-ICP-MS analysis of a prismatic tip of a euhedral zircon from a metanorite yielded an age of 174 ± 1 Ma, which is interpreted as age of intrusion for both lens (Keppie et al., 2004). Biotite from a gabbroic dike of the Tepejillo lens yielded a $^{40}Ar/^{39}Ar$ cooling age of 166 ± 2 Ma, whereas muscovite from a granite dike yielded a $^{40}Ar/^{39}Ar$ age of 161 ± 2 Ma (Keppie et al., 2004), suggesting excess argon in the biotite. Lower power increments of Late Cretaceous to Tertiary age can be observed in almost all $^{40}Ar/^{39}Ar$ analyses, implying that the Ayú Complex was affected by a later deformational event.

STOP 1-6 (W97.899842°, N18.113004°: Fig. 5)
Location: road section near the town La Providencia, on the road between Petlalcingo and Tonhuixtla.

Reactivation of a Triassic S-vergent thrust fault as a listric normal fault in the Middle-Late Jurassic. The Providencia shear zone forms a major structural feature between rocks of the Acatlán Complex (Tecomate Formation and Cosoltepec Formation) and the Ayú Complex and comprises weathered mylonites.

A micaceous metapsammite just south of the shear zone yielded only seventeen concordant analyses. Relatively narrow age spectra ranging from 194 to 339 Ma were obtained with the two youngest grains (190 ± 4, 193 ± 4 Ma) forming a mean of 192 ± 19 Ma (Early Jurassic). To the north of the shear zone, a mylonitic phyllite yielded a youngest detrital zircon age of 314 ± 4 Ma, which lies within the error of the mean of the three youngest grains with an age of 321 ± 30 Ma (Late Mississippian/Early Pennsylvanian). A graphite- and feldspar-bearing mylonitic metasedimentary rock, yielded two youngest detrital zircon ages of 281 ± 4 Ma and 295 ± 8 Ma with a mean age of 284 ± 71 Ma (Early Permian).

The presence of a major shear zone (Providencia Shear Zone) that separates the Acatlán Complex from the Ayú Complex was previously mapped as a thrust based on s-c fabrics in the hanging block (Malone et al., 2002; Keppie et al., 2004). However, $^{40}Ar/^{39}Ar$ cooling ages for amphibole of an amphibolite lens and muscovite from micaceous schists, north of the shearzone yielded cooling ages of ~214 Ma and ~224 Ma, respectively (Keppie et al., 2004). These fabrics are Late Triassic, and thus developed before or during the deposition of the Chazumba Lithodeme. It is envisaged that this Triassic shear zone was reactivated during or after the Middle Jurassic as a listric normal fault and formed the upper boundary of the exhuming Chazumba Lithodeme.

DAY 2
Moritz Kirsch and J. Duncan Keppie

Lower Permo-Carboniferous Arc Magmatism and Sedimentation on the Margin of Pangea-A

Kirsch, M., Keppie, J.D., Murphy, J.B., and Solari, L.A. in press. Permian-Carboniferous arc magmatism and basin evolution along the western margin of Pangea: geochemical and geochronological evidence from the eastern Acatlán Complex, southern Mexico: GSA Bulletin.

ABSTRACT

The Late Paleozoic evolution of Mexico records part of a continental arc that extends along the western margin of Pangea from western USA to the northern Andes. In the Acatlán Complex of southern Mexico, an arc assemblage consisting of a Permo-Carboniferous intrusion (Totoltepec pluton) and Permian sedimentary rocks (Tecomate Formation) offers a rare opportunity to examine events along the periphery of Pangea at the critical stage of final amalgamation.

The Totoltepec pluton ranges in composition from hornblendite and hornblende gabbro through diorite to tonalite, trondhjemite, granodiorite and monzo-granite. U-Pb LA-ICP-MS zircon analyses yield concordant ages of 306 ± 2 Ma in minor marginal mafic to ultramafic rocks and 289 ± 2 Ma for the main, more voluminous mafic to felsic intrusion. Major and trace element geochemistry of the Totoltepec rocks exhibit a tholeiitic to calc-alkaline character, high LILE/HFSE and flat REE patterns, which is typical of arc-related magmas. The precursor gabbroic rocks display εNd(t) values ranging from +1.3 to +3.3 (t = 306 Ma), whereas rocks from the main body of the pluton have εNd(t) values between −0.8 and +2.6 (t = 289 Ma).

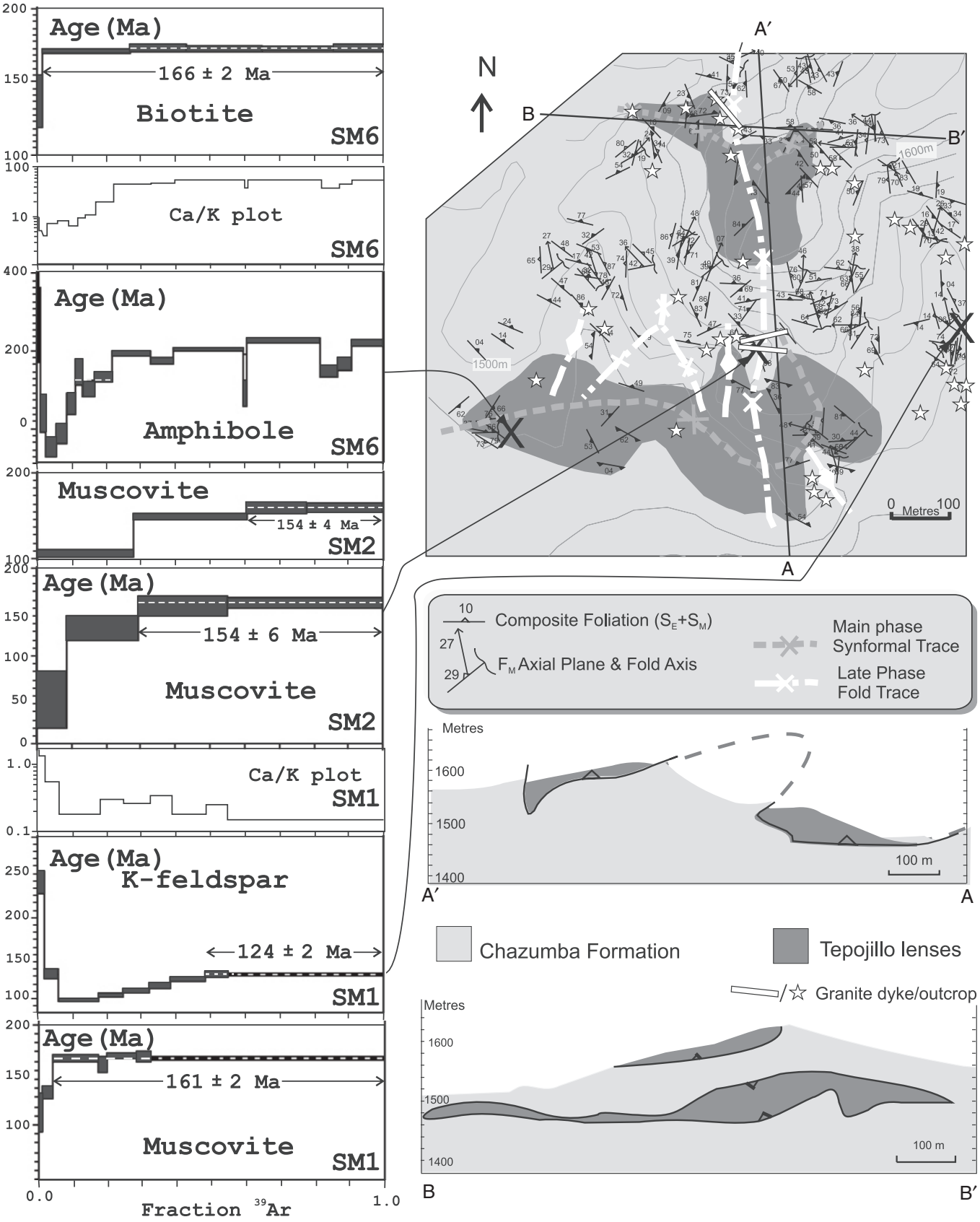

Figure 4. Stop 1-5: geological map, age data, and section of the Tepejillo ultramafic lens (after Keppie et al., 2004).

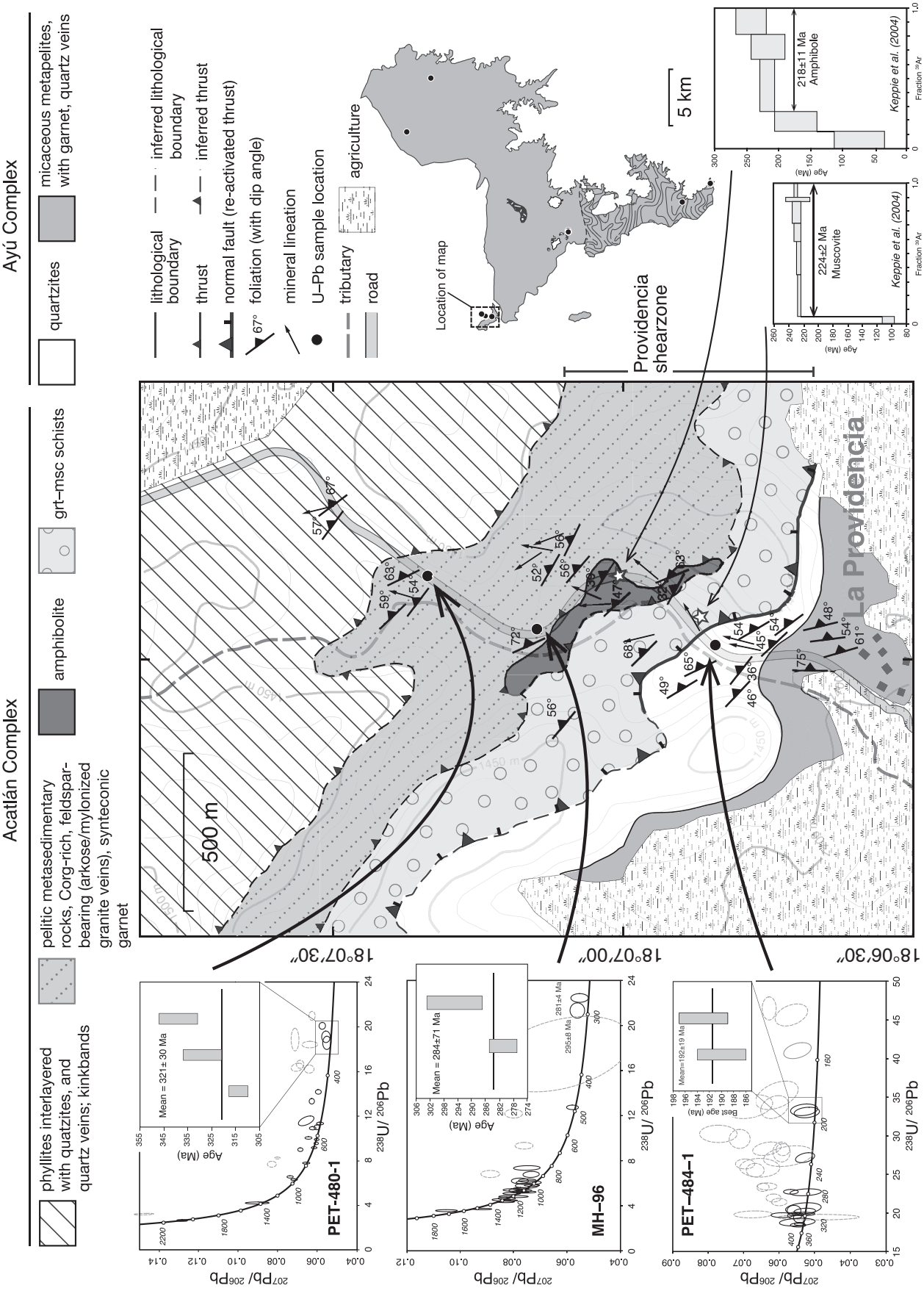

Figure 5. Stop 1-6: geological map and geochronology of the La Providencia shear zone (modified after Helbig et al., in press)

All of the samples are variably affected by wall rock assimilation, mixing and fractionation processes, but are more juvenile compared to contemporaneous arc-related igneous rocks in southern Mexico, suggesting the pluton was emplaced into thinner crust in a less mature part of the arc or along a fault that acted as a conduit for mantle-derived melts.

The Tecomate Formation consists of low-grade, poorly sorted, compositionally immature and largely unweathered metapsammites and metapelites. Several factors indicate derivation from the Permo-Carboniferous arc: (i) an arc-related geochemistry, (ii) εNd(t) values ranging from −5.7 to +0.3 (t = 280 Ma) that overlap those of the Totoltepec pluton, and (iii) detrital zircons with predominantly Permo-Carboniferous ages. The depositional age of the Tecomate Formation is constrained between the youngest detrital zircon population (ca. 280 Ma) and a published Ar/Ar age of 263 ± 3 Ma from the Tecomate Formation in the adjacent area. However, a metapsammite sample from the base of the Tecomate Formation yielded only Proterozoic zircons, indicating that deposition may have initiated earlier. Possible correlative sequences that may have been deposited in a similar peri-arc setting include the latest Pennsylvanian to Middle Permian Tecomate Formation type area, the latest Devonian to Lower Permian Patlanoaya Group, the Early to Middle Permian Tuzancoa Formation, the Middle Permian Los Hornos Formation, and the Olinalá Formation of Middle to Upper Permian age.

Kirsch, M., Keppie, J.D., Murphy, J.B. and Lee, J.K.W., in preparation. Structural history of the arc-related Totoltepec pluton, Acatlán Complex, southern Mexico: Syntectonic emplacement along a mid-crustal transpressional shear zone.

ABSTRACT

The 306–289 Ma tholeiitic to calc-alkaline Totoltepec pluton in the eastern Acatlán Complex, southern Mexico, is part of a Permo-Carboniferous continental magmatic arc along the western margin of Pangea. The pluton is a well-exposed, composite, felsic to ultramafic intrusive suite containing a conspicuous mesoscopic fabric, making it an ideal place to study the relationship between tectonic processes in magmatic arcs and pluton emplacement.

We use an integrated approach combining field observations, structural measurements, analysis of micro-fabrics, as well as Al-in-hornblende thermobarometry and $^{40}Ar/^{39}Ar$ thermochronology to decipher the structural evolution of the Totoltepec pluton. The data suggest that the pluton was emplaced in ~20 km depth and rapidly uplifted to allow it to cool to ~400 °C within 6 ± 2 Ma. The elongate pluton shape, parallel, decreasing temperature fabrics, similar crystallization and deformation ages and the rapid exhumation of the pluton speak for a syntectonic emplacement. A subvertical, fanning foliation and subhorizontal to subvertical lineations as well as the presence of internal, margin-parallel sinistral shear zones suggest emplacement along a transpressional fault. Hornblende-bearing diorites and tonalites within the low to medium-temperature solid-state domain in the southern part of the pluton exhibit a compositional and textural banding that is interpreted to have formed by a combination of steep igneous layering, layer-parallel dike injection and melt-enhanced deformation.

Although we were unable to document any regional-scale structures that may have controlled its intrusion, the timing and emplacement mechanism of the Totoltepec pluton is similar to that reported for syn-tectonic Late Carboniferous to Early Permian plutons along the Caltepec Fault zone that separates the Mixteca terrane from the Oaxacan Complex. Strike-slip tectonism along this fault may be associated with oblique subduction of the paleo-Pacific beneath the western margin of Pangea.

STOP 2-1. (W97.88385°, N18.214033°: Fig. 6)

Transpressional shear zone within the Totoltepec pluton near Santo Domingo Tonahuixtla. Here, strongly banded and foliated hornblende-bearing diorite and tonalite is intruded by felsic and mafic dikes at low angles to the WSW-striking planar fabric. Hornblende fish and asymmetrically boudinaged dikes consistently display sinistral kinematics. The crystallization age of the mafic rocks give an age of 289 ± 2 Ma (Keppie et al., 2004), whereas foliation-parallel muscovite in trondhjemite (1 km due SE) yield a $^{40}Ar/^{39}Ar$ age of 283 ± 1 Ma.

STOP 2-2 (W97.890711°, N18.208455°: Fig. 6)

Aplitic dikes intruding megacrystic hornblende diorite/ tonalite north of Santo Domingo Tonahuixtla. Dikes are mostly foliation-parallel, but are locally observed to cut the foliation at low angles. Some dikes contain an internal tectono-magmatic fabric parallel to the dike wall and dike-host contacts are sharp to irregular suggesting dike emplacement was syntectonic and occurred prior to complete crystallization of the host. The megacrystic hornblende-bearing rocks are laterally traceable. Whereas at this location, lineations are weakly developed or subhorizontal with sinistral kinematics, further east, between the villages of Tonahuixtla and Totoltepec, the rocks possess a strong down-dip mineral lineation and sigma-shaped tails on hornblende porphyroblasts suggest thrusting toward the south.

STOP 2-3 (W97.874964°, N18.207481°: Fig. 6)

Compositional/ textural banding in hornblende-bearing tonalites east of Tonahuixtla. Rocks at this stop have a mylonitic fabric and contain a conspicuous banding defined by a more or less rhythmic variation in grain size and modal proportions of feldspar and hornblende. Locally, these rocks exhibit gentle, ca. 2 m wavelength, fold-like structures resembling trough-banding characteristic of layered intrusions. These features indicate that the banding may have a complex, multi-stage history of development, involving magma chamber, injection as well as tectonic processes.

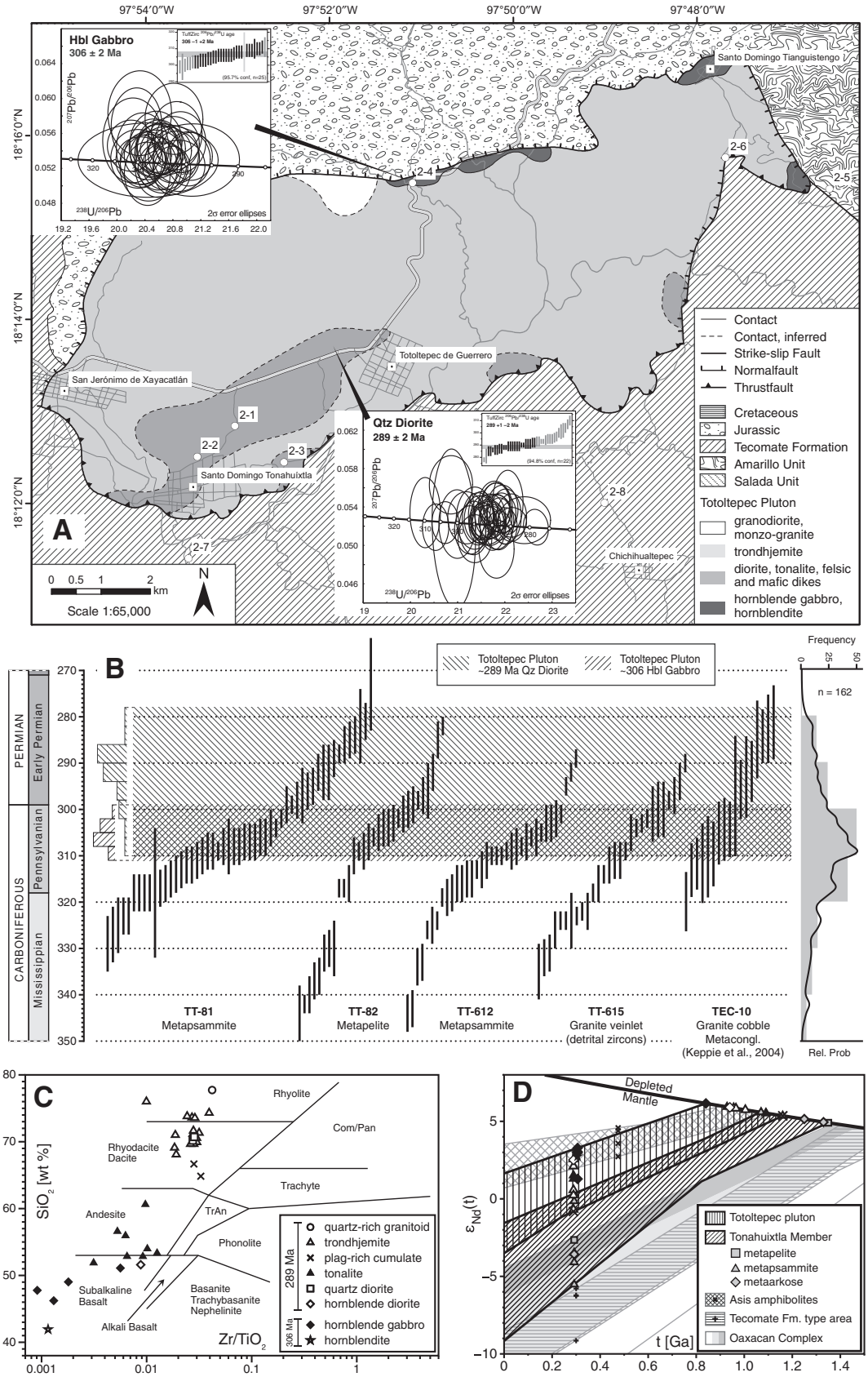

Figure 6. Stops 2-1 to 2-8: geological map of the Totoltepec pluton (after Kirsch et al., in press) showing field trip stops.

STOP 2-4 (W97.86816°, N18.218361°: Fig. 6)

Hornblende gabbro at the northern margin of the Totoltepec pluton in contact with Jurassic redbeds. This outcrop is located in one of three ca. 0.2–0.6 km^2, fault-bounded, precursor (306 ± 2 Ma) gabbroic phase, which is distributed along the northern and north-eastern margin of the pluton. Locally, these rocks are intruded by intensely deformed felsic dikes. To the north, the pluton is unconformably overlain by redbeds of inferred Jurassic age, which sit steeply against the pluton buttress due to a subsequent period of normal faulting.

STOP 2-5 (W97.851633°, N18.2581°: Fig. 6)

Amarillo Unit (new name), SE of Santo Domingo Tianguistengo. This unit is characterized by medium- to high-grade metasedimentary rocks locally intruded by amphibolite dikes. Youngest detrital zircons from a garnet schist sample indicate a maximum depositional age of 337 ± 4 Ma (Mississippian). The amphibolite dikes exhibit a MORB-like geochemistry with $\varepsilon_{Nd}(i)$ values of +5.2 to +7.6 and T_{DM} model ages between 333 and 433 Ma. These features are very similar to those documented in the Salada Unit (Morales-Gámez et al., 2008), on the western side of the Totoltepec pluton.

STOP 2-6 (W97.776016°, N18.257016°: Fig. 6)

Thrust contact between the Totoltepec pluton and the Tecomate Formation metasedimentary rocks. The exposed contact is a low-angle brittle-ductile thrust. At another location, this thrust is mylonitic and yielded a Middle Triassic $^{40}Ar/^{39}Ar$ age on muscovite. The contact is furthermore associated with a Fe-P-REE deposit containing the mineral association magnetite, apatite, barite, chlorite, quartz, chalcopyrite, and a cerium mineral. The mineralization is confined to two discrete, elongated bodies of ~100 m length coinciding with strong aeromagnetic anomalies.

STOP 2-7 (W97.794857°, N18.262697°: Fig. 6)

S-C fabrics in the Tecomate Formation ~1 km south of the margin of the Totoltepec pluton, indicating top-to-the-south thrusting. Thermochronological data from this area as well as other samples from the Tecomate Formation and Amarillo Unit reveal a regionally significant tectonothermal event of mid-Triassic age.

STOP 2-8 (W97.892266°, N18.190066°: Fig. 6)

Pebble metaconglomerates of the Tecomate Formation near Chichihualtepec. The pebbles from this outcrop, which are petrographically similar to the Totoltepec pluton trondhjemite, yielded zircons with ages between 320 and 264 Ma (Keppie et al., 2004). Morales-Gámez et al. (2009) conducted strain measurements in these rocks, documenting prolate spheroids typical of transtensional deformation. Rotated pebbles with asymmetric tails show top-to-the-south shear, which is consistent with other kinematic indicators in this area.

DAY 3

Gonzalo Galaz-Escanilla and J. Duncan Keppie

A High Pressure Zone within the Acatlán Complex: Uppermost Devonian: Lower Carboniferous Subduction and Extrusion under Extension during the Initial Stages of Pangea Amalgamation

Center of High Pressure Zone

Keppie, J.D., Nance, R.D., Dostal, J., Lee, J.K.W., and Ortega-Rivera, A. 2011 Constraints on the subduction erosion/extrusion cycle in the Paleozoic Acatlán Complex of southern Mexico: geochemistry and geochronology of the type Piaxtla Suite. Gondwana Research, doi:10.1016/j.gr.2011.07.020

ABSTRACT

The type high-pressure (HP) Piaxtla Suite in the Acatlán Complex of southern Mexico consists of retrogressed eclogite (amphibolite), megacrystic granitoids and high-grade metasedimentary rocks. Exhumation of these HP rocks has recently been interpreted as the result of extrusion into the upper plate, rather than by return flow up the subduction zone. Geochemical analyses of the retrograde eclogites indicate that they have a rift tholeiitic-transitional alkalic composition. These are closely associated with a megacrystic meta-granitoid that has yielded an intrusive age of 452 ± 6 Ma (concordant U-Pb zircon analyses) with inherited zircon populations at ca. 800–950 Ma and 1000–1200 Ma derived from the underlying basement, probably the Oaxacan Complex which borders the Acatlán Complex to the east. The bimodal nature of these igneous rocks and their close association with continentally-derived sedimentary rocks is similar to most HP rocks in the Acatlán Complex derived from a rifted passive margin. The youngest detrital zircon population in a metapsammite sample yielded an U-Pb age of 365 ± 15 Ma with older analyses distributed along a chord with an upper intercept of 1287 ± 29 Ma. The ca. 365 Ma age provides a maximum age for the time of deposition of this sample. $^{40}Ar/^{39}Ar$ ages from the retrogressed eclogites provided hornblende plateau ages of 342 ± 2 Ma and 344 ± 2 Ma, whereas muscovite from the granitoid and metapsammite yielded 334 ± 2 Ma plateau ages. These data constrain the subduction erosion-extrusion cycle to ≤35 my during which the rocks were taken to a depth of ca. 40 km at a rate of 2.7 km/my and back to the surface at 2.4 km/my. Such exhumation rates are slower than those in continent-continent collision zones, but similar to those in the Iberia-Czech Variscan belt where tectonic interpretation also suggests extrusion into the upper plate.

Western Boundary of High Pressure Zone: A High-Pressure Folded Klippe Explaced during the Lower Carboniferous at Tehuitzingo

Galaz E., Gonzalo, et al., in press. A high-pressure folded klippe at Tehuizingo on the western margin of an extrusion zone, Acatlán Complex, southern Mexico

ABSTRACT

The Acatlán Complex is divided into two blocks of low-grade metamorphic rocks by a central belt of high-pressure (HP) rocks, which at Tehuitzingo is composed of metabasites, serpentinite, granite and mica schist. 580–430 Ma detrital zircon ages indicate that these rocks were deposited adjacent or very close to the Gondwana supercontinent during the Early Paleozoic and are more consistent with a development on the southern margin of the Rheic Ocean rather than the Iapetus Ocean. These rocks were then removed by a subduction-erosion to depths of ~50km, reaching a metamorphic peak of ~16 kbar and 750 °C (eclogite facies). The HP rocks underwent rapid extrusion during a major Late Devonian-Pennsylvanian tectonothermal event indicated by $^{40}Ar/^{39}Ar$ analyses, which yielded ages of ~373 Ma (hornblende in metabasite) and of 328–317 Ma (muscovite in granite, mica schist and metabasite) that indicate cooling through ~570 °C and ~350 °C respectively, indicating a very high cooling rate of ~4.9–3.9 °C/m.y. During the extrusion process these rocks were affected by retrogression to amphibolite-epidote and green schist facies, and finally emplaced as a klippe on a greenschist facies psammite-pelite unit that constitutes the western block of the Acatlán Complex. Petrologic, deformational and geothermobarometric data suggest that west and east blocks belong to the same terrane, indicating that a subduction-erosion process and subsequent extrusion is more consistent with the genesis of the HP central belt than a collisional event as has been proposed. The P-T-t pattern of these HP rocks is consistent with subduction environments reported elsewhere in the world and suggests a serpentinite extrusion channel on the western margin of Pangea.

Eastern Boundary of High Pressure Zone: A Listric Normal Shear Zone Synchronous with Deposition of the Uppermost Devonian–Lower Permian Patlanoaya Group

Keppie, J.D., Nance, R.D., Ramos-Arias, M.A., Lee, J.K.W., Dostal, J., Ortega-Rivera, AQ., and Murphy, J.B. 2010. Late Paleozoic subduction and exhumation of Cambro-Ordovician passive margin and arc rocks in the northern Acatlán Complex, southern Mexico: geochronological constraints. Tectonophysics, v. 495, p. 213–229.

ABSTRACT

The origin and age of high pressure (HP) rocks is crucial for paleogeographic reconstruction because they either mark an oceanic suture or an extrusion zone within the upper plate. HP rocks in the San Miguel Las Minas area in the northern part of the complex has been inferred to be of early Paleozoic age and to mark oceanic sutures. However, blueschists in the northern part of the Acatlán Complex in southern Mexico have yielded Mississippian $^{40}Ar/^{39}Ar$ plateau ages of 344 ± 5 Ma for glaucophane and 338 ± 3 Ma and 337 ± 2 Ma for muscovite. These ages are slightly younger than recently published ages: a U-Pb zircon age of 353 ± 1 Ma from associated eclogite, and a 347 ± 3 Ma muscovite age from the tectonically overlying, greenschist facies Las Minas Unit. Taken together, these data indicate rapid cooling between 700° and 340°C in ca. 17 Myr. On the other hand, associated Ordovician Anacahuite Amphibolite cooled through ca. 500°C at 299 ± 6 Ma ($^{40}Ar/^{39}Ar$ on hornblende) suggesting a second, Permian period of exhumation. Protoliths of the high grade rocks include Cambrian-Ordovician, rift-passive margin, psammites, pelites, and tholeiitic dykes, an Ordovician mafic intrusion (Anacahuite Amphibolite dated at 470 ± 10 Ma: U-Pb zircon) and megacrystic granite (dated at 492 ± 12 Ma: U-Pb zircon), and arc-related mafic rocks of unknown age. These upper plate rocks are inferred to have been removed by subduction erosion and taken to depths between 35 and 55 km where they underwent blueschist-eclogite facies metamorphism. This was followed by rapid extrusion along a channel bounded by an easterly dipping, Mississippian, listric normal shear zone, and a thrust modified by a Permian dextral fault. Rocks above and below the extrusion zone are mainly Cambro-Ordovician rift-passive margin units, but a small vestige of the arc preserved as dikes cutting rocks lying unconformably beneath the fossiliferous latest Devonian-Lower Permian Patlanoaya Group. Since faunal data indicate that Pangea had amalgamated by the Mississippian, at which time the Acatlán Complex lay 1500–2000 km south of the Ouachita collisional orogen between Gondwana and Laurentia, it is inferred that subduction and extrusion of the high pressure rocks occurred on the active western margin of Pangea.

Ramos-Arias, M., Keppie, J.D., Ortega-Rivera, A., and Lee, J.W.K. 2008. Extensional late Paleozoic deformation on the western margin of Pangea, Patlanoaya area, Acatlán Complex, southern Mexico. Tectonophysics, v. 448, p. 60–76.

ABSTRACT

New mapping in the northern part of the Paleozoic Acatlán Complex (Patlanoaya area) records several ductile shear zones and brittle faults with normal kinematics (previously thought to be thrusts). These movement zones separate a variety of units that pass structurally upwards from: (i) blueschist-eclogitic metamorphic rocks (Piaxtla Suite) and mylonitic megacrystic granites (Columpio del Diablo granite ≡ Ordovician granites elsewhere in the complex); (ii) a gently E-dipping, listric, normal shear zone with top to the east kinematic indicators that formed under upper greenschist to lower amphibolite conditions; (iii) the Middle-Upper Ordovician Las Minas quartzite (upper greenschist facies psammites with minor interbedded pelites intruded by mafic dikes

and a leucogranite dike from the Columpio del Diablo granite) unconformably overlain by the Otate meta-arenite (lower greenschist facies psammites and pelites): roughly temporal equivalents are the Middle-Upper Ordovician Mal Paso unit and prelatest Devonian Ojo de Agua unit (interbedded metasandstone and slate, and metapelite and mafic minor intrusions, respectively)—the Otate and Mal Paso units are intruded by the massive, 461 ± 2 Ma, Palo Liso megacrystic granite: decussate, contact metamorphic muscovite yielded a $^{40}Ar/^{39}Ar$ plateau age of 440 ± 4 Ma; (iv) a steeply-moderately, E-dipping normal fault; (v) uppermost Devonian-Lower Permian sedimentary rocks (Patlanoaya Group: here elevated from formation status). The upward decrease in metamorphic grade is paralleled by a decrease in the number of penetrative fabrics, which varies from (i) three in the Piaxtla Suite, through (ii) two in the Las Minas unit (E-trending sheath folds deformed by NE-trending, subhorizontal folds with top to the southeast asymmetry, both associated with a solution cleavage), (iii) one in the Otate, Mal Paso, and Ojo de Agua units (steeply SE-dipping, NE-SW plunging, open-close folds), to (iv) none in the Patlanoaya Group. $^{40}Ar/^{39}Ar$ analyses of muscovite from the earliest cleavage in the Las Minas unit yielded a plateau age of 347 ± 3 Ma and show low temperature ages of ~260 Ma. Post-dating all of these structures and the Patlanoaya Group are NE-plunging, subvertical folds and kink bands. An E-W, vertical normal fault juxtaposes the low-grade rocks against the Anacahuite amphibolite that is cut by megacrystic granite sheets, both of which were deformed by two penetrative fabrics. Amphibole from this unit has yielded a $^{40}Ar/^{39}Ar$ plateau age of 299 ± 6 Ma, which records cooling through ~490 °C and is probably related to a Permo-Carboniferous reheating event during exhumation. The extensional deformation is inferred to have started in the latest Devonian (~360 Ma) during deposition of the basal Patlanoaya Group, lasting through the rapid exhumation of the Piaxtla Suite at ~350–340 Ma synchronous with cleavage development in the Las Minas unit, deposition of the Patlanoaya Group with active fault-related exhumation suggested by Mississippian and Early Permian conglomerates (~340 and 300 Ma, respectively), and continuing at least into the Middle Permian (≡ 260 Ma muscovite ages). The continuity of Mid-Continent Mississippian fauna from the USA to southern Mexico suggests that this extensional deformation occurred on the western margin of Pangea after closure of the Rheic Ocean.

STOP 3-1 (N18° 11.728′, W98° 14.690′ to N18° 11.652′, W98° 15.065′: Fig. 2)

Contact between a deformed, Ordovician megacrystic granitoid, a Tertiary dike, and the HP Piaxtla Suite at Piaxtla.

STOP 3-2 (UTM: 1405110/2023872: Fig. 7)

Thrust contact between Tehuitzingo serpentinite and polydeformed psammitic-pelitic rocks at Solozuchitl near Atopoltitlan.

The Piaxtla serpentinites are composed almost entirely of secondary minerals. Decussate, acicular and fibrous crystals serpentine aggregates make up 95% of the rock, magnetite, calcite, white mica and talc, and accessory chromite, clinochlore, undulose quartz, amphibole and epidote. This serpentinite are thrust over the low grade psammite-pelite unit along a gently NW-dipping thrust (320/15°), on which there are striae that plunge westwards (290/12°): associated recumbent folds, S-C fabrics and thrust horses indicate thrusting toward the west. Cutting across this thrust zone are several N-S vertical faults with subhorizontal striae.

The low grade psammite-pelite unit (498 ± 2 Ma, U-Pb detrital zircon; Galaz-Escanilla et al., in press) is composed mainly of primary minerals such as quartz, feldspar and zircon (accessory), which suggests a medium-grained quartz-arenitic (0.25–0.5 mm) and shaly (<0.06 mm grain size) protoliths respectively. The equilibrium secondary mineralogy is composed of quartz, albite ($Ab_{99–100}$), Mg-Fe-chlorite (ripidolite type), phengite, epidote, calcite and leucoxene, whose geothermobarometry indicated P-T conditions of ~2.7 kbar and ~350 °C (greenschist facies; Galaz-Escanilla and Keppie, in press).

STOP 3-3 (UTM: 140571085/2023811: Fig. 7)

Serpentinite, amphibolite, metabasite, Ordovician granitic and psammitic-pelitic rocks along the eastern margin of the Tehuitzingo serpentinite at Tecolutla.

In Tecolutla area outcrop a HP unit (eclogitic facies) that mainly consists of serpentinized harzburgite with small marginal fault blocks of metabasite, metagranitoid (485 ± 3 Ma, U-Pb zircon age: Galaz-Escanilla et al., in press) and mica schist (433 ± 3 Ma, U-Pb detrital zircon: Galaz-Escanilla et al., in press) juxtaposed by N-S structures. The serpentinized harzburgites contain elliptical metabasite lenses up to several meters in size, which have fine grained margins that may reflect an original intrusive relationship. The long axes of the elliptical lenses are parallel to the foliation indicating ductile deformation. On the other hand, the high-grade metasediments have a composite foliation where S_1 is parallel to a second S-C foliation with the S_2 planes subparallel to the border of the block and oriented ~128/27° (dip direction/dip angle), and C_2 planes oriented ~147/58°.

The HP unit is tectonically juxtaposed against a low grade psammite-pelitic unit along N-S structures. This unit has a planar fabric composed mainly of white mica and chlorite evidencing a low-temperature (greenschist) ductile deformation.

The geothermobarometry suggests a common prograde metamorphic history for the Tehuitzingo HP rocks: (a) a metamorphic peak eclogite facies of zoisite-amphibole, with a temperature of ~750 °C and a pressure of ~16 kbar; (b) retrogression to amphibolite-epidote facies, with a temperature of ~472 °C and variable pressures between ~7.1–3.4 kbar; (c) retrogression to greenschist facies with a temperature of ~360 °C and whose pressures were not obtained (Galaz-Escanilla et al., in press). The Piaxtla serpentinite contains three types of serpentine group minerals:

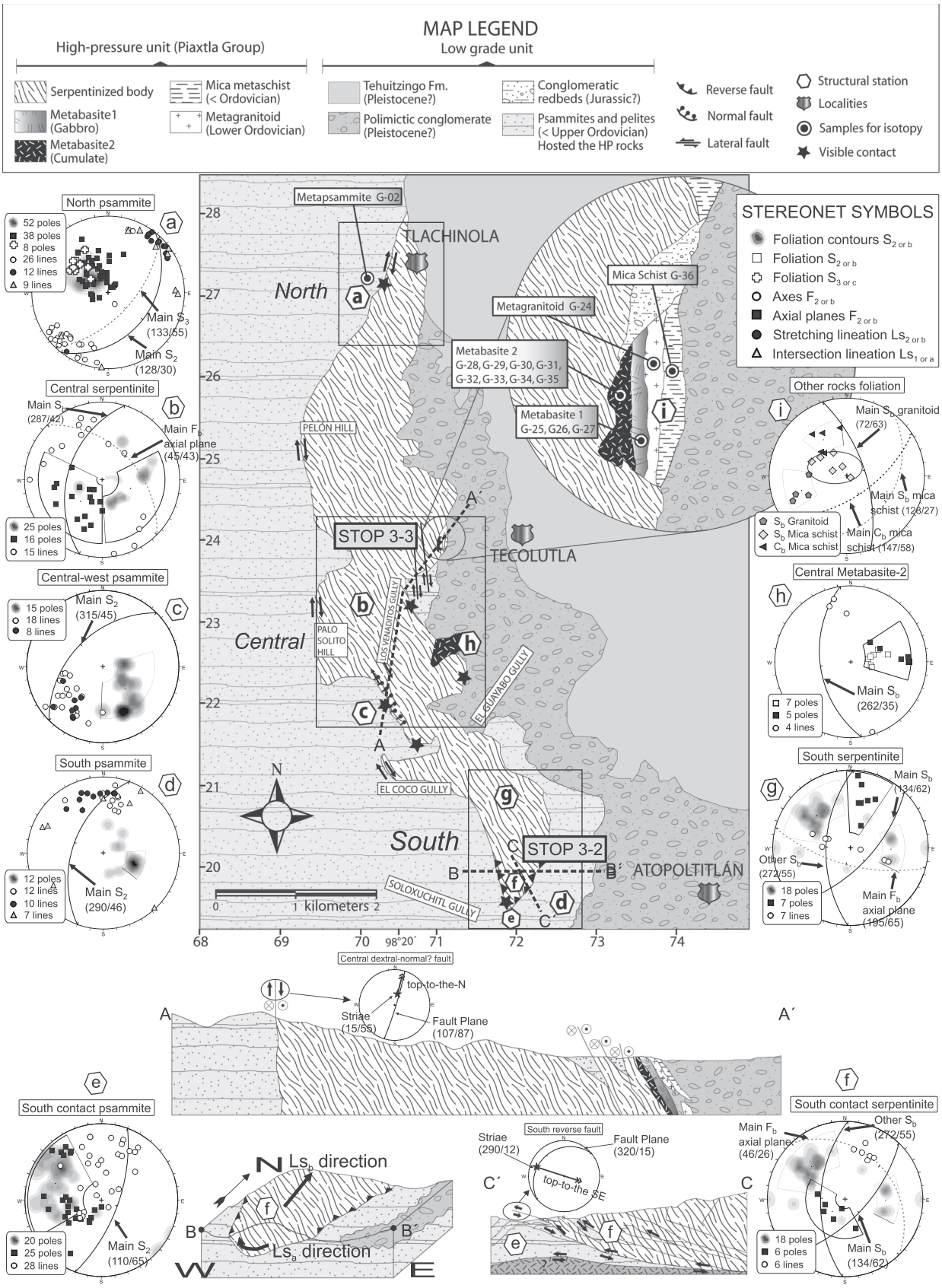

Figure 7. Stops 3-2 and 3-3: geological map, structural data, and section (after Galaz-Escanilla et al., in press).

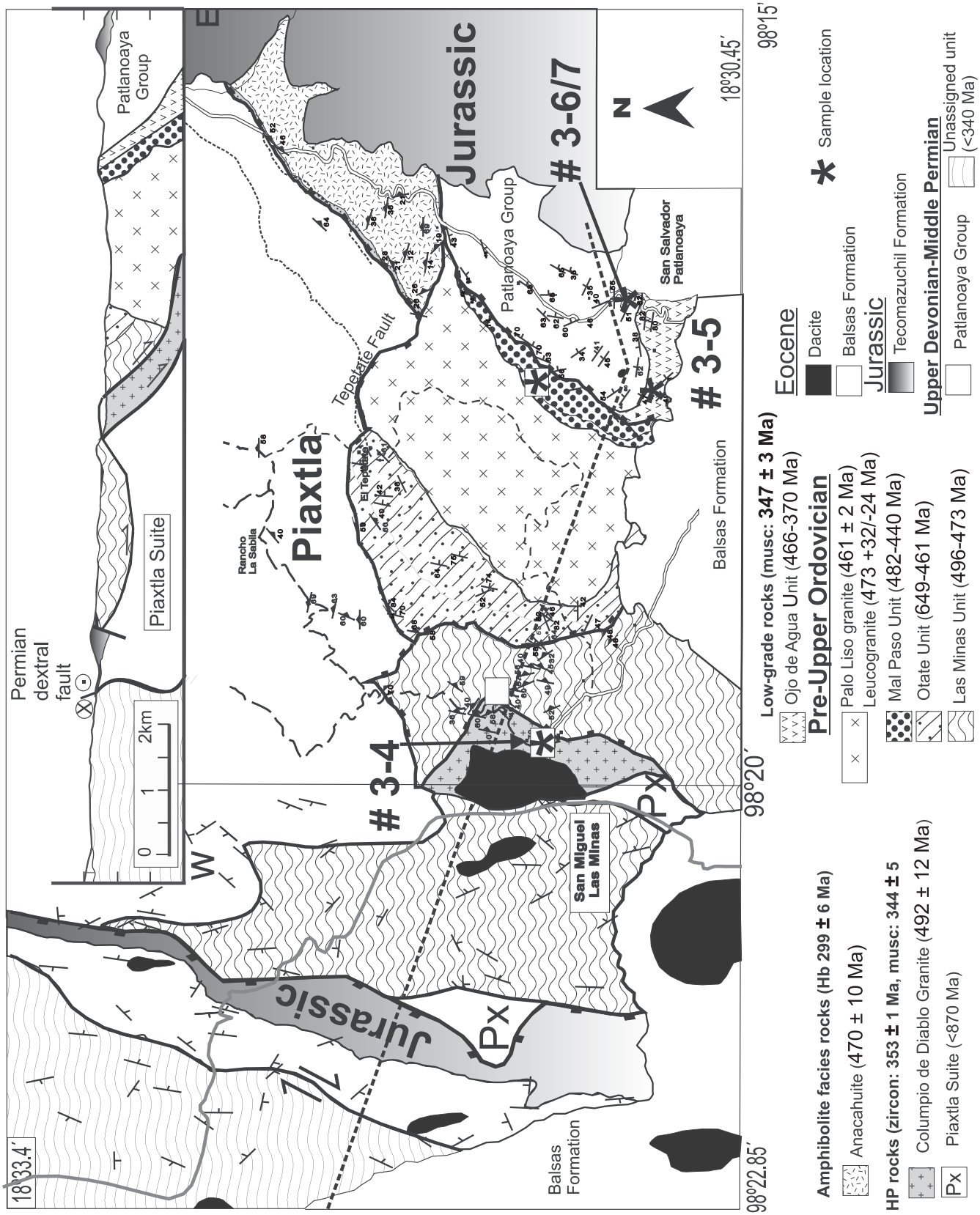

Figure 8. Stops 3-4, 3-5, 3-6 and 3-7: geological map and section (after Keppie et al., 2010).

chrysotile, lizardite and antigorite. Based on the stability field of the latter was estimated a P-T peak of ~550 °C and ~9 kbar (González-Mancera, 2001), however, has been reported in subduction zones antigorite reaching ~720 °C and high pressures of ~20 kbar (Ulmer and Trommsdorff, 1995).

The geochemistry data of the eclogitic mafic rocks indicate that these rocks have an arc affinity (author´s unpublished data). The P-T-t pattern of these rocks is consistent with subduction environments and serpentinite subduction channel exhumation (e.g., Guillot et al. 2009), where the driving forces for exhumation are a combination of buoyancy and channel flow coupled with underplating of slabs.

STOP 3-4 (N18° 31.051′, W98° 19.733′: Fig. 8)

Listric normal shear zone between megacrystic, Columpio del Diablo granitoid and Ordovician Las Minas unit.

The Columpio del Diablo megacrystic granite (492 ± 12 Ma, U-Pb zircon age: Keppie et al., 2010) consists of blastomylonitic granite containing quartz, K-feldspar (perthitic orthoclase), white mica, chlorite, epidote, and accessory opaque minerals. The megacrystic granite is cut by thin leucogranite sheets that consist mainly of quartz and potassium feldspar and are inferred to be a late differentiates of the granite. Structurally, the granite varies from an L-tectonite to an L-S tectonite with kinematic indicators, such as σ fabrics associated with the feldspars and generally vertical, extensional, quartz-filled fractures within the feldspars that indicate top-to-east movement along the contact with the Las Minas Unit: a minor, brittle fault has been superimposed on the contact. The Las Minas unit consists predominantly of polydeformed, low-grade psammites interbedded with thin pelitic phyllites, and intruded by many tholeiitic mafic dikes and sills (Keppie et al., 2008). The psammites consist mainly of quartz with minor muscovite, chlorite, and K-feldspar, and accessory zircon, whereas the phyllites are composed of muscovite, chlorite, quartz, and opaque minerals. The youngest concordant detrital zircon is dated at 496 ± 25 Ma (Keppie et al., 2008) The mafic intrusions contain amphibole (tremolite-actinolite), chlorite, epidote, quartz, plagioclase, muscovite, and accessory calcite, and opaque minerals. $^{40}Ar/^{39}Ar$ analyses of muscovite from the earliest cleavage in the Las Minas unit yielded a plateau age of 347 ± 3 Ma (Mississippian) and show low temperature ages of ~260 Ma.

STOP 3-5 (N18° 30.351′, W98° 17.57′: Fig. 8)

The Cerro Puntiagudo Formation of Strunian age (latest Devonian) is 63 m thick and consists of shale, sandstone, and limestone. It is overlain by conglomerates of the Potrerillo Formation (124 m thick) that consists of red sandstone with Oseagean fossils and conglomerate with large K-feldspar clasts: these clasts are inferred to have been derived from the nearby megacrystic granitoids. The Cerro Puntiagudo Formation rests unconformably upon the Ojo de Agua unit, which consists of finely bedded, black pelitic rocks intruded by green, fine grained, mafic dikes with an arc-related chemistry. These latter rocks are deformed by isoclinal, upright-steeply inclined, NE- and SE-trending, subhorizontal folds. The youngest detrital zircons in this unit are 466 ± 25 Ma (Keppie et al., 2008), abd 471 ± 9 Ma (Keppie et al., 2010).

STOP 3-6 (N18° 30.66′ W98° 17.78′: Fig. 8)

The La Junta Formation is a 126 m thick shale unit containing Missourian fossils; the Tepazulco Formation (193 m thick) is made up of interbedded limestone, shale, and sandstone and contains Virgilian-Missourian fossils. An Ordovician plug is faulted against the Patlanoaya Group at this locality.

STOP 3-7 (N18°31′, W°16.79′: Fig. 8)

The Lower Permian La Mesa, La Cuesta and La Cueva Formations consist of a conglomerate (45 m thick) and calcareous sandstone unit containing Wolfcampian fossils; interbedded shale and limestone with mid-Wolfcampian to middle Leonardian fossils; and sandstone (>280 m thick) containing late Leonardian fossils at its base.

REFERENCES CITED

Alva-Valdivia, L.M., Goguitchaichvli, A., Grajales, M., Flores de Dios, A., Urrutia-Fucugauchi, J., Rosales, C., and Morales, J., 2002, Further constraints for Permo-Carboniferous magnetostratigraphy: case study of the sedimentary sequence from San Salvador-Patlanoaya (Mexico): Comptes Rendus Geoscience, v. 334, p. 811–817, doi:10.1016/S1631-0713(02)01821-7.

Böhnel, H., 1999, Paleomagnetic study of Jurassic and Cretaceous rocks from the Mixteca terrane (Mexico): Journal of South American Earth Sciences, v. 12, no. 6, p. 545–556, doi:10.1016/S0895-9811(99)00038-3.

Bullard, E.C., et al., 1965, A symposium on continental drift-IV. The fit of the continents around the Atlantic: Philosophical Transactions of the Royal Society, v. 258, p. 41–51, doi:10.1098/rsta.1965.0020.

Fang, W., Van der Voo, R., Molina-Garza, R., Moran-Zenteno, D.J., and Urrutia-Fucugauchi, J., 1989, Paleomagnetism of the Acatlan terrane, southern Mexico: evidence for terrane rotation: Earth and Planetary Science Letters, v. 94, no. 1-2, p. 131–142, doi:10.1016/0012-821X(89)90089-7.

Galaz-Escanilla, G., Keppie, J.D., Lee, J.K.W., and Ortega-Rivera, A., in press, A high-pressure folded klippe at Tehuitzingo on the western margin of an extrusion zone, Acatlán Complex, southern Mexico: Gondwana Research.

González-Mancera, G., 2001, Mineralogía y petrología de las serpentinitas del cuerpo ultramáfico de Tehuitzingo, Estado de Puebla: Tesis de Maestría, Universidad Nacional Autónoma de México, 103p.

Guillot, S., Hattori, K., Agard, P., Schwartz, S., and Vidal, O., 2009, Exhumation Processes in Oceanic and Continental Subduction Contexts: A Review, *in* Lallemand, S., Funiciello, F., eds., Subduction Zone Geodynamics. Springer-Verlag Berlin Heidelberg, p. 175–205.

Helbig, M., Keppie, J.D., Murphy, B., and Solari, L., 2010, Jurassic Amphibolites of the Eastern Acatlan Complex (Southern Mexico) Related to Both Back-Arc Rifting and the Opening of the Gulf of Mexico?: Geological Society of America Abstracts with Programs, v. 42, no. 5, p. 679.

Irving, E., 1977, Drift of the major continents since the Devonian: Nature, v. 270, p. 304–309, doi:10.1038/270304a0.

Keppie, J.D., 2004, Terranes of Mexico revisited: A 1.3 billion year odyssey: International Geology Review, v. 46, no. 9, p. 765–794, doi:10.2747/0020-6814.46.9.765.

Keppie, D.F., and Keppie, J.D., in review, An alternative Pangean reconstruction for Middle America with the Chortis and Yucatan blocks in the Gulf of Mexico: implications for Mesozoic and Cenozoic tectonics: International Geology Review.

Keppie, J.D., Nance, R.D., Dostal, J., Ortega-Rivera, A., Miller, B.V., Fox, D., Powell, J., Mumma, S., and Lee, J.W.K., 2004, Mid-Jurassic Tectonothermal Event Superposed on a Paleozoic Geological Record in the Acatlán Complex of Southern Mexico: Hotspot Activity During the Breakup of Pangea: Gondwana Research, v. 7, p. 238–260, doi:10.1016/S1342-937X(05)70323-3.

Keppie, J.D., Dostal, J., Murphy, J.B., and Nance, R.D., 2008, Synthesis and tectonic interpretation of the westernmost Paleozoic Variscan orogen in southern Mexico: From rifted Rheic margin to active Pacific margin: Tectonophysics, v. 461, no. 1-4, p. 277–290, doi:10.1016/j.tecto.2008.01.012.

Keppie, J.D., Nance, R.D., Ramos-Arias, M.A., Lee, J.K.W., Dostal, J., Ortega-Rivera, A., and Murphy, J.B., 2010, Late Paleozoic subduction and exhumation of Cambro-Ordovician passive margin and arc rocks in the northern Acatlán Complex, southern Mexico: Geochronological constraints: Tectonophysics, v. 495, no. 3-4, p. 213–229, doi:10.1016/j.tecto.2010.09.019.

Kirsch, M., Keppie, J.D., Murphy, J.B., and Solari, L.A., in press, Permian–Carboniferous arc magmatism and basin evolution along the western margin of Pangea: geochemical and geochronological evidence from the eastern Acatlán Complex, southern Mexico: GSA Bulletin.

Malone, J., Nance, R.D., Keppie, J.D., and Dostal, J., 2002, Deformational history of part of the Acatlan Complex: Late Ordovician-early Silurian and early Permian orogenesis in southern Mexico: Journal of South American Earth Sciences, v. 15, no. 5, p. 511–524, doi:10.1016/S0895-9811(02)00080-9.

Morales-Gámez, M., Keppie, J.D., and Norman, M.D., 2008, Ordovician-Silurian rift-passive margin on the Mexican margin of the Rheic Ocean overlain by Carboniferous-Permian periarc rocks: Evidence from the eastern Acatlán Complex, southern Mexico: Tectonophysics, v. 461, p. 291–310, doi:10.1016/j.tecto.2008.01.014.

Morales-Gámez, M., Keppie, J.D., and Dostal, J., 2009, Carboniferous tholeiitic dikes in the Salada unit, Acatlán Complex, southern Mexico: a record of extension on the western margin of Pangea: Revista Mexicana De Ciencias Geológicas, v. 26, p. 133–142.

Pindell, J.L., and Dewey, J.F., 1982, Permo-Triassic reconstruction of western Pangaea and the evolution of the Gulf of Mexico/Caribbean region: Tectonics, v. 1, p. 179–211, doi:10.1029/TC001i002p00179.

Pindell, J.L., and Dewey, J.F., 1982, Permo-Triassic reconstruction of western Pangaea and the evolution of the Gulf of Mexico/Caribbean region: Tectonics, v. 1, p. 179–211, doi:10.1029/TC001i002p00179.

Smith, A.G., et al., 1981, Phanerozoic paleocontinental world maps. Cambridge University Press, Cambridge, 102 p.

Steiner, M.B., 2005, Pangean reconstruction of the Yucatan Block: Its Permian, Triassic, and Jurassic geologic and tectonic history, *in* Anderson, T.H., Nourse, J.A., McKee, J.W., and Steiner, M.B., eds. The Mojave-Sonora megashear hypothesis: Development, assessment, and alternatives. Geological Society of America Special Paper 393, p. 457–480. doi: 10.1130/2005.2393(17).

Talavera-Mendoza, O., Ruiz, J., Gehrels, G.E., Meza-Figueroa, D., Vega-Granillo, R., and Campa-Uranga, M., 2005, U-Pb geochronology of the Acatlán Complex and implications for the Paleozoic paleogeography and tectonic evolution of southern Mexico: Earth and Planetary Science Letters, v. 235, p. 682–699, doi:10.1016/j.epsl.2005.04.013.

Ulmer, P., and Trommsdorff, V., 1995, Serpentine Stability to Mantle Depths and Subduction-Related Magmatism: Science, v. 268, no. 5212, p. 858–861, doi:10.1126/science.268.5212.858.

Van der Voo, R., and French, R.B., 1974, Apparent polar wandering for the Atlantic-bordering continents: Late Carboniferous to Eocene: Earth-Science Reviews, v. 10, p. 99–119, doi:10.1016/0012-8252(74)90082-8.

Vega-Granillo, R., Meza-Figueroa, D., Ruiz, J., Talavera-Mendoza, O., and López-Martínez, M., 2009, Structural and tectonic evolution of the Acatlán Complex, southern Mexico: Its role in the collisional history of Laurentia and Gondwana: Tectonics, v. 28, no. 4, p. TC4008, doi:10.1029/2007TC002159.

Vega-Granillo, R., Talavera-Mendoza, O., Meza-Figueroa, D., Ruiz, J., Gehrels, G.E., and López-Martínez, M., 2007, Pressure-temperature-time evolution of Paleozoic high-pressure rocks of the Acatlán Complex (southern Mexico): Implications for the evolution of the Iapetus and Rheic Oceans: Geological Society of America Bulletin, v. 119, no. 9/10, p. 1249–1264, doi:10.1130/B226031.1.

Yañez, P., Patchett, P.J., Ortega-Gutierrez, F., and Gehrels, G.E., 1991, Isotopic studies of the Acatlán Complex, southern Mexico: Implications for Paleozoic North American Tectonics: Geological Society of America Bulletin, v. 103, no. 6, p. 817–828, doi:10.1130/0016-7606(1991)103<0817:ISOTAC>2.3.CO;2.

Printed in the U.S.A.

Capítulo 6

Discusión y conclusiones

6.1. Discusión

6.1.1. Origen de las rocas máficas de alta presión de Tehuitzingo

Los datos petrológicos y geoquímicos indican que las rocas máficas de alta presión (Suite Piaxtla) de Tehuitzingo corresponden a acumulados gabroicos intermedios a máficos, con afinidad toleítica de arcos de islas, y características típicas de magmas de antearco, similares a los generados actualmente en arcos oceánicos inmaduros. Esto es consistente con estudios realizados en la Serpentinita Tehuitzingo y sus lentes de cromititas (Proenza *et al.*, 2004), en las cuales la química de elementos del grupo de los platinoides y Au, indica que sus protolitos fueron fragmentos de litósfera oceánica formados en un ambiente de periarco. Este tipo de ofiolitas son típicas de arcos inmaduros, donde un régimen extensional en la placa superior permite la fusión de manto astenosférico hidratado (Shervais, 2001). Sin embargo, la única evidencia acerca de la posibilidad de un arco en el Complejo Acatlán es la presencia de clastos volcánicos y de una población de circones ígneos detríticos del Devónico Temprano–Misisípico (405–330 Ma), en rocas sedimentarias carboníferas que cubren los complejos Acatlán y Oaxaqueño (Keppie *et al.*, 2012a). Esto sugiere que las rocas máficas-ultramáficas que conforman la Suite Piaxtla en Tehuitzingo fueron formadas en la periferia de un naciente arco en el Complejo Acatlán durante el Devónico Temprano–Misisípico.

6.1.2. Génesis de las rocas metamórficas de alta presión del Complejo Acatlán: convergencia continental-continental vs continental-oceánica

Como se discutió en “Capítulo 1. Introducción”, las rocas metamórficas de alta presión son fundamentalmente formadas en regímenes convergentes, existiendo parámetros muy contrastantes que nos permiten discriminar si fueron formadas en convergencia continental-continental o continental-oceánica. Por ejemplo, las rocas extruidas en convergencia continental-continental (tipo alpina) se caracterizan por sus altas tasas de exhumación (sobre 20 mm/año) y gradientes termales (sobre 15 °C/km). En contraste, en

convergencia continental-oceánica (subducción), las tasas de exhumación varían entre 1–10 mm/año y sus gradientes termales son menores a 10 °C/km.

Las tasas de exhumación y gradientes termales de las rocas de la Suite Piaxtla en Tehuitzingo, Mimilulco y Piaxtla, varían entre 1.6–2.3 mm/año y 5.9–8.7 °C/km respectivamente (Fig. 5). Estos rangos son consistentes con un régimen convergente de subducción, ya sea de tipo acrecionario o serpentinítico (Fig. 6; Guillot *et al.*, 2004, 2009; Agard *et al.*, 2006, 2009). Esto sugiere que la Suite Piaxtla representa una zona de extrusión generada durante un proceso de subducción, como fue propuesto por Keppie *et al.* (2008a), en vez de una zona de sutura oceánica producto de uno o múltiples eventos de convergencia continental-continental (Ortega-Gutiérrez, 1999; Talavera-Mendoza *et al.*, 2005; Vega-Granillo *et al.*, 2007, 2009).

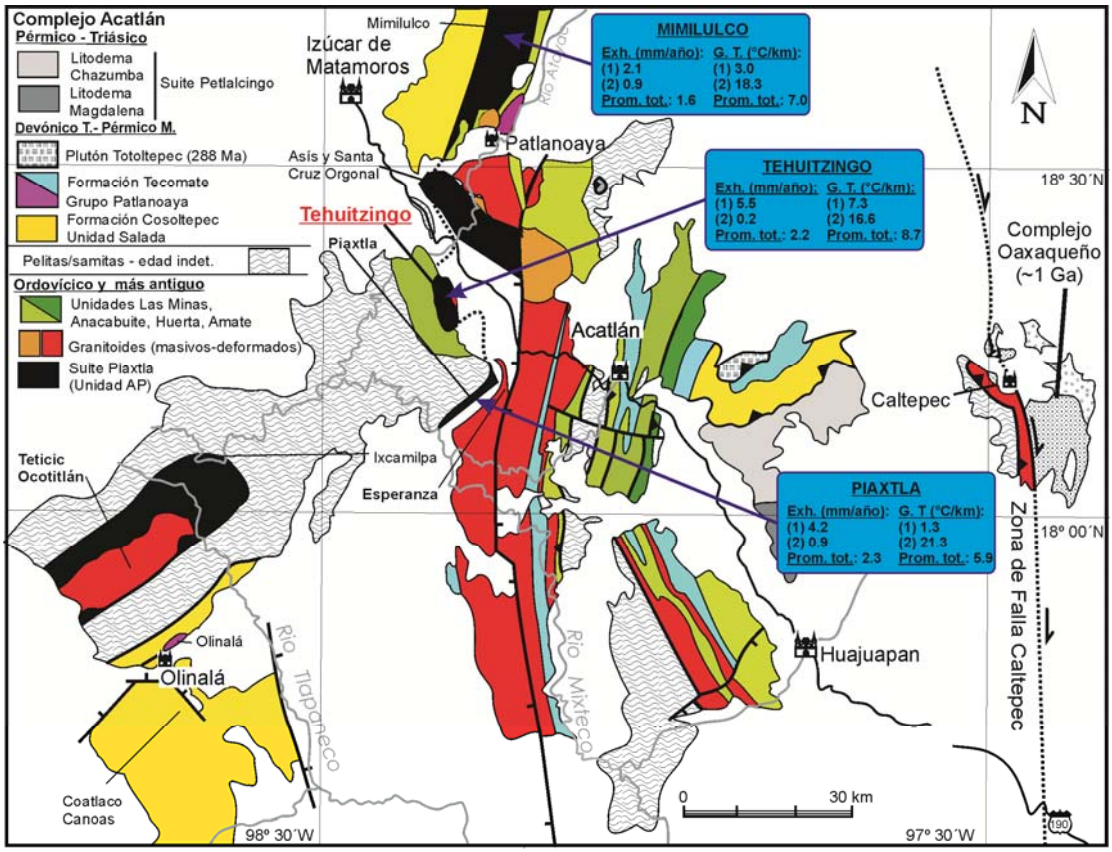

(1) primer periodo de exhumación entre facies eclogita y anfibolita
(2) segundo periodo de exhumación entre facies anfibolita y esquistos verdes

Fig. 5. Tasas de exhumación y gradientes termales de rocas de alta presión en el Complejo Acatlán. Cálculos realizados en rocas de Tehuitzingo (esta tesis), Mimilulco (Meza-Figueroa *et al.*, 2003; Vega-Granillo *et al.*, 2007; Elías-Herrera *et al.*, 2007) y Piaxtla (Vega-Granillo *et al.*, 2007; Meza-Figueroa *et al.*, 2003).

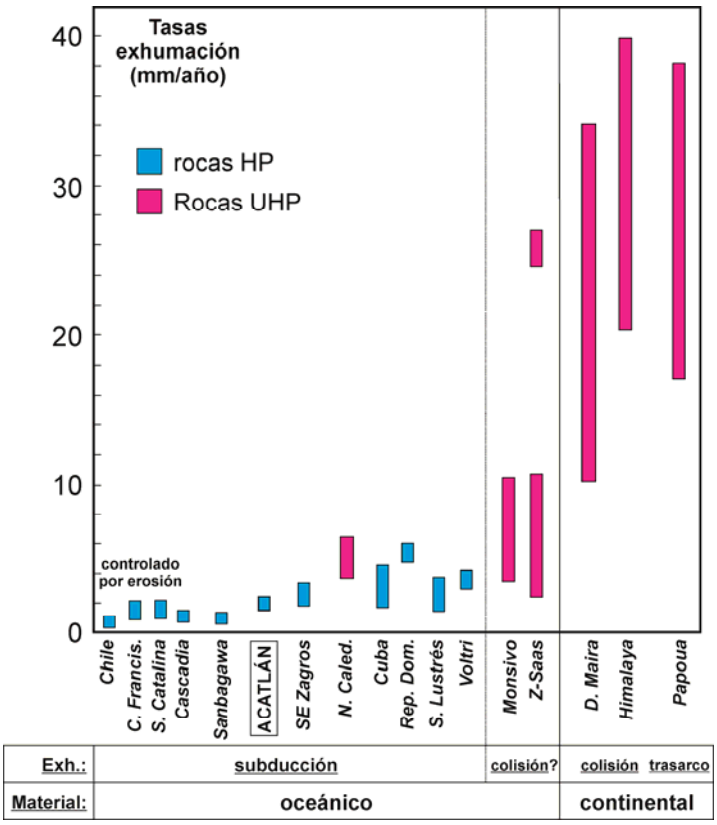

Fig. 6. Comparación de tasas de exhumación de rocas de alta presión alrededor del mundo. Notar el claro contraste entre convergencia en subducción vs continental. Modificado desde Agard *et al.* (2009).

Por otro lado, en subducción existen dos mecanismos mediante los cuales es posible generar y exhumar rocas de alta presión: acrecionario y serpentinítico (Guillot *et al.*, 2009; Agard *et al.*, 2009; Hattori *et al.*, 2010). Rocas metamórficas generadas mediante un prisma acrecionario no superan los ~20 km de profundidad máxima, exceptuando casos excepcionales en Chile (Glodny *et al.*, 2005, 2006) y Cascadia (Hyndman, 1995), donde alcanzan profundidades de ~40 km. En el caso de la Suite Piaxtla, sus patrones P-T-t, altas profundidades (50–55 km), además de la génesis en la cuña del manto de algunas de sus rocas, indican que su exhumación se produjo mediante un **canal de subducción serpentinítico** (Coleman, 1971; Guillot *et al.*, 2009; Agard *et al.*, 2009; Hattori *et al.*, 2010). Esta exhumación fue probablemente facilitada por el gran aumento volumétrico de las rocas ultramáficas durante su serpentinización en la cuña del manto (O'Hanley, 1996), conduciendo a la disminución de su densidad y en consecuencia al aumento de su flotabilidad. La baja densidad de lentes graníticos y metasedimentarios incluidos en la ofiolita Tehuitzingo, mejora la eficiencia de este proceso (e.g., Chemenda *et al.*, 2001). Las rocas metamórficas generadas y exhumadas mediante un canal de subducción serpentinítico

no superan los 60–70 km de profundidad (20–23 kbar, Guillot *et al.*, 2009; Agard *et al.*, 2009). Esto posiblemente debido a que a profundidades mayores la deshidratación de la losa y la cuña del manto impiden el proceso de serpentinización en peridotitas.

Por otro lado, un proceso de subducción-erosión que afectó a las rocas de alto grado del Complejo Acatlán durante el Devónico Temprano–Misisípico, es inferido por:

(1) el régimen de subducción determinado a partir del metamorfismo y extrusión de la Suite Piaxtla;

(2) durante un régimen de subducción, es el principal mecanismo que permite la remoción, enterramiento y consecuente metamorfismo de rocas de antearco/arco.

Este proceso habría actuado en protolitos de antearco/arco (serpentinita y acumulados de Tehuitzingo) pertenecientes a la Suite Piaxtla, sometiéndolas a altas presiones en profundidad (facies eclogita y esquistos azules). Posteriormente, estas rocas fueron extruidas en la cobertura de bajo grado del Complejo Acatlán por medio de un canal de subducción serpentinítico durante el Misisípico. La exhumación esta constreñida entre la edad del pico metamórfico de alta presión (facies eclogita o esquistos azules) en la Suite Piaxtla, donde existen dos consistentes edades U-Pb de 353 ± 1 en Mimilulco (Elías-Herrera *et al.*, 2007) y 346 ± 3 Ma en Asís (Middleton *et al.*, 2007), obtenidas desde circones interpretados como cogenéticos con el pico metamórfico (facies eclogita) Además existe una consistente edad granate-roca total de 352 ± 4 Ma (Estrada-Carmona, 2013), la cual es más confiable pues se obtuvo desde un mineral en equilibrio con la asociación mineral de alta presión.

6.2. Conclusiones

6.2.1. Evolución tectónica del Complejo Acatlán

Trabajos previos complementados con datos obtenidos en esta tesis, nos indican que la evolución tectónica paleozoica del Complejo Acatlán puede resumirse de la siguiente forma:

(1) *Ordovícico*: depósitos asociados a una secuencia de *rift* depositada sobre el margen pasivo sur del Océano Reico. El esquisto de mica de alto grado y la samita de bajo grado de Tehuitzingo, son correlacionables con esta secuencia y con depósitos de bajo grado ubicadas en el margen opuesto (este) del cinturón central de rocas de alta presión. Esta secuencia es contemporánea a la intrusión de una suite ígnea bimodal, constituida por granitoides y rocas máficas. Esto es consistente con edades U-Pb del Ordovícico Temprano, obtenidas en Tehuitzingo (Galaz *et al.,* 2013a) desde un granitoide de alto grado (485–482 Ma), un esquisto de mica de alto grado (~472 Ma) y una samita de bajo grado (481 Ma);

(2) *Devónico Medio:* inicio de un proceso de subducción sobre el margen occidental de Gondwana generando magmatismo de arco y depósitos de periarco al menos hasta el *Pérmico medio*;

(3) *Devónico Tardío–Pensilvánico*: proceso de subducción-erosión sobre el margen occidental de Gondwana, que afectó a los protolitos de antearco de la Suite Piaxtla en Tehuitzingo (Galaz *et al.*, 2013b). Este proceso permite que la placa oceánica remueva y entierre rocas de antearco/arco, produciéndose su deformación polifásica, migmatización y metamorfismo de alta P-T en profundidad. Los procesos de serpentinización desarrollados en la cuña del manto facilitan el aumento de la flotabilidad de este conjunto de rocas, así como su desacople con la placa superior. Esto posibilita la exhumación de la Suite Piaxtla por medio de un canal de subducción serpentinítico, permitiendo su yuxtaposición tectónica en la corteza superior de bajo grado durante el Misisípico (329–317 Ma). Este proceso se realizó a tasas de exhumación de 1.6–2.3 mm/año y con un gradiente termal promedio de ~7 °C/km (Galaz *et al.*, 2013a);

(4) *Pérmico–Triásico*: continuación de la subducción evidenciada por la intrusión de plutones asociados a arco volcánico. En la corteza se producen diversas zonas de cizalla dextral, N-S, de bajo grado (esquistos verdes) que obliteran la mayoría de los contactos originales entre la Suite Piaxtla y las rocas de bajo grado metamórfico. Simultáneamente, numerosos corrimientos con vergencia sur generan diversos depósitos de cuña clástica (Keppie *et al.*, 2006).

6.2.2. Extrusión en la placa superior: modelos numéricos vs modelos geológicos

Se han reportado diversos modelos geológicos relacionados a mecanismos de exhumación de terrenos metamórficos de alta presión alrededor del mundo. Estos modelos son construidos fundamentalmente a partir de datos petrológico-estructurales y geocronológicos, combinados con resultados obtenidos desde modelos numéricos y análogos. Recientemente se han postulado valiosos modelos geológicos asociados a la extrusión de rocas de alta presión tanto en márgenes convergentes colisionales (e.g., Liou *et al.*, 2004; Ernst *et al.*, 2005, 2010), como en subducción (e.g., Keppie *et al.*, 2008b; Hattori *et al.*, 2010). Adicionalmente, existen diversos trabajos que han modelado numéricamente los mecanismos de exhumación en regímenes de convergencia continental-continental (Chemenda *et al.*, 2001; Toussaint *et al.*, 2004; Warren *et al.*, 2008) y continental-oceánica (Gerya, *et al.*, 2002; Stöckhert y Gerya, 2005; Gorczyk *et al.*, 2007; Castro y Gerya, 2008). Estos modelos numéricos han permitido comprender el comportamiento en profundidad de diversos parámetros fundamentales en la exhumación de estas rocas, entre otros, patrones P-T-t, tasas de exhumación, gradientes termales, grado de desacople mecánico interplacas, etc. En general, las determinaciones desde modelos geológicos y numéricos tienen una gran consistencia, sin embargo, prácticamente la totalidad de los modelos numéricos, muestran un ascenso por medio de un flujo convoluto y/o diapírico en las etapas iniciales de exhumación del cuerpo metamórfico. Posteriormente, en profundidades más someras (~50 km), el material metamórfico es incorporado al canal de subducción o exhumado mediante estructuras preexistentes en una posición más interna de la placa superior. Este inicial mecanismo de exhumación convectivo y/o diapírico del cuerpo metamórfico ha sido sometido a un fuerte cuestionamiento, no logrando aún ser demostrado con datos geológicos concretos.

6.2.3. Modelo de extrusión: desafíos futuros

Los estudios relacionados con mecanismos de exhumación de rocas de alta presión en régimen de subducción (continental-oceánica), han aportado grandes avances en la comprensión de la tectónica de placas, permitiendo la reinterpretación de diversos terrenos

metamórficos de alta presión alrededor del mundo. Sin embargo, aún falta establecer importantes factores en la generación y exhumación de sus rocas:

(1) establecer si la velocidad y geometría de convergencia de la placa oceánica subductante influye en las tasas de exhumación de las rocas extruidas. Basado en modelos numéricos se ha propuesto que un canal de subducción con un flujo de retorno estable, requiere una tasa de subducción mínima (Gerya y Stöckhert, 2006), no obstante, este valor no ha sido determinado aún en modelos geológicos;

(2) determinar si existe alguna relación entre la edad de la placa subductante y el gradiente termal y/o tasa de exhumación de las rocas extruidas. Claramente placas jóvenes más calientes favorecen una subducción con altos gradientes termales iniciales;

(3) la temporalidad del evento de exhumación de la corteza oceánica con respecto a la duración del proceso de subducción. Existen ejemplos de exhumación en etapas iniciales (Cordillera Costa en Chile, Complejo Franciscano en EU), intermedias (Himalaya, Andes ecuatorianos), y finales (Nueva Caledonia, Alpes del oeste). Esto con el objetivo de determinar si la exhumación es sistemática o sólo se produce en particulares intervalos de tiempo durante el proceso de subducción.

(4) determinar si existe una proporción mínima de “material” boyante (sedimentos y peridotitas serpentinizadas), asociado a las rocas máficas-ultramáficas, requerido para que se produzca su exhumación.

Referencias Bibliográficas

Citas incluidas en el *Capítulo 1. Introducción* y *Capítulo 6. Discusión y conclusiones*. Las citas de los artículos incluidos en esta Tesis se encuentran contenidas en los mismos

Agard, P. Monié, P., Gerber, W., Omrani, J., Molinaro, M., Meyer, B., Labrousse, L., Vrielynck, B., Jolivet, L., Yamato, P., 2006. Transient, syn-obduction exhumation of Zagros blueschists inferred from P-T-deformation-time and kinematic constraints: implications for Neotethyan wedge dynamics. Journal of Geophysical Research, 111, B11401. doi:10.1029/2005JB004103.

Agard, P., Yamato, P., Jolivet, L., Burov, E., 2009. Exhumation of oceanic blueschists and eclogites in subduction zones: Timing and mechanisms. Earth-Science Reviews, 92, p. 53–79.

Anczkiewicz, R., Platt, J.P., Thirlwall, M.F., Wakabayashi, J., 2004. Franciscan subduction off to a slow start: evidence from high-precision Lu–Hf garnet ages on high grade-blocks. Earth and Planetary Science Letters, 225, p. 147–161.

Brun, J.P., Faccenna, C., 2008. Exhumation of high-pressure rocks driven by slab rollback. Earth and Planetary Science Letters, 272(1–2), p. 1–7, doi:10.1016/j.epsl.2008.02.038.

Brun, J.P., Sokoutis, D., 2007. Kinematics of the Southern Rhodope Core Complex (North Greece). International Journal of Earth Sciences, 96, p. 1079–1099, doi:10.1007/s00531-007-0174-2.

Butler, J.P., Beaumont, C., Jamieson, R.A., 2011. Crustal emplacement of exhuming (ultra) high-pressure rocks: will that be pro- or retro-side?. Geology, 39, p. 635–638.

Calderón-García, A., 1956. Estratigrafía del Mesozoico y tectónica del sur del Estado de Puebla, México: México D. F. Congreso Geológico Internacional 20, Libro-guía de la excursión A-11, p. 9–33.

Carballido-Sánchez, E.A., Delgado-Argote, L.A., 1989. Geología del cuerpo serpentinítico de Tehuitzingo, Estado de Puebla. Interpretación preliminar de su emplazamiento. Revista Mexicana de Ciencias Geológicas, 8(2), p. 134–148.

Castro, A., Gerya, T.V., 2008. Magmatic implications of mantle wedge plumes: Experimental study. Lithos, 103(1–2), p. 138–148.

Cerca, M., Ferrari, L., López-Martínez, M., Martiny, B., Iriondo, A., 2007. Late Cretaceous shortening and early Tertiary shearing in the central Sierra Madre del Sur, southern México: Insights into the evolution of the Caribbean-North American plate interaction. Tectonics, 26, TC3007, http://dx.doi.org/10.1029/2006TC001981.

Chemenda, A.I., Hurpin, D., Tang, J.-C., Stephan, J.-F., Buffet, G., 2001. Impact of arc-continent collision on the conditions of burial and exhumation of UHP/LT rocks: experimental and numerical modeling. Tectonophysics, 342, p. 137–161.

Coleman, R.G., 1971. Plate tectonic emplacement of upper mantle peridotites along continental edges. Journal of Geophysical Research, 76, p. 1212–1222.

Elías-Herrera, M., Ortega-Gutiérrez, F., 2002. Caltepec fault zone: An Early Permian dextral transpressional boundary between the Proterozoic Oaxacan and Paleozoic Acatlán complexes, southern México, and regional implications. Tectonics, 21(3), p. 220–234.

Elías-Herrera, M., Ortega-Gutiérrez, F., Sánchez-Zavala, J.L., Iriondo, A., Ortega-Rivera, A., 2007. Conflicting stratigraphic and geochronological data from the Acatlán Complex: "Ordovician" granite intrude metamorphic and sedimentary rocks of Devonian-Permian age. Eos Transactions AGU, 88(23), Joint Assembly Supplement, Abstract T41A-12.

Ernst, W.G., 2005. Alpine and Pacific styles of Phanerozic mountain building: subduction-zone petrogenesis of continental crust. Terra Nova, 17, p. 165–188.

Ernst, W.G., 2010. Subduction-zone metamorphism, calc-alkaline magmatism, and convergent-margin crustal evolution. Gondwana Research, 18(1), p. 8–16, doi:10.1016/j.gr.2009.05.010.

Ernst, W.G., Marayama, S., Wallis, S., 1997. Buoyancy-driven, rapid exhumation of ultrahigh-pressure metamorphosed continental crust. Proceedings of the National Academy of Science USA, 94, p. 9532–9537.

Estrada-Carmona, J., 2013. Magmatismo Ordovícico en el sur del Bloque Maya y metamorfismo de alta presión Misisípico en el Terreno Mixteca: Implicaciones para a evolución tectónica del noroeste de Gondwana durante el Paleozoico (Estudio geoquímico e isotópico y geocronometría por U-Pb y Lu-Hf. Tesis de Doctorado, Centro de Investigación Científica y de Educación Superior de Ensenada, México, 139 p.

Galaz, G., Keppie, J.D., Lee, J.K.W., and Ortega-Rivera, A., 2013a. A high-pressure folded klippe at Tehuitzingo on the western margin of an extrusion zone, Acatlán Complex, southern México. Gondwana Research, 23, p. 641–660.

Galaz, G., Keppie, J.D., Murphy, J.B., 2013b. Mafic forearc cumulates and associated rocks in the central high-pressure belt of the Acatlán Complex of southern México: geochemical constraints. International Geology Review, http://dx.doi.org/10.1080/00206814.2013.776806.

Gerya, T.V., Stöckhert, B., 2006. Two-dimensional numerical modeling of tectonic and metamorphic histories at active continental margins. International Journal of Earth Sciences, 95, p. 250–274.

Gerya, T.V., Stöckhert, B., Perchuk, A.L., 2002. Exhumation of high-pressure metamorphic rocks in a subduction channel: a numerical simulation. Tectonics, 21, p. 1056, doi:10.1029/2002TC001406.

Glodny, J., Echtler, H., Figueroa, O., Franz, G., Grafe, K., Kemnitz, H., Kramer, W., Krawczyk, C., Lohrmann, I., Lucassen, F., Melnick, D., Rosenau, M., Seifert, W., 2006. Long-Term Geological Evolution and Mass-Flow Balance of the South-Central Andes. In: Onken, O., Chong, G., Franz, G., Giese, P., Götze, H.J., Ramos, V.A., Strecker, M.R., Wigger, P., (Eds.), The Andes: Active Subduction Orogeny. Springer-Verlag Berlin Heidelberg, p. 401–428.

Glodny, J., Lohrmann, J., Echtler, H., Gräfe, K., Seifert, W., Collao, S., Figueroa, O., 2005. Internal dynamics of a paleoaccretionary wedge: Insights from combined isotope tectonochronology and sandbox modelling of the South-Central Chilean forearc. Earth and Planetary Science Letters, 231(1-2), p. 23–39.

González-Mancera, G., 2001. Mineralogía y petrología de las serpentinitas del cuerpo ultramáfico de Tehuitzingo, Estado de Puebla. Tesis de Maestría, Universidad Nacional Autónoma de México, México, 103 p.

Gorczyk, W., Guillot, S., Gerya, T.V., Hattori, K., 2007. Asthenospheric upwelling, oceanic slab retreat, and exhumation of UHP mantle rocks: Insights from Greater Antilles. Geophysical Research Letters, 34, L21309, doi:10.1029/2007GL031059.

Guillot, S., Hattori, K., Agard, P., Schwartz, S., Vidal, O., 2009. Exhumation Processes in Oceanic and Continental Subduction Contexts: A Review. In: Lallemand, S., Funiciello, F. (Eds.), Subduction Zone Geodynamics. Springer-Verlag Berlin Heidelberg, p. 175–205.

Guillot, S., Schwartz, S., Hattori, K., Auzende, A.L., Lardeaux, J.M., 2004. The Monviso ophiolitic Massif (Western Alps), a section through a serpentinite subduction channel. Journal of the Virtual Explorer, 16, Paper 3, p. 1–16.

Hattori, K., Wallis, S., Enami, M., Mizukami, T., 2010. Subduction of mantle wedge peridotites: Evidence from the Higashi-akaishi ultramafic body in the Sanbagawa metamorphic belt. Island Arc, 19, p. 192–207.

Huet, B., Le Pourhiet, L., Labrousse, L., Burov, E., Jolivet, L., 2011. Post-orogenic extension and metamorphic core complexes in a heterogeneous crust: the role of crustal layering inherited from collision. Application to the Cyclades (Aegean domain). Geophysical Journal International, 184, p. 611–625.

Hyndman, R.D., 1995. The lithoprobe corridor across the Vancouver Island and tectonic consequences of subduction. Canadian Journal of Earth Sciences, 32, p.1777–1802.

Jansen, J.B.H, Schuiling, R.D., 1976. Metamorphism on Naxos: Petrology and geothermal gradients. American journal of Science, 276, p. 1225–1253.

Kapp, P., Yin, A., Manning, C.E., Murphy, M., Harrison, T.M., Spurlin, M., Lin, D., Xi-Guang, D., Cun-Ming, W., 2000. Blueschist-bearing metamorphic core complexes in the Qiangtang block reveal deep crustal structure of northern Tibet. Geology, 28(1); p. 19–22.

Keppie, J.D., Dostal, J., Cameron, K.L., Solari, L.A., Ortega-Gutiérrez, F., López, R., 2003. Geochronology and geochemistry of Grenvillian igneous suites in the northern Oaxacan Complex, southern México: tectonic implications. Precambrian Research, 120, p. 365–389.

Keppie, J.D., Dostal, J., Miller, B.V., Ramos-Arias, M.A., Morales-Gámez, M., Nance, R.D., Murphy, J.B., Ortega-Rivera, A., Lee, J.W.K, Housh, T., Cooper, P., 2008a. Ordovician–earliest Silurian rift tholeiites in the Acatlán Complex, southern México: Evidence of rifting on the southern margin of the Rheic Ocean. Tectonophysics, 461, p. 130-156.

Keppie, J.D., Dostal, J., Murphy, J.B., Nance, R.D., 2008b. Synthesis and tectonic interpretation of the westernmost Paleozoic Variscan orogen in southern México: From rifted Rheic margin to active Pacific margin. Tectonophysics, 461, p. 277-290.

Keppie, J.D., Dostal, J., Murphy, J.B., Galaz-Escanilla, G., Ramos-Arias, M.A., Nance, R.D., 2012a. High pressure rocks of the Acatlán Complex, southern Mexico: Large-scale subducted Ordovician rifted passive margin extruded into the upper plate during the Devonian–Carboniferous. Tectonophysics, 560–561, p. 1–21.

Keppie, J.D., Nance, R.D., Dostal, J., Lee, J.K.W., Ortega-Rivera, A., 2012b. Constraints on the subduction erosion/extrusion cycle in the Paleozoic Acatlán Complex of southern México: Geochemistry and geochronology of the type Piaxtla Suite. Gondwana Research, 21, p. 1050–1065, doi:10.1016/j.gr.2011.07.020.

Keppie, J.D., Nance, R.D., Fernández-Suárez, J., Storey, C.D., Jeffries, T.E., Murphy, J.B., 2006. Detrital zircon data from the Eastern Mixteca Terrane, Southern México: Evidence for an Ordovician–Mississippian continental rise and a Permo-Triassic clastic wedge adjacent to Oaxaquia. International Geology Review, 48, 97–111.

Keppie, J.D., Nance, R.D., Murphy, J.B., Dostal, J., Braid, J.A., 2010a. The high-pressure Iberian–Czech belt in the Variscan orogen: Extrusion into the upper (Gondwanan) plate?. Gondwana Research, 17, 306–316, doi:10.1016/j.gr.2009.08.007.

Keppie, J.D., Nance, R.D., Ramos-Arias, M.A., Lee, J.K.W., Dostal, J., Ortega-Rivera, A., Murphy, J.B., 2010b. Late Paleozoic subduction and exhumation of Cambro–Ordovician passive margin and arc rocks in the northern Acatlán Complex, southern México: Geochronological constraints. Tectonophysics, 495, p. 213–229.

Kylander-Clark, A.R.C., Hacker, B.R., Mattinson, J.M., 2008. Slow exhumation of UHP terranes: titanite and rutile ages of the Western Gneiss Region, Norway. Earth and Planetary Science Letters, 272, p. 531–540.

Liou, J.G., Tsujimori, T., Zhang, R.Y., Katayama, I., Maruyama, S., 2004. Global UHP metamorphism and continental subduction/collision: the Himalayan mode. International Geology Review, 46, p. 1–27.

Lister, G.S., Banga, G., Feenstra, A., 1984. Metamorphic core complex of cordilleran type in the Cyclades, Aegean Sea, Greece. Geology, 12, p. 221–225.

Meza-Figueroa, D.M., 1998. Geochemistry and characterization of intermediate temperature eclogites from the Acatlán Complex, southern México [Ph.D. thesis]. Tucson, University of Arizona, 201 p.

Meza-Figueroa, D., Ruiz, J., Talavera-Mendoza, O., Ortega-Gutiérrez, F., 2003. Tectonometamorphic evolution of the Acatlán Complex eclogites (southern México). Canadian Journal of Earth Sciences, 40, p. 27–44.

Middleton, M.D., Keppie, J.D., Murphy, J.B., Miller, B.V., Nance, R.D., 2007. P-T-t constraints on exhumation following subduction in the Rheic Ocean: eclogitic Asís Lithodeme, Piaxtla Suite, Acatlán Complex, southern México. In: Linnemann, U., Nance, R.D., Zulauf, G., Kraft, P. (Eds.), The Geology of Peri-Gondwana: the Avalonian–Cadomian Belt, Adjoining Cratons and the Rheic Ocean. Geological Society of America, Special Paper 423, p. 489–509.

Morales-Gámez, M., Keppie, J.D., Dostal, J., 2009. Carboniferous tholeiitic dikes in the Salada unit, Acatlán Complex, southern México: A record of extension on the western margin of Pangea. Revista Mexicana de Ciencias Geológicas, 26(1), p. 133–142.

Murphy, J.B., Keppie, J.D., Nance, R.D., Miller, B.V., Dostal, J., Middleton, M., Fernández-Suárez, J., Jeffries, T.E., Storey, C.D., 2006. Geochemistry and U-Pb protolith ages of eclogitic rocks of the Asís Lithodeme, Piaxtla Suite, Acatlán Complex, southern México: Tectonothermal activity along the southern margin of the Rheic Ocean. Journal of the Geological Society, 163, p. 683–695.

O'Hanley, D.S., 1996. Serpentinites: Records of tectonic and petrological history. Oxford University Press, New York, 34, 277 p.

Ortega-Gutiérrez, F., 1981. La evolución tectónica premisisípica del sur de México. UNAM, Revista del Instituto de Geología, 5(2), p. 140–157.

Ortega-Gutiérrez, F., Elías-Herrera, M., Reyes-Salas, M., Macías-Romo, C., López, R., 1999. Late Ordovician–Early Silurian continental collisional orogeny in southern México and its bearing on Gondwana-Laurentia connections. Geology, 27, p. 719–722.

Ortega-Obregón, C., Murphy, J.B., Keppie, J.D., 2009. Geochemistry and Sm–Nd isotopic systematics of Ediacaran–Ordovician, sedimentary and bimodal igneous rocks in the western Acatlán Complex, southern México: Evidence for rifting on the southern margin of the Rheic Ocean. Lithos, 114, p. 155–167.

Proenza, J.A., Ortega-Gutiérrez, F., Camprubí, A., Trilla, J., Elías-Herrera, M., Reyes-Salas, M., 2004. Paleozoic serpentinite-enclosed chromitites from Tehuitzingo (Acatlán Complex, southern México): a petrological and mineralogical study. Journal of South American Earth Sciences, 16, p. 649–666.

Ramos-Arias, M.A., Keppie, J.D., Lee, J.W.K., Ortega-Rivera A., 2012. A Carboniferous high-pressure klippe in the western Acatlán Complex of southern México: implications for the tectonothermal development and paleogeography of Pangea. International Geology Review, 54, p. 1–20, doi: 10.1080/00206814.2011.580634.

Ramos-Arias, M.A., Keppie J.D., Ortega-Rivera A., Lee, J.W.K., 2008. Extensional Late Paleozoic deformation on the western margin of Pangea, Patlanoaya area, Acatlán Complex, southern México. Tectonophysics, 448, p. 60–76.

Reyes-Salas, A.M., 2003. Mineralogía y petrología de los Granitoides Esperanza del Complejo Acatlán, sur de México. Tesis doctoral, Universidad Autónoma del Estado de Morelos, México, 165 p.

Shervais, J.W., 2001. Birth, death, and resurrection: The life cycle of suprasubduction zone ophiolites. Geochemistry, Geophysics, Geosystems, 2, 2000GC000080.

Stöckhert, B., Gerya, T.V., 2005. Pre-collisional high pressure metamorphism and nappe tectonics at active continental margins: A numerical simulation. Terra Nova, 17, p. 102–110.

Talavera-Mendoza, O., Meza-Figueroa, D., De la Cruz, V.J.C., Vega-Granillo, R., 2002. Esquistos azules en el complejo Acatlán, (sur de México): Implicaciones tectonometamórficas. Reunión Anual de la Unión Geofísica Mexicana, Resumen, 22, p. 248.

Talavera-Mendoza, O., Ruiz, J., Gehrels, G.E., Meza-Figueroa, D.M., Vega-Granillo, R., Campa-Uranga, M.F., 2005. U-Pb geochronology of the Acatlán Complex and implications for the Paleozoic paleogeography and tectonic evolution of southern México. Earth and Planetary Science Letters, 235, 682–699.

Tolson, G., 2005. La falla Chacalapa en el sur de Oaxaca. En: Alaniz-Álvarez, S.A., Nieto-Samaniego, A.F. (Eds.), Grandes Fronteras Tectónicas de México. Boletín de la Sociedad Geológica Mexicana, Volumen Conmemorativo del Centenario, 52(1), p. 111–122.

Toussaint, G., Burov, E., Avouac, J.P., 2004. Tectonic evolution of a continental collision zone: a thermomechanical numerical model. Tectonics, 23(6), TC6003, p. 1–24. doi:10.1029/2003TC001604.

Vega-Granillo, R., Calmus, T., Meza-Figueroa, D., Ruiz, J., Talavera-Mendoza, O., López-Martínez M., 2009. Structural and tectonic evolution of the Acatlán Complex, southern México: Its role in the collisional history of Laurentia and Gondwana. Tectonics, 28, p. 1–25.

Vega-Granillo, R., Talavera-Mendoza, O., Meza-Figueroa, D., Ruiz, J., Gehrels, G., López-Martínez, M., De la Cruz-Vargas, J., 2007. Pressure-temperature evolution of Paleozoic high-pressure rocks of the Acatlán Complex (southern México): implications for the evolution of the Iapetus and Rheic Oceans. Geological Society of America Bulletin, 119(9–10), p. 1249–1264.

Warren, C.J., Beaumont, C., Jamieson, R.A., 2008. Modelling tectonic styles and ultra-high pressure (UHP) rock exhumation during the transition from oceanic subduction to continental collision. Earth and Planetary Science Letters, 267, p. 129–145.

Apéndice A

Análisis de microsonda electrónica, fórmulas estructurales minerales y análisis U-Pb de rocas del Complejo Acatlán en Tehuitzingo

Tabla A1. Análisis de microsonda y fórmulas estructurales de granates, basadas en 12 oxígenos.

Litología	**Granitoide (SP*)**		**Metabasita-1 (SP)**			**Esquisto de mica (SP)**			
Fase	**G24-c2.1**	**G24-c2.2**	**G27-c2.1**	**G27-c2.2**	**G27-c2.3**	**G12-c1.1**	**G12-c1.2**	**G12-c3.1**	**G12-c3.2**
SiO_2 (wt. %)	37.60	37.50	38.50	38.23	38.31	38.55	37.45	37.71	37.43
TiO_2	0.09	0.06	0.10	0.12	0.07	0.11	0.11	0.05	0.09
Al_2O_3	21.30	21.24	21.76	21.73	21.86	22.02	21.13	21.55	21.26
FeO	32.22	34.17	28.77	28.72	29.03	32.49	31.98	33.41	31.57
MnO	1.11	1.13	0.59	1.49	0.40	0.51	0.47	0.38	2.67
MgO	1.90	2.10	2.55	2.18	2.89	2.43	2.16	2.34	1.48
CaO	6.82	5.34	10.04	10.16	9.98	7.28	7.62	6.45	6.46
Total óxidos %	**101.03**	**101.53**	**102.29**	**102.63**	**102.54**	**103.38**	**100.90**	**101.89**	**100.95**
Almandino %	70.87	74.46	61.52	60.93	61.29	69.63	69.43	72.29	69.88
Piropo %	7.44	8.15	9.71	8.26	10.87	9.28	8.34	9.02	5.82
Espesartina %	2.47	2.49	1.27	3.19	0.86	1.11	1.04	0.83	5.97
Grosularia %	19.22	14.89	27.49	27.62	26.98	19.98	21.19	17.87	18.33
Fórmulas estructurales basadas en 12 oxígenos									
Si	2.99	2.98	2.99	2.97	2.97	2.98	2.98	2.97	2.99
Ti	0.01	0.00	0.01	0.01	0.00	0.01	0.01	0.00	0.01
Al_{tot}	1.99	1.99	1.99	1.99	1.99	2.01	1.98	2.00	2.00
$Fe^{+2}{}_{tot}$	2.14	2.27	1.87	1.87	1.88	2.10	2.13	2.20	2.11
Mn	0.07	0.08	0.04	0.10	0.03	0.03	0.03	0.03	0.18
Mg	0.22	0.25	0.29	0.25	0.33	0.28	0.26	0.27	0.18
Ca	0.58	0.45	0.83	0.85	0.83	0.60	0.65	0.54	0.55
Cationes totales	**8.01**	**8.02**	**8.01**	**8.03**	**8.03**	**8.01**	**8.03**	**8.02**	**8.01**
Al^{IV}	0.01	0.02	0.01	0.03	0.03	0.02	0.02	0.03	0.01
Al^{VI}	1.98	1.97	1.98	1.96	1.96	1.99	1.96	1.97	1.99
Mg #	9.50	9.87	13.64	11.94	15.07	11.77	10.73	11.09	7.69

*SP: Suite Piaxtla

Tabla A2. Análisis de microsonda y fórmulas estructurales de anfíboles, basadas en 23 oxígenos.

Litología	**Metabasita-1 (SP*)**				**Metabasita-2 (SP)**			
Fase	**G25-c1.1**	**G25-c1.2**	**G25-c2.1**	**G25-c2.2**	**G31-c1.1**	**G31-c1.2**	**G31-c2.1**	**G31-c2.2**
SiO_2 (wt. %)	52.27	53.01	49.79	49.90	49.09	49.28	46.81	46.61
TiO_2	0.02	0.00	0.11	0.12	0.11	0.09	0.18	0.18
Al_2O_3	2.74	0.91	6.34	5.56	8.03	7.77	9.65	9.55
FeO	7.69	7.08	8.55	8.23	6.71	6.05	6.95	6.97
MnO	0.00	0.00	0.00	0.00	0.00	0.00	0.00	0.00
MgO	19.43	20.57	17.83	18.20	18.33	18.52	18.12	17.95
CaO	12.03	12.45	10.78	10.70	10.71	10.95	11.14	11.64
Na_2O	1.07	0.51	2.15	1.91	2.59	2.50	2.87	2.67
K_2O	0.04	0.01	0.11	0.10	0.06	0.03	0.03	0.05
Tot. óxidos %	**95.28**	**94.54**	**95.65**	**94.72**	**95.61**	**95.20**	**95.75**	**95.62**
Volátiles	4.72	5.46	4.35	5.28	4.39	4.80	4.26	4.38
Fórmulas estructurales basadas en 23 oxígenos (anhidro con Fe^{+3} asumido= 0.125 de Fe total)								
Si	7.57	7.71	7.23	7.30	7.08	7.12	6.79	6.78
Ti	0.00	0.00	0.01	0.01	0.01	0.01	0.02	0.02
Al_{tot}	0.47	0.16	1.09	0.96	1.36	1.32	1.65	1.64
$Fe^{+2}{}_{tot}$	0.93	0.86	1.04	1.01	0.81	0.73	0.84	0.85
Mn	0.00	0.00	0.00	0.00	0.00	0.00	0.00	0.00
Mg	4.20	4.46	3.86	3.97	3.94	3.99	3.92	3.89
Ca	1.87	1.94	1.68	1.68	1.65	1.69	1.73	1.82
Na	0.30	0.14	0.60	0.54	0.72	0.70	0.81	0.75
K	0.01	0.00	0.02	0.02	0.01	0.01	0.00	0.01
Cationes tot.	**15.34**	**15.28**	**15.53**	**15.49**	**15.59**	**15.57**	**15.77**	**15.76**
Al^{IV}	0.43	0.29	0.77	0.70	0.92	0.88	1.21	1.22
Al^{VI}	0.04	-0.13	0.32	0.26	0.44	0.44	0.44	0.42
Mg #	81.84	83.81	78.81	79.78	82.97	84.52	82.29	82.12

*SP: Suite Piaxtla

Tabla A3. Análisis de microsonda y fórmulas estructurales de fengitas, basadas en 11 oxígenos.

Litología	**Granitoide (SP*)**					**Samita de bajo grado**					**Esquisto de mica (SP)**						
Fase	**G24-c1.1**	**G24-c1.2**	**G24-c1.3**	**G24-c2.1**	**G24-c2.2**	**G02-c1.1**	**G02-c1.2**	**G02-c3.1**	**G02-c3.2**	**G02-c3.3**	**G12-c1.1**	**G12-c1.2**	**G12-c1.3**	**G12-c2.1**	**G12-c2.2**	**G12-c2.3**	**G12-c3.2**
SiO_2	49.37	48.62	49.07	48.91	50.16	46.02	44.51	47.73	47.21	48.92	48.23	48.81	48.40	48.28	46.62	50.37	49.07
TiO_2	0.42	0.46	0.45	0.44	0.45	0.13	0.13	0.15	0.17	0.15	0.39	0.36	0.36	0.31	0.31	0.29	0.29
Al_2O_3	29.10	29.44	30.04	29.09	29.71	30.70	29.62	33.15	32.67	31.93	29.50	28.74	30.13	29.65	30.39	30.44	30.22
FeO	3.65	3.60	3.21	3.24	3.15	2.77	2.60	2.77	2.33	2.39	2.70	2.35	2.64	1.84	1.52	1.61	1.81
MnO	0.00	0.00	0.00	0.00	0.00	0.00	0.00	0.00	0.00	0.00	0.00	0.00	0.00	0.00	0.00	0.00	0.00
MgO	2.34	2.40	2.34	2.36	2.38	1.82	1.66	1.35	1.45	1.78	2.84	3.14	2.76	3.05	3.09	3.05	3.07
CaO	0.02	0.00	0.00	0.01	0.00	0.02	0.03	0.02	0.03	0.01	0.02	0.01	0.00	0.02	0.02	0.02	0.00
Na_2O	0.57	0.69	0.72	0.58	0.67	0.39	0.34	0.19	0.21	0.20	0.54	0.48	0.56	0.71	0.75	0.86	0.74
K_2O	9.37	9.68	9.86	9.34	9.37	9.46	9.48	8.98	9.33	9.51	9.71	9.63	9.57	9.25	9.23	9.25	9.34
Tot. óx.%	**94.84**	**94.88**	**95.68**	**93.95**	**95.89**	**91.30**	**88.36**	**94.34**	**93.39**	**94.90**	**93.92**	**93.51**	**94.43**	**93.11**	**91.93**	**95.87**	**94.54**
Volátiles	5.16	5.12	4.32	6.05	4.11	8.70	11.64	5.66	6.61	5.10	6.08	6.49	5.57	6.89	8.07	4.13	5.46
Total	100.00	100.00	100.00	100.00	100.00	100.00	100.00	100.00	100.00	100.00	100.00	100.00	100.00	100.00	100.00	100.00	100.00
Celadonita%	31.34	27.32	26.98	30.77	31.71	20.48	20.81	19.06	19.13	25.26	26.62	30.95	25.43	27.54	20.60	30.55	27.62
Muscovita%	62.79	65.60	65.69	63.19	61.56	74.75	74.94	78.27	77.97	72.38	67.61	64.16	68.44	64.83	70.51	60.76	64.62
Paragonita%	5.79	7.08	7.33	5.99	6.73	4.64	4.04	2.50	2.67	2.28	5.66	4.86	6.13	7.52	8.76	8.60	7.76
Margarita%	0.08	0.00	0.00	0.06	0.00	0.13	0.21	0.16	0.24	0.08	0.11	0.03	0.00	0.12	0.13	0.09	0.00
Fórmulas estructurales basadas en 11 oxígenos																	
Si	3.31	3.27	3.27	3.31	3.32	3.20	3.21	3.19	3.19	3.25	3.27	3.31	3.25	3.28	3.21	3.31	3.28
Al^{IV}	0.69	0.73	0.73	0.69	0.68	0.80	0.79	0.81	0.81	0.75	0.73	0.69	0.75	0.72	0.79	0.69	0.72
Total T	*4.00*	*4.00*	*4.00*	*4.00*	*4.00*	*4.00*	*4.00*	*4.00*	*4.00*	*4.00*	*4.00*	*4.00*	*4.00*	*4.00*	*4.00*	*4.00*	*4.00*
Ti	0.02	0.02	0.02	0.02	0.02	0.01	0.01	0.01	0.01	0.01	0.02	0.02	0.02	0.02	0.02	0.01	0.01
Al^{VI}	1.62	1.61	1.63	1.63	1.63	1.72	1.72	1.80	1.79	1.75	1.62	1.61	1.64	1.65	1.67	1.66	1.65
Fe_{tot} as Fe^{+2}	0.20	0.20	0.18	0.18	0.17	0.16	0.16	0.16	0.13	0.13	0.15	0.13	0.15	0.10	0.09	0.09	0.10
Mn	0.00	0.00	0.00	0.00	0.00	0.00	0.00	0.00	0.00	0.00	0.00	0.00	0.00	0.00	0.00	0.00	0.00
Mg	0.23	0.24	0.23	0.24	0.23	0.19	0.18	0.13	0.15	0.18	0.29	0.32	0.28	0.31	0.32	0.30	0.31
Total b	*2.08*	*2.08*	*2.06*	*2.07*	*2.06*	*2.08*	*2.07*	*2.10*	*2.08*	*2.07*	*2.08*	*2.08*	*2.09*	*2.08*	*2.09*	*2.06*	*2.08*
Ca	0.00	0.00	0.00	0.00	0.00	0.00	0.00	0.00	0.00	0.00	0.00	0.00	0.00	0.00	0.00	0.00	0.00
Na	0.07	0.09	0.09	0.08	0.09	0.05	0.05	0.02	0.03	0.03	0.07	0.06	0.07	0.09	0.10	0.11	0.10
K	0.80	0.83	0.84	0.81	0.79	0.84	0.87	0.77	0.80	0.81	0.84	0.83	0.82	0.80	0.81	0.77	0.80
Total a	*0.88*	*0.92*	*0.93*	*0.88*	*0.88*	*0.89*	*0.92*	*0.79*	*0.83*	*0.83*	*0.91*	*0.90*	*0.89*	*0.90*	*0.91*	*0.88*	*0.89*
Cat. tot.	**6.95**	**7.00**	**6.99**	**6.95**	**6.94**	**6.98**	**6.99**	**6.89**	**6.92**	**6.91**	**6.99**	**6.97**	**6.98**	**6.97**	**7.00**	**6.94**	**6.97**

*SP: Suite Piaxtla

Tabla A4. Análisis de microsonda y fórmulas estructurales de epidotas, basadas en 12.5 oxígenos

Litología	**Granitoide (SP*)**		**Metabasita-1 (SP)**			
Fase	**G24-c3.1**	**G24-c3.2**	**G27-c2.1**	**G27-c2.2**	**G25-c1.1**	**G25-c1.2**
SiO_2 (wt. %)	36.76	37.95	38.14	37.09	38.07	38.55
TiO_2	0.11	0.18	0.11	0.16	0.16	0.16
Al_2O_3	24.39	24.64	24.58	27.35	27.86	27.25
Cr_2O_3	0.01	0.02	0.00	0.00	0.00	0.05
Fe_2O_3	10.31	9.87	10.59	7.05	6.35	7.38
MnO	0.28	0.35	0.17	0.12	0.01	0.13
MgO	0.03	0.03	0.02	0.06	0.07	0.09
CaO	23.01	23.45	23.74	24.12	24.39	23.98
Na_2O	0.00	0.00	0.00	0.00	0.00	0.00
K_2O	0.00	0.00	0.00	0.00	0.00	0.00
Total óxidos%	**94.90**	**96.49**	**97.35**	**95.95**	**96.90**	**97.60**
Clinozoisita%	78.23	78.98	78.12	85.64	87.28	85.00
Pistachita%	21.11	20.20	21.49	14.09	12.70	14.70
Piemontita%	0.65	0.81	0.39	0.27	0.02	0.30
Fórmulas estructurales basadas en 12.5 oxígenos						
Si	3.00	3.03	3.03	2.96	2.99	3.01
Ti	0.01	0.01	0.01	0.01	0.01	0.01
Al_{tot}	2.34	2.32	2.30	2.57	2.58	2.51
Cr	0.00	0.00	0.00	0.00	0.00	0.00
$Fe^{+3}{}_{tot}$	0.63	0.59	0.63	0.42	0.38	0.43
Mn	0.02	0.02	0.01	0.01	0.00	0.01
Mg	0.00	0.00	0.00	0.01	0.01	0.01
Ca	2.01	2.01	2.02	2.06	2.05	2.01
Na	0.00	0.00	0.00	0.00	0.00	0.00
K	0.00	0.00	0.00	0.00	0.00	0.00
Cationes tot.	**8.01**	**8.00**	**8.00**	**8.04**	**8.02**	**8.00**
Al+Fe+Mn	2.99	2.94	2.94	3.00	2.96	2.95

*SP: Suite Piaxtla

Tabla A5. Análisis de microsonda y fórmulas estructurales de cloritas, basadas en 14 oxígenos.

Litología	**Granitoide (SP*)**				**Metabasita-1 (SP)**									
Fase	**G24-c1.1**	**G24-c1.2**	**G24-c2.1**	**G24-c2.2**	**G27-c1.1**	**G27-c1.2**	**G27-c2.1**	**G27-c2.2**	**G27-c2.1**	**G25-c1.1**	**G25-c1.2**	**G25-c1.3**	**G25-c2.1**	**G25-c2.2**
SiO_2 (wt.%)	24.42	25.03	24.74	25.24	27.58	27.29	26.22	26.85	26.18	26.64	26.81	27.02	27.03	27.02
TiO_2	0.05	0.06	0.03	0.03	0.08	0.09	0.00	0.01	0.03	0.02	0.01	0.02	0.03	0.02
Al_2O_3	21.59	21.40	21.10	20.89	21.05	20.32	18.67	20.06	21.42	21.37	21.45	20.84	21.83	22.11
Cr_2O_3	0.00	0.00	0.00	0.00	0.00	0.00	0.00	0.00	0.00	0.00	0.00	0.00	0.00	0.00
FeO	28.20	28.36	28.33	28.24	21.14	19.61	24.18	23.87	21.24	14.51	14.67	14.53	14.26	14.27
MnO	0.00	0.00	0.00	0.00	0.00	0.00	0.00	0.00	0.00	0.00	0.00	0.00	0.00	0.00
MgO	12.99	12.62	12.38	12.47	18.80	20.27	17.40	17.14	18.75	23.70	23.76	23.88	24.18	23.85
CaO	0.00	0.00	0.02	0.00	0.01	0.03	0.02	0.01	0.01	0.02	0.01	0.01	0.02	0.00
Na_2O	0.00	0.03	0.03	0.02	0.00	0.00	0.01	0.01	0.01	0.00	0.00	0.00	0.03	0.03
K_2O	0.01	0.00	0.00	0.00	0.00	0.00	0.03	0.00	0.00	0.01	0.01	0.00	0.01	0.01
Total óx.%	**87.26**	**87.49**	**86.62**	**86.89**	**88.66**	**87.60**	**86.53**	**87.95**	**87.65**	**86.25**	**86.71**	**86.29**	**87.39**	**87.30**
Volátiles	12.74	12.51	13.38	13.11	11.34	12.40	13.47	12.05	12.35	13.75	13.29	13.71	12.61	12.70
Total	100.00	100.00	100.00	100.00	100.00	100.00	100.00	100.00	100.00	100.00	100.00	100.00	100.00	100.00
Fe^{2+}+Mg	4.62	4.56	4.57	4.56	4.63	4.75	4.91	4.73	4.71	4.80	4.79	4.82	4.77	4.73
Clinocloro%	45.09	44.24	43.79	44.04	61.33	64.82	56.20	56.14	61.15	74.44	74.28	74.55	75.15	74.87
Chamosita%	54.91	55.76	56.21	55.96	38.67	35.18	43.80	43.86	38.85	25.56	25.72	25.45	24.85	25.13
Fórmulas estructurales basadas en 14 oxígenos														
Si	2.63	2.69	2.68	2.73	2.79	2.78	2.79	2.79	2.69	2.69	2.70	2.73	2.69	2.69
Ti	0.00	0.00	0.00	0.00	0.01	0.01	0.00	0.00	0.00	0.00	0.00	0.00	0.00	0.00
Al_{tot}	2.74	2.70	2.70	2.66	2.51	2.44	2.34	2.46	2.60	2.54	2.54	2.48	2.56	2.59
Cr	0.00	0.00	0.00	0.00	0.00	0.00	0.00	0.00	0.00	0.00	0.00	0.00	0.00	0.00
Fe^{+2}_{tot}	2.54	2.54	2.57	2.55	1.79	1.67	2.15	2.07	1.83	1.23	1.23	1.23	1.19	1.19
Mn	0.00	0.00	0.00	0.00	0.00	0.00	0.00	0.00	0.00	0.00	0.00	0.00	0.00	0.00
Mg	2.08	2.02	2.00	2.01	2.84	3.08	2.76	2.66	2.88	3.57	3.56	3.59	3.59	3.54
Ca	0.00	0.00	0.00	0.00	0.00	0.00	0.00	0.00	0.00	0.00	0.00	0.00	0.00	0.00
Na	0.00	0.01	0.01	0.00	0.00	0.00	0.00	0.00	0.00	0.00	0.00	0.00	0.01	0.00
K	0.00	0.00	0.00	0.00	0.00	0.00	0.00	0.00	0.00	0.00	0.00	0.00	0.00	0.00
Cat. tot.	**10.00**	**9.96**	**9.97**	**9.95**	**9.94**	**9.99**	**10.04**	**9.98**	**10.00**	**10.04**	**10.03**	**10.03**	**10.03**	**10.02**
Al^{IV}	1.37	1.31	1.32	1.27	1.21	1.22	1.21	1.21	1.31	1.31	1.30	1.27	1.31	1.31
Al^{VI}	1.37	1.39	1.38	1.38	1.31	1.22	1.13	1.25	1.29	1.24	1.24	1.21	1.25	1.28
Mg#	45.09	44.24	43.79	44.04	61.33	64.82	56.20	56.14	61.15	74.44	74.28	74.55	75.15	74.87

*SP: Suite Piaxtla

Tabla A5. Análisis de microsonda y fórmulas estructurales de cloritas, basadas en 14 oxígenos (*continuación*).

Litología	**Metabasita-2 (SP*)**				**Esquisto de mica (SP)**						**Samita de bajo grado**				
Fase	**G31-c1.1**	**G31-c1.2**	**G31-c2.1**	**G31-c2.2**	**G12-c1.1**	**G12-c1.2**	**G12-c1.3**	**G12-c2.1**	**G12-c3.1**	**G12-c3.2**	**G02-c1.1**	**G02-c1.2**	**G02-c3.1**	**G02-c3.2**	**G02-c3.3**
SiO_2 (wt.%)	29.25	27.37	27.86	27.15	24.08	23.94	23.62	22.30	24.87	23.87	25.81	27.36	24.61	23.64	24.17
TiO_2	0.01	0.03	0.02	0.01	0.02	0.05	0.07	0.01	0.03	0.04	0.08	0.02	0.05	0.02	0.02
Al_2O_3	22.07	21.71	20.88	21.42	21.33	20.38	22.13	23.33	22.49	22.73	23.40	23.54	21.81	22.60	22.98
Cr_2O_3	0.00	0.00	0.00	0.00	0.00	0.00	0.00	0.00	0.00	0.00	0.00	0.00	0.00	0.00	0.00
FeO	10.42	10.48	9.16	9.49	29.25	27.71	28.90	31.34	29.60	27.65	28.94	28.45	28.94	29.59	30.15
MnO	0.00	0.00	0.00	0.00	0.00	0.00	0.00	0.00	0.00	0.00	0.00	0.00	0.00	0.00	0.00
MgO	27.42	27.34	27.52	28.48	11.37	13.26	11.64	9.36	10.89	13.09	10.05	8.65	10.29	9.85	9.96
CaO	0.01	0.01	0.01	0.00	0.03	0.02	0.04	0.05	0.02	0.00	0.00	0.00	0.04	0.04	0.03
Na_2O	0.00	0.02	0.01	0.01	0.06	0.07	0.04	0.05	0.08	0.03	0.05	0.44	0.03	0.05	0.00
K_2O	0.00	0.00	0.00	0.01	0.05	0.02	0.01	0.02	0.05	0.00	0.40	0.59	0.41	0.21	0.17
Total óx.%	**89.17**	**86.95**	**85.45**	**86.56**	**86.21**	**85.44**	**86.46**	**86.44**	**88.02**	**87.42**	**88.72**	**89.05**	**86.18**	**85.99**	**87.49**
Volátiles	10.83	13.05	14.55	13.44	13.79	14.56	13.54	13.56	11.98	12.58	11.28	10.95	13.82	14.01	12.51
Total	100.00	100.00	100.00	100.00	100.00	100.00	100.00	100.00	100.00	100.00	100.00	100.00	100.00	100.00	100.00
Fe^{2+}+Mg	4.72	4.86	4.82	4.95	4.55	4.73	4.54	4.46	4.39	4.57	4.14	3.84	4.33	4.35	4.34
Clinocloro%	82.44	82.31	84.26	84.26	40.94	46.04	41.80	34.75	39.61	45.77	38.24	35.15	38.81	37.24	37.06
Chamosita%	17.56	17.69	15.74	15.74	59.06	53.96	58.20	65.25	60.39	54.23	61.76	64.85	61.19	62.76	62.94
Fórmulas estructurales basadas en 14 oxígenos															
Si	2.78	2.69	2.76	2.67	2.65	2.64	2.58	2.48	2.66	2.56	2.72	2.86	2.70	2.61	2.62
Ti	0.00	0.00	0.00	0.00	0.00	0.00	0.01	0.00	0.00	0.00	0.01	0.00	0.00	0.00	0.00
Al_{tot}	2.48	2.51	2.44	2.48	2.76	2.65	2.85	3.05	2.84	2.87	2.91	2.90	2.82	2.94	2.93
Cr	0.00	0.00	0.00	0.00	0.00	0.00	0.00	0.00	0.00	0.00	0.00	0.00	0.00	0.00	0.00
$Fe^{+2}{}_{tot}$	0.83	0.86	0.76	0.78	2.69	2.55	2.64	2.91	2.65	2.48	2.56	2.49	2.65	2.73	2.73
Mn	0.00	0.00	0.00	0.00	0.00	0.00	0.00	0.00	0.00	0.00	0.00	0.00	0.00	0.00	0.00
Mg	3.89	4.00	4.06	4.17	1.86	2.18	1.90	1.55	1.74	2.09	1.58	1.35	1.68	1.62	1.61
Ca	0.00	0.00	0.00	0.00	0.00	0.00	0.00	0.01	0.00	0.00	0.00	0.00	0.01	0.00	0.00
Na	0.00	0.00	0.00	0.00	0.01	0.01	0.01	0.01	0.02	0.01	0.01	0.09	0.01	0.01	0.00
K	0.00	0.00	0.00	0.00	0.01	0.00	0.00	0.00	0.01	0.00	0.05	0.08	0.06	0.03	0.02
Cat. tot.	**9.98**	**10.06**	**10.02**	**10.10**	**9.98**	**10.04**	**9.99**	**10.00**	**9.92**	**10.01**	**9.84**	**9.77**	**9.92**	**9.94**	**9.92**
Al^{IV}	1.22	1.31	1.24	1.33	1.35	1.36	1.42	1.52	1.34	1.44	1.28	1.14	1.30	1.39	1.38
Al^{VI}	1.26	1.20	1.20	1.14	1.41	1.29	1.43	1.53	1.50	1.43	1.64	1.76	1.51	1.55	1.55
Mg#	82.44	82.31	84.26	84.26	40.94	46.04	41.80	34.75	39.61	45.77	38.24	35.15	38.81	37.24	37.06

*SP: Suite Piaxtla

Tabla A6. Análisis de microsonda y fórmulas estructurales de feldespatos (8 ox.)

Litología	**Granitoide (SP*)**		**Metabasita-1 (SP)**		**Samita bajo grado**
Fase	**G24-c1.1**	**G24-c1.2**	**G27-c2.1**	**G25-c1.1**	**G02-c1.1**
SiO_2 (wt. %)	69.10	68.82	69.17	68.62	68.36
TiO_2	0.01	0.00	0.00	0.00	0.00
Al_2O_3	19.79	19.73	20.15	20.04	19.65
FeO	0.01	0.00	0.01	0.01	0.08
MgO	0.01	0.00	0.00	0.01	0.00
BaO	0.00	0.00	0.01	0.00	0.00
CaO	0.09	0.07	0.27	0.28	0.02
Na_2O	11.92	11.95	12.02	11.68	11.60
K_2O	0.03	0.02	0.05	0.06	0.03
Total óxidos%	**99.99**	**99.99**	**99.99**	**99.99**	**99.99**
Or%	0.14	0.10	0.25	0.31	0.17
Ab%	99.42	99.57	98.55	98.37	99.73
An%	0.43	0.33	1.20	1.32	0.10
Fórmulas estructurales basadas en 8 oxígenos					
Si	2.99	2.99	2.97	2.98	2.99
Ti	0.00	0.00	0.00	0.00	0.00
Al	1.01	1.01	1.02	1.02	1.01
Fe	0.00	0.00	0.00	0.00	0.00
Mg	0.00	0.00	0.00	0.00	0.00
Ba	0.00	0.00	0.02	0.00	0.00
Ca	0.00	0.00	0.01	0.01	0.00
Na	1.00	1.01	1.00	0.98	0.98
K	0.00	0.00	0.00	0.00	0.00
Cationes tot.	**5.01**	**5.01**	**5.02**	**5.00**	**4.99**

*SP: Suite Piaxtla

Tabla A7. Análisis de microsonda y fórmulas estructurales de titanitas, basadas en 20 oxígenos.

Litología	**Metabasita-2 (SP*)**			**Metabasita-1 (SP)**							
Fase	**G31-c1.1**	**G31-c2.1**	**G31-c2.2**	**G27-c1.1**	**G27-c1.2**	**G25-c1.1**	**G25-c1.2**	**G25-c1.1**	**G25-c1.2**	**G25-c2.1**	**G25-c2.2**
SiO_2 (wt. %)	30.73	30.78	30.72	30.55	30.50	30.58	30.25	0.66	0.11	30.65	30.68
TiO_2	36.68	36.79	36.68	37.51	37.22	37.36	36.83	93.19	93.54	36.45	36.44
Al_2O_3 IV	1.30	1.32	1.34	0.91	1.05	1.33	1.35	4.15	4.25	1.28	1.29
Al_2O_3 VI	0.00	0.00	0.00	0.00	0.00	0.00	0.00	0.00	0.00	0.00	0.00
FeO	0.22	0.18	0.27	0.31	0.34	0.19	0.19	0.10	0.09	0.15	0.24
MnO	0.04	0.05	0.05	0.03	0.03	0.03	0.04	0.00	0.00	0.01	0.03
MgO	0.01	0.01	0.00	0.01	0.00	0.02	0.00	0.03	0.00	0.00	0.02
CaO	28.96	29.16	28.70	29.14	28.83	28.99	29.35	2.06	1.57	29.31	29.20
Na_2O	0.00	0.00	0.00	0.00	0.00	0.00	0.00	0.00	0.00	0.00	0.00
K_2O	0.00	0.00	0.00	0.00	0.00	0.00	0.00	0.00	0.00	0.00	0.00
Total óxidos%	**97.94**	**98.30**	**97.76**	**98.45**	**97.98**	**98.50**	**98.00**	**100.18**	**99.56**	**97.85**	**97.89**
Fórmulas estructurales basadas en 20 oxígenos											
Si	1.02	1.02	1.02	1.01	1.02	1.01	1.01	0.02	0.00	1.02	1.02
Ti	0.92	0.92	0.92	0.94	0.93	0.93	0.92	2.32	2.34	0.91	0.91
Al IV	-0.02	-0.02	-0.02	-0.01	-0.02	-0.01	-0.01	0.98	1.00	-0.02	-0.02
Al VI	0.07	0.07	0.08	0.05	0.06	0.06	0.06	-0.82	-0.83	0.07	0.07
Fe	0.01	0.00	0.01	0.01	0.01	0.01	0.01	0.00	0.00	0.00	0.01
Mn	0.00	0.00	0.00	0.00	0.00	0.00	0.00	0.00	0.00	0.00	0.00
Mg	0.00	0.00	0.00	0.00	0.00	0.00	0.00	0.01	0.00	0.00	0.00
Ca	1.03	1.04	1.03	1.04	1.03	1.03	1.05	0.07	0.06	1.05	1.04
Na	0.00	0.00	0.00	0.00	0.00	0.00	0.00	0.00	0.00	0.00	0.00
K	0.00	0.00	0.00	0.00	0.00	0.00	0.00	0.00	0.00	0.00	0.00
H_2O	0.00	0.00	0.00	0.00	0.00	0.00	0.00	0.00	0.00	0.00	0.00
Cationes tot.	**3.04**	**3.04**	**3.03**	**3.03**	**3.03**	**3.03**	**3.04**	**2.58**	**2.57**	**3.04**	**3.04**

*SP: Suite Piaxtla

Tabla A8. Análisis U-Pb mediante LA-ICPMS a rocas del Complejo Acatlán, sur de México. Se analizó una samita de bajo grado (G-02), además de un granitoide (G-24) y esquisto de mica (G-36) de alta presión (Suite Piaxtla). Las edades concordantes son destacadas en negrita. Los errores se presentan como 1-sigma.

#	PROPORCIONES CORREGIDAS									EDADES CORREGIDAS (Ma)										
	$^{207}Pb/^{206}Pb$	±1σ	$^{207}Pb/^{235}U$	±1s	$^{206}Pb/^{238}U$	±1σ	$^{208}Pb/^{232}Th$	±1σ	Rho	$^{206}Pb/^{238}U$	±1σ	$^{207}Pb/^{235}U$	±1σ	$^{207}Pb/^{206}Pb$	±1σ	$^{208}Pb/^{232}Th$	±1σ	Best age (Ma)	±1σ	% disc
G-02 - Samita de bajo grado																				
Z59_077	0.0543	0.0008	0.3990	0.0059	0.0533	0.0003	0.0161	0.0002	0.34	334	2	341	4	385	31	322	4	334	2	2.1
ZZ2_037	0.06216	0.00081	0.51253	0.00764	0.05979	0.00044	0.02177	0.00054	0.49	374	3	420	5	680	28	435	11	374	3	11.0
Z45_060	0.0568	0.0005	0.5672	0.0067	0.0723	0.0005	0.0218	0.0003	0.62	450	3	456	4	483	20	435	6	450	3	1.3
ZZ2_002	0.05794	0.00064	0.6115	0.00752	0.07648	0.00042	0.02323	0.0003	0.44	475	3	485	5	528	23	464	6	475	3	2.1
ZZ2_014	0.05951	0.00095	0.63206	0.01106	0.07701	0.00055	0.02285	0.00032	0.41	478	3	497	7	586	33	457	6	478	3	3.8
Z13_022	0.0585	0.0012	0.6233	0.0145	0.0774	0.0008	0.0235	0.0003	0.42	480	5	492	9	548	43	470	7	480	5	2.4
ZZ2_016	0.05806	0.00081	0.62724	0.00999	0.07826	0.00059	0.02422	0.00039	0.48	486	4	494	6	532	29	484	8	486	4	1.6
Z66_086	0.0591	0.0010	0.6452	0.0116	0.0791	0.0005	0.0236	0.0003	0.34	491	3	505	7	569	36	472	6	491	3	2.8
Z49_065	0.0573	0.0008	0.6353	0.0088	0.0803	0.0004	0.0240	0.0003	0.34	498	2	499	5	504	27	479	7	**498**	**2**	0.2
ZZ2_035	0.0641	0.00082	0.72713	0.01067	0.08227	0.00052	0.02521	0.00018	0.45	510	3	555	6	745	27	503	4	510	3	8.1
Z32_045	0.0585	0.0009	0.6672	0.0108	0.0827	0.0005	0.0251	0.0003	0.38	512	3	519	7	550	33	501	6	512	3	1.3
Z38_052	0.0597	0.0009	0.6896	0.0124	0.0837	0.0008	0.0254	0.0004	0.56	518	5	533	7	591	32	507	7	518	5	2.8
Z76_098	0.0562	0.0007	0.6499	0.0092	0.0837	0.0005	0.0258	0.0003	0.41	518	3	508	6	462	28	514	6	518	3	-2.0
Z82_105	0.0575	0.0013	0.6633	0.0152	0.0836	0.0005	0.0252	0.0004	0.27	518	3	517	9	512	45	503	7	**518**	**3**	-0.2
Z72_093	0.0599	0.0008	0.6920	0.0097	0.0838	0.0004	0.0252	0.0003	0.37	519	3	534	6	598	27	503	6	519	3	2.8
Z67_087	0.0573	0.0008	0.6628	0.0100	0.0839	0.0005	0.0256	0.0003	0.37	520	3	516	6	503	30	510	7	**520**	**3**	-0.8
ZZ2_039	0.06057	0.00103	0.70123	0.013	0.08396	0.00062	0.02497	0.00035	0.4	520	4	540	8	624	36	499	7	520	4	3.7
Z73_094	0.0578	0.0009	0.6771	0.0115	0.0848	0.0005	0.0251	0.0004	0.32	525	3	525	7	523	34	500	7	**525**	**3**	0.0
ZZ2_028	0.06137	0.00147	0.72144	0.01804	0.08496	0.00059	0.02703	0.00081	0.29	526	4	552	11	652	51	539	16	526	4	4.7
ZZ2_019	0.06612	0.00119	0.78321	0.01566	0.08556	0.00074	0.02692	0.00048	0.44	529	4	587	9	810	36	537	9	529	4	9.9
ZZ2_020	0.06612	0.00119	0.78321	0.01566	0.08556	0.00074	0.02692	0.00048	0.44	529	4	587	9	810	37	537	9	529	4	9.9
Z11_020	0.0595	0.0008	0.7026	0.0097	0.0857	0.0004	0.0258	0.0003	0.34	530	2	540	6	584	26	515	6	530	2	1.9
Z25_036	0.0604	0.0009	0.7137	0.0115	0.0857	0.0005	0.0257	0.0003	0.34	530	3	547	7	617	33	513	7	530	3	3.1
ZZ2_034	0.05883	0.00065	0.69535	0.00926	0.08564	0.00064	0.02746	0.00038	0.56	530	4	536	6	561	24	548	7	530	4	1.1
Z91_116	0.0600	0.0008	0.7109	0.0098	0.0858	0.0004	0.0257	0.0003	0.33	531	2	545	6	602	28	513	6	531	2	2.6
Z47_063	0.0584	0.0011	0.6948	0.0138	0.0863	0.0005	0.0254	0.0003	0.29	533	3	536	8	543	41	508	6	**533**	**3**	0.6
Z84_107	0.0568	0.0008	0.6777	0.0101	0.0864	0.0005	0.0255	0.0003	0.36	534	3	525	6	483	28	508	6	534	3	-1.7
ZZ2_005	0.05979	0.00056	0.71447	0.00905	0.08656	0.00074	0.02774	0.00111	0.67	535	4	547	5	596	19	553	22	535	4	2.2
Z86_110	0.0588	0.0008	0.7109	0.0101	0.0876	0.0005	0.0267	0.0010	0.41	541	3	545	6	559	26	532	19	**541**	**3**	0.7
Z01_008	0.0595	0.0007	0.7207	0.0087	0.0877	0.0004	0.0278	0.0004	0.41	542	2	551	5	584	25	553	7	542	2	1.6
Z93_118	0.0595	0.0008	0.7234	0.0100	0.0880	0.0004	0.0264	0.0003	0.36	544	2	553	6	586	27	526	7	544	2	1.6
Z40_054	0.0592	0.0009	0.7304	0.0118	0.0893	0.0005	0.0263	0.0003	0.37	551	3	557	7	574	32	524	6	**551**	**3**	1.1
Z18_028	0.0587	0.0009	0.7248	0.0115	0.0896	0.0005	0.0269	0.0004	0.33	553	3	553	7	556	30	536	8	**553**	**3**	0.0
Z87_111	0.0603	0.0009	0.7445	0.0119	0.0898	0.0005	0.0270	0.0004	0.35	554	3	565	7	613	30	538	7	554	3	1.9
ZZ2_031	0.06017	0.00072	0.74823	0.01011	0.09005	0.00056	0.02637	0.00034	0.46	556	3	567	6	610	26	526	7	556	3	1.9
Z96_122	0.0595	0.0008	0.7419	0.0102	0.0904	0.0004	0.0265	0.0003	0.33	558	2	563	6	585	28	528	6	**558**	**2**	0.9
Z100_126	0.0597	0.0011	0.7465	0.0139	0.0906	0.0005	0.0267	0.0004	0.25	559	3	566	8	594	39	533	7	**559**	**3**	1.2

#	PROPORCIONES CORREGIDAS									EDADES CORREGIDAS (Ma)										
	$^{207}Pb/^{206}Pb$	±1σ	$^{207}Pb/^{235}U$	±1s	$^{206}Pb/^{238}U$	±1σ	$^{208}Pb/^{232}Th$	±1σ	Rho	$^{206}Pb/^{238}U$	±1σ	$^{207}Pb/^{235}U$	±1σ	$^{207}Pb/^{206}Pb$	±1σ	$^{208}Pb/^{232}Th$	±1σ	Best age (Ma)	±1σ	% disc
G-02 - Samita de bajo grado (*continuación*)																				
Z92_117	0.0592	0.0011	0.7480	0.0141	0.0915	0.0005	0.0272	0.0004	0.27	565	3	567	8	574	39	542	8	**565**	**3**	0.4
Z53_070	0.0595	0.0009	0.7586	0.0120	0.0926	0.0005	0.0272	0.0003	0.32	571	3	573	7	586	30	542	6	**571**	**3**	0.3
Z21_032	0.0596	0.0007	0.7633	0.0092	0.0928	0.0005	0.0276	0.0003	0.38	572	3	576	5	588	22	550	6	**572**	**3**	0.7
Z64_083	0.0612	0.0012	0.7862	0.0163	0.0930	0.0005	0.0270	0.0003	0.28	573	3	589	9	646	42	538	5	573	3	2.7
ZZ2_021	0.065	0.00078	0.83701	0.01363	0.09302	0.00102	0.03135	0.00213	0.68	573	6	617	8	774	25	624	42	573	6	7.1
Z29_041	0.0577	0.0010	0.7469	0.0132	0.0936	0.0005	0.0276	0.0003	0.28	577	3	566	8	519	37	551	6	577	3	-1.9
Z81_104	0.0571	0.0016	0.7383	0.0215	0.0937	0.0008	0.0279	0.0003	0.28	577	5	561	13	494	57	556	6	577	5	-2.9
Z27_039	0.0596	0.0009	0.7733	0.0123	0.0940	0.0005	0.0283	0.0004	0.34	579	3	582	7	588	33	564	8	**579**	**3**	0.5
Z74_095	0.0608	0.0009	0.7912	0.0126	0.0943	0.0007	0.0283	0.0004	0.48	581	4	592	7	632	29	565	7	581	4	1.9
Z44_059	0.0644	0.0009	0.8421	0.0125	0.0948	0.0005	0.0276	0.0003	0.33	584	3	620	7	755	29	550	6	584	3	5.8
Z34_047	0.0607	0.0011	0.7986	0.0153	0.0953	0.0006	0.0292	0.0005	0.36	587	4	596	9	629	38	583	9	**587**	**4**	1.5
Z51_068	0.0602	0.0006	0.7908	0.0088	0.0953	0.0005	0.0292	0.0004	0.45	587	3	592	5	609	20	582	7	**587**	**3**	0.8
Z54_071	0.0599	0.0007	0.7945	0.0104	0.0960	0.0005	0.0281	0.0003	0.4	591	3	594	6	599	24	560	6	**591**	**3**	0.5
Z71_092	0.0606	0.0007	0.8045	0.0106	0.0960	0.0005	0.0298	0.0004	0.4	591	3	599	6	627	25	594	8	591	3	1.3
Z50_066	0.0614	0.0010	0.8184	0.0146	0.0967	0.0005	0.0282	0.0003	0.32	595	3	607	8	654	34	563	6	595	3	2.0
ZZ2_001	0.06985	0.0044	0.93375	0.06576	0.09695	0.00103	0.02943	0.00024	0.22	597	6	670	35	924	125	586	5	597	6	10.9
Z75_096	0.0596	0.0010	0.7990	0.0141	0.0972	0.0005	0.0282	0.0003	0.29	598	3	596	8	588	36	563	6	**598**	**3**	-0.3
Z06_014	0.0605	0.0007	0.8214	0.0107	0.0983	0.0005	0.0291	0.0004	0.39	605	3	609	6	623	24	580	7	**605**	**3**	0.7
ZZ2_006	0.06453	0.00153	0.88001	0.02413	0.09891	0.00071	0.03029	0.0002	0.38	608	4	641	13	759	48	603	4	608	4	5.1
ZZ2_004	0.06481	0.00093	0.88622	0.01628	0.09918	0.00081	0.03036	0.00024	0.54	610	5	644	9	768	29	604	5	610	5	5.3
Z56_074	0.0605	0.0009	0.8340	0.0135	0.0999	0.0006	0.0298	0.0004	0.36	614	4	616	7	622	30	594	8	**614**	**4**	0.3
Z69_089	0.0610	0.0006	0.8453	0.0090	0.1002	0.0005	0.0307	0.0003	0.43	616	3	622	5	640	20	610	7	616	3	1.0
Z78_100	0.0607	0.0007	0.8467	0.0109	0.1009	0.0005	0.0299	0.0004	0.35	620	3	623	6	629	24	595	8	**620**	**3**	0.5
Z43_058	0.0619	0.0011	0.8634	0.0157	0.1011	0.0007	0.0311	0.0004	0.36	621	4	632	9	670	36	619	8	621	4	1.7
Z23_034	0.0609	0.0008	0.8586	0.0121	0.1020	0.0006	0.0293	0.0003	0.39	626	3	629	7	636	26	583	6	**626**	**3**	0.5
Z31_044	0.0606	0.0006	0.8606	0.0090	0.1028	0.0004	0.0307	0.0003	0.41	631	3	630	5	626	21	611	7	**631**	**3**	-0.2
Z83_106	0.0650	0.0010	0.9201	0.0161	0.1030	0.0007	0.0334	0.0006	0.41	632	4	662	9	773	31	665	13	632	4	4.5
Z94_119	0.0616	0.0008	0.8783	0.0122	0.1033	0.0005	0.0304	0.0003	0.36	633	3	640	7	660	27	605	6	**633**	**3**	1.1
Z90_114	0.0632	0.0011	0.9082	0.0171	0.1041	0.0006	0.0307	0.0004	0.29	639	3	656	9	714	38	611	8	639	3	2.6
Z62_081	0.0659	0.0007	0.9498	0.0108	0.1044	0.0006	0.0369	0.0004	0.47	640	3	678	6	804	21	733	9	640	3	5.6
ZZ2_024	0.06144	0.00074	0.88875	0.01192	0.10481	0.00063	0.03359	0.0004	0.44	643	4	646	6	655	26	668	8	**643**	**4**	0.5
Z16_026	0.0611	0.0010	0.8875	0.0183	0.1050	0.0014	0.0310	0.0005	0.63	644	8	645	10	644	32	617	9	**644**	**8**	0.2
Z98_124	0.0610	0.0007	0.8939	0.0140	0.1061	0.0011	0.0308	0.0004	0.64	650	6	648	7	641	25	614	8	**650**	**6**	-0.3
Z63_082	0.0614	0.0009	0.9066	0.0145	0.1070	0.0008	0.0341	0.0006	0.49	655	5	655	8	654	30	678	11	**655**	**5**	0.0
Z35_048	0.0609	0.0008	0.9275	0.0134	0.1102	0.0007	0.0321	0.0004	0.44	674	4	666	7	637	27	639	7	674	4	-1.2
ZZ2_029	0.06364	0.0007	0.98018	0.01283	0.11156	0.00079	0.03814	0.00053	0.54	682	5	694	7	730	23	757	10	682	5	1.7
Z02_009	0.0650	0.0018	1.0139	0.0309	0.1129	0.0014	0.0392	0.0011	0.39	690	8	711	16	775	62	777	21	690	8	3.0
Z22_033	0.0657	0.0014	1.0388	0.0249	0.1146	0.0008	0.0350	0.0002	0.38	700	5	723	12	798	41	696	5	700	5	3.2
Z26_038	0.0650	0.0009	1.0285	0.0159	0.1147	0.0008	0.0336	0.0005	0.42	700	4	718	8	774	30	667	9	700	4	2.5

#	PROPORCIONES CORREGIDAS									EDADES CORREGIDAS (Ma)										
	$^{207}Pb/^{206}Pb$	±1σ	$^{207}Pb/^{235}U$	±1s	$^{206}Pb/^{238}U$	±1σ	$^{208}Pb/^{232}Th$	±1σ	Rho	$^{206}Pb/^{238}U$	±1σ	$^{207}Pb/^{235}U$	±1σ	$^{207}Pb/^{206}Pb$	±1σ	$^{208}Pb/^{232}Th$	±1σ	Best age (Ma)	±1σ	% disc
G-02 - Samita de bajo grado (*continuación*)																				
Z85_108	0.0690	0.0013	1.0986	0.0227	0.1155	0.0009	0.0347	0.0005	0.39	704	5	753	11	898	36	690	10	704	5	6.5
Z10_018	0.0636	0.0006	1.0368	0.0116	0.1181	0.0007	0.0348	0.0004	0.49	719	4	722	6	729	19	691	7	**719**	**4**	0.4
Z61_080	0.0636	0.0009	1.0382	0.0186	0.1184	0.0007	0.0363	0.0002	0.57	721	4	723	9	729	30	721	4	**721**	**4**	0.3
ZZ2_027	0.06695	0.001	1.0998	0.01781	0.11889	0.00073	0.03674	0.00051	0.39	724	4	753	9	836	31	729	10	724	4	3.9
ZZ2_025	0.06255	0.00075	1.0515	0.01528	0.12168	0.001	0.03211	0.00048	0.56	740	6	730	8	693	25	639	9	740	6	-1.4
ZZ2_012	0.0646	0.00065	1.0953	0.01272	0.12283	0.00072	0.03592	0.0005	0.5	747	4	751	6	761	20	713	10	**747**	**4**	0.5
Z88_112	0.0643	0.0015	1.1018	0.0274	0.1240	0.0008	0.0368	0.0005	0.27	754	5	754	13	753	50	730	9	**754**	**5**	0.0
Z36_050	0.0688	0.0015	1.2294	0.0342	0.1303	0.0022	0.0396	0.0009	0.61	790	13	814	16	891	44	785	18	790	13	2.9
Z04_011	0.0658	0.0011	1.2123	0.0209	0.1335	0.0008	0.0379	0.0005	0.37	808	5	806	10	801	35	753	9	**808**	**5**	-0.2
ZZ2_009	0.07301	0.00139	1.3413	0.02945	0.13406	0.00147	0.0388	0.00054	0.5	811	8	864	13	1014	37	769	11	811	8	6.1
Z58_076	0.0656	0.0006	1.2328	0.0140	0.1351	0.0008	0.0427	0.0006	0.51	817	5	816	6	793	19	846	12	**817**	**5**	-0.1
ZZ2_022	0.06883	0.00067	1.2856	0.01773	0.13529	0.00131	0.04749	0.00066	0.71	818	7	839	8	894	20	938	13	818	7	2.5
ZZ2_018	0.07268	0.00094	1.3828	0.02048	0.13789	0.00098	0.05003	0.0007	0.49	833	6	882	9	1005	25	987	13	833	6	5.6
Z57_075	0.0694	0.0007	1.3319	0.0146	0.1390	0.0006	0.0422	0.0005	0.42	839	3	860	6	912	19	834	10	839	3	2.4
Z09_017	0.0705	0.0011	1.3641	0.0245	0.1402	0.0011	0.0406	0.0007	0.45	846	6	874	11	942	31	805	13	846	6	3.2
Z68_088	0.0666	0.0010	1.3104	0.0213	0.1425	0.0009	0.0421	0.0005	0.39	859	5	850	9	827	30	833	10	**859**	**5**	-1.1
Z17_027	0.0690	0.0009	1.3879	0.0197	0.1457	0.0008	0.0423	0.0006	0.39	877	5	884	8	898	25	837	11	**877**	**5**	0.8
ZZ2_038	0.07013	0.00113	1.41185	0.0268	0.14601	0.00096	0.0443	0.00029	0.46	879	5	894	11	932	33	876	6	879	5	1.7
Z08_016	0.0693	0.0010	1.4154	0.0223	0.1478	0.0007	0.0430	0.0006	0.3	889	4	895	9	909	29	850	11	**889**	**4**	0.7
ZZ2_003	0.07348	0.00073	1.6119	0.01863	0.15887	0.00092	0.04733	0.00062	0.51	950	5	975	7	1027	19	935	12	950	5	2.6
ZZ2_033	0.07331	0.00081	1.6554	0.02132	0.16342	0.00109	0.04997	0.00065	0.51	976	6	992	8	1023	22	986	13	976	6	1.6
Z20_030	0.0729	0.0010	1.7471	0.0263	0.1737	0.0010	0.0525	0.0009	0.37	1033	5	1026	10	1012	26	1033	18	**1012**	**26**	-0.7
Z60_078	0.0730	0.0010	1.7889	0.0273	0.1776	0.0011	0.0524	0.0007	0.4	1054	6	1041	10	1014	28	1032	13	1014	28	-1.2
Z41_056	0.0732	0.0007	1.7241	0.0187	0.1706	0.0008	0.0490	0.0005	0.44	1015	5	1018	7	1020	19	967	10	**1020**	**19**	0.3
Z89_113	0.0739	0.0010	1.8187	0.0274	0.1782	0.0010	0.0527	0.0008	0.36	1057	5	1052	10	1040	28	1037	15	**1040**	**28**	-0.5
ZZ2_032	0.07412	0.0007	1.7988	0.01959	0.1757	0.00097	0.05114	0.00061	0.5	1043	5	1045	7	1045	19	1008	12	**1045**	**19**	0.2
Z65_084	0.0749	0.0008	1.8619	0.0209	0.1801	0.0009	0.0526	0.0006	0.45	1068	5	1068	7	1065	20	1036	12	**1065**	**20**	0.0
ZZ2_036	0.07501	0.00065	1.782	0.02631	0.17196	0.00206	0.05581	0.00084	0.81	1023	11	1039	10	1069	17	1098	16	1069	17	4.3
ZZ2_030	0.07566	0.00076	1.8179	0.0223	0.17403	0.00124	0.05221	0.00068	0.57	1034	7	1052	8	1086	20	1029	13	1086	20	4.8
Z52_069	0.0761	0.0009	1.9789	0.0284	0.1885	0.0015	0.0548	0.0007	0.55	1113	8	1108	10	1098	22	1079	13	**1098**	**22**	-0.5
Z19_029	0.0761	0.0008	1.8816	0.0230	0.1793	0.0010	0.0548	0.0006	0.43	1063	5	1075	8	1099	21	1078	11	1099	21	1.1
ZZ2_010	0.07621	0.00099	1.8421	0.02637	0.17507	0.00105	0.05127	0.00072	0.42	1040	6	1061	9	1101	25	1011	14	1101	25	5.5
Z03_010	0.0766	0.0008	1.9285	0.0231	0.1824	0.0009	0.0522	0.0005	0.4	1080	5	1091	8	1110	23	1029	10	1110	23	1.0
ZZ2_011	0.07815	0.00133	1.8848	0.03525	0.17497	0.00136	0.05373	0.00091	0.41	1039	7	1076	12	1151	32	1058	17	1151	32	9.7
Z15_024	0.0795	0.0011	2.3015	0.0346	0.2097	0.0012	0.0593	0.0007	0.37	1227	6	1213	11	1185	26	1165	12	1185	26	-1.2
ZZ2_015	0.08034	0.00106	2.16284	0.03592	0.19525	0.00136	0.05836	0.00042	0.54	1150	7	1169	12	1205	25	1146	8	1205	25	1.6
Z14_023	0.0813	0.0011	2.3524	0.0327	0.2096	0.0010	0.0598	0.0007	0.34	1227	5	1228	10	1228	24	1175	13	**1228**	**24**	0.1
Z07_015	0.0969	0.0016	3.6344	0.0676	0.2720	0.0026	0.0765	0.0009	0.51	1551	13	1557	15	1566	28	1490	17	**1566**	**28**	0.4
Z46_062	0.0987	0.0008	3.8283	0.0350	0.2809	0.0012	0.0787	0.0008	0.48	1596	6	1599	7	1599	15	1530	15	**1599**	**15**	0.2

#	PROPORCIONES CORREGIDAS									EDADES CORREGIDAS (Ma)										
	$^{207}Pb/^{206}Pb$	±1σ	$^{207}Pb/^{235}U$	±1s	$^{206}Pb/^{238}U$	±1σ	$^{208}Pb/^{232}Th$	±1σ	Rho	$^{206}Pb/^{238}U$	±1σ	$^{207}Pb/^{235}U$	±1σ	$^{207}Pb/^{206}Pb$	±1σ	$^{208}Pb/^{232}Th$	±1σ	Best age (Ma)	±1σ	% disc
G-02 - Samita de bajo grado (*continuación*)																				
Z12_021	0.1065	0.0009	4.4004	0.0429	0.2995	0.0013	0.0838	0.0008	0.44	1689	7	1712	8	1740	15	1626	16	1740	15	1.3
ZZ2_023	0.10694	0.00177	4.38945	0.09375	0.29768	0.0025	0.08633	0.00068	0.52	1680	12	1710	18	1748	30	1674	13	1748	30	3.9
Z30_042	0.1146	0.0011	5.3578	0.0582	0.3386	0.0019	0.0930	0.0010	0.51	1880	9	1878	9	1873	17	1797	19	**1873**	**17**	-0.1
Z24_035	0.1206	0.0010	5.0592	0.0476	0.3036	0.0014	0.0853	0.0009	0.49	1709	7	1829	8	1965	14	1655	16	1965	14	6.6
Z97_123	0.1735	0.0013	11.2010	0.0984	0.4672	0.0021	0.1231	0.0012	0.5	2471	9	2540	8	2591	12	2347	22	2591	12	2.7
ZZ2_017	0.17948	0.00154	12.129	0.13223	0.48852	0.00327	0.13049	0.00157	0.62	2564	14	2614	10	2648	14	2479	28	2648	14	3.2
ZZ2_008	0.18249	0.0015	10.9951	0.12083	0.43698	0.0027	0.12022	0.00074	0.57	2337	12	2523	10	2676	13	2295	13	2676	13	12.7
Z37_051	0.1920	0.0014	12.8950	0.1288	0.4864	0.0032	0.1310	0.0013	0.66	2555	14	2672	9	2760	12	2488	23	2760	12	4.4
Z48_064	0.1921	0.0016	13.5360	0.1378	0.5103	0.0029	0.1387	0.0014	0.55	2658	12	2718	10	2761	14	2626	25	2761	14	2.2
ZZ2_013	0.21228	0.00185	15.066	0.15753	0.51397	0.00298	0.13231	0.00159	0.55	2674	13	2819	10	2923	14	2512	28	2923	14	8.5
Z05_012	0.2221	0.0016	15.0920	0.1327	0.4920	0.0024	0.1332	0.0013	0.56	2579	10	2821	8	2996	12	2527	24	2996	12	8.6
Z39_053	0.2518	0.0018	21.0760	0.1842	0.6061	0.0031	0.1567	0.0016	0.58	3054	12	3142	8	3196	11	2943	27	3196	11	2.8
Z77_099	0.2691	0.0026	23.1950	0.2670	0.6236	0.0041	0.1631	0.0023	0.56	3124	16	3235	11	3301	14	3054	40	3301	14	3.4
Z55_072	0.3017	0.0023	27.9920	0.2478	0.6718	0.0032	0.1688	0.0019	0.53	3313	12	3419	9	3479	11	3153	32	3479	11	3.1
#	PROPORCIONES CORREGIDAS									CORRECTED AGESEDADES CORREGIDAS (Ma)										
	$^{207}Pb/^{206}Pb$	±1σ	$^{207}Pb/^{235}U$	±1σ	$^{206}Pb/^{238}U$	±1σ	$^{208}Pb/^{232}Th$	±1σ	Rho	$^{206}Pb/^{238}U$	±1σ	$^{207}Pb/^{235}U$	±1σ	$^{207}Pb/^{206}Pb$	±1σ	$^{208}Pb/^{232}Th$	±1σ	Best age (Ma)	±1σ	% disc
G-24 - Metagranitoide de alta presión (Suite Piaxtla)																				
Z67_32	0.0580	0.0006	0.5918	0.0081	0.0740	0.0006	0.0216	0.0003	0.59	460	4	472	5	531	23	432	6	460	4	2.5
Z77_44	0.0581	0.0009	0.6167	0.0105	0.0772	0.0005	0.0228	0.0003	0.34	479	3	488	7	534	31	456	6	479	3	1.8
Z49_11	0.0584	0.0009	0.6219	0.0110	0.0773	0.0006	0.0236	0.0003	0.43	480	3	491	7	546	33	471	6	480	3	2.2
Z57_21	0.0582	0.0009	0.6184	0.0105	0.0773	0.0004	0.0229	0.0003	0.33	480	3	489	7	535	34	458	6	480	3	1.8
Z61_26	0.0582	0.0008	0.6197	0.0087	0.0773	0.0004	0.0230	0.0003	0.36	480	2	490	5	538	27	459	6	480	2	2.0
Z79_46	0.0603	0.0014	0.6453	0.0155	0.0777	0.0005	0.0232	0.0003	0.28	482	3	506	10	613	45	463	6	482	3	4.7
Z54_17	0.0571	0.0011	0.6159	0.0125	0.0782	0.0006	0.0232	0.0003	0.36	485	3	487	8	494	40	463	6	**485**	**3**	0.4
Z58_22	0.0627	0.0014	0.6761	0.0154	0.0782	0.0005	0.0243	0.0004	0.25	485	3	524	9	697	45	485	7	485	3	7.4
Z74_40	0.0618	0.0012	0.6701	0.0134	0.0787	0.0005	0.0230	0.0003	0.32	489	3	521	8	667	36	460	6	489	3	6.1
Z71_37	0.0579	0.0012	0.6443	0.0136	0.0806	0.0006	0.0233	0.0003	0.32	500	3	505	8	528	41	466	7	**500**	**3**	1.0
Z72_38	0.0581	0.0008	0.6762	0.0094	0.0844	0.0004	0.0244	0.0003	0.35	522	3	524	6	535	27	487	5	**522**	**3**	0.4
Z42_03	0.0602	0.0007	0.8416	0.0110	0.1014	0.0005	0.0302	0.0004	0.41	623	3	620	6	612	25	602	8	**623**	**3**	-0.5
Z76_43	0.0638	0.0011	0.9641	0.0174	0.1098	0.0007	0.0311	0.0004	0.34	672	4	685	9	735	32	618	8	672	4	1.9
Z60_24	0.0709	0.0013	1.1733	0.0242	0.1204	0.0012	0.0370	0.0006	0.48	733	7	788	11	955	34	735	12	733	7	7.0
Z56_20	0.0663	0.0009	1.1675	0.0165	0.1278	0.0007	0.0373	0.0005	0.4	775	4	785	8	817	26	740	10	775	4	1.3
Z63_28	0.0732	0.0008	1.5296	0.0207	0.1515	0.0009	0.0457	0.0003	0.56	909	5	942	8	1020	20	904	5	909	5	3.5
Z69_34	0.0726	0.0010	1.7174	0.0258	0.1718	0.0009	0.0495	0.0006	0.35	1022	5	1015	10	1003	27	977	11	**1003**	**27**	-0.7
Z62_27	0.0729	0.0008	1.8079	0.0218	0.1800	0.0009	0.0512	0.0007	0.42	1067	5	1048	8	1010	21	1009	13	1010	21	-1.8
Z46_08	0.0745	0.0010	1.8623	0.0268	0.1815	0.0011	0.0535	0.0008	0.43	1075	6	1068	10	1054	25	1053	14	**1054**	**25**	-0.7
Z41_02	0.0762	0.0012	1.8461	0.0315	0.1760	0.0010	0.0516	0.0007	0.34	1045	6	1062	11	1100	31	1018	14	1100	31	1.6
Z52_15	0.0764	0.0008	1.8651	0.0213	0.1769	0.0010	0.0468	0.0009	0.49	1050	6	1069	8	1105	19	924	17	1105	19	1.8

#	PROPORCIONES CORREGIDAS									CORRECTED AGESEDADES CORREGIDAS (Ma)										
	$^{207}Pb/^{206}Pb$	±1σ	$^{207}Pb/^{235}U$	±1σ	$^{206}Pb/^{238}U$	±1σ	$^{208}Pb/^{232}Th$	±1σ	Rho	$^{206}Pb/^{238}U$	±1σ	$^{207}Pb/^{235}U$	±1σ	$^{207}Pb/^{206}Pb$	±1σ	$^{208}Pb/^{232}Th$	±1σ	Best age (Ma)	±1σ	% disc
G-24 - Metagranitoide de Suite Piaxtla (*continuación*)																				
Z43_04	0.0811	0.0011	2.3631	0.0352	0.2115	0.0011	0.0596	0.0007	0.35	1237	6	1232	11	1223	26	1171	14	**1223**	**26**	-0.4
Z73_39	0.0822	0.0008	2.3455	0.0264	0.2069	0.0011	0.0669	0.0009	0.47	1212	6	1226	8	1251	18	1309	18	1251	18	1.1
Z64_29	0.0925	0.0010	3.9263	0.0611	0.3030	0.0033	0.0890	0.0011	0.71	1706	16	1619	13	1478	19	1723	20	1478	19	-5.4
Z70_35	0.0944	0.0010	3.7886	0.0511	0.2909	0.0023	0.0786	0.0009	0.58	1646	11	1590	11	1516	19	1530	18	1516	19	-3.5
Z51_14	0.1044	0.0010	4.3884	0.0481	0.3034	0.0018	0.0871	0.0011	0.53	1708	9	1710	9	1703	16	1688	20	**1703**	**16**	0.1
Z78_45	0.1111	0.0009	4.4959	0.0415	0.2937	0.0015	0.0842	0.0009	0.54	1660	7	1730	8	1817	13	1634	17	1817	13	4.0
Z47_09	0.1112	0.0021	4.6553	0.1155	0.3035	0.0024	0.0877	0.0006	0.47	1709	12	1759	21	1820	34	1699	11	1820	34	2.8
Z68_33	0.1131	0.0011	5.3260	0.0624	0.3419	0.0023	0.0929	0.0010	0.57	1896	11	1873	10	1850	16	1796	19	1850	16	-1.2
Z50_12	0.1133	0.0013	5.3291	0.0646	0.3406	0.0017	0.0943	0.0011	0.41	1889	8	1874	10	1852	18	1821	21	1852	18	-0.8
Z53_16	0.1141	0.0010	5.5101	0.0563	0.3505	0.0018	0.0958	0.0011	0.51	1937	9	1902	9	1866	15	1849	19	1866	15	-1.8
Z45_06	0.1145	0.0010	5.2760	0.0527	0.3345	0.0018	0.0933	0.0010	0.54	1860	9	1865	9	1872	15	1804	19	**1872**	**15**	0.3
Z80_47	0.1147	0.0010	5.2619	0.0524	0.3331	0.0017	0.0899	0.0010	0.53	1853	8	1863	9	1875	14	1740	18	**1875**	**14**	0.5
Z59_23	0.1149	0.0010	5.4068	0.0599	0.3416	0.0024	0.0927	0.0010	0.64	1894	12	1886	9	1878	14	1792	19	**1878**	**14**	-0.4
Z75_41	0.1150	0.0012	5.4537	0.0605	0.3441	0.0017	0.0944	0.0010	0.43	1906	8	1893	10	1880	16	1823	19	1880	16	-0.7
Z65_30	0.1156	0.0010	5.5230	0.0587	0.3467	0.0020	0.0939	0.0011	0.54	1919	10	1904	9	1890	15	1814	21	1890	15	-0.8
Z55_18	0.1159	0.0011	5.6268	0.0627	0.3516	0.0022	0.0979	0.0012	0.56	1942	11	1920	10	1894	16	1887	22	1894	16	-1.1
Z44_05	0.1206	0.0021	4.7186	0.0901	0.2838	0.0025	0.0835	0.0013	0.46	1610	12	1771	16	1965	27	1622	23	1965	27	9.1
Z48_10	0.1325	0.0012	6.9377	0.0788	0.3790	0.0026	0.1036	0.0011	0.59	2071	12	2103	10	2131	14	1992	21	2131	14	1.5
#	PROPORCIONES CORREGIDAS									EDADES CORREGIDAS (Ma)										
	$^{207}Pb/^{206}Pb$	±1σ	$^{207}Pb/^{235}U$	±1σ	$^{206}Pb/^{238}U$	±1σ	$^{208}Pb/^{232}Th$	±1σ	Rho	$^{206}Pb/^{238}U$	±1σ	$^{207}Pb/^{235}U$	±1σ	$^{207}Pb/^{206}Pb$	±1σ	$^{208}Pb/^{232}Th$	±1σ	Best age (Ma)	±1σ	% disc
G-36 - Esquisto de mica de Suite Piaxtla																				
Z48_064	0.0613	0.0109	0.5215	0.1027	0.0617	0.0018	0.0190	0.0005	0.35	386	11	426	69	649	362	381	10	**386**	**11**	9.4
Z93_118	0.0552	0.0008	0.5293	0.0081	0.0695	0.0004	0.0226	0.0004	0.4	433	3	431	5	418	32	451	8	**433**	**3**	-0.5
Z64_083	0.0605	0.0018	0.6062	0.0198	0.0726	0.0005	0.0224	0.0001	0.29	452	3	481	12	623	60	448	3	452	3	6.0
Z71_092	0.0557	0.0007	0.5641	0.0082	0.0734	0.0005	0.0238	0.0004	0.46	457	3	454	5	440	28	475	8	**457**	**3**	-0.7
Z38_052	0.0560	0.0006	0.5691	0.0071	0.0736	0.0004	0.0206	0.0004	0.46	458	3	457	5	454	22	412	9	**458**	**3**	-0.2
Z88_112	0.0592	0.0008	0.6053	0.0085	0.0741	0.0004	0.0227	0.0003	0.37	461	2	481	5	573	29	454	7	461	2	4.2
Z30_042	0.0619	0.0007	0.6394	0.0082	0.0748	0.0003	0.0231	0.0003	0.37	465	2	502	5	671	23	461	6	465	2	7.4
ZZ2_27	0.05689	0.00063	0.58965	0.00736	0.075	0.00044	0.02268	0.00027	0.46	466	3	471	5	487	23	453	5	**466**	**3**	1.1
Z59_077	0.0562	0.0008	0.5937	0.0094	0.0765	0.0004	0.0227	0.0003	0.32	475	2	473	6	461	32	454	6	**475**	**2**	-0.4
Z44_059	0.0571	0.0007	0.6042	0.0078	0.0767	0.0004	0.0233	0.0003	0.39	477	2	480	5	494	24	466	6	**477**	**2**	0.6
Z32_045	0.0606	0.0020	0.6434	0.0244	0.0770	0.0007	0.0238	0.0002	0.33	478	4	504	15	625	66	475	4	478	4	5.2
Z05_012	0.0565	0.0007	0.6032	0.0084	0.0774	0.0004	0.0235	0.0003	0.37	480	2	479	5	472	27	469	6	**480**	**2**	-0.2
Z02_009	0.0569	0.0008	0.6147	0.0096	0.0784	0.0005	0.0242	0.0004	0.43	486	3	487	6	487	30	483	8	**486**	**3**	0.2
Z45_060	0.0565	0.0008	0.6109	0.0092	0.0784	0.0004	0.0233	0.0003	0.36	486	3	484	6	471	29	465	6	**486**	**3**	-0.4
Z29_041	0.0566	0.0009	0.6201	0.0106	0.0794	0.0005	0.0244	0.0003	0.34	493	3	490	7	475	33	487	7	**493**	**3**	-0.6
Z55_072	0.0615	0.0014	0.6730	0.0152	0.0796	0.0004	0.0245	0.0004	0.24	493	3	523	9	657	44	490	7	493	3	5.7

#	PROPORCIONES CORREGIDAS									EDADES CORREGIDAS (Ma)										
	$^{207}Pb/^{206}Pb$	±1σ	$^{207}Pb/^{235}U$	±1σ	$^{206}Pb/^{238}U$	±1σ	$^{208}Pb/^{232}Th$	±1σ	Rho	$^{206}Pb/^{238}U$	±1σ	$^{207}Pb/^{235}U$	±1σ	$^{207}Pb/^{206}Pb$	±1σ	$^{208}Pb/^{232}Th$	±1σ	Best age (Ma)	±1σ	% disc
G-36 - Esquisto de mica de Suite Piaxtla (*continuación*)																				
Z33_046	0.0568	0.0014	0.6216	0.0160	0.0796	0.0005	0.0235	0.0004	0.24	494	3	491	10	482	51	469	8	**494**	**3**	-0.6
Z27_039	0.0596	0.0011	0.6568	0.0131	0.0799	0.0005	0.0252	0.0004	0.31	495	3	513	8	588	38	503	7	495	3	3.5
Z87_111	0.0592	0.0008	0.6577	0.0093	0.0803	0.0004	0.0254	0.0003	0.39	498	3	513	6	575	28	506	7	498	3	2.9
Z75_096	0.0565	0.0005	0.6298	0.0067	0.0808	0.0004	0.0267	0.0003	0.44	501	2	496	4	472	21	532	6	501	2	-1.0
Z90_114	0.0571	0.0010	0.6370	0.0123	0.0809	0.0006	0.0231	0.0004	0.36	501	3	500	8	497	41	461	7	**501**	**3**	-0.2
Z92_117	0.0578	0.0009	0.6494	0.0104	0.0813	0.0004	0.0250	0.0003	0.33	504	3	508	6	523	34	499	6	**504**	**3**	0.8
ZZ2_11	0.0591	0.00071	0.671	0.00942	0.08184	0.0006	0.02634	0.00034	0.52	507	4	521	6	571	24	525	7	507	4	2.7
Z76_098	0.0578	0.0006	0.6892	0.0082	0.0864	0.0004	0.0261	0.0003	0.37	534	2	532	5	523	24	520	6	**534**	**2**	-0.4
Z35_048	0.0579	0.0009	0.6972	0.0111	0.0873	0.0005	0.0260	0.0003	0.34	540	3	537	7	526	30	520	7	**540**	**3**	-0.6
Z13_022	0.0588	0.0022	0.7300	0.0314	0.0901	0.0009	0.0279	0.0002	0.35	556	5	557	18	559	78	556	5	**556**	**5**	0.2
Z04_011	0.0623	0.0010	0.7871	0.0189	0.0916	0.0012	0.0282	0.0004	0.73	565	7	590	11	684	33	562	7	565	7	4.2
ZZ2_13	0.06318	0.00114	0.8685	0.0175	0.09969	0.00075	0.0306	0.00024	0.39	613	4	635	10	714	36	609	5	613	4	3.5
Z61_080	0.0614	0.0006	0.8481	0.0088	0.1000	0.0005	0.0296	0.0004	0.45	614	3	624	5	655	19	589	7	614	3	1.6
Z81_104	0.0628	0.0011	0.8730	0.0156	0.1009	0.0006	0.0315	0.0004	0.31	620	3	637	8	700	35	628	9	620	3	2.7
ZZ2_17	0.06904	0.0009	0.97235	0.0172	0.10218	0.00123	0.04255	0.00051	0.68	627	7	690	9	900	25	842	10	627	7	9.1
Z63_082	0.0653	0.0009	0.9445	0.0148	0.1032	0.0009	0.0235	0.0004	0.55	633	5	675	8	782	26	469	8	633	5	6.2
Z65_084	0.0626	0.0008	0.9331	0.0132	0.1080	0.0006	0.0318	0.0004	0.4	661	3	669	7	695	26	633	7	661	3	1.2
ZZ2_16	0.06438	0.00114	1.12091	0.02476	0.12628	0.00108	0.03868	0.00032	0.53	767	6	763	12	754	34	767	6	**767**	**6**	-0.5
ZZ2_20	0.0751	0.00105	1.3198	0.02434	0.12718	0.00153	0.05671	0.00079	0.65	772	9	854	11	1071	26	1115	15	772	9	9.6
ZZ2_7	0.0731	0.00095	1.333	0.03292	0.13305	0.00279	0.04629	0.0006	0.85	805	16	860	14	1017	24	915	12	805	16	6.4
Z24_035	0.0680	0.0019	1.3523	0.0534	0.1443	0.0021	0.0439	0.0005	0.73	869	12	869	23	868	54	869	10	**869**	**12**	0.0
Z51_068	0.0712	0.0007	1.4534	0.0162	0.1481	0.0007	0.0449	0.0002	0.48	890	4	911	7	962	18	887	4	890	4	2.3
Z28_040	0.0687	0.0009	1.4219	0.0217	0.1501	0.0008	0.0456	0.0002	0.39	901	4	898	9	890	25	902	5	**901**	**4**	-0.3
ZZ2_35	0.07104	0.00065	1.473	0.01622	0.14996	0.00093	0.04341	0.00052	0.56	901	5	919	7	959	17	859	10	901	5	2.0
Z94_119	0.0686	0.0008	1.4366	0.0189	0.1518	0.0011	0.0454	0.0006	0.56	911	6	904	8	886	23	898	11	**911**	**6**	-0.8
ZZ2_31	0.06953	0.0007	1.459	0.01687	0.15179	0.00088	0.04649	0.00056	0.49	911	5	914	7	915	19	918	11	**911**	**5**	0.3
Z85_108	0.0710	0.0007	1.5161	0.0190	0.1549	0.0010	0.0469	0.0003	0.61	928	6	937	8	957	19	927	6	928	6	1.0
ZZ2_18	0.0713	0.00063	1.54353	0.01742	0.15701	0.00093	0.04754	0.00028	0.57	940	5	948	7	966	17	939	5	940	5	0.8
ZZ2_19	0.07256	0.00061	1.5764	0.01609	0.15728	0.00091	0.05134	0.00062	0.57	942	5	961	6	1002	16	1012	12	942	5	2.0
Z78_100	0.0701	0.0009	1.5238	0.0217	0.1577	0.0008	0.0478	0.0002	0.41	944	4	940	9	931	24	945	4	**944**	**4**	-0.4
Z70_090	0.0717	0.0008	1.5799	0.0191	0.1596	0.0008	0.0472	0.0006	0.41	954	4	962	8	979	21	933	11	**954**	**4**	0.8
ZZ2_10	0.07405	0.00163	1.6392	0.03832	0.16	0.00126	0.04753	0.00067	0.34	957	7	985	15	1043	41	939	13	957	7	2.8
ZZ2_6	0.07133	0.00114	1.5868	0.02898	0.16123	0.00142	0.0469	0.00075	0.48	964	8	965	11	967	30	926	14	**964**	**8**	0.1
Z84_107	0.0725	0.0011	1.6907	0.0273	0.1692	0.0010	0.0506	0.0008	0.37	1008	6	1005	10	999	30	997	15	**999**	**30**	-0.3
Z57_075	0.0729	0.0008	1.7931	0.0219	0.1784	0.0010	0.0529	0.0007	0.44	1058	5	1043	8	1011	21	1043	13	1011	21	-1.4
ZZ2_21	0.07316	0.00063	1.7025	0.01825	0.16833	0.00108	0.04764	0.00076	0.6	1003	6	1009	7	1018	16	941	15	**1018**	**16**	1.5
ZZ2_15	0.07333	0.00063	1.65988	0.017	0.16416	0.00097	0.04956	0.0003	0.57	980	5	993	6	1023	16	978	6	1023	16	1.3
Z74_095	0.0734	0.0009	1.7360	0.0228	0.1715	0.0009	0.0501	0.0007	0.41	1020	5	1022	8	1024	24	988	13	**1024**	**24**	0.2
ZZ2_36	0.07336	0.00068	1.7022	0.01931	0.16784	0.00109	0.05033	0.0007	0.58	1000	6	1009	7	1024	17	993	13	1024	17	2.3

#	PROPORCIONES CORREGIDAS									EDADES CORREGIDAS (Ma)										
	$^{207}Pb/^{206}Pb$	±1σ	$^{207}Pb/^{235}U$	±1σ	$^{206}Pb/^{238}U$	±1σ	$^{208}Pb/^{232}Th$	±1σ	Rho	$^{206}Pb/^{238}U$	±1σ	$^{207}Pb/^{235}U$	±1σ	$^{207}Pb/^{206}Pb$	±1σ	$^{208}Pb/^{232}Th$	±1σ	Best age (Ma)	±1σ	% disc
G-36 - Esquisto de mica de Suite Piaxtla (*continuación*)																				
Z53_070	0.0735	0.0009	1.9104	0.0250	0.1882	0.0010	0.0530	0.0007	0.4	1111	5	1085	9	1029	22	1044	13	1029	22	-2.4
Z25_036	0.0736	0.0009	1.7836	0.0233	0.1759	0.0009	0.0502	0.0007	0.41	1044	5	1039	9	1030	23	991	13	**1030**	**23**	-0.5
ZZ2_23	0.07378	0.00063	1.7127	0.02047	0.16799	0.00139	0.0463	0.0006	0.7	1001	8	1013	8	1035	16	915	12	1035	16	3.3
Z49_066	0.0738	0.0010	1.7572	0.0248	0.1731	0.0010	0.0522	0.0008	0.39	1029	5	1030	9	1036	24	1029	15	**1036**	**24**	0.1
Z95_120	0.0739	0.0007	1.7228	0.0223	0.1689	0.0015	0.0514	0.0006	0.7	1006	8	1017	8	1038	19	1013	12	1038	19	1.1
ZZ2_29	0.07396	0.00087	1.70978	0.02432	0.16767	0.00109	0.05057	0.00035	0.52	999	6	1012	9	1040	22	997	7	1040	22	1.3
Z23_034	0.0744	0.0007	1.7400	0.0204	0.1694	0.0010	0.0524	0.0007	0.53	1009	6	1023	8	1053	19	1032	13	1053	19	1.4
Z66_086	0.0745	0.0008	1.9060	0.0211	0.1853	0.0009	0.0548	0.0007	0.42	1096	5	1083	7	1056	19	1077	14	1056	19	-1.2
ZZ2_4	0.07455	0.00061	1.828	0.01815	0.17723	0.00099	0.0545	0.00065	0.57	1052	5	1056	7	1056	15	1073	12	**1056**	**15**	0.4
Z21_032	0.0748	0.0011	1.8526	0.0295	0.1796	0.0010	0.0504	0.0007	0.34	1065	5	1064	11	1064	28	993	13	**1064**	**28**	-0.1
ZZ2_5	0.07498	0.00068	2.034	0.02152	0.1963	0.00106	0.05692	0.00068	0.52	1155	6	1127	7	1068	17	1119	13	1068	17	-8.1
Z91_116	0.0752	0.0007	1.8881	0.0210	0.1820	0.0010	0.0536	0.0006	0.47	1078	5	1077	7	1073	20	1056	12	**1073**	**20**	-0.1
Z10_018	0.0753	0.0008	1.9502	0.0236	0.1879	0.0009	0.0545	0.0008	0.41	1110	5	1099	8	1075	21	1073	15	1075	21	-1.0
Z40_054	0.0753	0.0011	1.8416	0.0280	0.1774	0.0011	0.0519	0.0008	0.4	1052	6	1060	10	1075	26	1023	16	**1075**	**26**	0.8
Z72_093	0.0757	0.0014	1.8763	0.0374	0.1800	0.0011	0.0567	0.0009	0.3	1067	6	1073	13	1086	37	1115	16	**1086**	**37**	0.6
Z58_076	0.0758	0.0008	1.8110	0.0218	0.1732	0.0009	0.0534	0.0008	0.42	1030	5	1049	8	1089	20	1051	15	1089	20	1.8
Z60_078	0.0759	0.0009	2.0647	0.0268	0.1972	0.0010	0.0592	0.0009	0.38	1160	5	1137	9	1092	23	1163	17	1092	23	-2.0
Z56_074	0.0759	0.0010	2.0132	0.0287	0.1924	0.0011	0.0553	0.0008	0.41	1134	6	1120	10	1093	24	1088	15	1093	24	-1.3
Z16_026	0.0761	0.0009	1.9660	0.0259	0.1873	0.0010	0.0546	0.0008	0.42	1107	5	1104	9	1097	22	1075	15	**1097**	**22**	-0.3
Z67_087	0.0764	0.0007	1.9911	0.0210	0.1889	0.0009	0.0549	0.0007	0.45	1116	5	1112	7	1106	18	1081	13	**1106**	**18**	-0.4
Z96_122	0.0764	0.0010	1.9671	0.0284	0.1870	0.0012	0.0547	0.0008	0.44	1105	6	1104	10	1106	27	1076	16	**1106**	**27**	-0.1
ZZ2_2	0.07646	0.00067	1.8466	0.0202	0.17477	0.00114	0.04849	0.00078	0.6	1038	6	1062	7	1107	16	957	15	1107	16	6.2
Z20_030	0.0765	0.0008	1.9382	0.0213	0.1836	0.0008	0.0532	0.0006	0.4	1086	5	1094	7	1108	19	1047	12	**1108**	**19**	0.7
Z52_069	0.0768	0.0007	1.8787	0.0303	0.1770	0.0023	0.0545	0.0008	0.81	1051	13	1074	11	1115	18	1072	16	1115	18	2.1
ZZ2_32	0.0768	0.00115	1.82032	0.03532	0.17189	0.00133	0.05163	0.00037	0.58	1023	7	1053	13	1116	28	1017	7	1116	28	8.3
Z100_126	0.0768	0.0011	1.9885	0.0366	0.1877	0.0015	0.0564	0.0004	0.53	1109	8	1112	12	1117	27	1109	8	**1117**	**27**	**0.3**
Z39_053	0.0769	0.0024	1.9733	0.0656	0.1866	0.0022	0.0558	0.0011	0.36	1103	12	1106	22	1118	57	1098	21	**1118**	**57**	0.3
Z43_058	0.0771	0.0009	2.1461	0.0264	0.2017	0.0011	0.0619	0.0010	0.44	1184	6	1164	9	1124	20	1213	19	1124	20	-1.7
Z73_094	0.0776	0.0009	2.0777	0.0271	0.1940	0.0010	0.0559	0.0007	0.39	1143	5	1141	9	1137	23	1099	14	**1137**	**23**	-0.2
Z89_113	0.0781	0.0012	1.8711	0.0324	0.1734	0.0015	0.0505	0.0010	0.5	1031	8	1071	11	1149	31	996	19	1149	31	3.7
ZZ2_28	0.07813	0.00101	1.86825	0.03502	0.17342	0.00196	0.05199	0.00058	0.68	1031	11	1070	12	1150	24	1024	11	1150	24	10.3
Z22_033	0.0782	0.0008	2.0234	0.0329	0.1876	0.0018	0.0562	0.0005	0.73	1108	10	1123	11	1153	18	1106	10	1153	18	1.3
Z26_038	0.0783	0.0009	2.1894	0.0266	0.2026	0.0011	0.0606	0.0008	0.43	1189	6	1178	8	1155	20	1189	15	1155	20	-0.9
Z07_015	0.0786	0.0008	2.1590	0.0245	0.1990	0.0011	0.0575	0.0007	0.47	1170	6	1168	8	1163	19	1130	13	**1163**	**19**	-0.2
ZZ2_22	0.07862	0.00073	2.1933	0.02392	0.20176	0.00115	0.05897	0.00071	0.52	1185	6	1179	8	1163	17	1158	14	**1163**	**17**	-1.9
Z47_063	0.0789	0.0008	2.0758	0.0406	0.1898	0.0032	0.0544	0.0015	0.87	1120	17	1141	13	1170	18	1071	29	1170	18	1.8
ZZ2_3	0.07899	0.00103	2.1382	0.03061	0.19588	0.00118	0.05662	0.00074	0.41	1153	6	1161	10	1172	24	1113	14	**1172**	**24**	1.6
ZZ2_14	0.07997	0.00104	2.1892	0.03264	0.19833	0.00145	0.05905	0.00089	0.49	1166	8	1178	10	1196	24	1160	17	**1196**	**24**	2.5
Z18_028	0.0805	0.0008	2.0969	0.0296	0.1889	0.0016	0.0565	0.0005	0.66	1115	8	1148	10	1209	17	1110	9	1209	17	2.9

#	PROPORCIONES CORREGIDAS									EDADES CORREGIDAS (Ma)										
	$^{207}Pb/^{206}Pb$	±1σ	$^{207}Pb/^{235}U$	±1σ	$^{206}Pb/^{238}U$	±1σ	$^{208}Pb/^{232}Th$	±1σ	Rho	$^{206}Pb/^{238}U$	±1σ	$^{207}Pb/^{235}U$	±1σ	$^{207}Pb/^{206}Pb$	±1σ	$^{208}Pb/^{232}Th$	±1σ	Best age (Ma)	±1σ	% disc
G-36 - Esquisto de mica de Suite Piaxtla (*continuación*)																				
Z62_081	0.0807	0.0008	2.3783	0.0265	0.2135	0.0011	0.0618	0.0008	0.43	1247	6	1236	8	1214	19	1212	15	1214	19	-0.9
ZZ2_26	0.0807	0.00068	2.1737	0.02244	0.19488	0.00117	0.05874	0.0007	0.58	1148	6	1173	7	1214	15	1154	13	1214	15	5.4
Z68_088	0.0811	0.0009	2.3468	0.0280	0.2098	0.0010	0.0619	0.0007	0.39	1228	5	1227	8	1223	21	1214	14	**1223**	**21**	-0.1
Z69_089	0.0817	0.0009	2.3242	0.0286	0.2061	0.0011	0.0626	0.0009	0.45	1208	6	1220	9	1239	21	1228	18	1239	21	1.0
Z41_056	0.0821	0.0012	2.4408	0.0370	0.2156	0.0013	0.0635	0.0009	0.38	1259	7	1255	11	1247	25	1244	17	**1247**	**25**	-0.3
Z19_029	0.0829	0.0012	2.4012	0.0390	0.2096	0.0013	0.0617	0.0008	0.39	1227	7	1243	12	1267	27	1211	15	1267	27	1.3
ZZ2_25	0.08292	0.00108	2.3725	0.03459	0.20753	0.00137	0.05743	0.00069	0.45	1216	7	1234	10	1267	24	1129	13	1267	24	4.0
Z83_106	0.0830	0.0009	2.3098	0.0285	0.2017	0.0011	0.0650	0.0010	0.46	1185	6	1215	9	1268	21	1273	18	1268	21	2.5
Z97_123	0.0832	0.0010	2.5647	0.0334	0.2234	0.0011	0.0647	0.0009	0.39	1300	6	1291	10	1274	24	1268	17	**1274**	**24**	-0.7
Z36_050	0.0832	0.0009	2.2259	0.0270	0.1938	0.0010	0.0574	0.0007	0.41	1142	5	1189	8	1275	20	1129	13	1275	20	4.0
Z82_105	0.0832	0.0010	2.3486	0.0304	0.2045	0.0010	0.0654	0.0011	0.37	1200	5	1227	9	1275	23	1280	21	1275	23	2.2
Z54_071	0.0833	0.0012	2.4532	0.0369	0.2133	0.0012	0.0647	0.0010	0.36	1246	6	1258	11	1276	25	1268	20	**1276**	**25**	1.0
ZZ2_34	0.08331	0.00082	2.477	0.03032	0.21534	0.00155	0.06466	0.00078	0.59	1257	8	1265	9	1276	18	1266	15	**1276**	**18**	1.5
Z46_062	0.0837	0.0010	2.5249	0.0337	0.2184	0.0013	0.0648	0.0008	0.44	1273	7	1279	10	1285	22	1270	16	**1285**	**22**	0.5
ZZ2_1	0.08511	0.00102	2.4043	0.03377	0.2044	0.00149	0.05305	0.00085	0.52	1199	8	1244	10	1318	21	1045	16	1318	21	9.0
ZZ2_9	0.08557	0.00076	2.6445	0.02884	0.22363	0.00141	0.06399	0.00077	0.58	1301	7	1313	8	1328	16	1254	15	1328	16	2.0
Z11_020	0.0861	0.0016	2.1952	0.0410	0.1838	0.0009	0.0560	0.0008	0.27	1088	5	1180	13	1340	33	1102	15	1340	33	7.8
Z42_057	0.0876	0.0010	2.8090	0.0343	0.2325	0.0012	0.0685	0.0010	0.44	1347	6	1358	9	1373	19	1340	18	1373	19	0.8
Z06_014	0.0907	0.0015	3.1788	0.0618	0.2542	0.0015	0.0750	0.0004	0.43	1460	8	1452	15	1441	30	1461	8	**1441**	**30**	-0.6
Z86_110	0.0916	0.0010	3.3002	0.0407	0.2605	0.0015	0.0789	0.0013	0.45	1492	7	1481	10	1460	20	1536	24	**1460**	**20**	-0.7
Z37_051	0.0948	0.0010	3.3021	0.0568	0.2448	0.0034	0.0873	0.0011	0.81	1411	18	1482	13	1525	17	1691	21	1525	17	4.8
ZZ2_24	0.0984	0.00092	3.9133	0.04352	0.2875	0.00175	0.08582	0.00103	0.54	1629	9	1616	9	1594	16	1664	19	1594	16	-2.2
ZZ2_8	0.10685	0.00097	4.4048	0.04684	0.29824	0.00164	0.08373	0.001	0.52	1683	8	1713	9	1746	15	1625	19	1746	15	3.6
ZZ2_33	0.11067	0.00102	4.9191	0.06229	0.32054	0.00279	0.09399	0.00113	0.69	1792	14	1806	11	1810	16	1816	21	**1810**	**16**	1.0
Z08_016	0.1121	0.0010	4.9531	0.0914	0.3199	0.0051	0.0883	0.0018	0.87	1789	25	1811	16	1833	16	1709	33	1833	16	1.2
Z17_027	0.1121	0.0010	5.3083	0.0546	0.3433	0.0017	0.0967	0.0012	0.47	1902	8	1870	9	1833	15	1866	21	1833	15	-1.7
Z31_044	0.1128	0.0010	5.1341	0.0512	0.3298	0.0016	0.0937	0.0011	0.48	1837	8	1842	8	1845	14	1809	21	**1845**	**14**	0.3
Z12_021	0.1134	0.0011	5.2595	0.0539	0.3361	0.0015	0.0941	0.0011	0.43	1868	7	1862	9	1855	16	1817	21	**1855**	**16**	-0.3
Z77_099	0.1135	0.0010	5.3472	0.0525	0.3412	0.0017	0.0941	0.0011	0.49	1892	8	1876	8	1857	15	1818	21	1857	15	-0.9
Z14_023	0.1139	0.0010	5.1323	0.0548	0.3263	0.0019	0.0921	0.0011	0.56	1821	9	1841	9	1863	15	1781	21	1863	15	1.1
Z15_024	0.1148	0.0011	5.5988	0.0631	0.3531	0.0021	0.1033	0.0013	0.53	1949	10	1916	10	1877	16	1987	25	1877	16	-1.7
Z34_047	0.1148	0.0010	5.5090	0.0558	0.3476	0.0017	0.1014	0.0013	0.49	1923	8	1902	9	1877	14	1951	24	1877	14	-1.1
Z03_010	0.1257	0.0012	6.4650	0.0685	0.3728	0.0018	0.1025	0.0012	0.46	2043	9	2041	9	2039	16	1973	23	**2039**	**16**	-0.1
Z01_008	0.1260	0.0011	5.7098	0.0604	0.3281	0.0019	0.0947	0.0011	0.54	1829	9	1933	9	2043	14	1829	21	2043	14	5.4